NASA Tech Briefs

National
Aeronautics and
Space
Administration

Water-hyacinth technology, an imaginative new approach to wastewater treatment, has emerged from research in a NASA application project. Shown here being harvested at a Florida demonstration site, water hyacinths purify wastewater by absorbing and metabolizing pollutants — at a fraction of the cost of conventional sewage treatment. Side benefits under study are the conversion of harvested hyacinths to fuel gas, fertilizer, and animal feed. [See the bottom of page A1.]

Vol. 5, No. 3 Fall 1980

About the NASA Technology Utilization Program

The National Aeronautics and Space Act of 1958, which established NASA and the United States civilian space program, requires that "The Administration shall provide for the widest practicable and appropriate dissemination of information concerning its activities and the results thereof."

To help carry out this objective, NASA's Technology Utilization (TU) Program was established in 1962. Now, as an element of NASA's Technology Transfer Division, this program offers a variety of valuable services to help transfer aerospace technology to nonaerospace applications, thus assuring American taxpayers maximum return on their investment in space research; thousands of spinoffs of NASA research have already occurred in virtually every area of our economy.

The TU program has worked for engineers, scientists, technicians, and businessmen; and it can work for you.

NASA Tech Briefs

Tech Briefs is published quarterly and is free to engineers in U.S. industry and to other domestic technology transfer agents. It is both a current-awareness medium and a problem-solving tool. Potential products . . . industrial processes . . . basic and applied research . . . shop and lab techniques . . . computer software . . . new sources of technical data . . . concepts . . . can be found here. The short section on New Product Ideas highlights a few of the potential new products contained in this issue. The remainder of the volume is organized by technical category to help you quickly review new developments in your areas of interest. Finally, a subject index makes each issue a convenient reference file.

Further Information on Innovations

Although some new technology announcements are complete in themselves, most are backed up by Technical Support Packages (TSP's). TSP's are available without charge and may be ordered by simply completing a TSP Request Card found at the back of this volume. Further information on some innovations is available for a nominal fee from other sources, as indicated. In addition, Technology Utilization Officers at NASA Field Centers will often be able to lend necessary guidance and assistance.

Patent Licenses

Patents have been issued to NASA on some of the inventions described, and patent applications have been submitted on others. Each announcement indicates patent status, if applicable.

Other Technology Utilization Services

To assist engineers, industrial researchers, business executives, city officials, and other potential users in applying space technology to their problems, NASA sponsors Industrial Applications Centers. Their services are described on page A7. In addition, an extensive library of computer programs is available through COSMIC, the Technology Utilization Program's outlet for NASA-developed software.

Applications Program

NASA conducts applications engineering projects to help solve public-sector problems in such areas as safety, health, transportation, and environmental protection. Applications teams, staffed by professionals from a variety of disciplines, assist in this effort by working with Federal agencies and health organizations to identify critical problems amenable to solution by the application of existing NASA technology.

Reader Feedback

We hope you find the information in *NASA Tech Briefs* useful. A reader-feedback card has been included because we want your comments and suggestions on how we can further help you apply NASA innovations and technology to your needs. Please use it; or if you need more space, write to the Director, Technology Transfer Division, P. O. Box 8757, Baltimore/Washington International Airport, Maryland 21240.

NASA Tech Briefs

National
Aeronautics and
Space
Administration

FALL 1980
Volume 5, Number 3

COVERS: The photographs on the front and back covers illustrate developments by NASA and its contractors that have resulted in commercial and nonaerospace spinoffs. To find out more about the Water-Hyacinth Technology, Circle 89 on the TSP Request Card at the back of this issue of NASA Tech Briefs. [Also see the related article "Treating Domestic Wastewater With Water Hyacinths" on page 336.] To find out more about the Noise-Absorption Technology, Circle 90.

About This NASA Publication

NASA Tech Briefs, a quarterly publication, is distributed free to qualified U.S. citizens to encourage commercial application of U.S. space technology. For information on publications and services available through the NASA Technology Utilization Program, write to the Director, Technology Transfer Division, P. O. Box 8757, Baltimore/Washington International Airport, Maryland 21240.

"The Administrator of National Aeronautics and Space Administration has determined that the publication of this periodical is necessary in the transaction of the public business required by law of this Agency. Use of funds for printing this periodical has been approved by the Director of the Office of Management and Budget."

Change of Address

If you wish to have NASA Tech Briefs forwarded to your new address, use one of the Subscriptions cards enclosed in the back of this volume of NASA Tech Briefs. Be sure to check the appropriate box indicating change of address.

Communications Concerning Editorial Matter

For editorial comments or general communications about NASA Tech Briefs, you may use the Feedback card in the back of NASA Tech Briefs, or write to: The Publications Manager, Technology Transfer Division (ETD-6), NASA Headquarters, Washington, DC 20546. Technical questions concerning specific articles should be directed to the Technology Utilization Officer of the sponsoring NASA Center (addresses listed on page A4).

1979 Index

To obtain a copy of the 1979 Index to NASA Tech Briefs, Circle 91 on the TSP Request Card at the back of this issue.

Acknowledgements

NASA Tech Briefs is published quarterly by the National Aeronautics and Space Administration, Technology Utilization Branch, Washington, DC: Administrator: **Robert A. Frosch;** Director, Technology Transfer Division: **Floyd I. Roberson;** Publications Manager: **D. W. Orrick.** Prepared for the National Aeronautics and Space Administration by **Logical Technical Services Corp.:** Editor-in-Chief: **Jay Kirschenbaum;** Art Director: **Ernest Gillespie;** Assistant Editor: **Jerome Rosen;** Chief Copy Editor: **Oden Browne;** Staff Editors: **Donald Blattner, Ted Selinsky, George Watson:** Graphics: **Concetto Auditore, Conrad Carlock, Luis Martinez, Janet McCrie;** Editorial & Production: **Richard Johnson, Jeanne Bonner, Rose Giglietti, Marena Gutman, Kathi Norklun, Michael Stanton, Vincent Susinno, John Tucker, Ernestine Walker.**

NASA TU SERVICES

NASA TECHNOLOGY UTILIZATION NETWORK

★ TECHNOLOGY UTILIZATION OFFICERS

Charles C. Kubokawa
Ames Research Center
Code AU: 240-2
Moffett Field, CA 94035
(415) 965-5151

Gussie Anderson
Hugh L. Dryden Flight Research Center
Code OD/TU Office - Room 2015
Post Office Box 273
Edwards, CA 93523
(805) 258-3311, Ext. 787

Donald S. Friedman
Goddard Space Flight Center
Code 702.1
Greenbelt, MD 20771
(301) 344-6242

John T. Wheeler
Lyndon B. Johnson Space Center
Code AT-3
Houston, TX 77058
(713) 483-3809

Raymond J. Cerrato
John F. Kennedy Space Center
Code PT-STA-1
Kennedy Space Center, FL 32899
(305) 867-2780

John Samos
Langley Research Center
Mail Stop 139A
Hampton, VA 23665
(804) 827-3281

Harrison Allen, Jr.
Lewis Research Center
Mail Code 7-3
21000 Brookpark Road
Cleveland, OH 44135
(216) 433-4000, Ext. 6422

Aubrey D. Smith
George C. Marshall Space Flight Center
Code AT01
Marshall Space Flight Center, AL 35812
(205) 453-2224

D. W. Orrick
NASA Headquarters
Code ETD-6
Washington, DC 20546
(202) 755-2244

John H. Warden
NASA Resident Office-JPL
4800 Oak Grove Drive
Pasadena, CA 91103
(213) 354-6420

Gilmore H. Trafford
Wallops Flight Center
Code OD
Wallops Island, VA 23337
(804) 824-3411, Ext. 201

● INDUSTRIAL APPLICATIONS CENTERS

Aerospace Research Applications Center
1201 East 38th Street
Indianapolis, IN 46205
John M. Ulrich, director
(317) 264-4644

Computer Software Management and Information Center (COSMIC)
Suite 112, Barrow Hall
University of Georgia
Athens, GA 30602
Harold G. Hale, Jr., director
(404) 542-3265

Kerr Industrial Applications Center
Southeastern Oklahoma State University
Durant, OK 74701
Robert Oliver, director
(405) 924-0121, Ext. 413

NASA Industrial Applications Center
701 LIS Building
University of Pittsburgh
Pittsburgh, PA 15260
Paul A. McWilliams, executive director
(412) 624-5211

New England Research Applications Center
Mansfield Professional Park
Storrs, CT 06268
Daniel Wilde, director
(203) 486-4533

North Carolina Science and Technology Research Center
Post Office Box 12235
Research Triangle Park, NC 27709
Peter J. Chenery, director
(919) 549-0671

Technology Applications Center
University of New Mexico
Albuquerque, NM 87131
Stanley Morain, director
(505) 277-3622

NASA Industrial Applications Center
University of Southern California
Denny Research Building
University Park
Los Angeles, CA 90007
Robert Mixer, acting director
(213) 743-6132

■ STATE TECHNOLOGY APPLICATIONS CENTERS

NASA/University of Florida State Technology Applications Center
311 Weil Hall
University of Florida
Gainesville, FL 32611
Ronald J. Thornton, director
Gainesville: (904) 392-6760
Orlando: (305) 275-2706
Tampa: (813) 974-2499

NASA/University of Kentucky State Technology Applications Program
109 Kinkead Hall
University of Kentucky
Lexington, KY 40506
William R. Strong, manager
(606) 258-4632

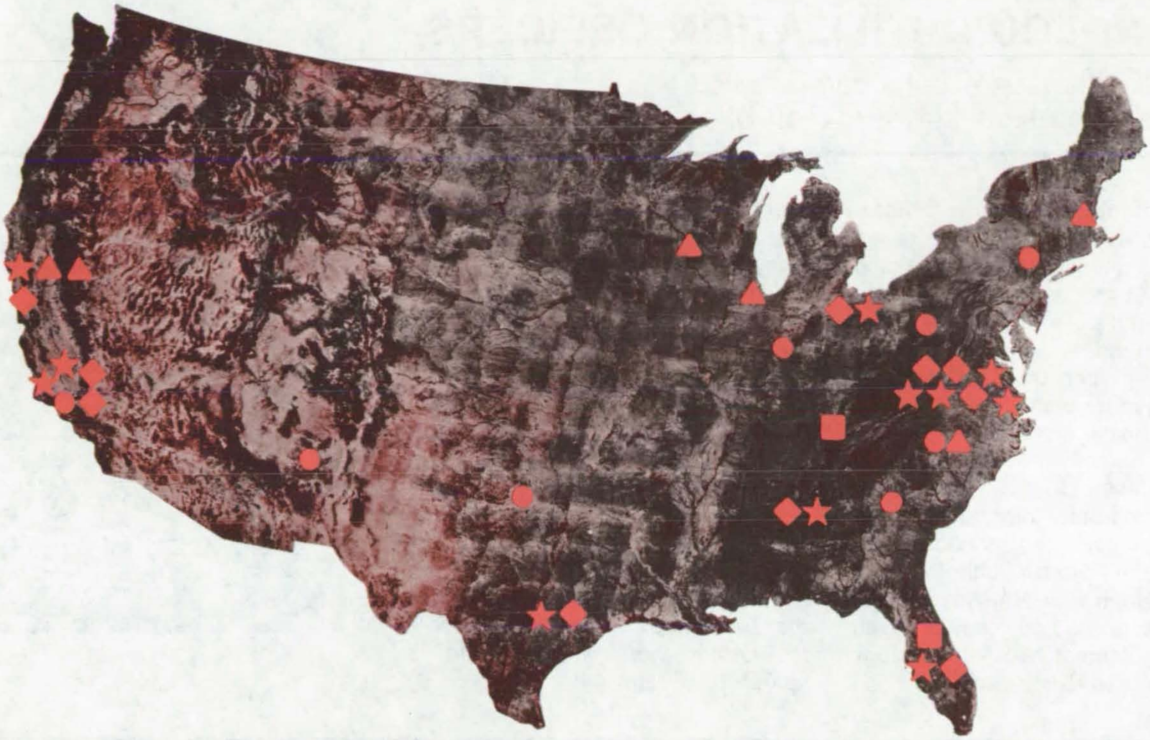

◆ PATENT COUNSELS

Robert F. Kempf
Asst. Gen. Counsel for patent matters
NASA Headquarters
Code GP-4
400 Maryland Avenue, SW.
Washington, DC 20546
(202) 755-3954

Darrell G. Brekke
Ames Research Center
Mail Code: 200-11A
Moffett Field, CA 94035
(415) 965-5104

Paul F. McCaul
Hugh L. Dryden Flight Research Center
Code OD/TU Office - Room 2015
Post Office Box 273
Edwards, CA 93523
(213) 354-2734

John O. Tresansky
Goddard Space Flight Center
Mail Code: 204
Greenbelt, MD 20771
(301) 344-7351

Marvin F. Matthews
Lyndon B. Johnson Space Center
Mail Code: AM
Houston, TX 77058
(713) 483-4871

James O. Harrell
John F. Kennedy Space Center
Mail Code: SA-PAT
Kennedy Space Center, FL 32899
(305) 867-2544

Howard J. Osborn
Langley Research Center
Mail Code: 279
Hampton, VA 23665
(804) 827-3725

Norman T. Musial
Lewis Research Center
Mail Code: 500-311
21000 Brookpark Road
Cleveland, OH 44135
(216) 433-4000, Ext. 346

Leon D. Wofford, Jr.
George C. Marshall Space Flight Center
Mail Code: CC01
Marshall Space Flight Center, AL 35812
(205) 453-0020

Monte F. Mott
NASA Resident Office-JPL
Mail Code: 180-601
4800 Oak Grove Drive
Pasadena, CA 91103
(213) 354-2700

▲ APPLICATION TEAMS

William N. Fetzner, director
Advisory Center for Medical Technology and Systems
University of Wisconsin
1500 Johnson Drive
Madison, WI 53706
(608) 263-2735

Edmund R. Bangs, director
IIT Research Institute
10 West 35th Street
Chicago, IL 60616
(312) 567-4191

Doris Rouse, director
Research Triangle Institute
Post Office Box 12194
Research Triangle Park, NC 27709
(919) 541-6256

Tom Anyos, director
SRI International
333 Ravenswood Avenue
Menlo Park, CA 94026
(415) 326-6200, Ext. 2864

Eugene Schmidt, program coordinator
Stanford University School of Medicine
Cardiology Division
Biomedical Technology Transfer
703 Welch Road, Suite E-4
Palo Alto, CA 94304
(415) 497-5353

David MacFadyen, project director
Technology + Economics
2225 Massachusetts Avenue
Cambridge, MA 02140
(617) 491-1500

TECHNOLOGY UTILIZATION OFFICERS

Technology transfer experts can help you
apply the innovations in NASA Tech Briefs.

The Technology Utilization Officer
at each NASA Field Center is an applications engineer who can help you make use of new technology developed at his center. He brings you NASA Tech Briefs and other special publications, sponsors conferences, and arranges for expert assistance in solving technical problems.

Technical assistance,
in the form of further information about NASA innovations and technology, is one of the services available from the TUO. Together with NASA scientists and engineers, he can often help you find and implement NASA technology to meet your specific needs.

Technical Support Packages (TSP's)
are prepared by the center TUO's. They provide further technical details for articles in NASA Tech Briefs. This additional material can help you evaluate and use NASA technology. You may receive most TSP's free of charge by using the TSP Request Card found at the back of this issue.

Technical questions about articles
in NASA Tech Briefs are answered in the TSP's. When no TSP is available, or you have further questions, contact the Technology Utilization Officer at the center that sponsored the research [see page A4].

NASA INVENTIONS AVAILABLE FOR LICENSING

Over 3,500 NASA inventions are available for licensing
in the United States — both exclusive and nonexclusive.

Nonexclusive licenses
for commercial use of NASA inventions are encouraged to promote competition and to achieve the widest use of inventions. They must be used by a negotiated target date but are usually royalty-free.

Exclusive licenses
may be granted to encourage early commercial development of NASA inventions, especially when considerable private investment is required. These are generally for 5 to 10 years and usually require royalties based on sales or use.

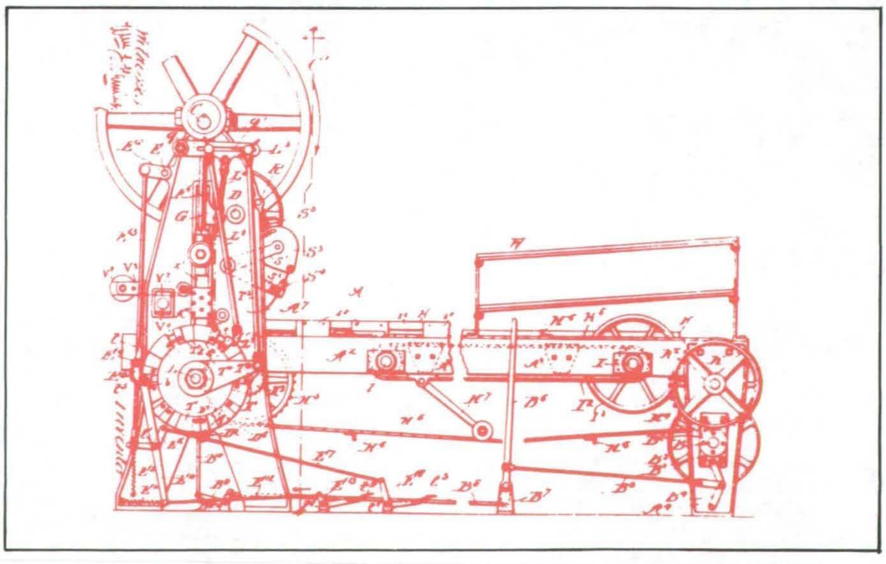

Additional licenses available
include those of NASA-owned foreign patents. In addition to inventions described in NASA Tech Briefs, *"NASA Patent Abstract Bibliography"* (PAB), containing abstracts of all NASA inventions, can be purchased from National Technical Information Service, Springfield, VA 22161. The PAB is updated semiannually.

Patent licenses for Tech Briefs
are frequently available. Many of the inventions reported in NASA Tech Briefs are patented or are under consideration for a patent at the time they are published. The current patent status is described at the end of the article; otherwise, there is no statement about patents. If you want to know more about the patent program or are interested in licensing a particular invention, contact the Patent Counsel at the NASA Field Center that sponsored the research [see page A5]. Be sure to refer to the NASA reference number at the end of the Tech Brief.

APPLICATION TEAMS

Technology-matching and problem-solving assistance to public-sector organizations

Application engineering projects are conducted by NASA to help solve public-sector problems in such areas as safety, health, transportation, and environmental protection. Some application teams specialize in biomedical disciplines; others, in engineering and scientific problems. Staffed by professionals from various disciplines, these teams work with other Federal agencies and health organizations to identify critical problems amenable to solution by the application of existing NASA technology.

Public-sector organization *representatives can learn more about application teams by contacting a nearby NASA Field Center Technology Utilization Office [see page A4].*

INDUSTRIAL APPLICATIONS CENTERS

Computerized access to nearly 10 million documents worldwide

Computerized information retrieval from one of the world's largest banks of technical data is available from NASA's network of Industrial Applications Centers (IAC's). The IAC's give you access to 1,800,000 technical reports in the NASA data base and to more than 10 times that many reports and articles found in 140 other computerized data bases.

The major sources include:

- *750,000 NASA Technical Reports*
- *Selected Water Resources Abstracts*
- *NASA Scientific and Technical Aerospace Reports*
- *Air Pollution Technical Information Center*
- *NASA International Aerospace Abstracts*
- *Chem Abstracts Condensates*
- *Engineering Index*
- *Energy Research Abstracts*
- *NASA Tech Briefs*
- *Government Reports Announcements*

and many other specialized files on food technology, textile technology, metallurgy, medicine, business, economics, social sciences, and physical science.

The IAC services range from tailored literature searches through expert technical assistance:

- *Retrospective Searches:* Published or unpublished literature is screened, and documents are identified according to your interest profile. IAC engineers tailor results to your specific needs and furnish abstracts considered the most pertinent. Complete reports are available upon request.
- *Current-Awareness Searches:* IAC engineers will help design a program to suit your needs. You will receive selected monthly or quarterly abstracts on new developments in your area of interest.
- *Technical Assistance:* IAC engineers will help you evaluate the results of your literature searches. They can help find answers to your technical problems and put you in touch with scientists and engineers at appropriate NASA Field Centers.

Prospective clients *can obtain more information about the services offered by NASA IAC's by contacting the nearest IAC [see page A4] or by checking the IAC box on a TSP Request Card in this issue.*

STATE TECHNOLOGY APPLICATIONS CENTERS

Technical information services for industry and state and local government agencies

Local government and industry in Florida and Kentucky can utilize the services of NASA's State Technology Applications Centers (STAC's). The STAC's differ from the Industrial Applications Centers described on page A7, primarily in that they are integrated into existing state technical assistance programs and serve only the host state, whereas the IAC's serve multistate regions.

Many data bases, including the NASA base and several commercial bases, are available for automatic data retrieval through the STAC's. Other services such as document retrieval and special searches are also provided. (The STAC's normally charge a fee for their services.)

To obtain information *about the services offered by NASA STAC's, write or call the STAC in your state* *[see page A4]*.

COSMIC®

An economical source of computer programs developed by NASA and other government agencies

A vast software library is maintained by COSMIC — the Computer Software Management and Information Center. COSMIC gives you access to approximately 1,600 computer programs developed for NASA and the Department of Defense and selected programs for other government agencies. Programs and documentation are available at reasonable cost.

Available programs range from management (PERT scheduling) to information science (retrieval systems) and computer operations (hardware and software). Hundreds of engineering programs perform such tasks as structural analysis, electronic circuit design, chemical analysis, and the design of fluid systems. Others determine building energy requirements and optimize mineral exploration.

COSMIC services go beyond the collection and storage of software packages. Programs are checked for completeness; special announcements and an indexed software catalog are prepared; and programs are reproduced for distribution. Customers are helped to identify their software needs; and COSMIC follows up to determine the successes and problems and to provide updates and error corrections. In some cases, NASA engineers can offer guidance to users in installing or running a program.

Information about programs *described in NASA Tech Briefs articles can be obtained by completing the COSMIC Request Card at the back of this issue. Just circle the letters that correspond to the programs in which you are interested.*

NEW PRODUCT IDEAS

NEW PRODUCT IDEAS are just a few of the many innovations described in this issue of NASA Tech Briefs and having promising commercial applications. Each is discussed further on the referenced page in the appropriate section in this issue. If you are interested in developing a product from these or other NASA innovations, you can receive further technical information by requesting the TSP referenced at the end of the full-length article or by writing the Technology Utilization Office of the sponsoring NASA center (see page A4). NASA's patent-licensing program to encourage commercial development is described on page A8.

Wrench for Smooth or Damaged Fasteners

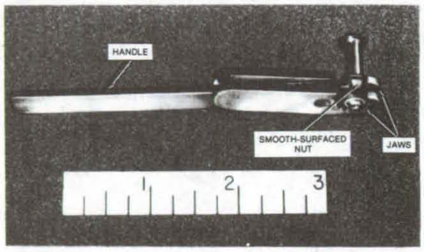

Smooth-surfaced or damaged fasteners that cannot be gripped by a conventional wrench can be unscrewed by a special wrench. It can be used in tight spaces and will not damage adjacent structures. The wrench consists of a central handle and two independent jaws with serrated teeth. The teeth are placed on the fastener to be removed, and the handle is rotated until the fastener is gripped with a positive locking action. Rotation of the wrench handle removes the fastener.
(See page 380.)

Quick Mixing of Epoxy Components

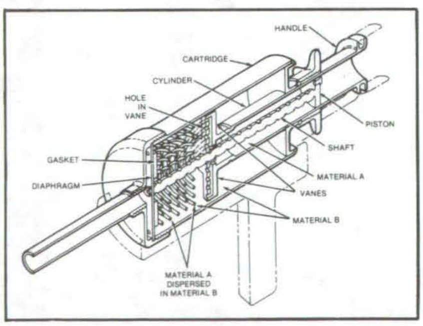

Two materials would be mixed quickly, thoroughly, and in precise proportion by a proposed disposable cartridge. The cartridge would mix components of fast-curing epoxy resins, with no mess, just before they are used. It could also be used in the home and in industry for caulking, sealing, and patching. The materials (A and B) to be mixed are initially isolated by a cylindrical wall within the cartridge. The cylinder has vanes, with holes in them, at one end and a handle at the opposite end. When the handle is pulled, grooves on a shaft rotate the cylinder so that the vanes rotate to extrude material A uniformly into material B.
(See page 379.)

Composites With Nearly-Zero Thermal Expansion

A new composite of graphite fibers and glass fibers in a plastic resin matrix has a near-zero coefficient of thermal expansion and high elastic modulus. The material is unusually strong, stiff, and thermally stable. As a mounting material for antennas, mirrors, and lenses, the glass/graphite composite would minimize structural distortion and misalinement.

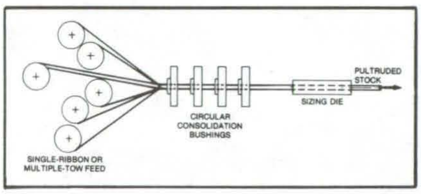

Rods of the composite are made by pulling a preimpregnated ribbon of glass and graphite fiber through a die. When the materials are combined in the proper proportion, the graphite contracts and the glass and resin expand as the temperature increases. The matrix for the fiber may be a polysulfone, an epoxy, a polyimide, or other resin.
(See page 323.)

Spraying Suspensions Uniformly

Coarse, multi-ingredient suspensions are sprayed on a surface smoothly and uniformly with the aid of a nozzle attachment for a commercial spray gun. The new nozzle attachment is contoured internally to suppress overspray and to prevent the spray from segregating. From its conical

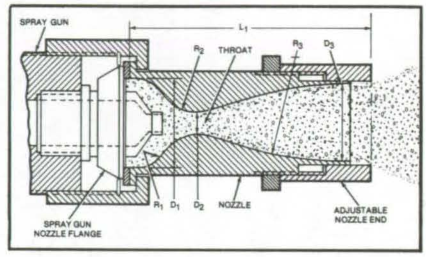

inlet, the nozzle converges smoothly to a throat, then diverges in a bell-shaped chamber that allows the suspension to flow uninterruptedly without building up turbulently in the nozzle. The end of the nozzle is adjustable and can be extended or retracted to avoid dripping when the inlet pressure, pump pressure, or density of the mixture changes.
(See page 374.)

Contour-Measuring Tool for Composite Layups

With the help of a simple handtool, contours and complex shapes are formed from laminae of resin-impregnated fabric. The new contouring tool,

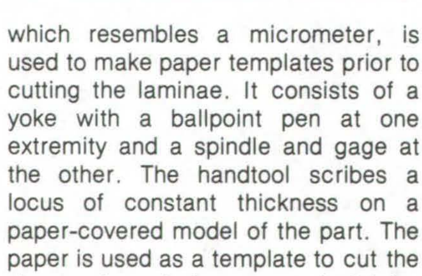

which resembles a micrometer, is used to make paper templates prior to cutting the laminae. It consists of a yoke with a ballpoint pen at one extremity and a spindle and gage at the other. The handtool scribes a locus of constant thickness on a paper-covered model of the part. The paper is used as a template to cut the sheet of resin-impregnated fabric. Several such layers are stacked and cured to form a composite layup with the same shape as the original part.
(See page 383.)

Lightweight Terminal Board

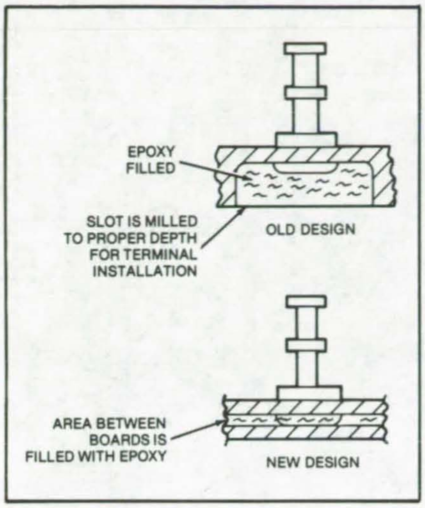

A new sandwich construction for terminal boards reduces fabrication time and produces thinner boards with better insulation consistency, better appearance, and less weight. The new method also permits closer spacing of the terminal posts. The method starts with a thin (0.031-inch) sheet of polyimide and consists of drilling, inserting terminal posts, upsetting the ends, and then bonding a second sheet to the upset side as a continuous insulation member. The resulting sandwich is lighter and much cheaper than the single board.

(See page 392.)

Versatile Modular Scaffolds

Movable and fixed modular scaffolds can be tailored to most scaffolding needs by interconnecting only four

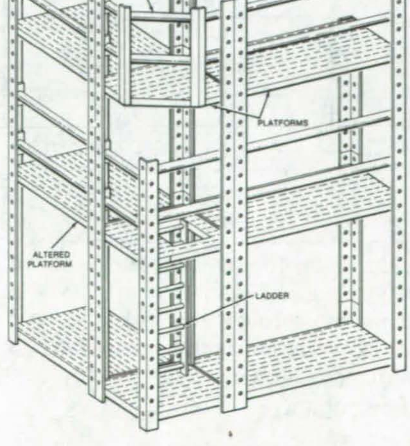

basic structural elements: platforms, rails, vertical-support angles, and a stiffener. Standard nuts and bolts are used to join elements, simplifying construction and reducing costs. The scaffolds are rigid and can be made any length. They are stable on unlevel ground and can extend to well over 50 feet in height. The scaffolds allow for internal elevators and for wheels and air mounts so that the same elements can be used for a standing or a movable scaffold.

(See page 372.)

Energy-Reduction Concept for Incandescent Lamps

A concept for a coated spherical light fixture may allow an ordinary incandescent lamp to produce more light for a given wattage. The fixture, coated on the inside with a thin layer of infrared-reflecting material, would be installed over the light bulb. Instead of infrared energy being lost, it would be directed back to the incandescent lamp filament by the selective coating.

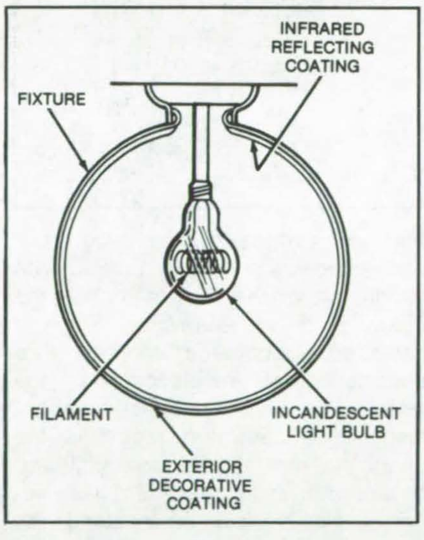

The reflected energy would aid the electric current in heating the filament and would allow a lower-wattage light bulb to produce the same amount of light as a higher wattage bulb in an ordinary light fixture.

(See page 304.)

Economical Ultraviolet Radiometer

Ultraviolet radiation from Sun and sky, integrated over the celestial hemisphere, is measured by an

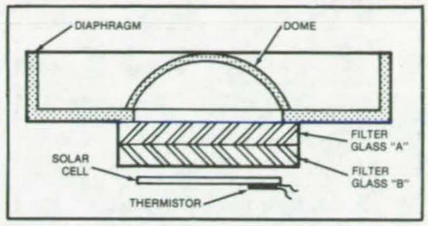

economical, cosine-corrected radiometer. Suitable for field use, the new radiometer has possible applications in testing materials for the effects of ultraviolet exposure and in studies of solar-cell degradation. It consists of a cup-shaped diaphragm and diffusing dome to obtain a cosine-corrected response, two filters that select the wavelength range, and a silicon solar cell. The two-component filter controls the response within a passband around 300 to 400 nm.

(See page 301.)

Acoustic Lens

A fluorocarbon gas contained by a plastic membrane is an effective lens for sound waves. In tests, the lens substantially improved the accuracy of sound "maps" of turbulent airflow. It could also be used to record sound-intensity patterns in the design of speakers, lecture halls, and auditoriums. The lens is fabricated by clamping together two membranes of thin plastic and filling the enclosed space with a fluorocarbon gas. Since the speed of sound in the gas is considerably less than in air, the lens refracts and focuses the sound waves,

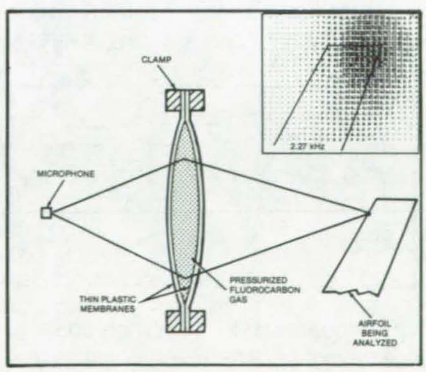

analogous to focusing light by a glass lens. The focal length is adjusted simply by changing the gas pressure, which changes the lens curvature.

(See page 345.)

Reshaping Tube Ends for Welding

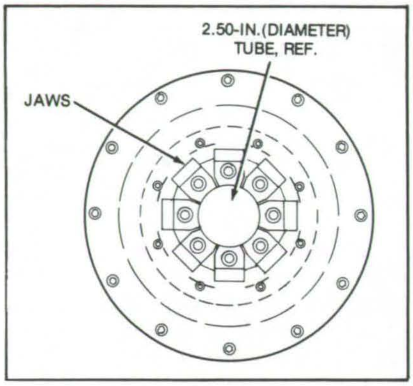

Roundness is restored to tube ends prior to welding by a semiautomatic tool. The hydraulically operated tool can be mounted on a workbench and is small enough to be moved easily from one factory area to another. It consists of two major parts: an "expander" that opens up the out-of-round tube so that a plug can be inserted and a "crimper" that compresses the tube into shape around the plug. After using the expander, hydraulic pressure is applied, and the jaws of the crimper swage the tube around the plug so that it assumes the proper shape. The present design handles a range of tube sizes, from 1/4 to 2-1/2 in.
(See page 373.)

Torque-Wrench Extension

A torque-wrench extension makes it easy to install and remove fasteners that are beyond the reach of typical wrenches or are located in narrow spaces that prevent full travel of the wrench handle. At the same time the new tool reads the applied torque accurately. The wrench drive system,

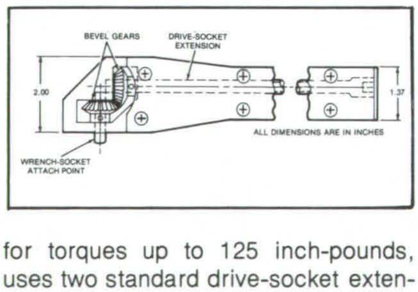

for torques up to 125 inch-pounds, uses two standard drive-socket extensions in an aluminum frame. The extensions are connected to a bevel gear that turns another bevel gear. The gears produce a 1:1 turns ratio through a 90° translation of the axis of rotation. The output bevel gear has a short extension that is used to attach a 1/4-inch drive socket.
(See page 378.)

Four-Cell Solar Tracker

A very sensitive Sun tracker has four solar cells surrounded by a cylindrical mirror. When added to a declination-angle/hour-angle drive, it can orient a solar collector or a solar mirror accurately for maximum illumination. Signal conduction leads from

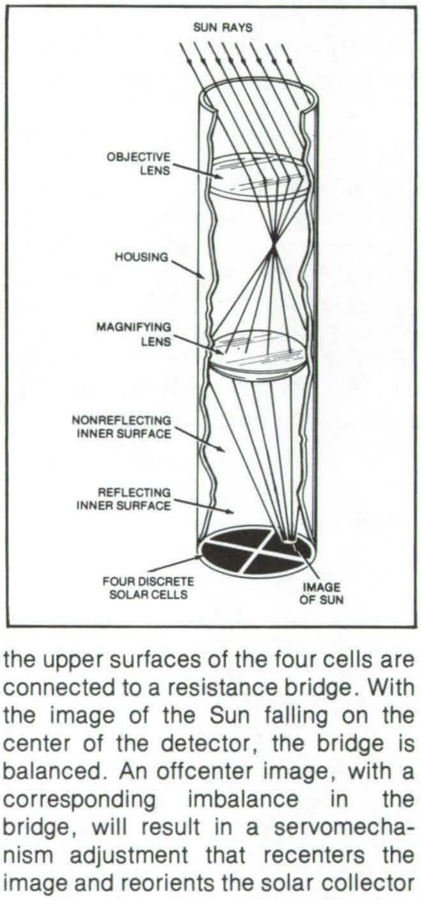

the upper surfaces of the four cells are connected to a resistance bridge. With the image of the Sun falling on the center of the detector, the bridge is balanced. An offcenter image, with a corresponding imbalance in the bridge, will result in a servomechanism adjustment that recenters the image and reorients the solar collector or solar mirror for maximum illumination. The cylindrical mirror extends the acquisition angle of the device by reflecting the Sun image back onto the solar cells.
(See page 298.)

Cleaving Machine for Hard Crystals

Hard crystalline materials such as lithium fluoride (LiF) are cleaved in thin sections by a new semiautomatic machine. The yield of undistorted LiF crystals is almost 100 percent, even

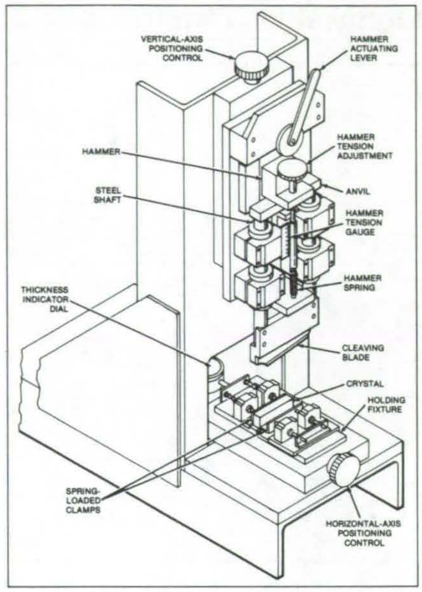

when the cleaved section is only 1/32 inch thick. The machine contains a spring-activated hammer that limits the penetration of a blade and controls the shock that cleaves the crystal. A fixture with spring-loaded clamps precisely locates and holds the crystal, restraining it in an ideal position for cleaving. The crystal then splays apart.
(See page 367.)

Compact Table-Tilting Mechanism

Optical components would be oriented precisely by a proposed motorized device for manipulating objects attached to a plane tilt table. The mechanism is compact, simple, and has low backlash. It consists of a drive motor, a rotatable disk, a rigid link,

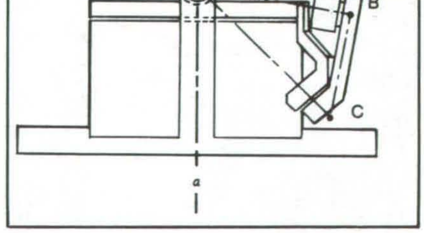

and a table. The motor rotates about a vertical axis, and the motion is converted through the disk and rigid link to rotation of the table about a perpendicular axis.
(See page 376.)

Electronic Components and Circuits

Hardware, Techniques, and Processes

Ultrastable Automatic Frequency Control

The center frequency of a wideband AFC circuit drifts only a few hundredths of a percent per day.

Lyndon B. Johnson Space Center, Houston, Texas

Designers of FM modulators using a voltage-controlled oscillator (VCO) must minimize carrier-frequency drift while allowing for wide modulation-frequency deviations. Adding automatic frequency control (AFC) to the VCO is a standard solution to the carrier-drift problem; however, conventional AFC may not suffice when the stability requirements are very tight.

A new circuit adds several new features to conventional AFC. Originally developed for the Space Shuttle payload communications simulator, the circuit stabilizes a 1.7-MHz FM subcarrier to better than 0.4 percent over 24 hours, while allowing a modulation-frequency deviation of ±160kHz. The operating temperature range is 0° to 50° C.

The major elements of an AFC loop are a frequency discriminator, which converts frequency deviations to an error voltage, and a loop filter, which removes the modulating signal from the error voltage. In wideband FM receivers, a pulse-averaging circuit containing a monostable multivibrator is usually used as the discriminator. However, the monostable pulse width and voltage levels vary with changes in temperature, supply voltage, and external timing components. As a result, the error voltage can fluctuate even if the modulation frequency does not change. These fluctuations appear as a drift of the center frequency.

The new AFC (see figure) minimizes discriminator pulse-width variations by using a highly stable crystal oscillator and a digital counting circuit, rather than a monostable multivibrator. Variations in discriminator voltages are compensated for by adding a correction voltage, obtained by subtracting the discriminator output from a reference voltage. The signals are buffered through separate amplifiers on the same integrated-circuit chip, so that both are subjected to the same temperature effects.

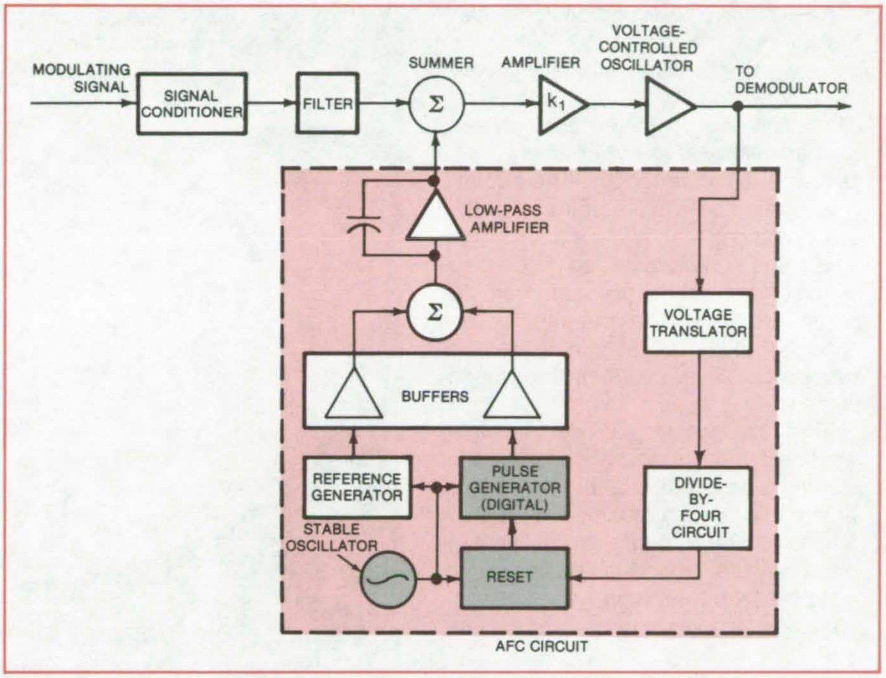

The improved **Automatic Frequency Control Circuit** is a negative-feedback loop that regulates a wideband FM voltage-controlled oscillator. Since the circuit responds only to relatively slow frequency drifts and the modulation signal has a high-pass characteristic, the AFC does not interfere with normal FM operation. The combination of the stable oscillator, reset circuit, and pulse generator constitutes a time-averaging discriminator. A digital counter in the pulse generator replaces the monostable multivibrator found in previous circuits.

If the pulses from the VCO are very short, propagation delay can also introduce error. The input to the reset circuit is therefore passed through a divide-by-four circuit. The input pulse width is quadrupled, and the propagation delay becomes insignificant.

The new AFC circuit has been built with transistor-transistor-logic (TTL) integrated circuits. Its performance has surpassed specifications; for example, the total drift at room temperature, recorded over a 24-hour period, is only ±100 Hz.

This work was done by Andy Furiga and Donald J. Sabourin of Motorola, Inc., for **Johnson Space Center.** *For further information, including detailed circuit drawings of the AFC, Circle 1 on the TSP Request Card.*

Inquiries concerning rights for the commercial use of this invention should be addressed to the Patent Counsel, Johnson Space Center [see page A5]. Refer to MSC-18679.

Fast Microwave Switching Power Divider

Power from a single input is divided among any 12 of 120 output terminals and is redistributed in 0.6 μs.

Goddard Space Flight Center, Greenbelt, Maryland

A microwave switching power divider has one input terminal and 120 output terminals. Power that is fed into the input terminal is divided equally (to within ± 0.5 dB) among 12 of the output terminals and can be switched to any other set of 12 outputs in 0.6 microseconds. The circuitry is located between a pair of parallel ground planes that define a microwave cavity and is reciprocal, so it can also be used for combining signals from 12 ports into one. The circuitry is on opposite sides of a thin dielectric substrate located between the ground planes.

The fast switching divider/combiner was built for use in an electronically-steered S-band antenna, but it can also divide and switch microwave energy among other networks such as filters or phase shifters. The design is not restricted to 120 terminals nor to the selection of 12; other numbers can be used just as well.

As shown in the figure, the center conductor of a coaxial cable is connected to the center of a copper disk on the dielectric substrate. The outer conductor of the coaxial cable is connected to the ground planes (the top ground plane is not shown).

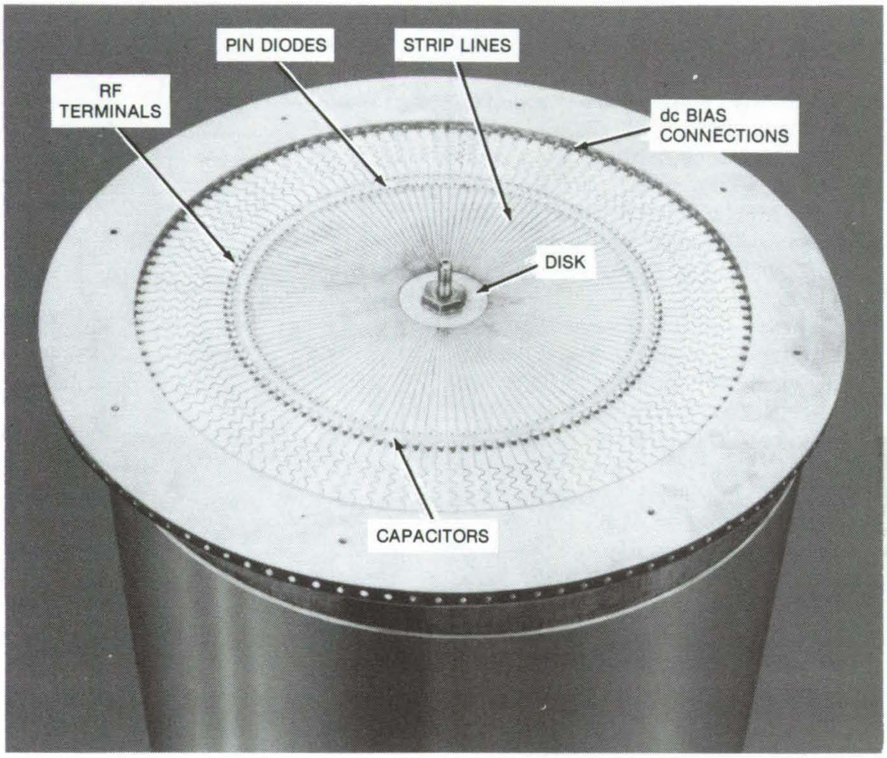

In this S-band **Switching Power Divider**, shown with one ground plane removed, microwave power from a coaxial line excites a disk that feeds many radial strip transmission lines. The 1.9-lb (0.87-kg) unit has an outer diameter of 22 cm.

Strip transmission lines are connected radially every 3° around the circumference of the disk; each line includes a PIN diode (for opening or closing the line) and a dc-blocking capacitor and tapers to 50 ohms impedance at its output terminal. A dc voltage applied to a diode biases it for conduction or nonconduction. The voltage is applied through an RF choke that presents very high impedance to the microwave signal; the choke isolates the microwave signal from the dc-blocking capacitor, and the capacitor keeps the dc voltage off the RF output cable.

The radius of the disk and the widths of the strip lines leaving it are chosen so that when 12 of the lines are closed and terminated in 50 ohms and the other 108 lines are open, the input impedance is also 50 ohms.

The PIN diodes have low insertion loss and high switching speed. A microprocessor or other source supplies dc bias current to switch the diodes.

Optimum power division (with respect to the uniformity of phase and amplitude) occurs when the output ports are symmetrically spaced about the circumference. The uniformity degrades slowly as the symmetric case is transformed (one port at a time) into the worst-case asymmetry where all the output ports are adjacent. Even this arrangement still gives good performance.

The switching divider/combiner built for the S-band antenna weighs only 865 grams, has an overall diameter of 22 cm, and is 3.3 cm high. The central disk has a radius of 1.24 cm, and the strip lines are 4.34 cm long.

This work was done by Russell W. Johnson and Ronald J. Stockton of Ball Corp. for **Goddard Space Flight Center**. *For further information, Circle 2 on the TSP Request Card.*

This invention is owned by NASA, and a patent application has been filed. Inquiries concerning nonexclusive or exclusive license for its commercial development should be addressed to the Patent Counsel, Goddard Space Flight Center [see page A5]. Refer to GSC-12420.

High-Power Solid-State Microwave Transmitter

Outputs from individual amplifier modules are phased and then combined in a multielement array feed antenna.

NASA's Jet Propulsion Laboratory, Pasadena, California

Although solid-state microwave amplifiers are more reliable than traveling-wave tubes (TWT's), they do not normally measure up to the high power-output levels possible with a TWT. Solid-state reliability and high power are both realized, however, with a new multielement microwave transmitter. In the new design, an input microwave signal is divided among many low-power solid-state amplifiers and then recombined in the proper phase to transmit a high-power output.

In an X-band antenna built for transmissions from deep space, the input is divided among 32 solid-state amplifiers that drive an equal number of in-phase radiating elements. For microwave power input at 1.11 watts, the amplifier transmits an output power level of 22.09 watts, while dissipating 77.96 watts of dc power. The basic design can be scaled up or down in size and power-handling capability for applications such as radar and other small-angle scanning.

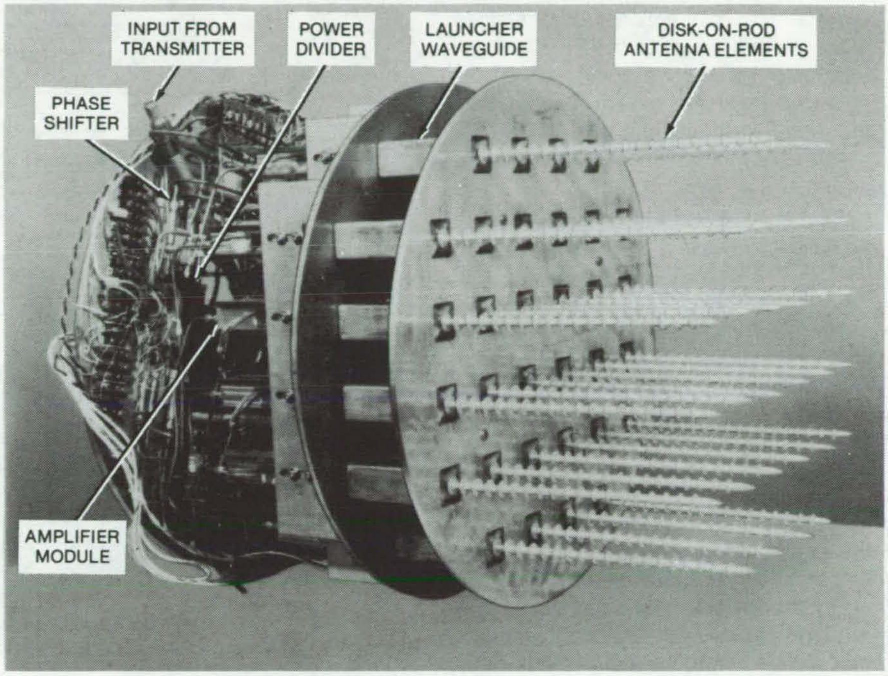

An **Array of Radiating Elements**, fed by paralleled solid-state amplifiers, combines its outputs to transmit a powerful signal from deep space to Earth. This arrangement gives solid-state reliability at a high power level.

The photograph of the combiner shows the input port, the power divider, the line-stretcher phase shifters, the amplifier modules, and the array feed for recombining the amplified signal. The power divider (in this case, a combination of 4- and 8-way dividers) splits the input power 32 ways. The phase shifters equalize the phasing of the 32 separated signal paths prior to injection into the 32 radiating elements.

The solid-state amplifiers operate at X-band. Each is a three-stage microstrip configuration housed in an H-frame chassis. The amplifier input power is 20 milliwatts; its output is 750 milliwatts at 8.415 GHz, with a minimum gain of 15 dB and efficiency greater than 25 percent. The GaAs field-effect transistors selected for the three-stage amplifier are rated at 1/4, 1/2, and 1 watt, respectively, with a total dc input power of 2.9 watts maximum. By using fixed 3-bit phase shifters and variable line stretchers, the relative phase difference among 32 amplifiers at the final array assembly is held to 2.5°, which contributes less than a 0.01-dB loss to the array beam phase efficiency.

In the power amplifier module, the 3-bit phase shifter (45°, 90°, and 180°) is included on the microstrip to combine signals in phase in the array; the desired phase is selected during testing. Line-stretcher phase shifters, having phase shifts of about 90°, are located in the input circuit between the 32-way power divider and the inputs to the amplifiers. These shifters compensate for most of the residual phase differences between the amplifiers.

The output of each amplifier module is isolated by a ferrite circulator and third port load. This protects the amplifier output stage and minimizes the array mismatch loss in the event of an amplifier failure.

This work was done by James F. Boreham, Bruce L. Conroy, Richard B. Postal, and Donald G. Yenche of Caltech for **NASA's Jet Propulsion Laboratory.** *For further information, including details of mechanical design and construction, Circle 3 on the TSP Request Card.*

Inquiries concerning rights for the commercial use of this invention should be addressed to the Patent Counsel, NASA Resident Office-JPL, [see page A5]. Refer to NPO-14803.

Antenna Feed for Linear and Circular Polarization

Hybrid elements transmit linear polarization and receive circular polarization without switching losses.

NASA's Jet Propulsion Laboratory, Pasadena, California

An S-band bidirectional communications network transmits a linearly-polarized radio wave and receives a circularly polarized wave. No waveguide switches are required in the proposed network, which uses only hybrid junctions, a diplexer, and a four-probe antenna. The linearly polarized downlink would be used on a NASA spacecraft for studies of the Earth ionosphere and for investigation of the solar corona.

A circularly-polarized radio wave consists of two orthogonal linearly polarized waves that are 90° out of phase. The NASA deep-space telecommunication links normally transmit and receive in circular polarization to avoid orientation problems. To meet the requirement for a linearly polarized downlink, the spacecraft antenna feed is modified to put all of the transmitted power into linear polarization only. The ground receiving antenna is also modified to automatically track and record the incoming plane of the linear polarization.

The figure shows an antenna feed with orthogonal coupling probes P_1, P_2, P_3, and P_4. In the transmit mode (color arrows), the diplexer connects the transmitter to 180° hybrid A, which excites probes P_1 and P_2 out of phase, producing a linearly polarized wave.

In the receive mode (black arrows), probes P_1 and P_2 are connected to 180° hybrid A; probes P_3 and P_4, 90° out of phase with P_1 and P_2, are connected to 180° hybrid B. The diplexer connects hybrid A to the 90° hybrid, and hybrid B delivers an orthogonal signal to the 90° hybrid; these two inputs are delivered in phase to the receiver.

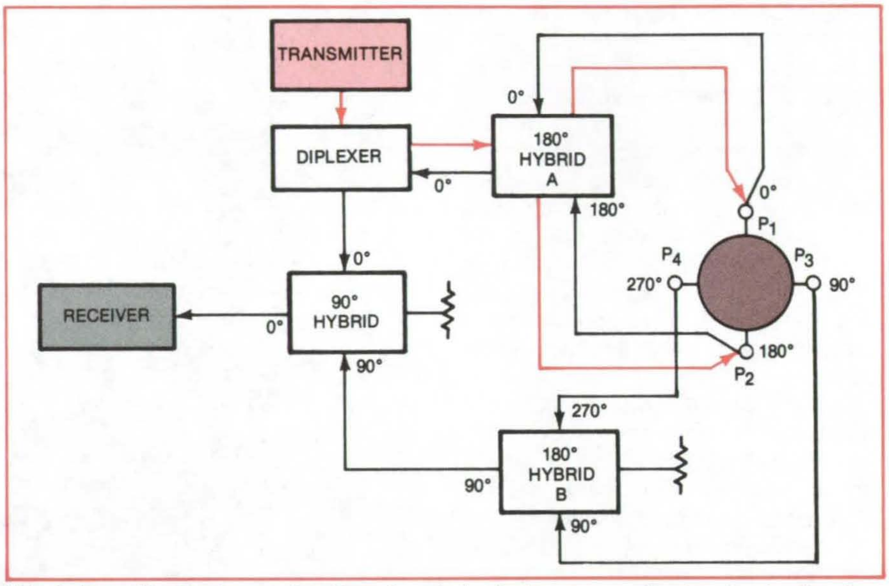

This Antenna System transmits a linearly-polarized microwave radio signal, yet a circularly-polarized incoming signal is received without polarization-mismatch losses. Other circuit arrangements are possible, using additional transmitters and receivers.

The hybrids can be implemented as waveguide, strip-line, or coaxial components. Possible configurations are the 3-dB coupler, the "rat-race," and the "magic-tee."

This work was done by Dan A. Bathker and Boris L. Seidel of Caltech for **NASA's Jet Propulsion Laboratory.** *For further information, Circle 4 on the TSP Request Card.*

This invention is owned by NASA, and a patent application has been filed. Inquiries concerning nonexclusive or exclusive license for its commercial development should be addressed to the Patent Counsel, NASA Resident Legal Office-JPL [see page A5]. Refer to NPO-14810.

Signal Conditioner for Nickel Temperature Sensors

Simple circuit conditions sensor signal for readout on a strain-gage recorder.

Lyndon B. Johnson Space Center, Houston, Texas

A strain-gage monitor can be used to read the output of a 50-ohm nickel temperature sensor if the sensor output is first conditioned through a simple circuit. Shown in the figure, the signal conditioner saves time and reduces instrumentation costs when both strain and temperature are being measured in the same setup.

In the standard application of a strain-gage monitor, the gage is inserted in one arm of a Wheatstone bridge, and the monitor measures strain by recording the departures from bridge balance. With the new circuit, a 50-Ω nickel temperature sensor replaces the strain gage, and the readings of the monitor are related to the temperature of the sensor.

The circuit consists of a few resistors, a switch, and a "matching" network available commercially (Vishay Intertechnology, Inc., Micro-Measurements Division, Part # LST-10F-350B, or equivalent). The 50-Ω nickel temperature sensor is attached to two input terminals on the module, and the

strain-gage recorder is attached to the output bulkhead connector. The bridge excitation voltage is applied through pins A and D (or A and F), and the bridge output is read between pins C and B (or C and E).

The matching network makes the 50-Ω temperature sensor look like one-half of a 350-Ω Wheatstone bridge at 70° F (21.1° C). It also linearizes the sensor output. With resistors R_1 and R_2 installed, the bridge is complete when the switch is in the "operate" mode. Resistors R_3 and R_4 are connected to the output when the switch is set to "zero" so that the bridge can be zeroed.

This work was done by Robert R. Walker of Rockwell International Corp. for **Johnson Space Center**. *No further documentation is available.*
MSC-18367

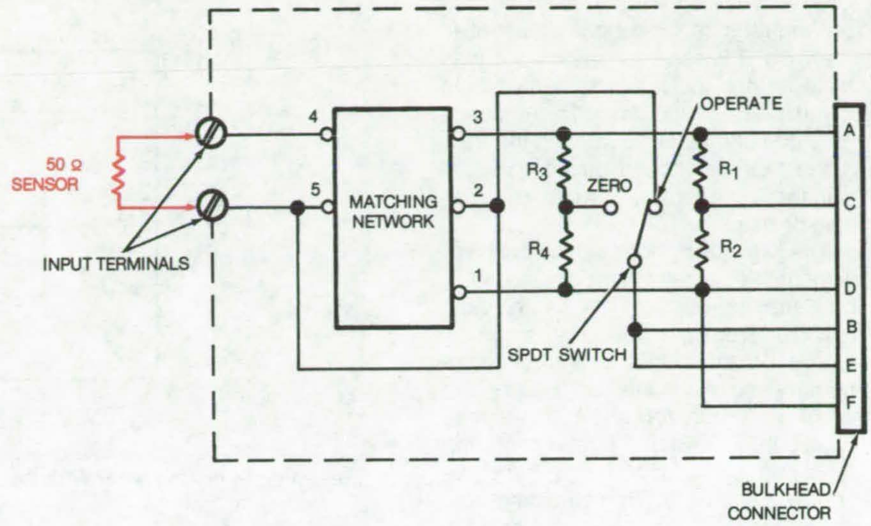

The **Resistance of a Nickel Temperature Sensor**, at the circuit input terminals, is converted to a strain reading on the recording equipment at the output. Resistors R_1 through R_4 are 350-Ω, ± 0.1 percent, wire-wound.

Efficient, Lightweight dc/dc Switching Converter

Efficient converters have the desirable input properties of a boost power stage and output properties of a buck power stage.

Lewis Research Center, Cleveland, Ohio

A dc-to-dc converter offers higher efficiency (95 as compared to 65 percent), lower output-voltage ripple, reduced EMI, and smaller size. As a general converter, the circuit output voltage is less than or larger than the input voltage, depending on the duty ratio of the transistor switch. New circuit arrangements allow both input and output currents to be nonpulsating, and capacitive energy transfer is used rather than the usual inductive energy transfer.

Variations of the fundamental circuit allow some important extensions not achievable with conventional switching converters.

In the basic circuit (Figure 1), a dc input voltage source (V_g) is connected to an input inductor L_1 that is connected to capacitor C_1. A switch S_1 alternately connects either the junction between L_1 and C_1 or the junction between C_1 and inductor L_2 to a common point between the source and the load. Inductor L_2 is connected in series with the load R. A filter capacitor C_2 is connected across the load.

Switch S_1 can be implemented with a transistor and a diode (Q_1 and D_1 in Figure 2). The transistor is initally in its nonconductive state, and C_1 charges from the voltage source V_g through the inductance since diode D_1 is forward-biased. At that time the collector of the transistor is positive with respect to its emitter. When a switching pulse turns the transistor on, it becomes conductive. This grounds the side of the capacitor connected to the transistor. The diode is thus back-biased, and the capacitance discharges through the inductance L_2 into the load. When the switching pulse drops, the transistor is cut off, storage

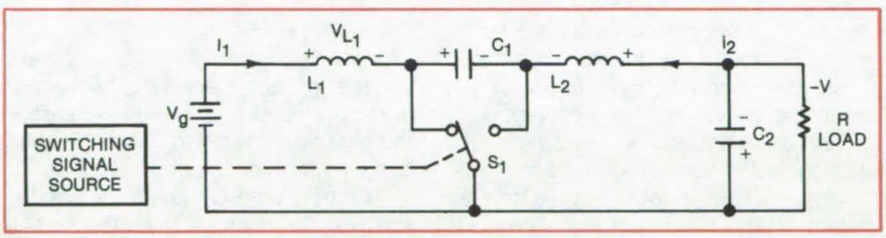

Figure 1. **A dc-to-dc Converter With Capacitive Energy Transfer**

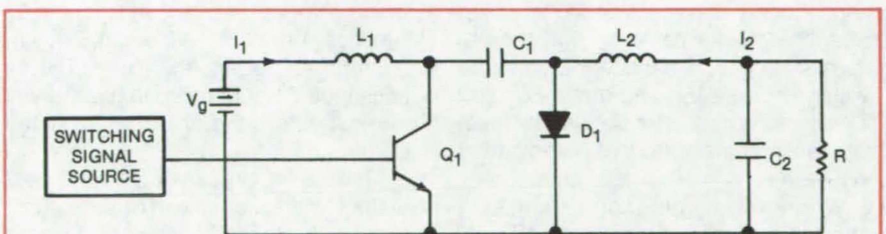

Figure 2. **A dc-to-dc Converter Using Bipolar Transistor and Diode To Replace Switch**

(continued on next page)

capacitor C_1 again charges, and output inductance L_2 supplies current to the load. Thus the transistor is driven by a train of pulses from a switching signal source, and diode D_1 responds as a complementary switch to the transistor being switched off and on. Capacitor C_1 is thus an energy-transferring device.

The two inductances can be coupled, without affecting the basic dc coversion, by a transformer with a 1:1 turns ratio and the direction of coupling shown in Figure 3. In that circuit, L_1 and L_2 are the primary and secondary windings T_1 and T_2 of a 1:1 transformer. A single-pole, double-throw switch S_1 represents the functions of the diode and transistor shown in Figure 2. This switching converter (Figure 3) is the only one (besides the straightforward cascade-connected boost and buck converters) in which transformer coupling of the input and output inductances is possible. The input or the output current ripple can be reduced by an order of magnitude or more compared with the noncoupled counterparts. In fact, either input or output current ripple can be made zero. Also, instead of two cores for two noncoupled inductors, a single transformer core may be used. The switching converter in Figure 3 has the simplest possible structure (single 1:1 transformer, commutation capacitor C_1, and switch S_1); yet efficiency and performance are high (both input and output currents are nonpulsating), and size and weight are minimized.

In many applications of dc-to-dc switching converters, the input and output circuits must be dc isolated. A circuit with such isolation and with the capability for multiple outputs with different polarities and magnitudes is shown in Figure 4. The modification requires two capacitors C_3 and C_4 in place of the capacitor C_1 and requires the insertion of a 1:1 transformer such that the primary T_3 connects capacitor C_3 and the voltage source V_g, and the secondary T_4 connects capacitor C_4 and the load. Operation is similar to that of the circuit in Figure 1.

When Q_1 is not conducting, C_3 charges through primary winding T_3, inducing a voltage in secondary winding T_4, which charges up C_4. Diode D_1 is conductive at this time. When the transistor Q_1 becomes conductive, C_3 discharges through primary T_3, inducing a voltage in secondary T_4. The voltage acress C_4 and the voltage induced in the secondary winding add and supply current through L_2 to the load.

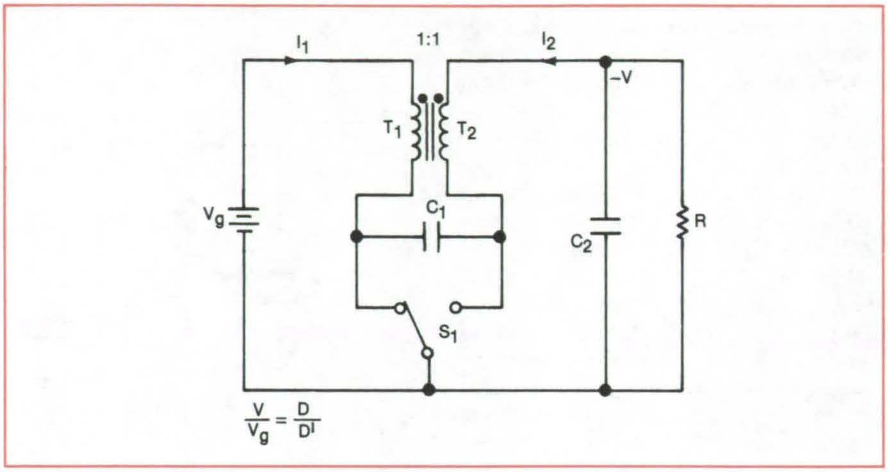

Figure 3. **A dc-to-dc Converter With Coupled Inductors**

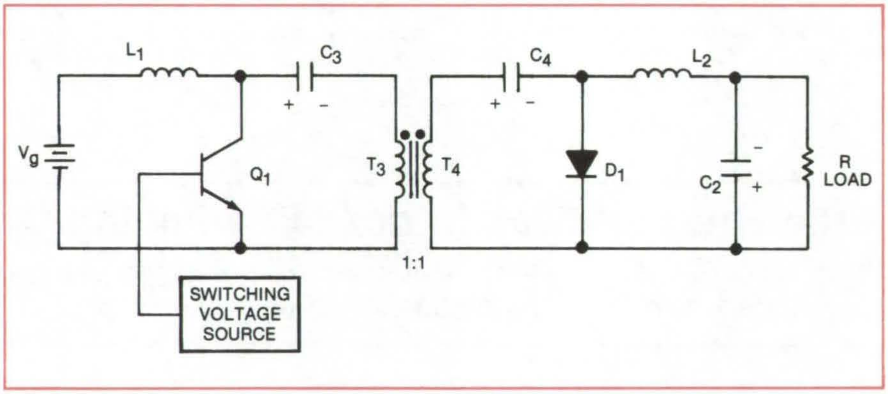

Figure 4. **Isolated dc-to-dc Converter**

The next time Q_1 becomes nonconductive, C_3 charges from the voltage source V_g, causing current flow through T_3 and inducing a voltage across T_4, which charges C_4 again. At that time, L_2 supplies current to the load, maintaining a nonpulsating output current. The capacitance C_2 connected in parallel with the load filters the ripple in the output current.

These new circuits outperform each of the three so-far-known basic converter power stages (buck, boost, buck/boost) since they have the desirable input properties of the boost power stage and the desirable output properties of the buck power stage; yet they perform the general conversion function (increase or decrease of input voltage) of a conventional buck/boost power stage with considerably higher efficiency.

This work was done by S. Cuk and R. D. Middlebrook of the California Institute of Technology for **Lewis Research Center**. *Further information may be found in NASA CR-135174 (N78-29351/NSP), "Modeling, Analysis, and Design of Switching Converters" ($17). A copy may be purchased (prepayment required) from the National Technical Information Service, Springfield, Virginia 22161.*

Title to this invention has been waived under the provisions of the National Aeronautics and Space Act [42 U.S.C. 2457(f)] to the California Institute of Technology, Pasadena, California 91125.
LEW-12809

28-Channel Rotary Transformer

Each channel handles digital data at 1 megabaud.

NASA's Jet Propulsion Laboratory, Pasadena, California

A 28-channel transformer for a 6-year Jupiter mission has been proposed to transmit power and digital data across a rotating interface. Tests on transformer components for two channels showed clean transmission of a 1-MHz square wave.

Each channel uses a separate ferrite-core rotary transformer capable of a 1-megabaud (1-megabit-per-second) data rate. The torus-shaped transformers are spaced along the rotor like beads on a string (see figure); there is no inherent limit to the number of channels.

The rather large airgap in the transformer magnetic circuit, required for rotary motion, is contrary to conventional transformer design since it increases leakage inductance and magnetizing current. Fortuitously, the large gap also permits a simpler, single-ended data drive circuit. In a core with no airgap, the dc bias imposed by such a circuit could drive the core into saturation.

Special ferrite cores offering good high-frequency response are manufactured to tolerances of 1 mil (25 μm). In a prototype, the rotor and stator each had two 5-turn windings, allowing experiments with either 5 or 10 turns.

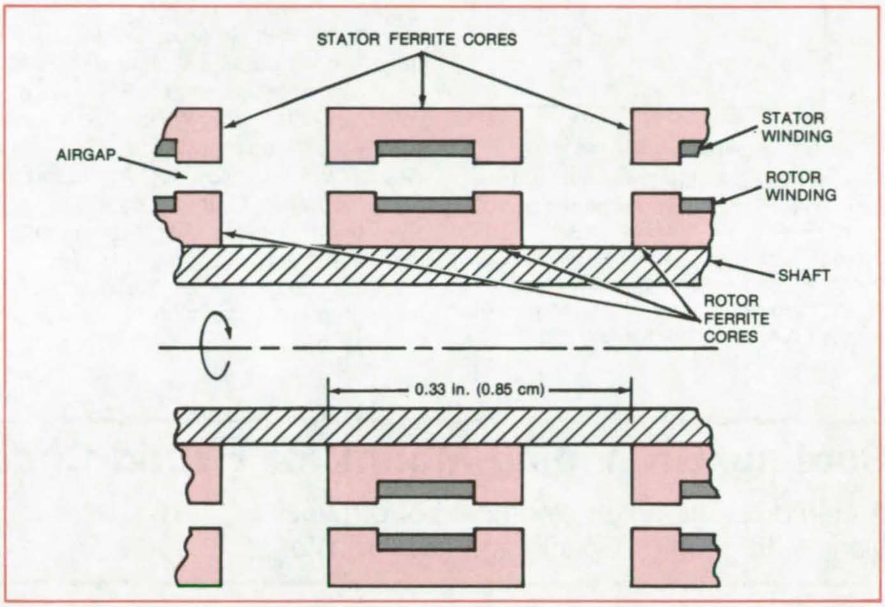

The **Rotary Transformer Array** has many parallel data channels, each with up to 1-megabaud data rate. The ferrite-cored transformers are spaced at 0.33-in. (0.85-cm) intervals along the rotor. The space between the transformers reduces crosstalk.

Previous rotary transformers have generally been single-channel units limited to end-of-shaft use at data rates of 15 kilobaud or less. Mechanical sliprings can also be used, but they require driving power to overcome contact friction, and they suffer gradual contact wear, noise, and bounce.

This work was done by Colonel W. T. McLyman of Caltech for **NASA's Jet Propulsion Laboratory.** *For further information, Circle 5 on the TSP Request Card.*
NPO-14861

Improving MOS Minority-Carrier Lifetime

Fluorine implantation can increase minority-carrier lifetime in silicon by a factor of 100.

NASA's Jet Propulsion Laboratory, Pasadena, California

Fluorine ion implantation can increase minority-carrier generation lifetime in silicon by a factor of up to 100 or so. In MOS (metal-oxide semiconductor) applications this can increase power efficiency by improving conduction when a voltage is applied across a pn junction.

Other findings of a study of the effects of fluorine as an impurity in silicon are as follows: Fluorine implantation does not increase microdefects at the silicon surface when thin oxide layers are grown; and fluorine appears to "getter" impurities at or near the silicon surface without adversely affecting MOS electrical parameters. Thus, there is no apparent need to remove fluorine often left on wafer surfaces after processing.

The effects of fluorine ion implantation were studied with a series of wafers from a ⟨100⟩ n-type, 1- to 3-Ω-cm Czochralski ingot. These were

(continued on next page)

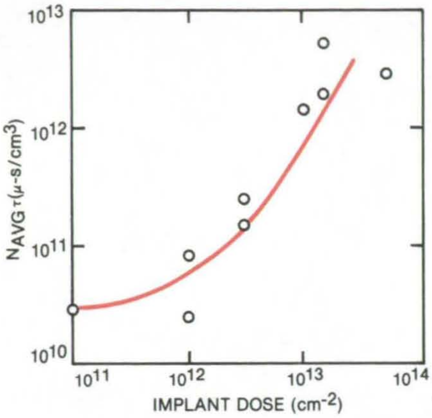

Minority-Carrier Lifetime in Silicon increases by more than a factor of 100 at high fluorine implant doses. The ordinate actually shows the product of lifetime and doping concentration N_{AVG}; however, the dependence of N_{AVG} on dose is relatively weak.

implanted at doses from 10^{11} to 5×10^{13} atoms per square centimeter. At the 150-keV ion kinetic energy used for implantation, the ions penetrate about 0.32 μm into the silicon.

Capacitor contact areas of 2×10^{-3} cm^2 were prepared on the wafers to permit measurements of capacitance versus voltage and versus time. (The capacitor dielectric was a 0.07-μm thermally-grown gate oxide layer.) A calculator-controlled system was used for these measurements. [See "Automated Tester for MOS Devices" (NPO-14088) on page 3 of *NASA Tech Briefs*, Vol. 3, No. 1.] A modified Zerbst analysis of these data yielded the minority-carrier-lifetime results shown in the figure.

Upon completion of the electrical measurements, the wafers were examined for microdefects. This required stripping off the capacitors to expose the base silicon surface. Etching showed no difference in the density of stacking faults and dislocation loops between implanted wafers and unimplanted controls; but such defects were formed below the surface at the depth of the fluorine ions. These deeper defects were detected by etching after growing (and then removing) an additional 1.1-μm oxide layer to expand the microdefects enough to reach the surface.

This work was done by Richard H. Cockrum, Seung P. Li, and Simon Prussin of Caltech for **NASA's Jet Propulsion Laboratory.** *For further information, Circle 6 on the TSP Request Card.*
NPO-14738

Cooling/Grounding Mount for Hybrid Circuits

A clamp ensures high electrical performance along with good grounding and heat transfer.

Lyndon B. Johnson Space Center, Houston, Texas

A new mounting for hybrid integrated-circuit modules allows extremely-short input and output connections so that the voltage standing-wave ratio (VSWR) is kept low. At the same time, the mounting ensures adequate grounding and efficient heat removal from the module.

The module is inserted in a rectangular clamp. The lead pins on the base of the module are inserted in a circuit board in the conventional way, and the circuit board is placed on a ground plane. Bosses on the ground plane pass through cutouts in the circuit board, and the clamp is attached to the ground plane by bolts (see figure).

Because the module leads are directly connected to the circuit board, VSWR is low and the circuit introduces no undue delay in processing a signal. Also, because the clamp is in close contact with the module and the ground plane, heat flows readily from the module to the metal plane, which serves as a sink for both heat and current.

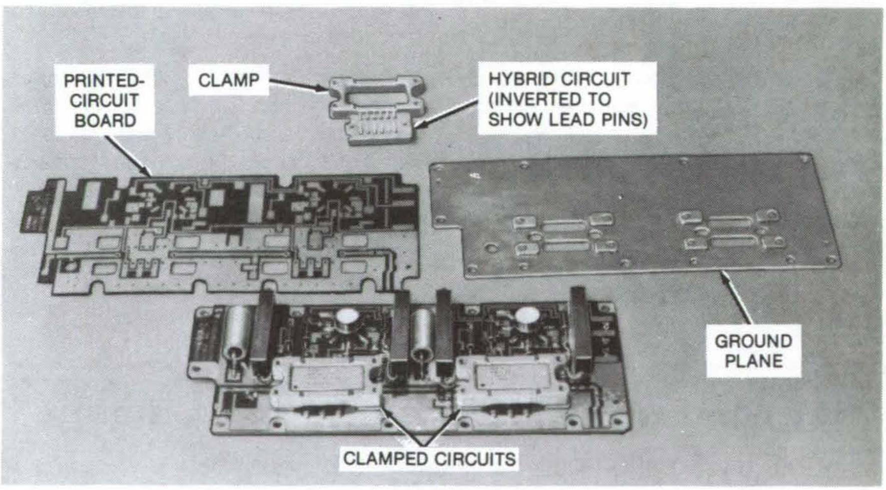

Rectangular Clamps Hold Hybrid Circuits on a printed-circuit board, in contact with a heat-conductive grounding plane. The assembled hybrid circuit, with clamps and ground plane in place, is an automatic-gain-control network for a first-stage intermediate-frequency amplifier.

The clamp mounting is superior to attaching ground straps to the module or connecting the module leads to the circuit board through jumpers.

This work was done by Bruce Bagstad, Robert Estrada, and Harold Mandel of TRW, Inc., for **Johnson Space Center.** *For further information, Circle 7 on the TSP Request Card.*
MSC-18728

Electronic Systems

Hardware, Techniques, and Processes

Common Data Buffer

Time-shared interface speeds data processing in a distributed computer network.

John F. Kennedy Space Center, Florida

The processing of information by a distributed network of computers proceeds much more efficiently if the network is linked by a time-shared data buffer (memory), access to which is sequenced such that each of the computers in the network appears to be the only computer using the buffer. Although originally developed as part of a 64-processor checkout, command, and control system for space vehicles and their ground facilities (see figure), the common data buffer can also serve as the interface and communications medium in a nonaerospace distributed computer complex. Its architecture is flexible, and it can be used with any computer and/or processing language, as long as the information interchange protocol is agreed upon by the users.

In operation, the buffer temporarily stores data, messages, and commands along with error-correcting information that assures proper retrieval of this information even when a certain portion of the buffer is inoperative as a result of failed hardware. A two-level high-speed scanning approach, with "look ahead" at the lowest level, is responsible for routing information to and from the computers in the network to the buffer. The buffer can be partitioned to protect certain reserved areas of memories from being overwritten by unauthorized computers in the network. Each of the connected central-processing units (CPU's) may have such an area, which is protected by address-validity logic to prevent accidental alteration of that memory.

A portion of the buffer is reserved for a series of "first-in, first-out" memory stacks supported by auxiliary hardware. These stacks allow any CPU to interrupt any other CPU in the network. Up to 64 interrupt vectors may be written to each stack, such that each CPU services, on a "first-come" basis, interrupts from each of the other CPU's connected to the buffer. A "stack-not-empty" condition is processed by the auxiliary hardware as an interrupt to the CPU belonging to the stack.

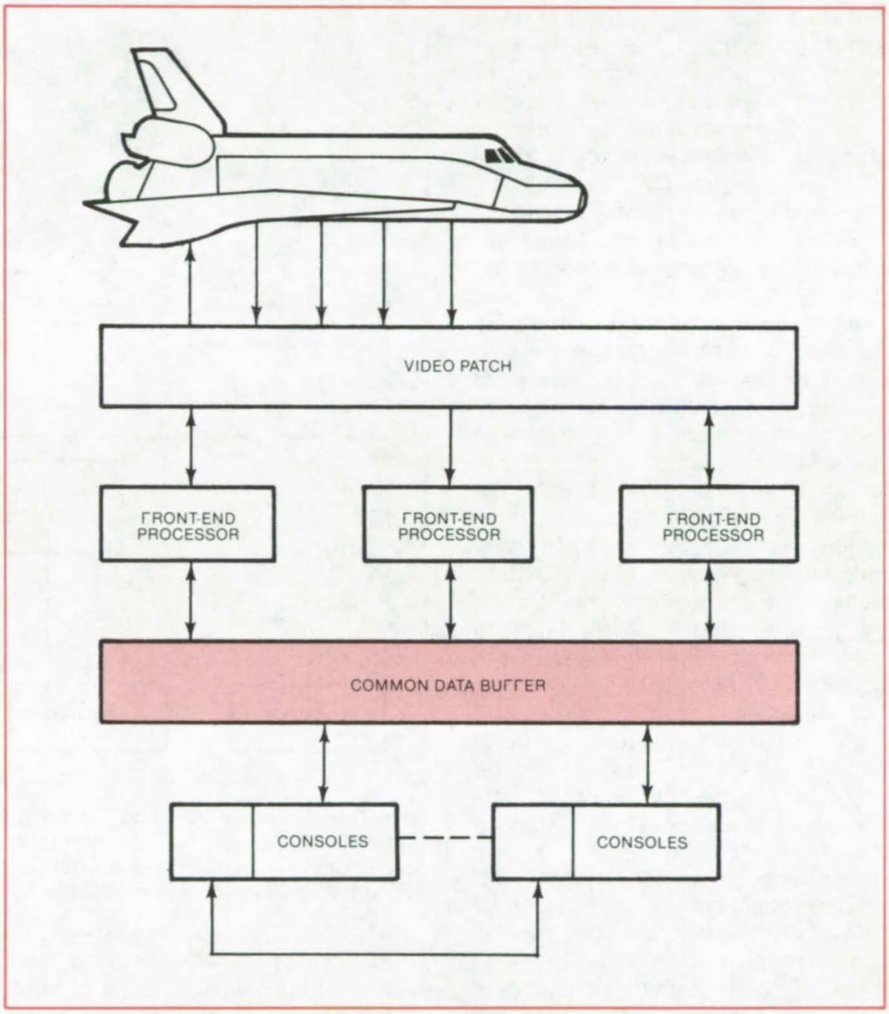

The **Common Data Buffer** is the primary interface between all the minicomputers participating in the Space Shuttle prelaunch checkout.

The buffer address structure and the memory are protected by an error-correcting code to protect and correct transactions to and from the buffer from noise or failed components. Bit-planar memory organization supports this feature. Redundant power is supplied to all components of the buffer, and certain critical timing and clock circuits have spare logic functions installed and may be selected by the flip of a switch.

This work was done by Frank Byrne of **Kennedy Space Center**. *For further information, including block diagrams and circuit descriptions that detail the operation of the system, Circle 8 on the TSP Request Card.*

This invention is owned by NASA, and a patent application has been filed. Inquiries concerning nonexclusive or exclusive license for its commercial development should be addressed to the Patent Counsel, Kennedy Space Center [see page A5]. Refer to KSC-11048.

Simultaneous Disk Storage and Retrieval

An efficient format handles simultaneous disk reads and writes.

John F. Kennedy Space Center, Florida

Data at rates of up to 150,000 16-bit words per second are concurrently recorded on disk by one minicomputer and accessed by another, using a format of memory blocks, buffering algorithm, and time-sequence addressing. Developed for the Space Shuttle prelaunch checkout, control, and monitoring system, the format allows near-real-time recording and access to the data.

As indicated in the block diagram, all Shuttle prelaunch operations are governed by 64 nominally independent minicomputers linked by an interface called a common data buffer (see preceding article). A minicomputer known as the Processed-Data Recorder (PDR) records the prelaunch transactions through the common data buffer for storage on tape and disk. Concurrently, another minicomputer, the Shared Peripheral Area (SPA) System, retrieves the disk-recorded data for further processing.

Transactions between the minicomputers occur at a rate such that up to 54,272 16-bit words may have to be recorded by the PDR each second. SPA requests for access to the data on disk may occur once every 77.222 milliseconds.

These rapid and concurrent storage and access requests are handled without losing data by selecting the data-block size and a buffering algorithm to hold incoming data temporarily while the SPA is reading from the disk. In addition, each of the addresses of the data on disk is quickly identified by a directory format that uses the times of start and end of each data request by the PDR as an index. Data are written sequentially, so all times of start and end for a data request are unique.

The PDR reads data in block sizes of 118 words and attaches a 10-word header, which describes and identifies the start and end times of all the data within a block. The data plus the header constitute a logical record of 128 words, which is the exact size of a sector on disk.

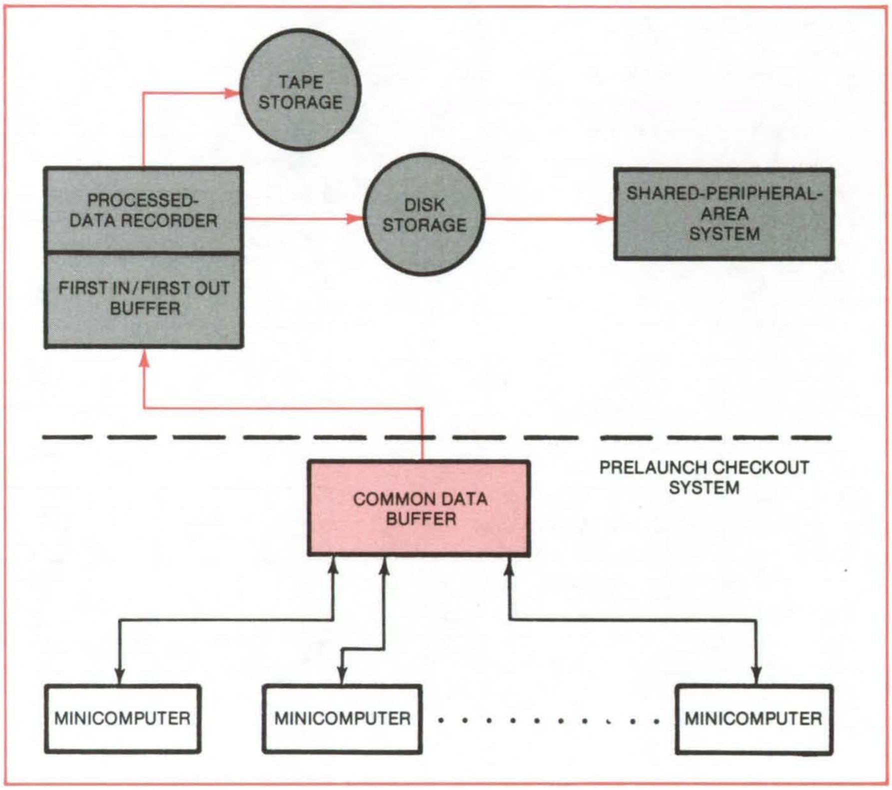

Data Transferred to Disk and Tape are a record of the minicomputer/minicomputer transactions through the common data buffer. In this simplified schematic of the Space Shuttle prelaunch checkout and control system, data at high rates are concurrently stored on and read from disk.

To prevent excessive "seeking" and loss of recorded data, the PDR issues a priority select, which lets the in-process SPA request complete and which allows subsequent requests come only from the PDR, until the PDR has finished writing all its backed-up data to disk. The PDR then lets the SPA begin a new request.

To allow the SPA to have access to the disk, the PDR has sufficient buffering area to hold all incoming data while the SPA request is being exercised. Also the algorithm for updating the directories minimizes "seeking" and does not interfere with the normal recording algorithm.

Although it was developed to handle a data rate of 54,000 words per second, the buffering algorithm has been tested successfully at data rates up to 68,000 words per second. A modified buffering algorithm to allow transfer of varying block sizes to disk has been tested at better than 150,000 words/second, and proposed modifications of the way the directory is recorded on disk should up the rate to 160,000 words/second.

This work was done by F. E. Levine of IBM Corp. for **Kennedy Space Center**. *For further information, Circle 9 on the TSP Request Card.*

Inquiries concerning rights for the commercial use of this invention should be addressed to the Patent Counsel, Kennedy Space Center [see page A5]. Refer to KSC-11167.

Four-Quadrant CCD Analog Multiplier

Sequential processing technique improves accuracy when multiplying CCD-array signals by a weighting function.

Langley Research Center, Hampton, Virginia

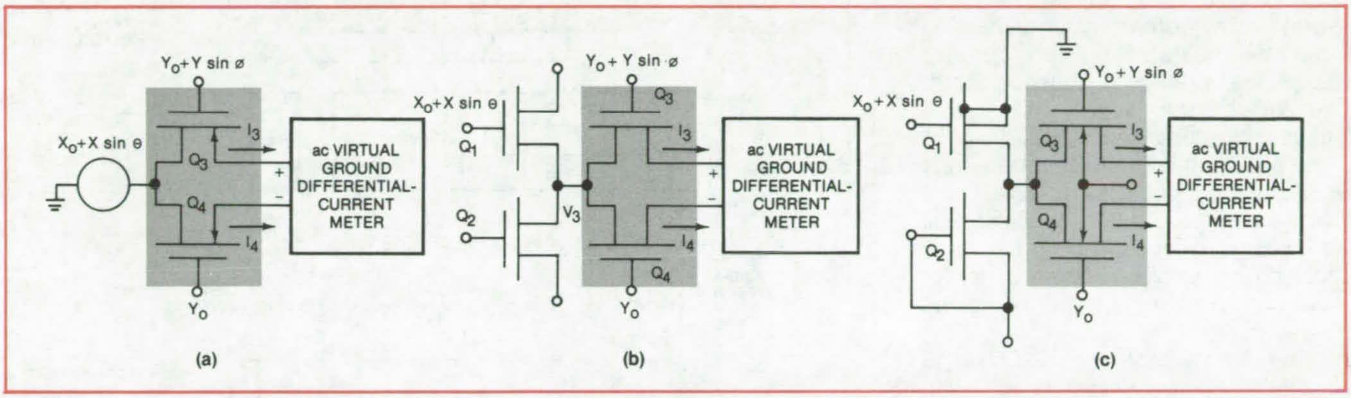

Figure 1. **One Cell of an MOS Multiplier Array** is shown in its simplest form in (a); in (b) the signal applied to the drain node is buffered; a CMOS implementation is illustrated in (c).

The multiplication of each element of a charge-coupled-device (CCD) array by a weighting function is usually necessary to remove offsets brought about by the applied bias voltages. However, a constant weighting function is not always sufficiently general for applications such as vector/matrix products or sums of products for analog correlators. Often with such vector or matrix products, ac coupling is not convenient for removing constant or slowly varying offsets, since a single true four-quadrant sum of products is needed after the analog data have been distributed into the vector/matrix component locations.

Analog correlator multipliers use two schemes to cancel the undesired output contributions arising from the prerequisite biases. The first is spontaneous cancellation by multiple "nominally identical" devices; and the second is sequential cancellation, where the same devices are used repeatedly to form the multiple products. A single device then successively subtracts the products, eliminating the effects of MOS-array threshold nonuniformities.

The multiplication function can be performed with MOS transistors operating in the "triode" region. A diagram of a balanced multiplier is shown in Figure 1a. When the signals are derived from the floating gate of a

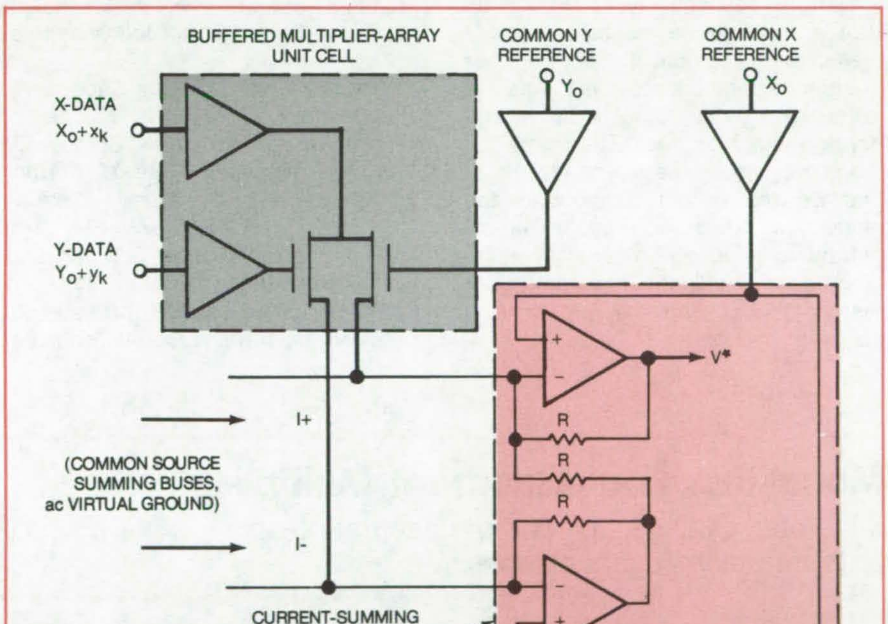

Figure 2. **Current-Summing Amplifiers and a Differential Current-to-Voltage Converter** are connected to the CCD-array output. The output voltage is processed in a four-step sequence by the circuit of Figure 3.

CCD, the signal should be applied to the gate of the minimum-geometry MOS transistor to reduce parasitic signal loading. Furthermore, to avoid unwanted interaction, the signal from a floating gate should not be connected directly to the drains of Q_3 and Q_4.

One solution is to use a buffer with voltage gain, which can be either a source follower or an inverter. Figure 1b shows a balanced multiplier using a buffer to drive the drain node of the multiplier. For inverting buffers the unequal dc voltage levels of the two

(continued on next page)

signals may be inconvenient. For instance, if both signals are derived from CCD's on the same structure, it is desirable to have the two signals at the same dc level. This difficulty can be circumvented by using complementary MOS circuits as shown in Figure 1c.

A CMOS/CCD analog multiplier array (or any other analog multiplier) can be operated in a four-step sequence to remove erroneous contributions to the output from array threshold nonuniformities. In this sequential multiplying scheme, all the undesired product terms associated with the threshold voltage deviations are canceled sequentially in the same multiplying transistor. The circuitry for accomplishing this is shown in Figures 2 and 3.

The performance of the CCD/MOS multiplier was investigated with Fourier analysis. Two signals of different frequencies were applied to the drain (X-channel) and gate (Y-channel), respectively. The desired sum and difference frequency components were compared to the other frequency components to measure the distortion of the output from a true four-quadrant product. Distortion can be expressed as the rejection ratio of the desired output voltage to the undesired output voltage. A 40-dB harmonic rejection value was equivalent to a multiplier accuracy of 1 percent. (Also see the two articles following this one.)

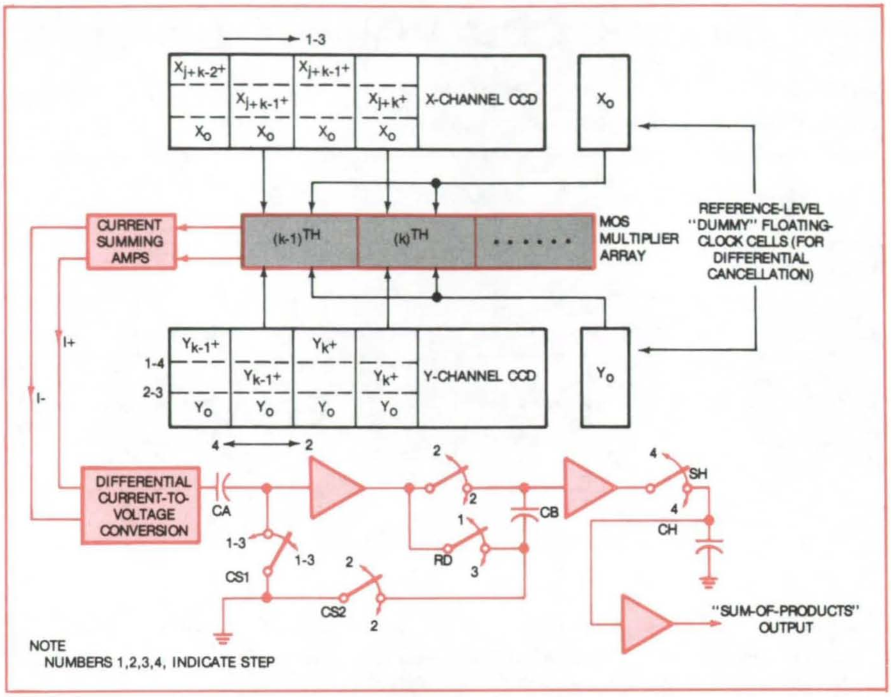

Figure 3. The **Four-Quadrant MOS Analog Multiplier Array** generates a "sum-of-products" output, in which threshold nonuniformity among the array elements is canceled. (See the article following this one for a summary of the circuit equations.)

This work was done by Charles W. Brooks and Donald R. Lampe of Westinghouse Electric Corp. for **Langley Research Center.** *Further information may be found in NASA CR-145334 [N79-14796/NSP], "The Investigation of Charge Coupled Device Correlation Techniques"* [**$11**]. *A copy may be purchased [prepayment required] from the National Technical Information Service, Springfield, Virginia 22161.*

Title to this invention has been waived under the provisions of the National Aeronautics and Space Act [42 U.S.C. 2457(f)] to the Westinghouse Electric Corp., 1310 Beulah Road, Pittsburgh, PA 15235.
LAR-12332

Monolithic Four-Quadrant Multiplier

Integrated CCD version is more accurate than a discrete component processor.

Langley Research Center, Hampton, Virginia

If the four-quadrant sequential processor shown in Figure 3 of the preceding article is implemented with discrete capacitors, resistors, switches, and operational amplifiers, its accuracy is limited by such factors as sample-and-hold (S/H) acquisition speed, S/H droop rate, and possible stray pickup by the card-mounted discrete components. Such problems would be eliminated, however, in a monolithic or integrated version incorporated on the same chips as the multiplier array.

For the discrete-element processor, four distinct products are generated sequentially in a perfectly uniform array of multiplying devices:

$$A = \sum_k (X_o + x_k) \cdot (Y_o),$$

$$B = \sum_k (X_o + x_k) \cdot (Y_o + y_k),$$

$$C = \sum_k (X_o) \cdot (Y_o + y_k),$$

$$D = \sum_k (X_o) \cdot (Y_o)$$

The ideal result then becomes:

$$Z = (B - A) + (D - C)$$
$$= \sum_k (x_k) \cdot (y_k)$$

A monolithic implementation of the part of the processor that is downstream of the current-to-voltage converter is shown in Figure 1. This version is for differential current summing; an analogous circuit has been designed for single-sided current summing. Both devices use the

stabilized charge injection or filled/spill scheme.

The charge metered and read while switch $\emptyset_0$ is activated is given by $Q^* = (C_{IN})$. With the "differential" processor, if the current-summing-to-voltage converters have an effective offset or threshold difference of Δ, while the resultant output voltages are $K\pm$, the sequence of charge packets metered on C_{IN} and collected on C_{OUT} becomes:

$$Q_1 = Q^* + C_{IN}\left| \Delta + (A+) - (A-)\right|$$

$$Q_2 = Q^* + C_{IN}\left|(B-) - \Delta - (B+)\right|$$

$$Q_3 = Q^* + C_{IN}\left| \Delta + (C+) - (C-)\right|$$

$$Q_4 = Q^* + C_{IN}\left|(D-) - \Delta - (D+)\right|$$

With all four charge packets added algebraically on the output capacitor:

$$Q = \sum_{1}^{4} Q_K$$
$$= 4Q^* + C_{IN}\,(\delta A - \delta B + \delta C - \delta D)$$

With the "single-sided" processor, the total charge added to C_{OUT} becomes:

$$Q = Q_1 + Q_2$$
$$= 2Q^* + C_{IN}\,(A - B + C - C)$$

Most multipliers generate product currents that are then combined in a way that eliminates the effects of array nonuniformities. Furthermore, the node into which the product currents flow often should be a virtual ground. Figure 2a shows this concept schematically, with the product current converted directly into a voltage by the operational amplifier and resistor R.

Simple monolithic approximations compatible with CCD fabrication are also illustrated in Figure 2, but they require appreciable bias currents from the current source Q_2 to increase the transconductance of the "grounded base" transistor Q_1 and thus better approximate a virtual ground. The techniques shown in Figures 2b and 2c convert the currents into voltages with a suitable bias for direct application to the input gates of the sequential processor. With transistor Q_1 operating in the saturation or "pentode" region, the actual current-to-voltage conversion is performed by resistor R, which must accurately be established and matched in duplicate at every location where differential current-to-voltage conversion occurs.

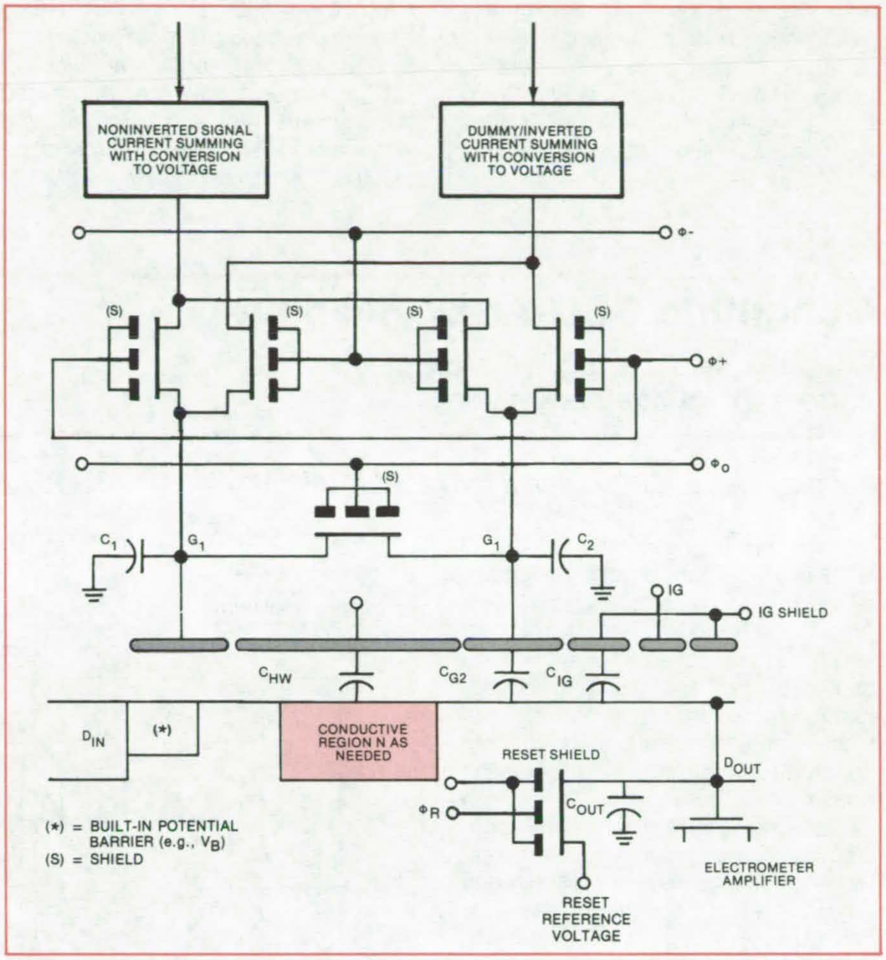

Figure 1. **Monolithic Configuration** for a "differential" sequential processor is less susceptible to noise than one that uses discrete components. A monolithic "single-sided" processor has also been designed.

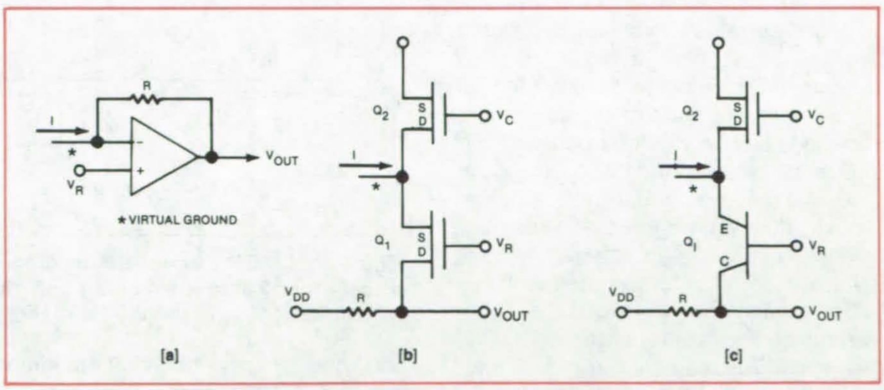

Figure 2. **Three Single-Sided Current-to-Voltage Converters** are compatible with CCD-array fabrication: (a) shows the circuit concept; (b) and (c) show MOS and MOS/bipolar implementations, respectively.

For this reason it is preferable to have only one such pair of resistors per "sum-of-products" device, rather than one pair for each multiplier in the array.

The schemes of Figures 2b and 2c have been computer-modeled. The results predict that the distortion added by the circuits, beyond that of the basic multiplier, is negligible. Since, typically, the distortion rejection performance of the CCD sequential processor well exceeds that of the multipliers, the complete monolithic

(continued on next page)

device should perform substantially better than previous devices.

This work was done by Donald R. Lampe of Westinghouse Electric Corp. for **Langley Research Center.** *Further information may be found in NASA CR-145334 [N79-14796/NSP], "The Investigation of Charge Coupled Device Correlation Techniques" [*$11*]. A copy may be purchased [prepayment required] from the National Technical Information Service, Springfield, Virginia 22161.*

Title to this invention has been waived under the provisions of the National Aeronautics and Space Act [42 U.S.C. 2457(f)] to the Westinghouse Electronic Corp., 1310 Beulah Road, Pittsburgh, PA 15235.
LAR-12330A

Monolithic CCD-Array Readout

Circuit is self-biasing, with differential current-to-voltage conversion.

Langley Research Center, Hampton, Virginia

The multiplying elements for a CCD MOS analog signal processor require a readout with dc-balanced virtual-ground input nodes, the dc bias of which is controlled by a voltage applied to another node. One conceptual and two simplistic forms of a single-sided or unbalanced readout are shown in Figure 2 of the preceding article.

Since most analog multipliers consist of counterbalancing elements, yielding currents that are subtracted to cancel threshold nonuniformities, it is desirable to obtain the differential current directly from noninteracting high-impedance current sources that are added in parallel. The high impedances can feed a high resistance, for converting small differential signal currents into large signal voltages.

The use of a large resistor in the single-sided circuits of the preceding article is severely limited because the full bias current needed to increase the G_M of the virtual-ground stage must flow through that resistor. Consequently, a pair of such circuits with smaller resistors, mated with the differential monolithic sequential processor, gives smaller differential signal voltages. The result is reduced signal-to-noise ratio or the need for a larger-area sequential processor to maintain the same ratio.

A possible CMOS circuit to subtract the two currents (canceling the dc bias components) and allow higher resistances to be used is illustrated in Figure 1. The circuit consists partly of a dc-balanced pair of virtual-ground stages. The remainder is the basic current-differencing part of the circuit

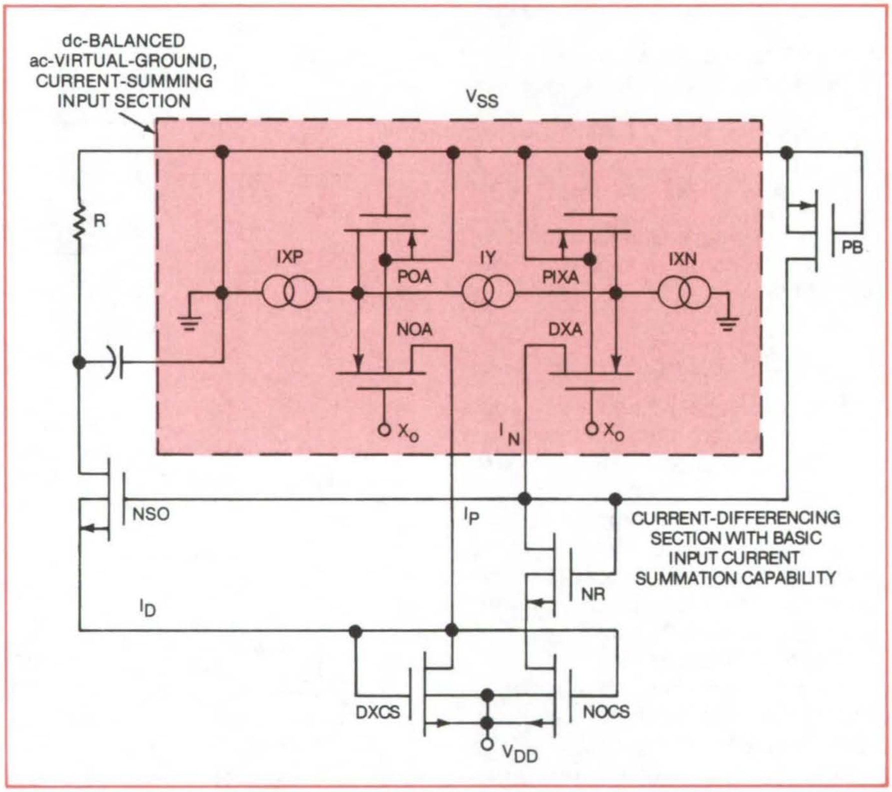

Figure 1. **CMOS Current-Dfferencing Readout** consists of a dc-balanced pair of virtual ground stages (in color) and current-differencing circuit that is similar to a current mirror. I_D is the differential readout current.

and closely resembles a modified current mirror; i.e., the currents through transistors DXCS and NOCS, which are nominally matched, try to establish themselves at very nearly equality:

$$I_D + I_P = I_N + \Delta I \qquad (1)$$

I_P and I_N are the signal (IXP, IXN, IY) plus bias currents for the two counterbalancing legs of the multiplier, as fed into their respective ac-virtual-ground nodes; ΔI is a fixed incremental offset current to enable readout of bipolar current differentials; and I_D is the differential readout current.

When a completely-quadruply-balanced triode multiplier cell replaces the test sources (IXP, IXN, IY), the circuit of Figure 2 results.

The transistors to the left of the dashed line are those belonging to the selected multiplier cell and need to be

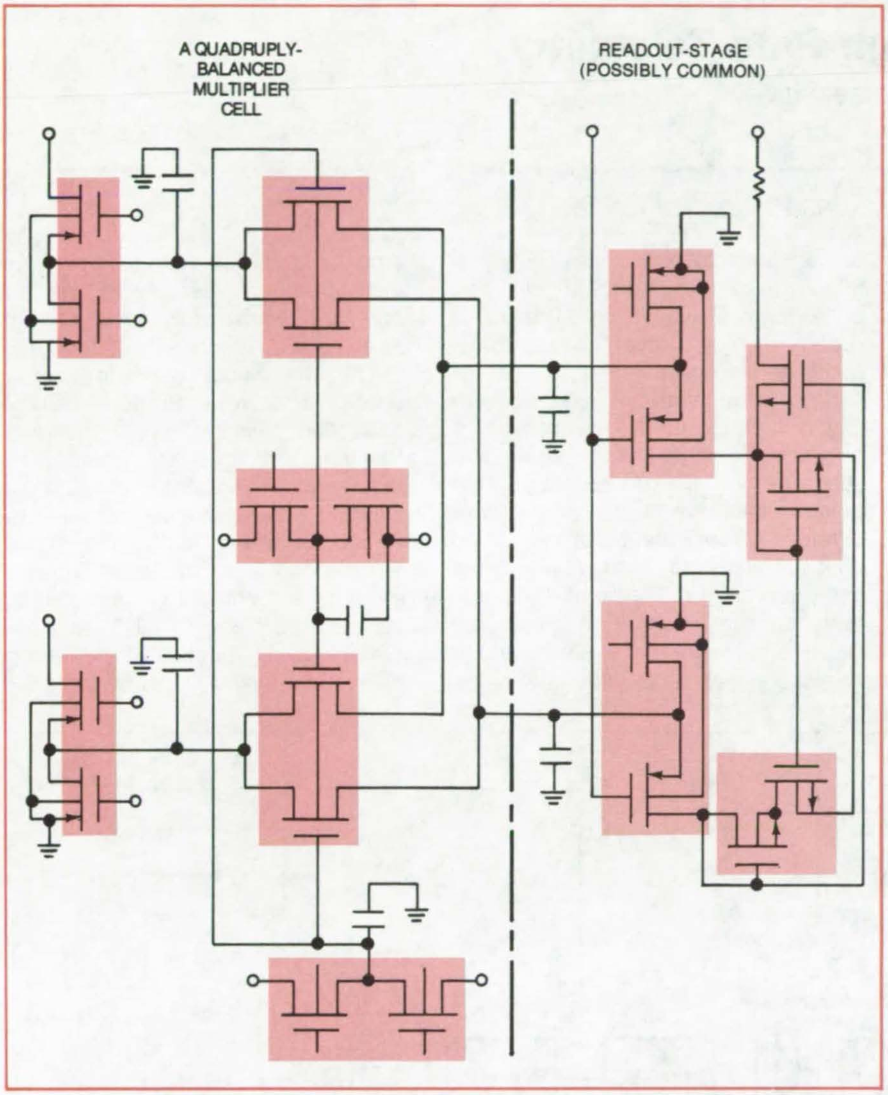

Figure 2. **CMOS Correlator Cell With Self-Bias and Differential Current-to-Voltage Readout** is shown in a form suitable for a monolithic implementation.

Feature	V_{DD}	CMRR (dB)	Differential Gain (dB)	V(48)	Equivalent Transconduction Sensitivity: Output Current Shift/Threshold Shift
Balanced, Higher Voltage	-15	72.9	-3.5	-2.116	N/A
Balanced	-12	49.6	-3.7	-1.762	N/A
0.2-V Increase in (NOA) Pinchoff	-12	46.1	-3.8	-1.593	8.45 μV
0.2-V Increase in (DXA) Pinchoff	-12	52.3	-3.5	-1.938	8.8 μV
0.2-V Increase in (DXCS) Threshold	-12	51.8	-5.7	-0.594	58.4 μV

CMOS Readout Circuit Sensitivity and Performance were calculated from a computer model.

duplicated for each such multiplier within the correlator chip. The remaining elements form part of the readout and may be scaled according to the number of multipliers involved as a single common readout stage.

Assuming the bias currents for the ac-virtual-ground stages are given by IB±:

$$I_P = (IB+) + (IXP) - (IY) \quad (2)$$

$$I_N = (IB-) + (IXN) + (IY) \quad (3)$$

Combining with the previous equation gives:

$$I_D = (\Delta I) + 2(IY) + |(IXN) - (IXP)| + |(IB-) - (IB+)| \quad (4)$$

For MOS "triode" multipliers, IXP and IXN are the drain/source currents when a common signal is applied to both drains; any ac component of the common drain signal cancels, assuming that the matched pair of MOSFET triodes is truly identical.

Equation 4 indicates that the fixed bias current, ΔI, is comparable to the worst case of unbalance for the virtual-ground stage biases plus the unbalance between the nominally-matched multiplier MOSFET's plus the peak signal excursion. Consequently, the common-mode rejection ratio (CMRR) for this circuit is:

$$CMRR = \frac{IX_{IN}}{IX_{OUT}}$$

This parameter as well as other measures of performance have been modeled using the commercially-available ISPICE routine. The results, showing circuit CMRR, differential gain, and sensitivity, are given in the table.

This work was done by Dave L. Farnsworth, Donald R. Lampe, and Tom J. Shutt of Westinghouse Electric Corp. for **Langley Research Center.** *Further information may be found in NASA CR-145334 [N79-14796/NSP], "The Investigation of Charge Coupled Device Correlation Techniques" [**$11**]. A copy may be purchased [prepayment required] from the National Technical Information Service, Springfield, Virginia 22161.*
LAR-12376

Receiver Array for High-Rate Telemetry

A proposed system improves the sensitivity of a telemetry station network.

NASA's Jet Propulsion Laboratory, Pasadena, California

An RF (radio-frequency) arraying system proposed for high-rate telemetry receiving stations promises to increase the receiver signal-to-noise ratio. [Also see the following related article "Arrayed Receivers for Low-Rate Telemetry" (NPO-14590).] The ratio will be improved in proportion to the number of the arrayed receivers. Marginal high-rate satellite telemetry signals, which are frequently lost due to system, atmosphere, and galactic noises, will come in more clearly.

A simplified setup using one primary and one slave receiver is shown in the illustration. Each is equipped with its own antenna to pick up an RF signal that is phase-modulated with telemetry or a ranging waveform. The other receivers, not shown, have corresponding input signals.

Since antennas 1 and 2 are physically separated, the phase shift on the RF carrier and square-wave subcarrier and the group delay on the data in the receiving system 2 are different from the corresponding phase shifts and modulation group delay in system 1. The combined noise from all the sources is measured relative to reference-temperature loads connected to the low-noise amplifier input (during the measurement) and is designated as the operating equivalent system temperature.

The first local oscillator signal, which is derived from a voltage-controlled oscillator (VCO_1) through frequency multiplier XM, is fed to the first mixer X and provides a noisy estimate (due to receiver noise) of the RF-carrier phase to the first mixer. The second local oscillator signal in system 1 is derived from a frequency standard common to all N receiving systems and is applied to the second mixer. The mixed signal is applied to

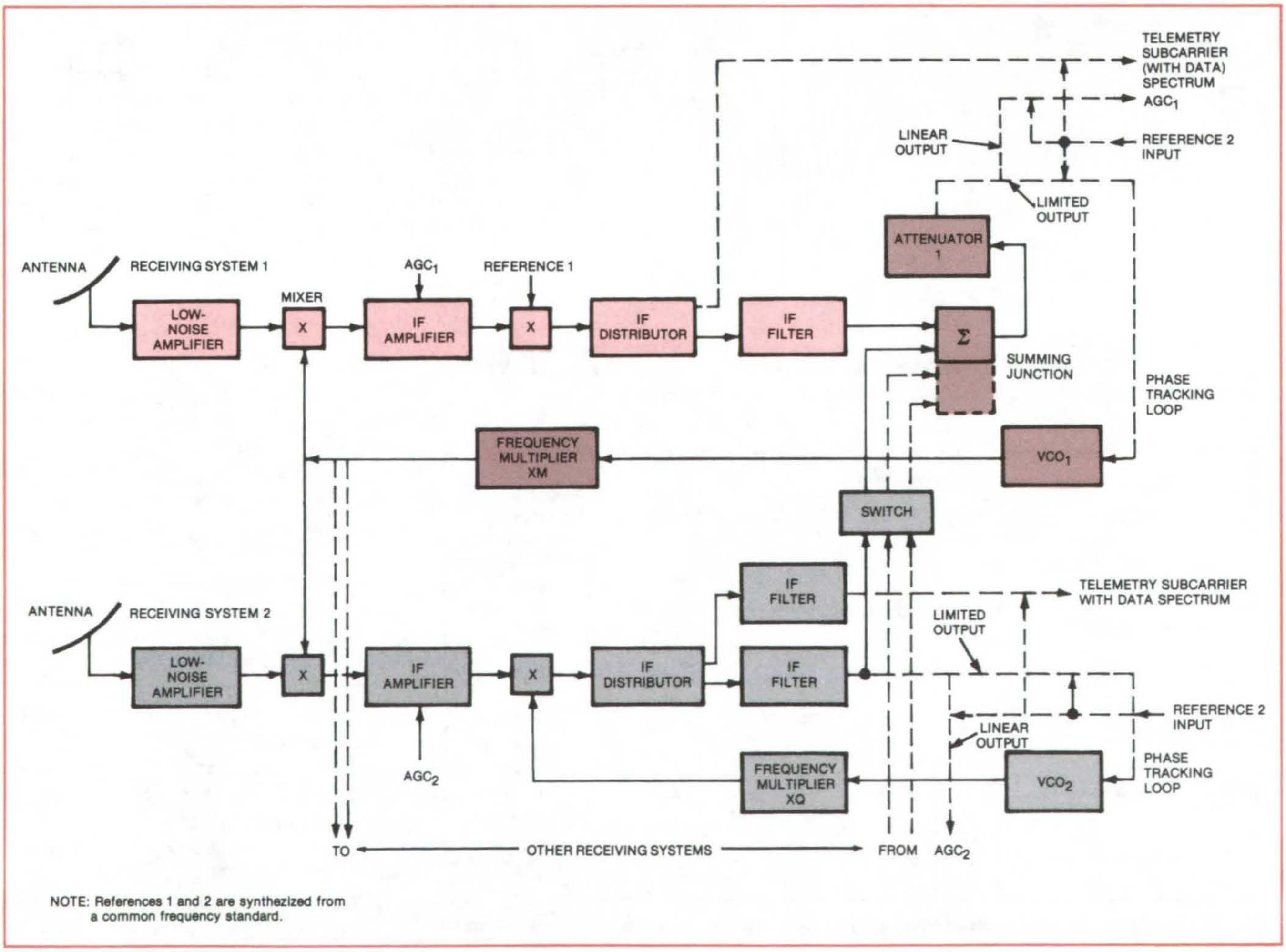

RF Carrier Array uses two receiver systems to improve the signal-to-noise ratio of high-rate telemetry signals. The signals separately processed by each system are coherently combined at the summing junction to produce an improved signal-to-noise ratio. Two receivers improve the ratio by 2.7 dB; three receivers, by 4.1 dB; and four, by 4.6 dB.

the IF distribution amplifier and then to the IF filter that removes the sidebands.

A similar process occurs in system 2 up to the second mixer. There the second local oscillator signal is derived from VCO_2 through a frequency multiplier XQ, and it provides an estimate of the RF-carrier input phase to the second mixer in system 2. A phase shifter in series with a reference input 2 sets the RF phase equal to the RF phase of system 1 at the input to the summing junction.

The carrier-phase noise that is fed from system 2 into the summing junction is small (because of much-narrower closed-loop noise bandwidths) relative to the phase noise error on the first local oscillator. Carrier signals fed into the summing junction are coherent with a small differential phase jitter. The sum of the two coherent signals becomes an output with an improved signal-to-noise ratio as compared to the single receiving system. An additional improvement is made by arraying more receiver systems.

This work was done by Milton H. Brockman and Mahlon Easterling of Caltech for **NASA's Jet Propulsion Laboratory.** *For further information, Circle 10 on the TSP Request Card.*

This invention has been patented by NASA [U.S. Patent No. 4,186,347]. Inquiries concerning nonexclusive or exclusive license for its commercial development should be addressed to the Patent Counsel, NASA Resident Office-JPL [see page A5]. Refer to NPO-14579.

Arrayed Receivers for Low-Rate Telemetry

A proposed method to maintain a low detection threshold of low-rate telemetry receiving stations

NASA's Jet Propulsion Laboratory, Pasadena, California

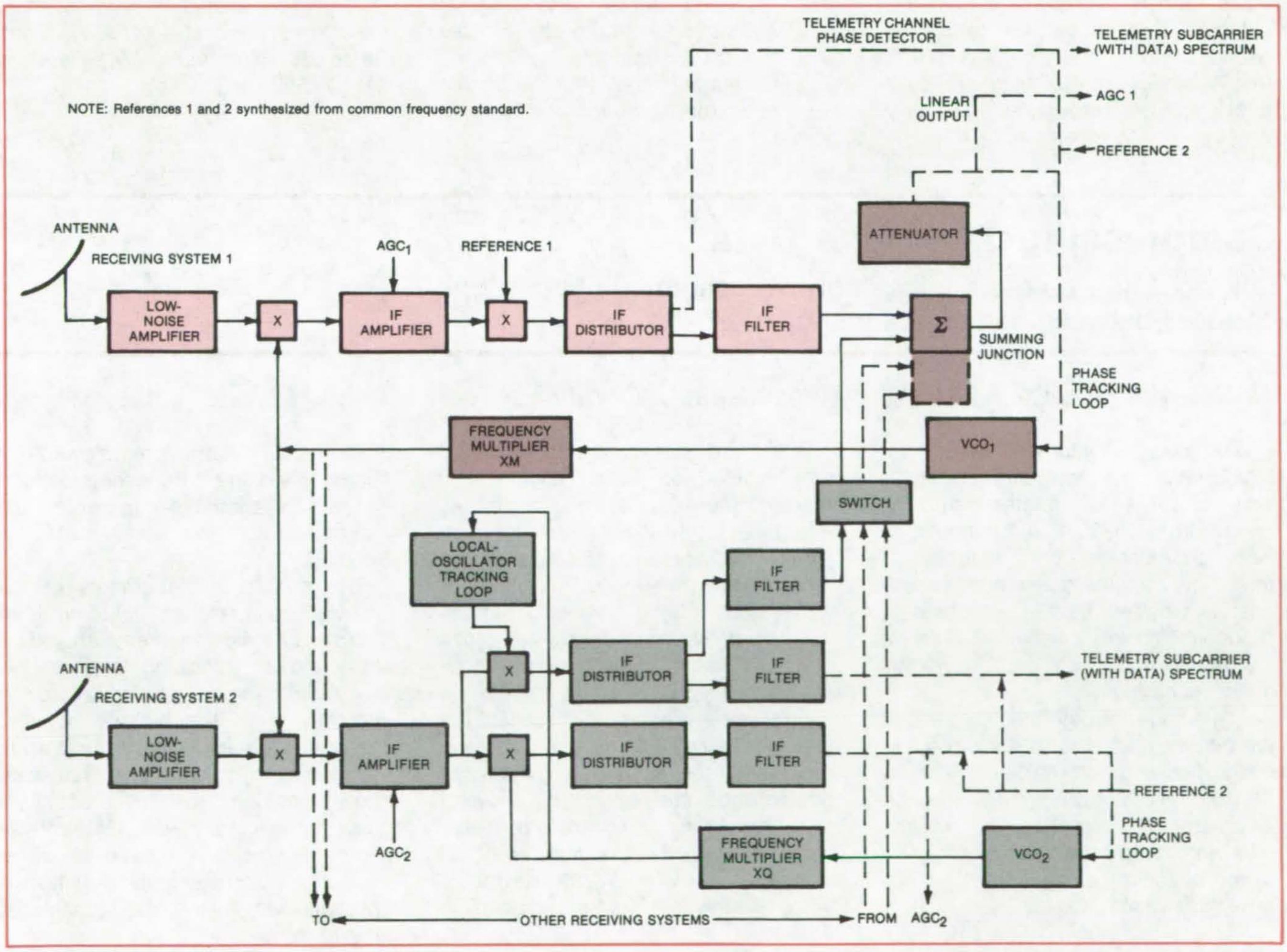

RF Carrier Array includes one master and one slave receiving systems to improve the overall signal-to-noise ratio. The system can be expanded to N slave systems to improve further the signal-to-noise ratio. This scheme reduces the detection threshold of low-rate telemetry signals transmitted from spacecraft, improving the overall communications efficiency.

(continued on next page)

An RF arraying system proposed for low-rate telemetry receiving stations [also see the preceding related article "Receiver Array for High-Rate Telemetry" (NPO-14579)] promises to increase the system signal-to-noise ratios. The scheme incorporates a local-oscillator tracking loop operating a 0.1-Hz bandwidth in a group of 1-Hz-bandwidth slave receivers.

A simplified scheme using one main and one slave receiver is shown in the illustration. Additional receiving systems can be added to improve further the signal-to-noise ratio of the station.

Both systems receive an RF signal phase modulated with telemetry and/or a ranging waveform. Receiving system 1 incorporates a low-noise amplifier, a mixer, an IF (intermediate frequency) amplifier, another mixer, an IF distribution amplifier, and a filter.

System 2 is similarly arranged up to the second mixer, and its signal-to-noise ratio is nearly equal to that of system 1 at that point. A second local-oscillator signal in system 2 is derived from a voltage-controlled crystal oscillator (VCO_2) through a frequency multiplier (XQ). The phase of the VCO_2 is modified by the differences in carrier phase plus any differences in carrier phase relative to system 1.

The second local-oscillator signal includes the estimate of the RF carrier input phase to the lower second mixer (system 2). The phase estimate is derived from a phase-locked loop with a closed-loop noise bandwidth that is a small fraction of the closed-loop noise bandwidth of the RF carrier-phase tracking loop in system 1. Hence the noise on the phase estimate is much less than that on the VCO_1 output.

When arraying many receiving systems, the cumulative phase noise at the summing junction is kept small relative to the phase noise in system 1 by including an additional second mixer (upper mixer) shown in system 2, with the second local oscillator fed to this additional second mixer through a narrow-band phase-locked local-oscillator tracking loop. The phase noise on the output of the local VCO_2 is small compared to the phase noise at its input. Consequently, the second local-oscillator signal that feeds the additional (upper) second mixer in system 2 has a very small amount of noise on its phase estimate.

System 2 has two second IF distribution amplifiers. The upper IF distribution amplifier accepts the output of the upper second mixer and in turn provides its output signal to the upper IF carrier filter (and to the telemetry IF channel) in system 2.

Additional filtering of the phase estimate in system 2 with subsequent coupling through the additional (upper) second mixer, IF distribution amplifier, and IF filter provide the near-maximum signal-to-noise ratio improvement for RF carrier arraying.

This work was done by Milton H. Brockman and Mahlon F. Easterling of Caltech for **NASA's Jet Propulsion Laboratory.** *For further information, Circle 11 on the TSP Request Card.*

This invention has been patented by NASA [U.S. Patent No. 4,186,347]. Inquiries concerning nonexclusive or exclusive license for its commercial development should be addressed to the Patent Counsel, NASA Resident Office-JPL [see page A5]. Refer to NPO-14590.

Compressing TV-Image Data

In processing before coding, only line segments with high contrast between samples are shortened.

NASA's Jet Propulsion Laboratory, Pasadena, California

A data compression method permits high-quality reconstruction of television pictures from relatively-narrow-bandwidth signals. The method may help to increase the capacity of television transmissions, both broadcast and cable. It may also help to reduce the size of the storage medium for video recordings and for digital audio recordings.

The number of data bits assigned to the picture elements (pixels) in a TV-image line segment is determined by the amount of activity in that segment. A segment composed of widely-different sample values is assigned fewer bits than a segment that has fewer variations.

A TV line is divided into 64 small data blocks, or pixels. In the new method (see figure), logic circuits assign an activity estimator to each block. The activity estimator is the "information-preserving" number of bits — that is, the estimated minimum number of bits to code a given block that will permit its exact reconstruction.

The activity estimators for all the blocks in a line are added. The total represents the estimated number of bits to code the entire line, allowing exact reconstruction of the part of the image contained in that line. The total is compared with a predetermined value of allowable bits for transmission of a line. If N bits are allowed for coding a line and if the estimator total exceeds N, then the number of bits estimated for the line must be reduced.

This means that segments of the line must be shortened. Logic circuitry determines which segments should be shortened, or truncated, and by how much. Truncation is applied first to the segments with the highest activity. The principle here is that truncation is less damaging to segments that have large transitions than to those with small transitions. Thus, high-activity segments are prime candidates for truncation because the average transition between their data samples is larger.

After data for a line have been preprocessed by selective truncation, the bits are applied to an adaptive variable-length coder (AVLC). The AVLC automatically selects the best of several optional codes for the line and encodes the line accordingly for transmission. The selection is based on the length of strings of zeros in the data stream; the longer the zero strings, the fewer the bits in the code.

The truncation during preprocessing means that the reconstructed image will have less detail than the original. However, when the data compression method was used on the Galileo satellite for pictures of Earth's surface, the image degradation was imperceptible.

This work was done by Edward E. Hilbert, Jun-Ji Lee, Robert F. Rice, and Alan P. Schlutsmeyer of Caltech for **NASA's Jet Propulsion Laboratory.** *For further information, Circle 12 on the TSP Request Card.*
NPO-14823

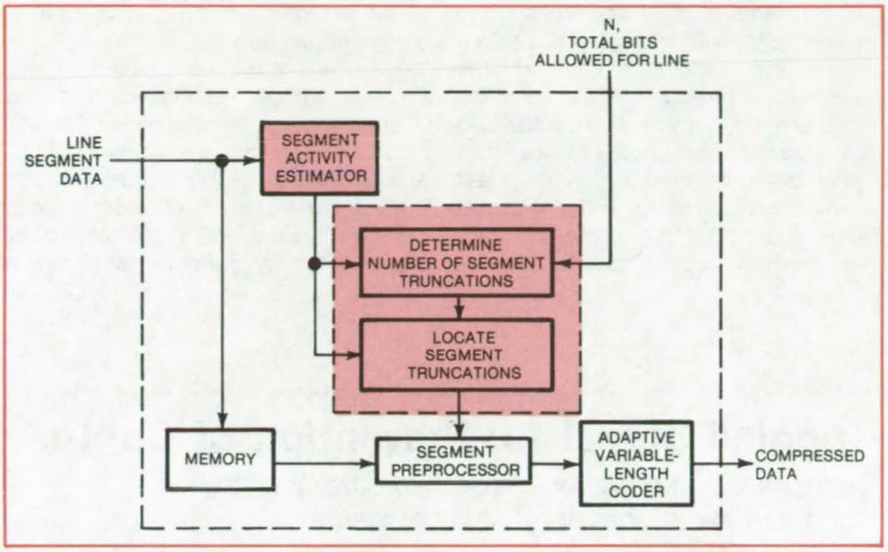

An **Activity Estimator Is Calculated** for each segment of an image line. The estimator is used in conjunction with the allowable bits per line, N, to determine the number of bits needed to code each segment and which segments can best tolerate truncation. The preprocessed line data are then passed to the adaptive variable-length coder, which selects the optimum transmission code.

Real-Time Image Enhancement

A proposed method of extracting low-level features from digital images

NASA's Jet Propulsion Laboratory, Pasadena, California

A successfully tested technique can be used to extract edges from digital images in "real time" (30 frames/s). It is a pipelined system that employs a "vision" algorithm, the Sobel gradient operator. This processor accepts binary image data from an imaging system (such as a charge-coupled device and an A-to-D imaging converter) and produces an edge map. The edge processor is being fabricated on an n-MOS LSI chip. Such a system could be used to locate objects on a moving belt, in deep-sea mining, in coal mining, in real-time control of robotic planetary rovers, and the like.

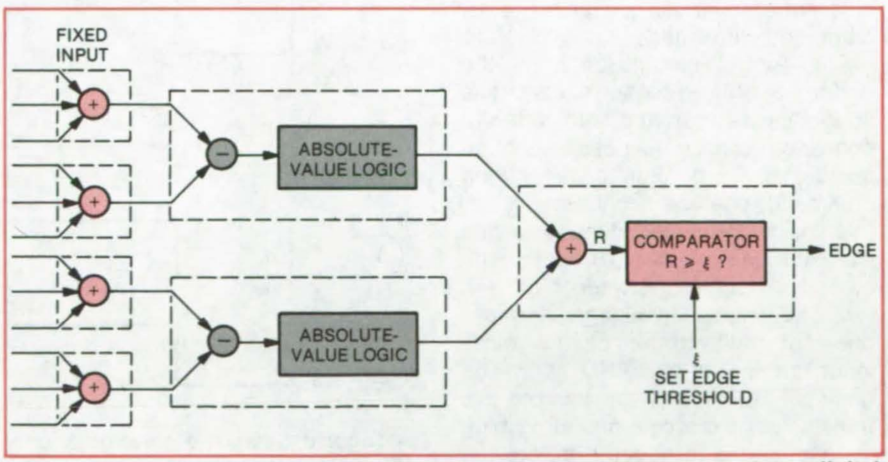

Sobel Gradient Operator is implemented on an LSI chip that processes input digital image data to produce image-edge information. The operator is partitioned into three parts, with the 3-input adder in the first part, the difference and absolute value cells in the second part, and an adder and a comparator in the third part.

A scene to be analyzed is imaged onto a photoarray, and the output is converted into an 8-bit binary number for each pixel of the image. For experimental purposes a 3-by-3 window was chosen; larger windows should work equally well. As the pixel values of the digitized picture are shifted through pixel buffers, the 3-by-3 window effectively moves through the digital picture. The pixel values from the window are then fed into the edge-enhancement pipeline. In this scheme the 3-by-3 window becomes discontinuous at the end of each image line and also at the end of each frame (blanking).

The operation is depicted in the illustration. The front section of four

(continued on next page)

3-input adders is followed by two subtracters and a logic block that forms the absolute value of the previous subtraction. The resulting absolute values are then added to produce the Sobel gradient value, R. A threshold comparator in the last section compares R with a preset edge threshold and indicates whether the gradient value is greater or less than the threshold (that is, whether an edge is present).

The entire system is based on MOS LSI technology. Compared to bipolar technologies, the charges in the MOS devices leak away slowly, making it possible to store the data reliably for 1 to 2 ms between different pipeline sections. The MOS transistors are symmetrically switching and can be used as simple on/off switches either to transmit or isolate data from section to section. Finally, the MOS design is more reliable because of reduced package count and reduced number of interconnections.

This work was done by Vincent S. Wong of Caltech for **NASA's Jet Propulsion Laboratory.** *For further information, Circle 13 on the TSP Request Card.*
NPO-14281

Toggled Signal for Prevention of Control Errors

Redundant command lines use two different "true" signals to avoid common failure modes.

Lyndon B. Johnson Space Center, Houston, Texas

Like a security vault that can be opened only when two keys are turned simultaneously, control-system functions can be protected against accidental excitation by using an AND gate that requires two high inputs to produce a high output. The activating command from the controlling logic circuit or controlling operator goes to the AND gate through two paths, so an erroneous high signal in one path cannot set the function into operation. Moreover, in analogy to keys of different shapes, the signals sent through the two paths can have different coding to protect against common failure modes.

The control circuit for firing the Space Shuttle reaction jets (see figure) uses two paths with different codes to minimize the possibility of an accidental firing. For a real firing command, one line simply goes high; this line is connected directly to one input terminal of the AND gate. The other line toggles between high and low. The toggled signal is applied to a one-shot multivibrator at the other input terminal of the AND gate. The one-shot is triggered by the positive transition of the toggle and stays high as long as it is retriggered before the monostable delay period ends. Thus both inputs to the AND gate are held high so the jets can operate.

A jet-firing command is generated in the computer and transmitted to a demultiplexer. The command is split along two paths in the demultiplexer, producing outputs from separate electronic cards.

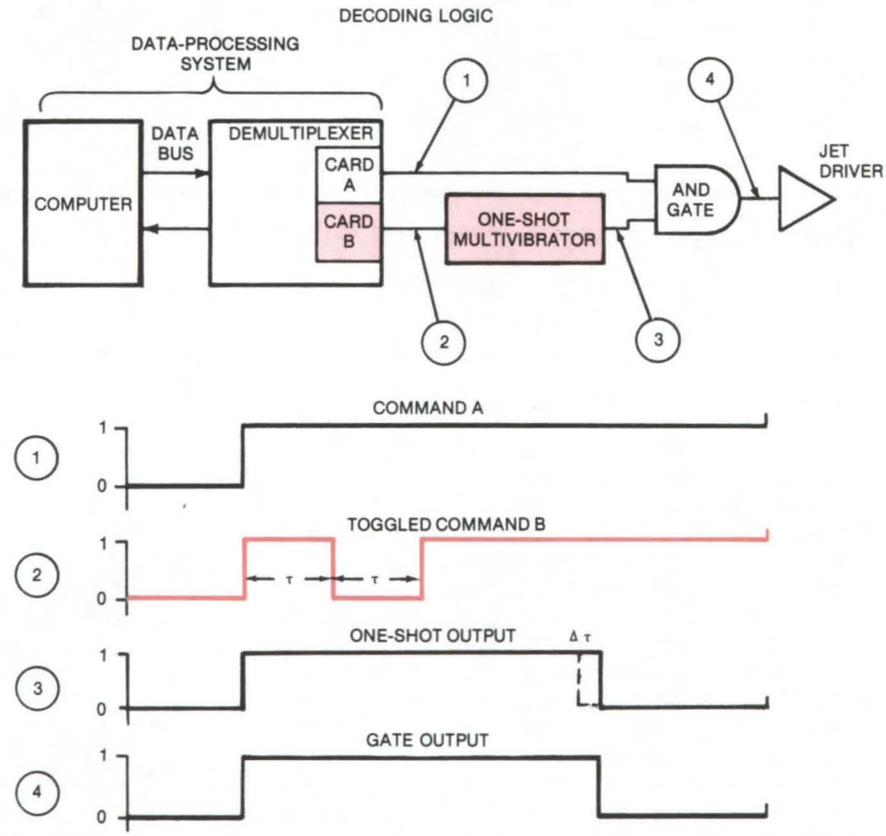

A **Toggled Command** prevents erroneous activation of reaction jets on the Space Shuttle. When the jets are required to fire, commands "A" and "B" combine to drive the AND gate high and turn them on. A failure in line "B" after two toggle pulses is illustrated by the graphs.

The one-shot in series with the toggle line, which has a delay of ($2\tau + \Delta\tau$), maintains the signal at a high level at the input to the AND gate. The one-shot retriggers before it has timed out, to maintain a continuous output as required to activate the jet driver. A failure in the toggle line after two pulses is illustrated by the graphs in the figure.

Failure modes upstream of the output cards still could cause both

card outputs to fail high. However, firing a jet requires command line "B" to toggle between high and low with a period 2τ while "A" remains high. A failure that causes both "A" and "B" to go high simultaneously causes a single jet pulse. Since "B" does not drop back to zero, the one-shot cannot be retriggered, so the jet turns off and remains off.

In the Shuttle application, the single pulse is acceptable. In other applications, additional logic may be desirable to avoid the single pulse; e.g., a third ANDed input from a second multiplexer/demultiplexer.

This work was done by Charles E. Wyllie of Honeywell Inc. for **Johnson Space Center.** *No further documentation is available.*
MSC-18779

Converting a Digital Filter to Its Analog Equivalent

Two methods complement each other for implementing the analog equivalent of a digital filter.

Lyndon B. Johnson Space Center, Houston, Texas

Two proposed procedures for converting a digital filter into an analog filter could simplify the analysis of digital control systems. By converting to the continuous frequency domain, various mathematical techniques for analyzing the stability and response of analog systems can be brought to bear on a digital system.

Given a digital filter in the w-domain:

$$G(w) = \left(\frac{\nu_D}{\nu_N}\right)^2 \frac{w^2 + 2\xi_N \nu_N w + \nu_N{}^2}{w^2 + 2\xi_D \nu_D w + \nu_D{}^2}$$

where

$$w = \frac{z+1}{z-1} \text{ and } z = e^{St}$$

$t \equiv$ sampling period, seconds.

Then the equivalent S filter is obtained by:

1. Direct Conversion Method

$$G(S) = \left(\frac{\omega_D}{\omega_N}\right)^2 \frac{S^2 + 2\xi_N \omega_N S + \omega_N{}^2}{S^2 + 2\xi_N \omega_D S + \omega_D{}^2}$$

where

$$\omega_N = \frac{2}{t}\,\frac{\pi}{180}\,\tan^{-1} \nu_N \text{ radians per second}$$

$$\omega_D = \frac{2}{t}\,\frac{\pi}{180}\,\tan^{-1} \nu_D \text{ radians per second}$$

or by:

2. Inverse of Tustin's Method

$$G(S) = \left(\frac{\omega_D}{\omega_N}\right)^2 \frac{S^2 + 2\xi_N \omega_N S + \omega_N{}^2}{S^2 + 2\xi_D \omega_D S + \omega_D{}^2}$$

where

$$\omega_N = \frac{2}{t} \nu_N \text{ radians per second}$$

$$\omega_D = \frac{2}{t} \nu_D \text{ radians per second}$$

Figure 1. The **Analog Equivalent G[S] of a Digital Filter G[w]** can be obtained by two conversion schemes.

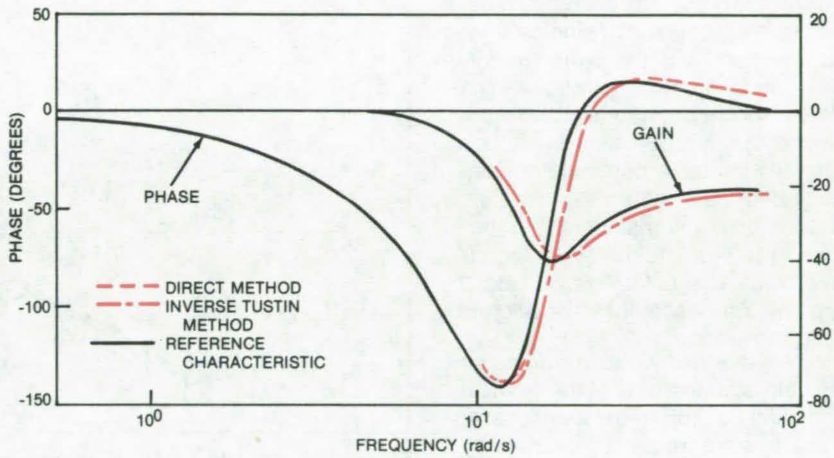

Figure 2. The reference **Response of a Banding Filter Is Matched** at low frequency by either the direct or inverse of Tustin's method. At frequencies above 10 radians per second, the direct method gives a better match. The curves are not drawn in the regions where they merge with the reference.

The two methods, outlined in Figure 1, are a direct conversion method and an inverse of Tustin's method for converting an analog filter into an equivalent digital filter. Tustin's method is already in use; the direct method is new. Together, the procedures form a complementary pair: Filters that cannot be implemented to the required accuracy using one method can usually be implemented by the other method. Both require only direct computations and are therefore simpler and more efficient than previous iterative techniques or methods that require "ad hoc" adjustment of filter parameters.

The procedures have been tested on low-frequency digital filters used in the Space Shuttle flight-control system. One is a banding filter (see Figure 2), and the other is a rolloff filter. For both cases, either method matches the reference response in the low-frequency range from zero to 10 radians per second. Above 10 radians per second, the direct method gives a better match for the banding filter, while the inverse of Tustin's method is better for the rolloff filter. In general, both methods are exercised; the one that gives the best match in the frequency range of interest is selected.

This work was done by John F. L. Lee of Honeywell Inc. for **Johnson Space Center.** *For further information, Circle 14 on the TSP Request Card.*
MSC-18587

Airborne Meteorological Data-Collection System

Aircraft position and weather data are collected, formatted, and relayed to ground from in-flight commercial jets.

Lewis Research Center, Cleveland, Ohio

An airborne data acquisition and communication system called ASDAR (Aircraft to Satellite Data Relay) has been developed as a result of a joint NASA/NOAA (National Oceanic & Atmospheric Administration) project to provide an improved source of meteorological data for weather forecasting.

The ASDAR system collects meteorological information (wind speed, wind direction, and static air temperature) and aircraft position data (latitude, longitude, and altitude) from wide-body jet aircraft instrumentation during flight and automatically converts and formats the data, adds time references, and transmits this information to the ground via synchronous meteorological satellite relay using a group of four satellites positioned around the world.

Much of the U.S. weather originates in the data-sparse areas of the tropical regions and the Southern Hemisphere. These areas are frequently crossed by many of the modern, wide-body jet aircraft of the B-747 and DC-10 types on regular routes. These aircraft contain navigation and data systems capable of providing latitude, longitude, altitude, wind speed, wind direction, and outside air temperature. Conventionally, the pilot records this information manually and submits it for use at the terminus of a flight. Conventionally, up to 24 hours may be required for a report to get into the weather data bank. Manual recording and data entry can be a source of errors making the data unusable or suspect.

The ASDAR system consists of a data acquisition and control unit to acquire, store, and format these data automatically; a transmitter to relay the formatted data via satellite to the ground; and a clock to time the data sampling and transmission periods. The data are relayed to the ground via NOAA Geostationary Operational Environmental Satellites (GOES) and then to the National Meteorological

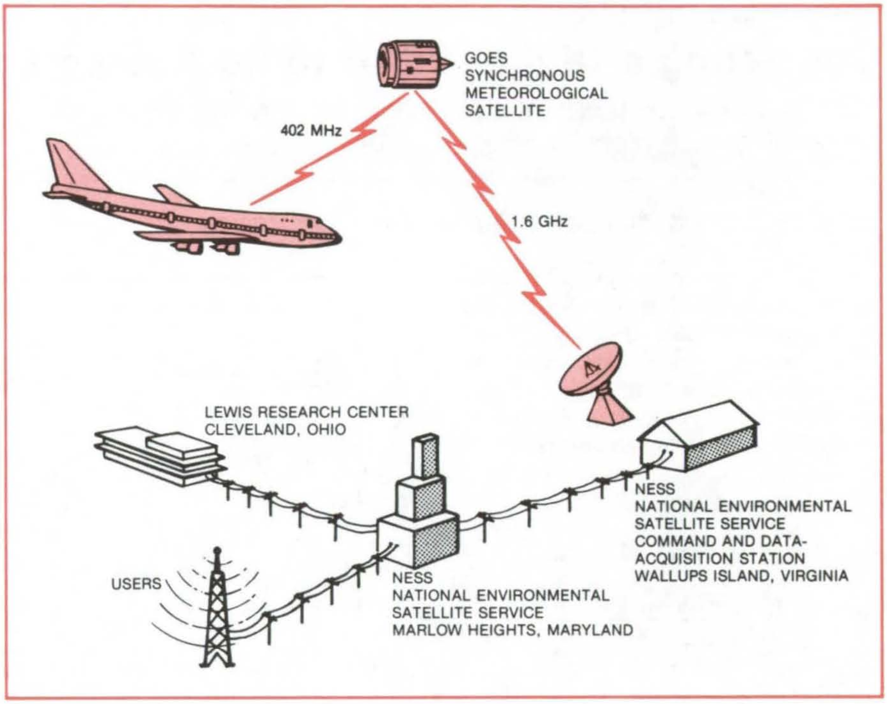

Figure 1. **Aircraft-to-Satellite Meteorological Data** are relayed to the ground to aid in weather forecasting. In normal operation, eight complete sets of data are acquired over a 1-hour period and transmitted to the satellite at a precise time each hour.

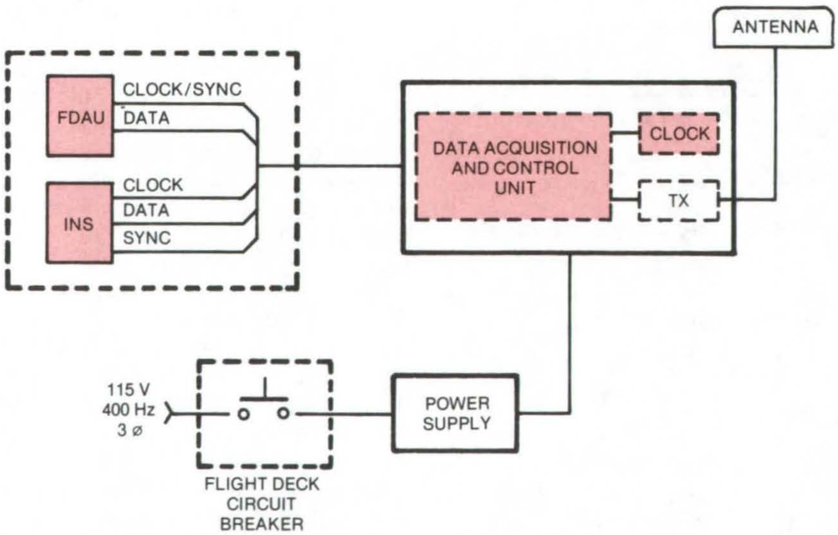

Figure 2. The **Data Acquisition and Control Unit** (DACU) receives information from the aircraft Inertial Navigation System (INS) and the Flight Data Acquisition Unit (FDAU). A battery-powered clock determines the data sampling time and transmission time for the microprocessor-based controller.

Center to aid in weather forecasting (see Figure 1).

The B-747 aircraft in commercial airline service use an Inertial Navigation System (INS) and a Flight Data Acquisition Unit (FDAU) as standard avionics equipment. These two units serve as sources of the data necessary to provide the wind speed and direction and static outside air temperature at a specific latitude, longitude, and altitude. The INS provides latitude, longitude, wind direction, and wind speed as serial BCD (binary coded decimal) data. The FDAU system provides altitude and outside static air temperature in the form of PCM (pulse-code modulation) serial data. These data are the same as are normally manually reported by airline pilots in the form of aircraft reports. The ASDAR reports are formatted on board in a manner similar to these reports. As a result of the onboard formatting prior to transmission, the messages received on the ground require little processing to be suitable for insertion onto the Global Telecommunications System and, subsequently, into the weather data base.

The major elements of the ASDAR system are the electronics unit, the antenna, and the power supply. These are interconnected as shown in Figure 2. Data from the aircraft INS and FDAU are fed into the Data Acquisition and Control Unit (DACU). A battery-powered clock is included in the electronics unit with the DACU. The clock output is used by the microprocessor-based controller to determine the data sampling times and transmission times. In normal operations, eight complete sets of data are acquired over a 1-hour period and transmitted to the satellite at a precise time each hour. The DACU provides all the necessary scaling to the data and stores them in International Alphabet. At the appropriate time each hour, the DACU turns the transmitter on and delivers a biphase data signal to phase-modulate its carrier. The ASDAR system was designed to survive and operate in the below-deck electronic equipment area of commercial aircraft; the only external part of significance is the antenna mounted on top of the fuselage.

To date, 17 systems have been installed on the 747 aircraft of eight national and international airlines and on the U.S. Air Force C-141. Performance has been excellent, with the ASDAR fleet returning 800 to 1,000 data sets daily. The data have been consistently high-quality and are being used routinely to generate worldwide weather maps of significantly improved accuracy. Because it retrieves and transmits data automatically and is inherently accurate, ASDAR can require less labor than when collecting and processing data manually, as is now done.

ASDAR has other potential uses. It could locate aircraft precisely and could selectively reroute them in near-real time to conserve fuel by taking advantage of favorable winds. (NOAA has a plan underway to install ASDAR on hundreds of aircraft worldwide.) Slightly modified, ASDAR could help in the search for a downed aircraft by continuously transmitting its location on a separate emergency channel.

This work was done by James W. Bagwell and Bruce G. Lindow of **Lewis Research Center.** *Further information may be found in NASA TM-78992 [N78-33283/NSP], "An Airborne Meteorological Data Collection System Using Satellite Relay [ASDAR]"* [**$5**]. *A copy may be purchased [prepayment required] from the National Technical Information Service, Springfield, Virginia 22161.*

LEW-13346

Receiving Signals of Any Polarization

Two-channel detection accommodates linear, circular, and elliptical polarization in the same receiving unit.

NASA's Jet Propulsion Laboratory, Pasadena, California

Losses due to polarization mismatch are avoided with a radio receiver that handles signals of any polarization—linear, left- or right-circular, or elliptical. The polarization-diversity receiver employs an orthomode transducer, a device that breaks a signal down into two components—one with right-circular and the other with left-circular polarization—regardless of the polarization of the original signal. (Any polarization can be separated into left- and right-circular components.)

The components are processed separately in two receiver channels having approximately-equal time delay. Each channel is phase-locked to the same reference signal so that the signals to the phase detectors in both channels are in phase and add coherently when they are combined.

The polarization-diversity receiver is proposed for an Earth station for linearly-polarized telemetry transmissions from a spinning satellite [see "Antenna Feed for Linear and Circular Polarization" (NPO-14810) on page 270 of this issue of *NASA Tech Briefs*]. The telemetry signals are received at the ground station by a circularly polarized antenna. Because the linearly polarized signals are transmitted from a spinning source, the plane of polarization is continuously changing. Compensation for the changing plane of polarization comes from treating the linearly polarized wave as a superposition of two circularly polarized waves, allowing reception by a circularly polarized antenna.

The two outputs of the receiver orthomode transducer are fed to two RF amplifiers for low-noise amplification (see figure). From there, the signals proceed through the closed-loop receiver channels where they are phase-locked to the reference.

(continued on next page)

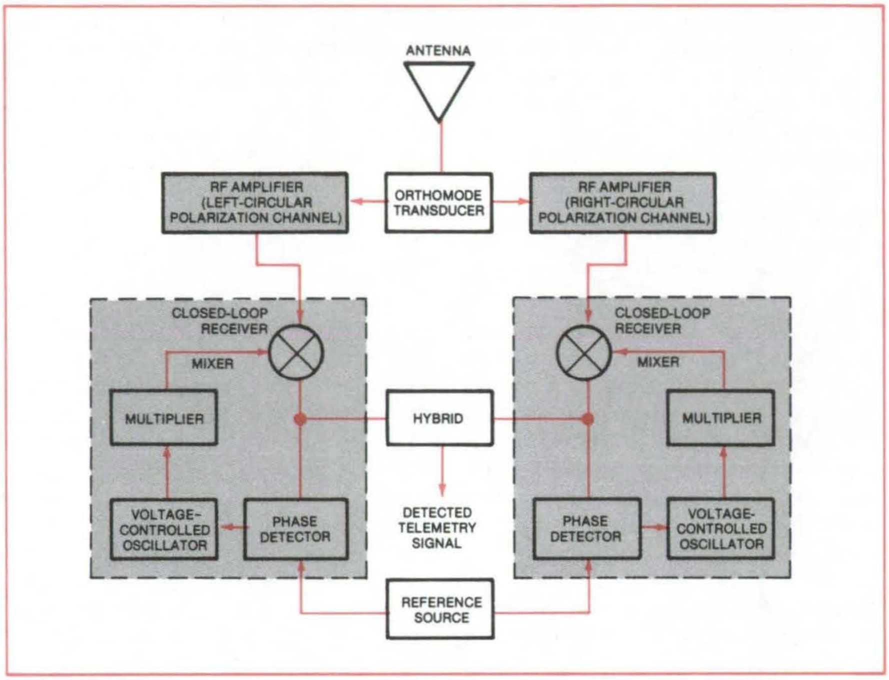

Separated into Left-Circular and Right-Circular Polarizations, a telemetry signal is detected in two channels, then recombined so that the data can be extracted. The two channels allow any polarization to be processed.

The synchronization source is derived from the Earth-station timing signals.

The gain in each channel must be controlled according to the polarization of the received signal. If the received signal is linearly polarized, both channels have equal gain. For circular polarization, one channel has zero gain; and for elliptical polarization, the ratio of the gains in the two channels is greater than zero but less than one. Under these conditions, the signal-to-noise ratio at the hybrid circuit is about the same as that of a receiver matched to the signal polarization when it is operated at a reasonable margin above threshold.

This work was done by John E. Ohlson, Boris L. Seidel, and Charles H. Stelzried of Caltech for **NASA's Jet Propulsion Laboratory.** *For further information, Circle 15 on the TSP Request Card. NPO-14836*

Portable Zero-Delay Assembly

The instrument accurately calibrates a translator for ground-station ranging-system time delay measurements.

NASA's Jet Propulsion Laboratory, Pasadena, California

A portable zero-delay device (PZDA) is the basic reference standard used to calibrate the time delays of an S- and X-band ground-station ranging system that has both transmit and receive paths. The PZDA is used to calibrate the delays of a station Doppler translator connected to an uplink sampling point and downlink signal-injection points into S- and X-band masers. After calibrating the translator path with the PZDA, the translator becomes the field instrument for measuring station time delays on a routine basis. For ground stations having antennas with severe multipath errors, the accuracy of the calibrated translator method is an order of magnitude better than that obtainable with calibrating instruments mounted on the surface of the antenna.

Before use in the field, the time delay of the PZDA is calibrated using a back-to-back method shown in the figure. The assembly on the right is under test; the one on the left is the comparison standard. The standard is also a portable zero-delay assembly, but the S-X isolators are reversed to permit reverse signal flow.

When the PZDA is used at each deep-space station, the calibration involves two measurements. In the first, the Doppler translator path between the uplink sampling and the maser injection points is replaced by the PZDA and its associated test cables and attenuators. With the assembly installed, ranging measurements are made and noted.

The second measurement consists of changing the delay path back to the normal translator path with the exception that the test cables and attenuators are connected in series with the normal translator-path cables. The adjustable attenuators of the PZDA are set to zero, and the fixed pads are replaced by pads of lower value to produce the same received-signal

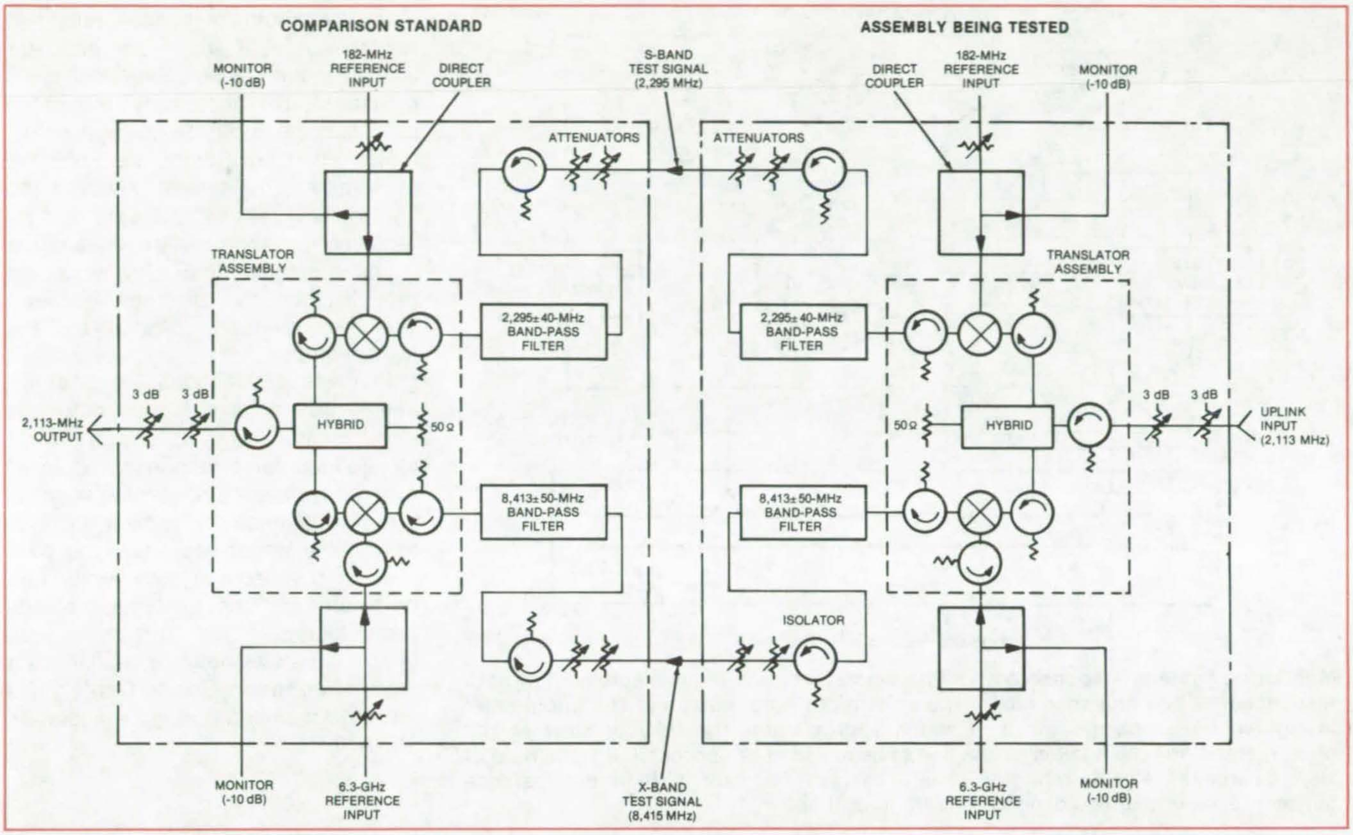

Portable Zero-Delay Assemblies are calibrated by use of the back-to-back method. The comparison standard differs from the device being tested in that S-X isolators are reversed to permit signal flow in the reverse direction. After the calibration PZDA is used in the field to calibrate time delays of deep-space network ground-station ranging systems. This approach may also be used in calibrating microwave links in other communication systems transmitting large quantities of digital data.

levels as those of the first measurement. Range measurements are again made and noted. The translator-path delay can then be determined by subtracting the first measurement from the second and adding in the delay of the portable zero-delay assembly.

This work was done by Manuel M. Franco, Tommy Y. Otoshi, and Edward J. Serhal, Jr., of Caltech for **NASA's Jet Propulsion Laboratory.** *For further information, Circle 16 on the TSP Request Card.*
NPO-14671

Photometer Used for Response Time Measurement

A photometer measures the response time of a servocontrol system.

Lyndon B. Johnson Space Center, Houston, Texas

Measuring light intensities is the standard application of a photometer, but this sensitive optical instrument, with its extremely narrow field of view and fast response, can also be put to some less obvious uses. In tests of the servocontrol systems of space vehicles, for example, a photometer is used as a motion detector for measuring response speed and acceleration.

To measure the response time of a servocontrol system, the photometer senses output movement shortly after an operator activates a hand-controlled input. The time delay is measured on an X/T recorder. In this application (see figure) the output is the motion of attitude-indicator indices; however, the photometer could also be sighted on the cursor of a cathode-ray tube, on a meter pointer, or even a pencil mark on a piece of paper taped to an object.

When the photometer with a very small acceptance angle (2 minutes of arc) is sighted on an edge of the cursor, the cursor motion across the field of view changes the photometer output signal. The delay between the activation of the hand controller and the signal change is the system response time.

(continued on next page)

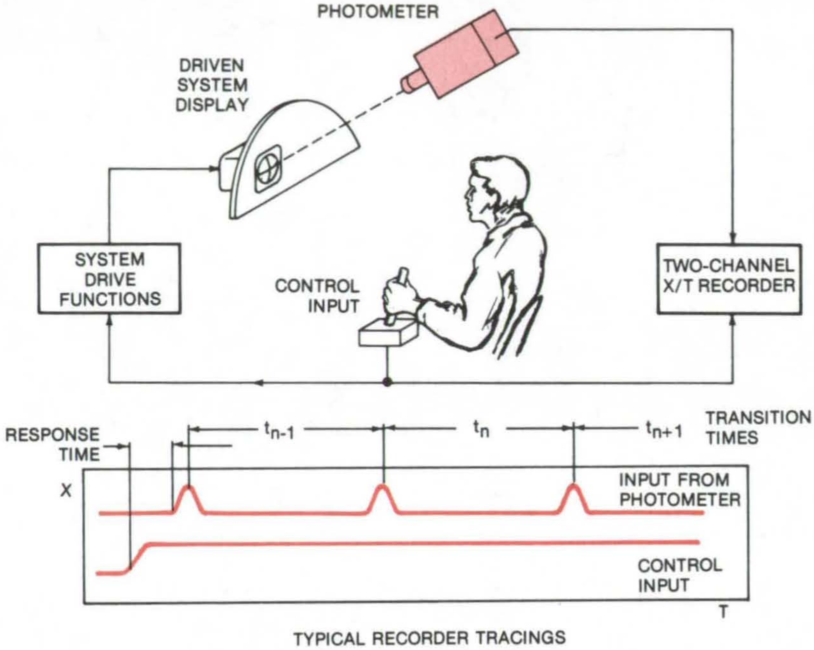

Monitoring System Response With a Photometer permits the measurement of both response time and response rate of the system driving the display. The photometer is sighted on a line the width of which approximates the field of view of the photometer. The time it takes for the line to be replaced by another line in the field of view equals the signal transition time. The response rate is then the distance between lines in degrees divided by transition time.

In use, both response time and response rate of an attitude indicator in the Shuttle Mission Simulator were measured. The photometer is sighted on a line the width of which approximates that of the field of the photometer. The time it takes for the line to move across the field and be replaced by another line equals the signal transition time. The response rate is then the distance between lines, in degrees, divided by the transition time.

In these applications the photometer is acting as a motion detector. With suitable targets, any open- or closed-loop servo response and servo rate, as well as computer lag, can be measured without perturbing the system. If the target has equally spaced lines on it, speed and acceleration can be determined from the times the lines are detected.

This work was done by Anibal J. da Silva of **Johnson Space Center.** *No further documentation is available.*
MSC-18712

Physical Sciences

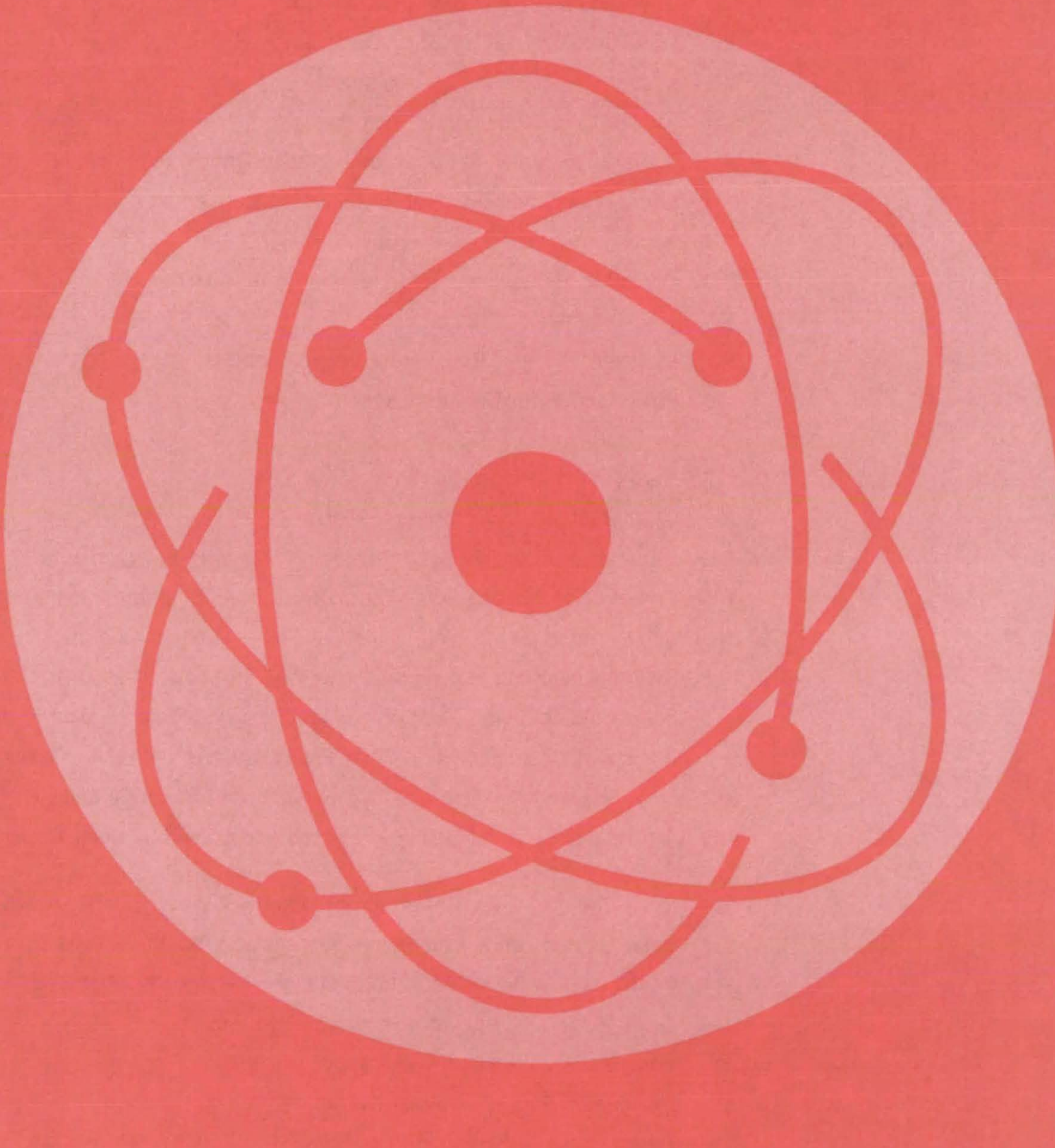

Hardware, Techniques, and Processes

Books and Reports

Multiplexed Logic Controls Solar-Heating System

Inexpensive sensors and logic circuits select from four operating modes.

Marshall Space Flight Center, Alabama

A controller for solar heating uses inexpensive thermocouples as temperature sensors and uses simple logic circuits to select among four operating modes. The sensor signals are multiplexed through the same amplifier, instead of each being processed by separate amplifiers. Errors caused by differing amplifier characteristics are therefore avoided. Control is based on temperature differences (rather than on absolute temperatures).

The controller was built for a solar heater in which air is the heat-transfer medium (see figure). The thermocouples sense temperatures at four locations: at the solar collector, at the top and bottom of the rock storage bed, and at the heated building. The logic circuits control dampers, a circulating fan, and an auxiliary heater, arranging the heating system in one of four configurations, or modes:

- Mode 1 heats the building directly from the collector. The logic selects mode 1 when the collector temperature is greater than the building temperature by a predetermined amount and the building thermostat calls for heat.
- Mode 2 stores heat in the rock bed. It is selected when the collector temperature is higher than the temperature at the top of the rock bed by a predetermined amount and the building thermostat is not calling for heat.
- Mode 3 heats the building from the rock bed. It is selected when the temperature at the bottom of the rock bed is greater than the building temperature by a predetermined amount and the thermostat calls for heat.
- Mode 4 heats the building with the auxiliary heater. It is selected when the collector and rock bed temperatures are low and the thermostat calls for heat.

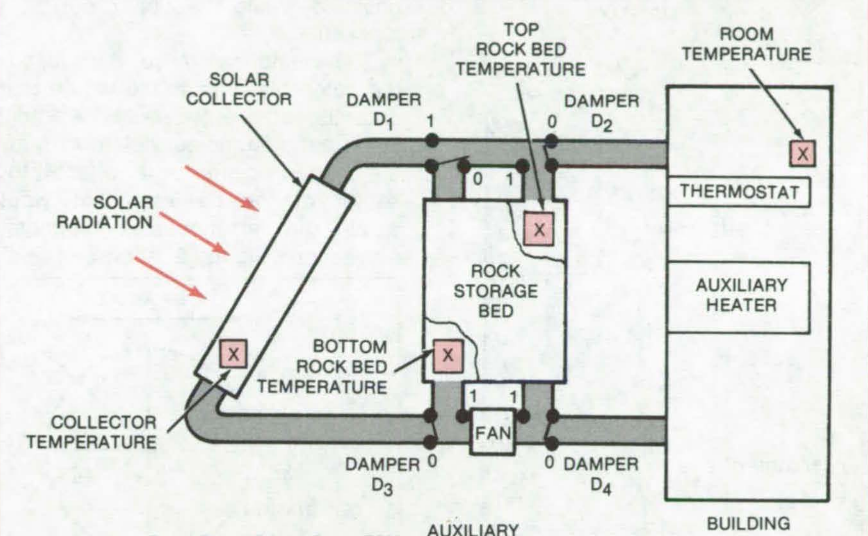

	D_1	D_2	D_3	D_4	FAN	AUXILIARY HEATER
MODE 1	0	1	1	1	ON	OFF
MODE 2	0	0	1	0	ON	OFF
MODE 3	1	1	0	1	ON	OFF
MODE 4	0	0	0	0	OFF	ON

Four Thermocouples Monitor the Temperatures at key points in this solar-heating system. On command from logic circuitry, dampers open and close to direct airflow. The table shows damper positions and fan and auxiliary heater status for each of the solar-heater operating modes.

Copper/constantan thermocouples with high-voltage change with temperature — about 0.023 mV/°F (0.041 mV/°C) — produce relative temperature measurements that are accurate within 2° F (1.1° C). Unlike thermistors, the thermocouples do not require an external electrical power supply, do not have to be selected for matched characteristics, and are relatively inexpensive.

The thermocouple outputs go to a multiplexer that alternately connects differential thermocouple voltages to an amplifier. Another amplifier and synchronized multiplexer connect the appropriate voltages representing preset temperature differences to a third amplifier, which compares the differential signals and provides mutliplexed outputs to the logic circuitry. The logic circuits decide on the proper operating mode and operate relays to control damper solenoids, the fan motor, and the auxiliary heating unit. [A detailed description of the circuit may be found in "Multichannel Temperature Controller for Solar Heating" (MFS-23775) on page 203 of *NASA Tech Briefs*, Vol. 3, No. 2.]

This work was done by James R. Currie of **Marshall Space Flight Center.** *For further information, Circle 17 on the TSP Request Card.*

This invention is owned by NASA, and a patent application has been filed. Inquiries concerning nonexclusive or exclusive license for its commercial development should be addressed to the Patent Counsel, Marshall Space Flight Center [see page A5]. Refer to MFS-25287.

Four-Cell Solar Tracker

A very sensitive tracking device for control of collector or mirror drives

NASA's Jet Propulsion Laboratory, Pasadena, California

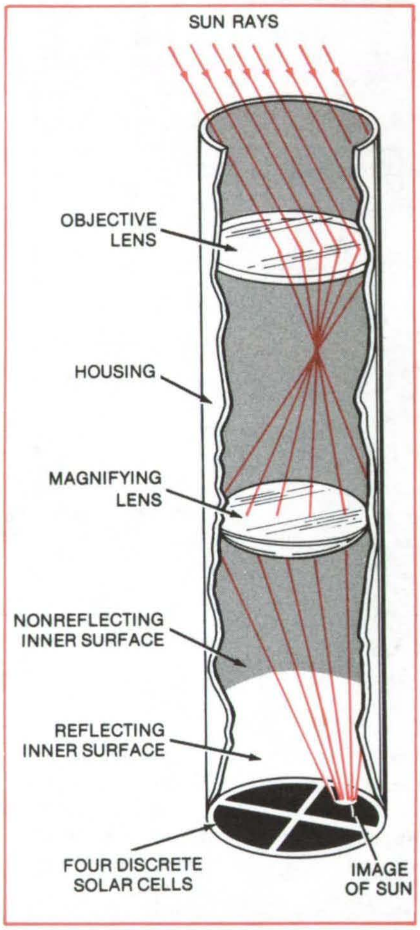

Figure 1. This **Sun Tracker,** consisting of an optical telescope and four solar cells, generates signals that keep the cylinder pointed at the Sun throughout the day. Roughly 40 cm in length, it can properly orient solar collectors or mirrors for maximum energy collection.

A prototype Sun tracker has four solar cells surrounded by a cylindrical mirror. When added to a declination-angle/hour-angle drive, it can orient a solar collector or solar mirror accurately for maximum illumination.

Figure 1 shows the lenses and detectors. The objective lens gathers incoming light from the Sun; and the magnifying lens focuses a sharp image of the solar disk, magnifying its motion across the detectors to enhance sensitivity. The inside of the lower portion of the housing is polished, while the upper portion is blackened.

The cylindrical mirror surrounding the detectors reflects the image back onto the adjacent detector element, but is not of sufficient height to return the image to center or to reflect it to a sector of the detector that would cause an erroneous or opposite correction. Figure 2 shows possible Sun image positions with different pointing errors and illustrates the capability of the cylindrical mirror to accommodate overtravel or wide-angle acquisition.

Signal conduction leads from the upper surfaces of the four cells are connected to a resistance bridge. With the image of the Sun falling on the center of the detector, the bridge is

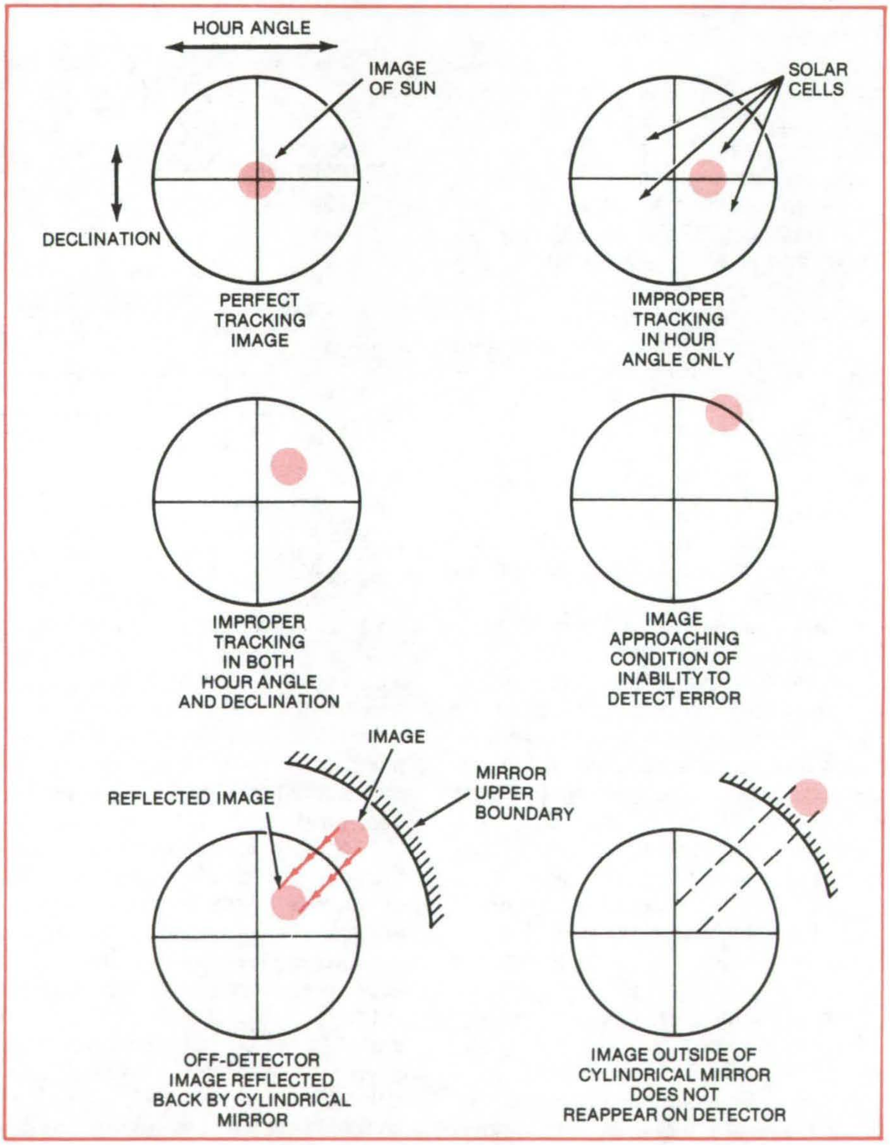

Figure 2. Each **Solar Cell** generates a voltage proportional to the part of the solar image it receives; the voltages drive servomotors that keep the image centered. Note how the mirrored portion of the cylinder extends the range of image excursion that can be corrected.

balanced. An offcenter image, with a corresponding imbalance in the bridge, will result in a servomechanism adjustment that recenters the image and reorients the solar collector or solar mirror for maximum illumination.

The sum of the voltages from the four cells remains nearly constant as long as no part of the Sun image moves off the circular boundary of the cells. When the light is reflected back to the detector array by the cylindrical mirror, the output falls off about 10 percent, which in most cases does not seriously affect tracking.

Standard electronic amplifier, comparator, and intensity measuring circuits may be used with the output signals from the detector to produce extremely close tracking. The detector may also be adapted to other types of tracking systems such as altitude/azimuth drives.

This work was done by C. Martin Berdahl of Caltech for **NASA's Jet Propulsion Laboratory.** *For further information, Circle 18 on the TSP Request Card.*
NPO-14811

Offset Paraboloidal Solar Concentrator

The new design increases solar gathering efficiency by 3 to 4 percent by eliminating shadowing and blocking of solar rays.

NASA's Jet Propulsion Laboratory, Pasadena, California

A section of a conventional paraboloid, offset from its major axis, is used as a reflector in a solar concentrator. The offset paraboloid is 3 to 4 percent more efficient in gathering solar rays than a conventional paraboloid because neither the receiver nor its support interferes with the incoming rays as they pass from the Sun to the reflector to the receiver. In addition, the offset paraboloid has certain maintenance advantages.

In a conventional solar concentrator, the receiver is supported at the focus of a paraboloid by a structure that blocks some of the incoming light and some of the reflected light. The result is shadowing and a loss in concentrator efficiency.

The non-axisymmetric reflector, receiver, and support is illustrated in the figure. Two parallel arms extending from the base support the reflector. Two other arms extend from the base and join approximately at the focal point of the concentrator, where the receiver is mounted.

The paraboloid and receiver support arms are pivoted about the apex of a truncated tetrahedron-truss base. Wheels are mounted at the three corners of the base triangle of the tetrahedron. A bull gear on a low, short pedestal below ground level, at the center of the base triangle, provides azimuth drive. The concentrator may also be driven in azimuth through a cable wrapped around the pedestal with a pinion and drive attached to the tetrahedron base.

The entire concentrator support can be located either below or above ground level for waist-high servicing of the receiver. A pivot in the reflector support arms allows the reflector to be folded toward the receiver and stowed. Since wind loading on the stowed structure is reduced, the cost of building a foundation can be lowered. Moreover, the concentrator is easily cleaned and serviced in the stowed position.

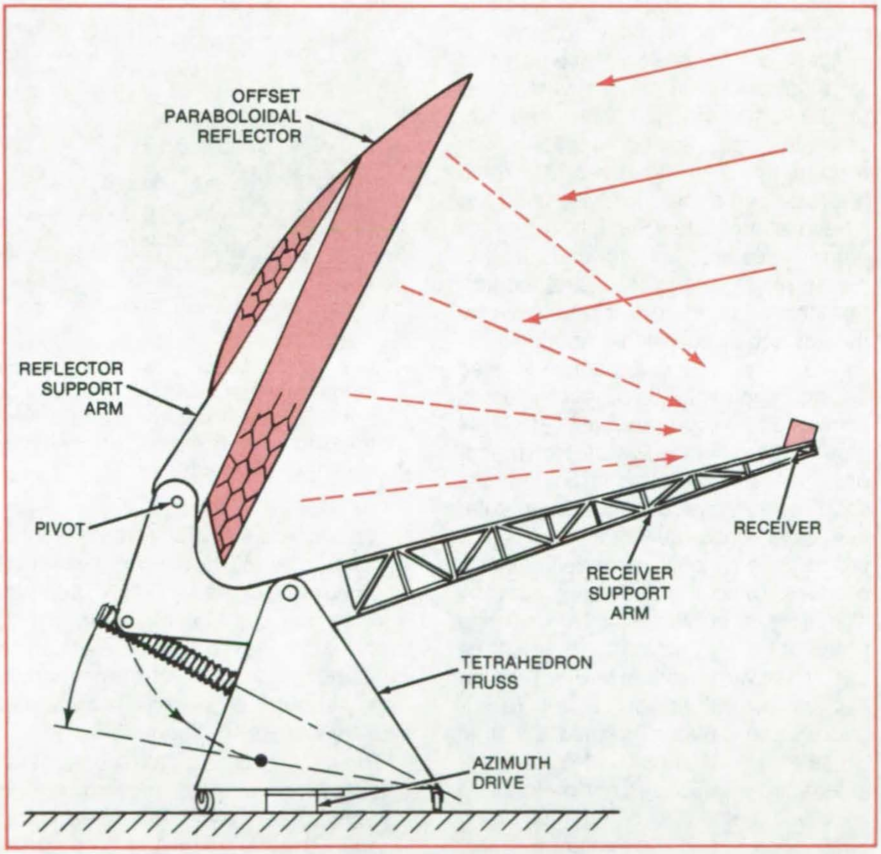

The **Offset-Paraboloidal Reflector** receives all of the incoming light and reflects it without obstruction to the receiver. Because the reflector can be folded toward the receiver, wind loading is reduced and maintenance is made easier.

This work was done by Edwin Y. Chow of Caltech for **NASA's Jet Propulsion Laboratory.** *For further information, Circle 19 on the TSP Request Card.*
NPO-14846

Miniature Personal UV Solar Dosimeter

Small light-powered meter measures accumulated radiation in the ultraviolet or other selected regions.

Langley Research Center, Hampton, Virginia

A miniature integrating light meter originally developed for use in space has many other possible applications. Small enough to be worn unobtrusively, it can measure accurately the radiation dose accumulated for a few minutes or over a period of weeks. It can measure total light or selected wave bands, such as UV or IR.

The primary practical advantages of the dosimeter are its potentially low cost, small size, accuracy, and adaptability to specific wave-band measurements. Medical applications suggested include as a research tool for studies of skin cancer, vitamin D production, and jaundice and for possible use in conjunction with treatments involving Sunlight exposure. It could be further used to measure integrated Sunlight for solar-energy design, for agriculture and meteorology, and to study and monitor the stability of materials and environmental and occupational lighting.

The meter uses a planar-diffused silicon photovoltaic detector as a sensor and a commercially available electrochemical coulometer to measure light accumulation. Conventional solar dosimeters use a silicon solar cell or a photomultiplier tube as a sensor. Solar cells are designed to produce maximum power output by matching internal resistivity during manufacture to the loads they will be used to power. While useful for power applications, their low shunt resistance is the cause of limited dynamic range and poor linearity if a constant low-impedance load is not maintained across the junction when measuring light. The need to maintain this artificial load to insure operation in the short-circuit-current mode reduces sensitivity unless supplemented by external signal-conditioning electronics that make the meters too complex and bulky for a miniature personal meter.

In contrast, the photovoltaic detector has a shunt resistance on the order of megohms and behaves more nearly as an ideal current source under typical loading conditions for light measurement. Reasonable variations in load resistance within the measurement circuit will not adversely affect photocurrent linearity. This linearity allows the use of a small, inexpensive, commercially-available electrolytic coulometer for photocurrent integration without the desensitizing shunt resistor across the junction.

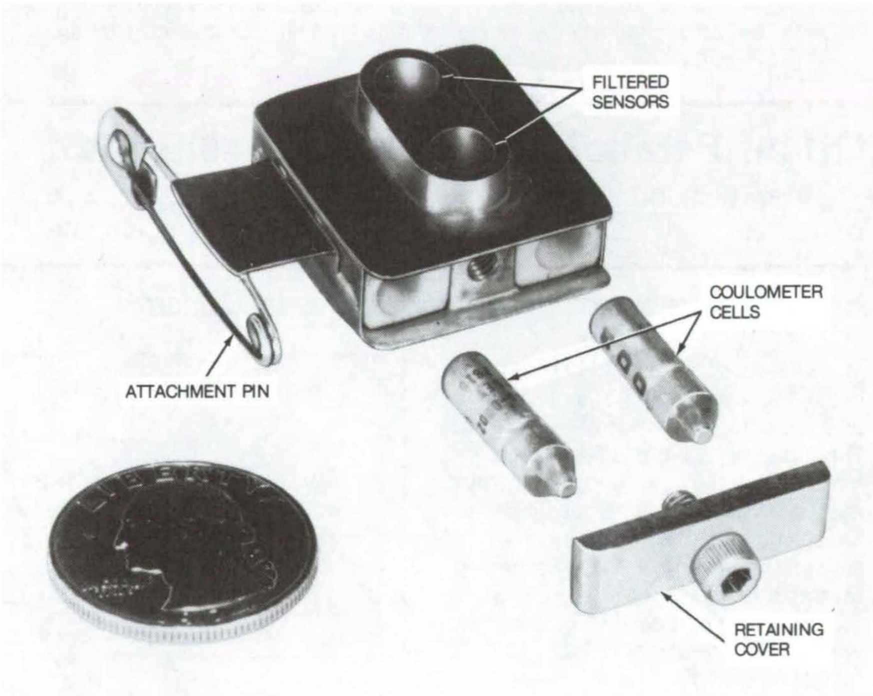

Figure 1. **UV Solar Dosimeter** currently undergoing tests was assembled from components that weigh 5 g and occupy 1.4 cm^3 exclusive of packaging. Under normal daylight, exposure over the band 250 to 400 nm was readily measurable on an hourly-to-a-weekly basis, with daily measurements being the best tradeoff between sensitivity and integration range.

The electrochemical coulometer selected accurately measures the quantity of electrical charge passing through it by transferring a mass of silver directly proportional to the input charge. Since the plating and deplating of silver are the only electrochemical reactions taking place, the coulometer operates with virtually 100 percent charge efficiency. Total radiation is determined by measuring the time required to deplate the silver using a constant current source.

Since virtually all of the photocurrent is recorded linearly, the junction area required is reduced from several square centimeters to a few square millimeters, yet sensitivity is sufficient to allow optical filtration for wave-band selection.

Figure 1 shows a prototype dosimeter currently being tested, and Figure 2 is a schematic of the dosimeter and a cell-readout circuit. There is also commercially available equipment for automatic readout and reset of the cells.

The dosimeter can be used to detect selected wave bands by using filters. The pair of cells in Figure 2a is used to measure a selected band of UV radiation. One filter, Schott UG-11, blocks light in the visible and admits UV (250 to 400 nm) and IR (mostly 660 to 800 nm). The other filter, Schott WG-305, blocks UV from 250 to 320 nm, passes UV from 320 to 400 nm, and passes IR. The difference between the radiation accumulations in the cell with the first filter only and

in the cell with both filters is the UV radiation over the wave band 250 to 320 nm. This example is of particular interest because it simulates the spectral response of human skin erythema and could be useful in clinical studies.

The coulometric cells currently retail for less than $5 and are accurate to within 2 percent. They can record up to 3,600 mA-s and are reusable indefinitely. The sensor can be larger or smaller, depending on the bandwidth and application desired. It was found that statistically significant readings of UV exposure in the 250-to-400-nm band can be obtained in open shade in 1 minute with only 5 mm^2 of filtered detector area per sensor.

The sensor is readily calibrated (relating mA-s reading to J/cm^2) in the laboratory using standard photometric procedures. The dosimeter should be packaged to allow the spring-loaded cells to be removed and replaced easily in the field. They can be read by removing the cell and using a circuit like that in Figure 2b. It would probably be most convenient to mail them to a central location.

This work was done by Richard R. Adams, Ian O. MacConochie, and Bordie D. Poole, Jr., of **Langley Research Center.** *For further information, Circle 20 on the TSP Request Card.*

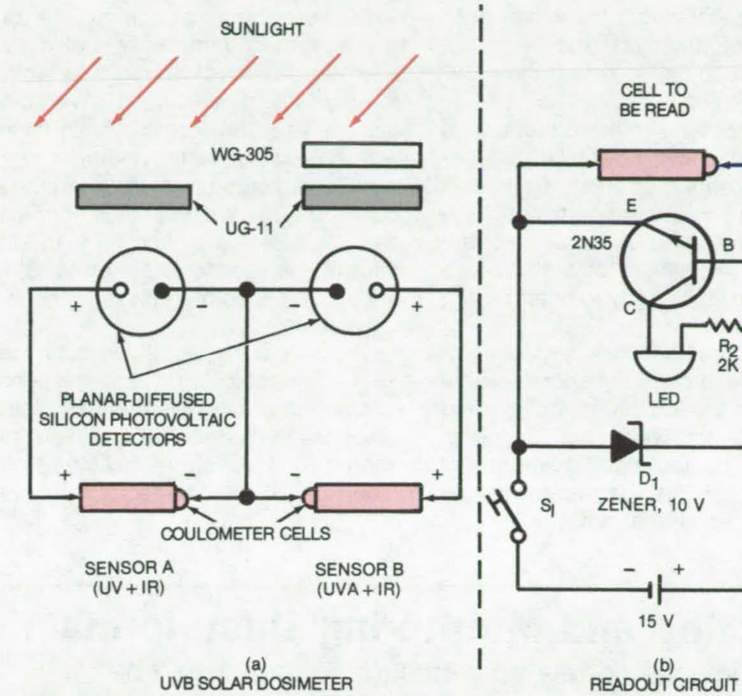

Figure 2. **Measurement and Readout Circuits** for the UV dosimeter are simple and inexpensive to build. The two-cell dosimeter, on the left, uses selective filters to allow measurement of a specific UV band. In the readout circuit on the right, the battery, R_3, and D_1 form a constant voltage source. When S_1 is closed, R_1 sets the read current through the cell to a constant 1 mA. When all the silver has been deplated, cell resistance increases abruptly, causing the transistor to conduct and the LED to light; then S_1 is opened. The product of the current and the time (monitored by a stopwatch) is proportional to the amount of silver transferred.

This invention is owned by NASA, and a patent application has been filed. Inquiries concerning nonexclusive or exclusive license for its commercial development should be addressed to the Patent Counsel, Langley Research Center [see page A5]. Refer to LAR-12469.

Economical Ultraviolet Radiometer

Compact cosine-corrected radiometer measures total ultraviolet insolation.

NASA's Jet Propulsion Laboratory, Pasadena, California

The simple, economical ultraviolet radiometer shown in the figure is suitable for field use. The new radiometer measures the ultraviolet radiation from Sun and sky, integrated over the celestial hemisphere. It has possible applications in testing materials for the effects of ultraviolet exposure and in studies of solar-cell degradation by ultraviolet.

The components of the radiometer include:

- a cup-shaped diaphragm and diffusing dome to obtain a cosine-corrected response,

(continued on next page)

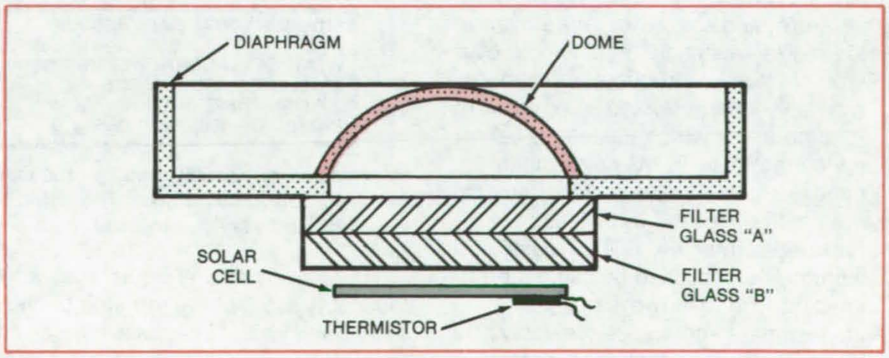

This **Ultraviolet Filter Radiometer** has cosine-corrected response. The radiometer is approximately 2 in. (5 cm) in diameter.

• two filters that select the wavelength range to be detected, and
• a silicon solar cell to detect the ultraviolet radiation.

The radiometer diffusing dome is made from sheet polytetrafluoroethylene. It covers a circular aperture in the bottom of the cup-shaped diaphragm. The radius of curvature of the dome and the height of the cup are determined empirically to optimize the cosine correction.

The radiometer uses a two-component filter to control response within a passband around 300 to 400 nm and to obtain a long-wavelength cutoff at 400 nm. The passband response is optimized for 300 to 400 nm and extends to about 280 nm.

Because the radiation arrives diffusely rather than as a collimated beam, absorptive rather than interference filters are used. The filter glasses used are commercially available. Glass A has the required long-wavelength cutoff near 400 nm and is chemically stable. Since this filter also has a low-level passband in the infrared, a second filter (glass B) is added to absorb radiation in that unwanted region.

The detector is a silicon solar cell with enhanced ultraviolet response characteristics. To achieve linear response to the incident radiation, the short-circuit current is measured with a current-to-voltage operational amplifier circuit. Its output may be fed to a data logger.

The solar-cell sensitivity varies a few percent over the temperature range expected in field use. To monitor temperature, a thermistor is attached to the back of the cell and connected to a bridge circuit. The thermistor data can be used to correct the radiometer readings for temperature.

This work was done by Clay H. Seaman of Caltech and Roger S. Estey of Kirk-Mayer, Inc., for **NASA's Jet Propulsion Laboratory.** *For further information, Circle 21 on the TSP Request Card.*
NPO-14843

Predicting and Monitoring Duststorms

Satellite images correlated with surface data would be transformed into color maps depicting duststorms.

NASA's Jet Propulsion Laboratory, Pasadena, California

A proposed duststorm-monitoring system combines surface data with stereoimage data from two geosynchronous satellites viewing the same area, or a geostationary satellite capable of providing stereoimages. The combined information would be processed at a field center, using correlation and image-enhancement algorithms. A series of maps generated this way would reveal the storm direction, warning areas in the path of the storm from zero to 24 hours before they are struck.

Duststorms are generally associated with large-scale meteorological events, such as rapidly-changing surface pressure, humidity, air temperature, and soil temperature over an area. The resulting high winds over eroding areas produce dustclouds, typically characterized by upward rotating fronts with a dustcloud center appearing 7° to 25° C colder than the edges. Such temperature gradients are easily recorded by satellite via IR (infrared) imaging. The dustcloud altitude is established by using stereoimaging from the two satellites. Thus an estimate could conceivably be made, from the dust in the atmosphere, of the amount of soil eroded. These data could be useful for agricultural productivity forecasts.

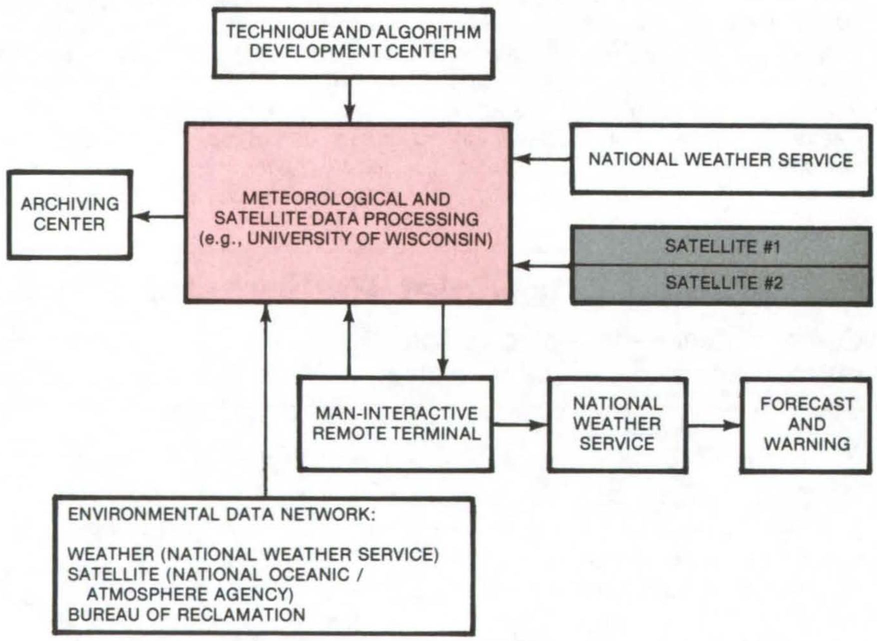

Information on Duststorms is processed by a terminal receiving signals from two geosynchronous satellites. The satellite information is correlated with that of other agencies and services to produce a series of maps of the storm area.

The accompanying figure shows all the inputs available to the field center. The IR and visible images are received from the two satellites; meteorological data are accessed through telephone links to several existing agencies. For example, the Data Archiving Center of the University of Wisconsin collects weather data from the Weather Service. The university also has its own meteorological data-processing system. In addition, the University of Wisconsin receives satellite data directly from two current geosynchro-

nous satellites and archives the data for processing.

The visible-image data and the IR data can be combined and registered on a grid. The images would be validated by reference to surface-data maps provided by the other agencies and recorded on photographic plates.

As an alternative, the analog video-tape-recorded frames may be digitized for further processing. The video-image is transformed by a digitizer into pixels. The pixel value associated with the IR image is split into bands, using color codes corresponding to recorded temperature gradients. The result is a composite map of superimposed visual and infrared images clearly defining the temperature gradients of the duststorm area. A series of these maps produced over a relatively-short time period would indicate the storm direction and is used in predicting its path.

This work was done by Peter M. Woiceshyn of Caltech for **NASA's Jet Propulsion Laboratory.** *For further information, Circle 22 on the TSP Request Card.*
NPO-14277

Noise Suppression in Forward-Scattering Optical Instruments

Apertures and stops reduce noise due to light scattered by the instrument optics.

Langley Research Center, Hampton, Virginia

Signal-to-noise ratio in forward-scattering optical instruments is increased by a combination of apertures and stops located at conjugate points in the receiver optics. Light scattered from the optics (such as from dust on the transmitter lens) is blocked, while light scattered from the sample volume is hardly affected.

The technique suppresses noise caused by scattered light in the forward-scattering laser velocimeter illustrated schematically in the figure. The transmitter optics cross and focus four laser beams at a point of interest in the sample region of a flow field. The receiver lens forms an image at the detector of light scattered from the sample.

The aperture plate next to the transmitter lens contains holes just large enough to pass the laser beams. Thus, it serves two functions: It is a baffle that stops stray light, and it is the aperture through which all light that passes through the transmitter optics must pass. The receiver lens, in addition to forming an image of the sample at the detector, also forms an image of the aperture plate at a plane that lies between the lens and the detector. If a stop plate that is the inverse of the aperture plate is placed in this plane, it will block the main laser beams and any undesired scattered light that passes through the aperture plate from the transmitter optics. The blockage of light scattered from the sample volume is minimal.

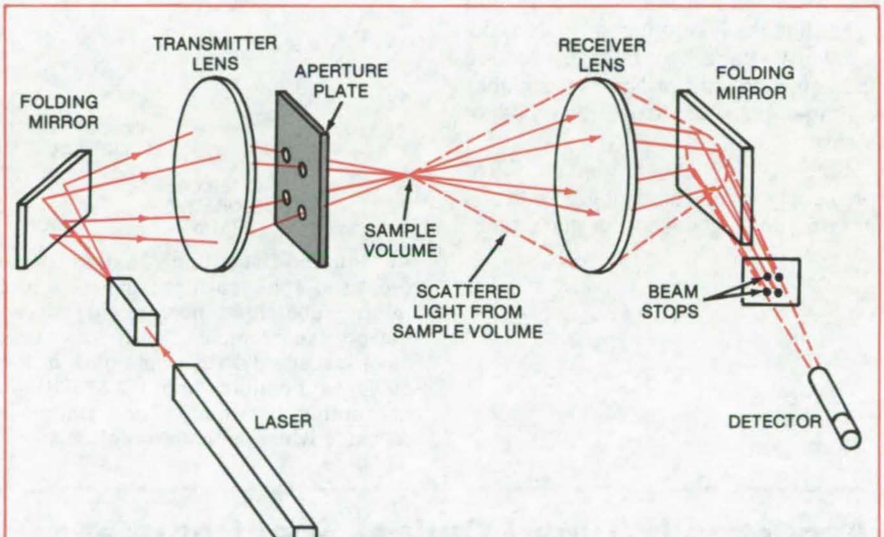

Apertures and Stops Reduce Noise due to scattered light in this laser velocimeter. The apertures and stops are placed and sized as if they were real, inverse images of each other in the receiver lens. Only light scattered from the sample volume reaches the detector.

Development of a prototype laser velocimeter is complete. The noise-suppression technique increased the signal-to-noise ratio on the order of 15 dB. The technique is not restricted to laser velocimeters and is applicable to other forward-scattering optical instruments.

This work was done by John M. Franke and Luther R. Gartrell of **Langley Research Center.** *No further documentation is available.*
LAR-12730

Energy-Reduction Concept for Incandescent Lamps

Reusable infrared reflector proposed to maintain
filament temperature and reduce power requirements

Lyndon B. Johnson Space Center, Houston, Texas

A concept for a coated, spherical light fixture may allow ordinary incandescent lamps to produce more light for a given wattage. The fixture, coated on the inside with a thin layer of infrared-reflecting material, would be installed over the light bulb (see figure). Instead of infrared energy being lost, it would be directed back to the incandescent lamp filament by the selective coating. The reflected energy would aid the electric current in heating the filament and would allow a lower-wattage light bulb to produce the same amount of light as a higher wattage bulb in an ordinary light fixture.

Some incandescent lamps have previously been assembled with an infrared coating inside the glass bulb.

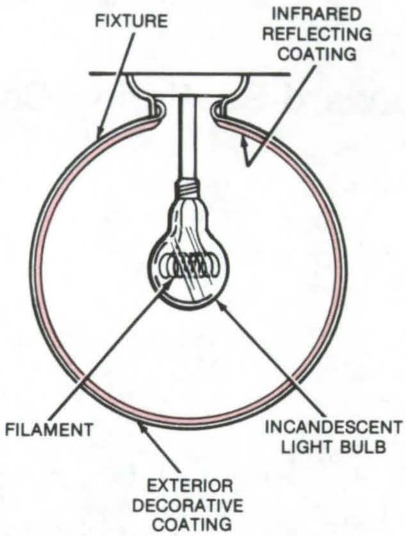

An **Infrared-Reflecting Coating** on a proposed spherical light fixture would return substantial heat energy to an incandescent lamp so that it draws less electrical energy, yet would glow at the same temperature (about 2,870 K) as conventional lamps. The globe is reusable when lamps are replaced.

This scheme is costly, however, since the coating is expensive and has to be discarded when the bulb burns out. With the coating as part of a separate fixture, it can be used indefinitely over the lifetimes of many lamps.

The fixture must be spherical to reflect the infrared energy back to the filament of the light bulb. To make it more attractive, the fixture could have a decorative exterior coating. Work would have to be done to select the optimum reflective-coating material and thickness and to choose a compatible substrate.

This work was done by Kenneth H. Vorhaben of Lockheed Electronics Co., Inc., for **Johnson Space Center.** *No further documentation is available.* *MSC-18757*

Acoustically-Tuned Optical Spectrometer

A novel lens arrangement corrects for aberrations
and gives a resolution of 0.7 seconds of arc.

NASA Headquarters, Washington, D.C.

A new imaging spectrometer can be electronically tuned to view an object at a selected wavelength between 6,500 and 14,000 angstroms. The spectrometer includes a two-element birefringent crystal in an acoustically-tunable optical filter (ATOF). Although such two-element ATOF devices are effective filters, they normally introduce severe optical aberrations when used for imaging; however, the new spectrometer corrects these aberrations with a cylindrical lens tilted away from the optical axis. The spectrometer combines 15-Å spectral resolution with a spatial resolution of 0.7 seconds of arc (as compared to 5 seconds of arc in a previous ATOF spectrometer).

The filter employs a pair of crossed calcite polarizers. One polarizer is placed at the filter input and the other at its output face. The acoustically tuned element between the polarizers is a birefringent calcium molybdate crystal (see figure). Acoustic waves generated by a radio-frequency voltage-controlled oscillator and a piezoelectric transducer propagate along the axis of the ATOF. Light from the object is polarized by the input polarizer and passes through the crystal in the same direction as the acoustic waves. The light interacts with the acoustically strained crystal in such a way that only a narrow range of wavelengths (determined by the acoustic frequency) is converted to the orthogonal polarization state. At the output end, the second polarizer passes the filtered wavelengths.

The ATOF actually consists of two pieces of calcium molybdate separated by an air gap at an angle of 28° with the normal to the optical axis. The purpose of the second piece is to redirect the light so that it emerges parallel to the axis. However, because

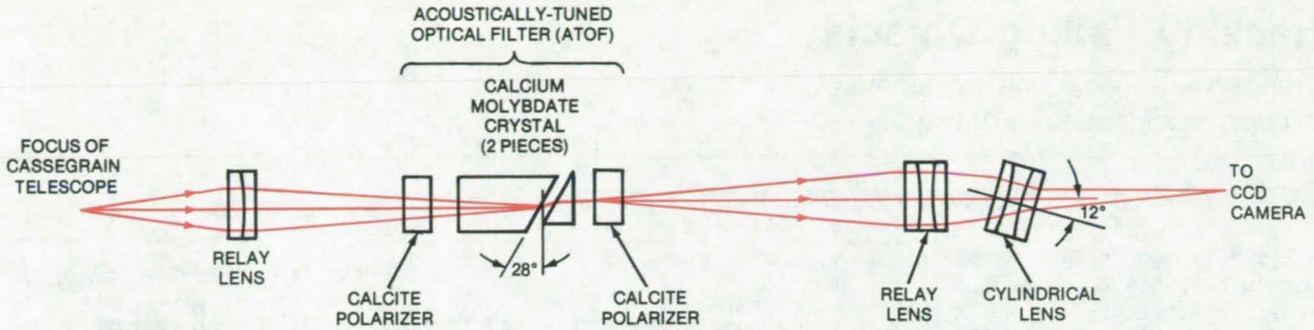

In an **Imaging Acoustic/Optical Spectrometer,** light from a telescope is relayed by a doublet lens to an acoustically-tuned optical filter. The selected wavelengths are relayed by a triplet lens to a charge-coupled-device camera. An intervening cylindrical lens, tilted at a 12° angle, corrects for astigmatism and coma introduced by the two-element birefringent crystal in the filter.

the rays are almost tangent to the 28° faces, severe astigmatism and coma are introduced.

A simple cylindrical lens could correct the astigmatism, but not the coma. However, if an achromatic cylindrical lens is tilted 12° from the optical axis, the off-axis aberration of the lens would compensate for the extreme coma and also correct the astigmatism.

The beam from the tilted cylindrical lens is directed to a charge-coupled-device (CCD) camera, which converts the light image to an electrical signal for recording and display on a screen.

This work was done by Edward Sklar of American Science and Engineering, Inc., for **NASA Headquarters.** *For further information, Circle 23 on the TSP Request Card.*
HQN-10924

Combined Photovoltaic and Thermal-Storage Module

Wax, a phase-change heat absorber, cools the module and stores energy for space and water heating.

NASA's Jet Propulsion Laboratory, Pasadena, California

A proposed photovoltaic module would use a phase-change heat-absorbing wax to reduce peak temperatures, thus increasing its electrical efficiency. In addition, the heat absorber could make the module more cost-effective by storing thermal energy for air and water heating.

The photovoltaic module normally operates at a cell temperature of 41° to 47° C. However, as the temperature increases, the open-circuit voltages decrease linearly by about 2.2 millivolts per °C, reducing the power output.

The aluminum box enclosing the photovoltaic module can incorporate a heat absorber that will limit the temperature rise. It has been found that eicosane, a wax having a melting point of 36.7° C (4° to 7° C less than the normal operating temperature of the module) reduces the module temperatures by about 5 percent and improves the diurnal power output by 2 to 2.5 percent.

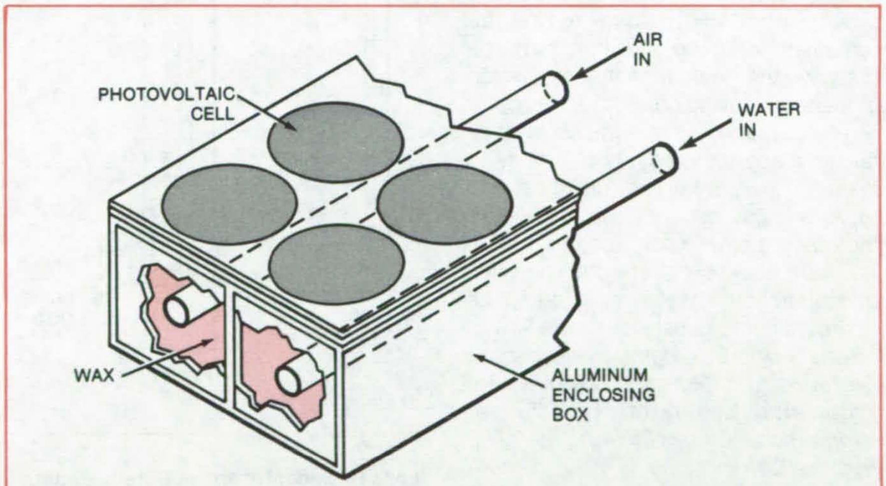

A **Wax Phase-Change Heat Absorber** reduces the photovoltaic module operating temperature while storing the latent heat of fusion. This heat can be used for water and space heating by passing conduits containing air or water through the module.

Although reducing the photovoltaic module temperature by using a wax phase-change material makes the module more expensive, the added costs could be offset if the thermal energy stored in the material is utilized. This could be done by circulating building air or water to be heated through the thermal-storage area. At the wax melting point, more energy can be stored with about 15 percent less weight than with water.

This work was done by James W. Stultz of Caltech for **NASA's Jet Propulsion Laboratory.** *For further information, Circle 24 on the TSP Request Card.*
NPO-14591

Tracking Falling Objects

A moving lens follows the movement of an object accelerated by gravity.

NASA's Jet Propulsion Laboratory, Pasadena, California

Objects in free fall are viewed at constant magnification by an optical carriage mechanism. The object is viewed continuously by a movie or TV camera for studies of the dynamics of free fall. A prototype is used in experiments on the formation of glass coatings on nuclear fuel pellets as they fall under the influence of gravity.

As shown in the figure, the system consists of an optical carriage on a vertical track and a fixed telescope that is attached to a camera. The carriage holds a lens that collimates rays of light reflected from the falling object. To have constant magnification, the distance from the object to the lens is equal to the focal length of the lens, and the telescope is focused at infinity.

The carriage travels on the vertical track, composed of an H-beam, as it falls with the object. Three wheels, with grooved edges to minimize rolling friction, guide the carriage along the beam. A small motor supplies the power needed to overcome the remaining drag so that the carriage matches the gravitational acceleration of the freely falling object.

The carriage has been used to track falling glass spheres about 2 cm in diameter over a vertical distance of 2 m. A long fluorescent lamp, parallel to the object path, illuminates the object. The light could be strobed for a series of stop-action images, or it could be operated continuously for movie films.

This work was done by Robert E. Frazer of Caltech for **NASA's Jet Propulsion Laboratory**. *For further information, Circle 25 on the TSP Request Card.*

This invention is owned by NASA, and a patent application has been filed. Inquiries concerning nonexclusive or exclusive license for its commercial development should be addressed to the Patent Counsel, NASA Resident Office-JPL [see page A5]. Refer to NPO-14813.

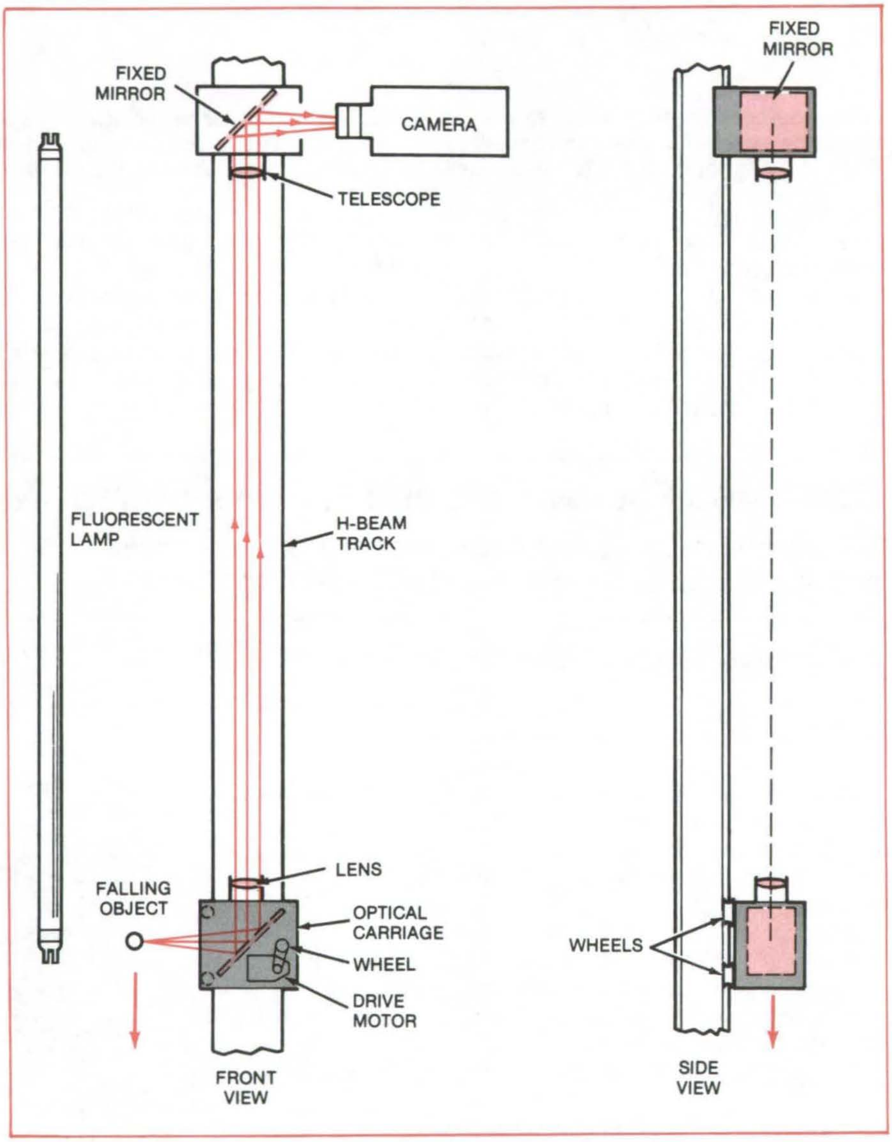

Lenses and Mirrors maintain constant magnification regardless of the distance between the moving carriage and the fixed telescope.

Diplexer for Laser-Beam Heterodyne Receiver

A four-prism interferometer superposes a local-oscillator beam on the signal beam, with all power output through one port.

Goddard Space Flight Center, Greenbelt, Maryland

The signal and local-oscillator beams of a laser communications system are combined in an interferometric diplexer that delivers all of the incident light energy to a single output port. The superposed beams, with phase fronts parallel, can then be directed onto a mixer to generate a difference frequency carrying the signal information, as in other heterodyne detection systems.

The three major advantages of the interferometric diplexer over laser-beam combiners used in the past are:
1. All of the power of the signal and local-oscillator beams emerges from one port, which is determined by the adjustable position of one of the prisms.
2. The output port is spatially separated from the input ports.
3. There is no limitation on how large the frequency difference between the two signals may be.

The diplexer, presently under construction, consists of four 90° prisms, as shown in the figure. The perpendicular faces of each prism are covered with either beam splitters or mirrors. Three of the prisms are fixed, but the top one can be translated along the direction of input beam 2.

Collimated beams entering at inputs 1 and 2 are split into two paths: One path propagates to the right and around the lower part of the configuration, and the other path propagates upward and around the upper part of the configuration. The two beams recombine at the second beam splitter, so both input beams contribute to both output ports. The path-length difference is adjusted by translating the movable prism.

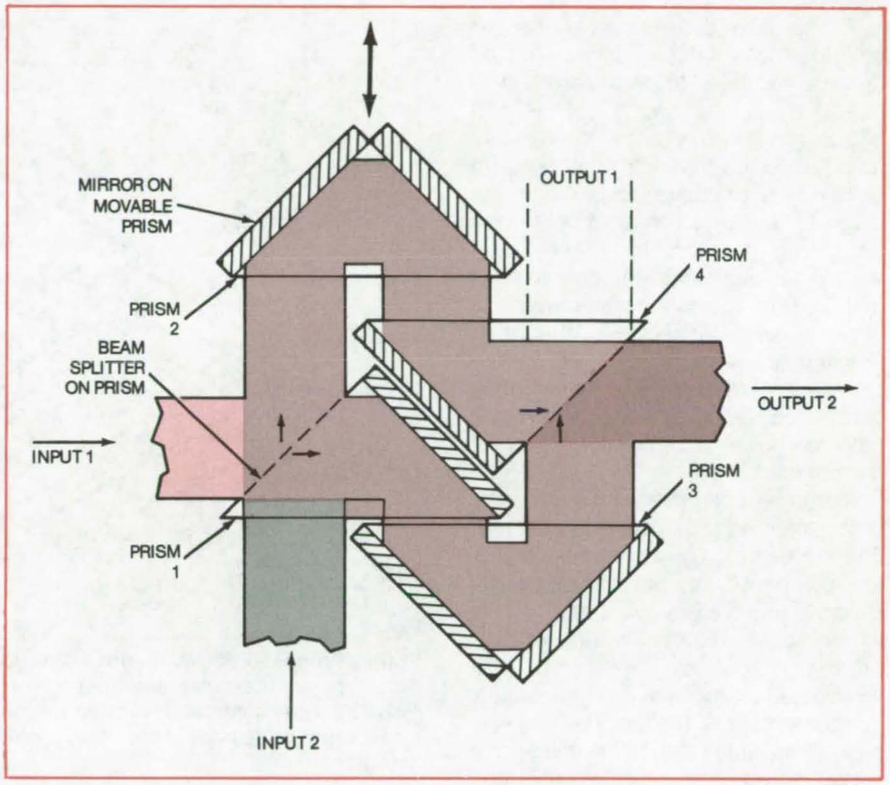

This **Diplexer for Laser Beams** superposes a local-oscillator beam on a signal beam. The movable prism can be positioned so that all of the incident energy in both beams emerges from just one of the two possible output ports — here, output 2. If an additional half wavelength is added to the path difference, then all the light exits from output 1 and no light emerges from output 2.

For each input frequency, the difference in path lengths can be adjusted to give constructive interference at either output port 1 or output port 2. To satisfy the condition of constructive interference simultaneously for both frequencies, the path difference is set at $c/2\Delta f$ (where c is the speed of light and Δf is the difference between the two frequencies). The movable prism is moved toward the fixed prisms for a large Δf value and is moved away for a small Δf. No limitation exists for large Δf values; but for low Δf, diffraction losses degrade the transmission function.

This work was done by Gerhard Koepf of Phoenix Corp. for **Goddard Space Flight Center**. *For further information, Circle 26 on the TSP Request Card.*
GSC-12589

Powerful Copper Chloride Laser

Flowthrough design avoids overheating in a 300-W laser amplifier.

NASA's Jet Propulsion Laboratory, Pasadena, California

The proposed high-power copper chloride pulsed laser shown in the figure is expected to produce a 300-W beam at wavelengths of 510.6 and 578.2 nm. Two design innovations give an up-to-thirtyfold increase in power over previous copper chloride lasers: (1) Heat is removed by flowing the lasing gas through the system, allowing larger lasing volumes; and (2) fast, uniform excitation discharges are obtained with transverse, rather than longitudinal, electrodes. Preliminary tests with experimental dissociating electrodes and pulsed discharges have demonstrated the feasibility of the concept.

In copper chloride vapor lasers, the lasing efficiency is about 1 percent. The remaining 99 percent of the energy from the pulsed discharge must be removed to avoid heating the vapor above the maximum temperature at which lasing will occur. In a low-power laser, the heat is simply conducted away by the walls of the small-bore tube that contains the vapor. However, the small tube volume has limited the output of previous copper chloride lasers to about 10 W. Large increases in power require amplifiers with cross sections too large to cool by conduction.

In the proposed laser, copper vapor and a buffer gas (e.g., helium) are pumped through the amplifier just fast enough to prevent its temperature from exceeding 3,000 K as it is heated by the pulsed discharge. (Above 3,000 K, certain excited copper states are overpopulated, and a population inversion cannot occur.)

The design parameters of the proposed laser are based on experiments with hollow-cathode discharges (for dissociating copper chloride) and fast-rise-time pulse discharges (to produce a population inversion). Data from the hollow-cathode discharge work indicate that the copper chloride vapor is dissociated predominately into ground-state copper atoms. In the experiments with fast transverse pulse discharges, lasing occurred at buffer gas pressures between about 100 and 200 torr (1.3 to 2.6×10^5 N/m^2), pulse repetition rates between 1 and 2×10^4 Hz, and 8 to 10 kV peak voltage drop between the electrodes.

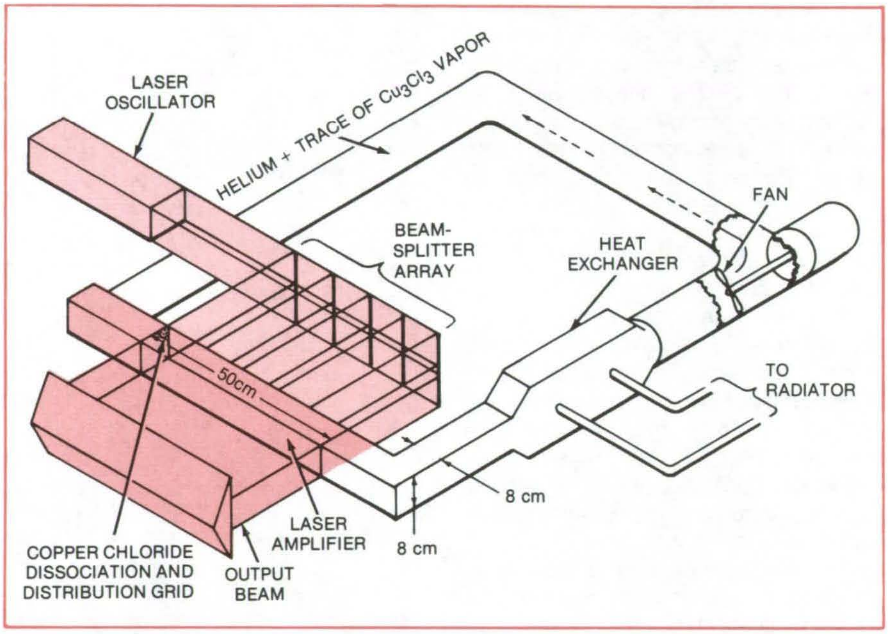

In this **Proposed 300-W Copper Chloride Laser,** a fast-rise-time transverse pulsed discharge in the laser amplifier pumps the lasing gas. Lasing occurs between resonant and metastable excited states in copper. Copper chloride is dissociated into ground-state copper atoms by a hollow-cathode grid at the entrance to the laser amplifier.

To create a population inversion between the resonant and metastable states of the copper atom that are involved in the lasing, the pumping must be fast. This is possible with low-inductance pulsed-discharge circuits that give an initial rate of current rise of about 10^{10} amperes per second and pulse widths of about 100 ns.

This work was done by Thomas J. Pivirotto of Caltech for **NASA's Jet Propulsion Laboratory.** *For further information, Circle 27 on the TSP Request Card.*

This invention is owned by NASA, and a patent application has been filed. Inquiries concerning nonexclusive or exclusive license for its commercial development should be addressed to the Patent Counsel, NASA Resident Office-JPL [see page A5]. Refer to NPO-14782.

Books and Reports

These reports, studies, and handbooks are available from NASA as Technical Support Packages (TSP's) when a Request Card number is cited; otherwise they are available from the National Technical Information Service.

Heat for Film Processing From Solar Energy

A commercial film-processing lab gets most of its hot-water energy from the Sun.

A solar water-heating system for a commercial building is described in a final report. Installed in the Iris Images photo laboratory in Mill Valley, California, the system furnishes 59 percent of the hot-water requirements for photographic film processing. The 120-page report describes the site and building, the solar-energy system, and problems and modifications. It analyzes performance and economics, and it supplies drawings and an operation and maintenance manual.

The system uses 640 ft^2 (60 m^2) of flat-plate collectors on the roof to produce 6 gallons of hot water per minute at at least 100° F (38° C) for 8 hours per day. The hot water is stored in tanks having a total capacity of 360 gallons (1,332 liters). The solar-heated water from the tanks passes through an auxiliary gas-fired heater, which adds heat if necessary to raise the water to the required temperature. The hot water is then piped to the film processors and to six sinks and two bathrooms.

The film processors require water at temperatures between 75° and 100° F (24° and 38° C), depending on the type of film being developed. The hot water from the solar panels and auxiliary heater is mixed with cold water to the desired temperature at each unit.

A low-temperature (less than 120° F, 49° C) industrial process such as film developing is an ideal application for solar heating. With a constant year-round daytime load, storage requirements are minimized and solar utilization is maximized. High collector efficiency can be expected because of the relatively-low hot-water temperature.

The solar collectors are not prefabricated, but instead were constructed on the site. The collector array faces due south and is tilted 36° from the horizontal. It consists of a bank of 12 collector panels and another bank of 4 collector panels, each panel measuring 4 by 10 ft (1.2 by 4 m). The first bank has an aluminum absorber plate that is bonded to copper tubing. The second bank has a copper absorber plate that is soldered to copper tubing. Both absorber plates are coated with flat black paint. A single panel of coated fiberglass covers the collectors. The report cautions that onsite fabrication is practical only where skilled, low-cost labor is available.

To prevent damage from freezing, a pump circulates water through the collector array whenever the temperature of either collector-bank absorber plate is below 36° F (2.2° C). If there is a power failure at freezing temperatures, the system automatically drains the collectors and exterior pipes.

This work was done by Interactive Resources, Inc., for **Marshall Space Flight Center.** *Further information may be found in DOE/NASA CR-161414 [N80-22781/NSP], "Solar Process Water Heat for the Iris Images Custom Color Photo Lab" [$10]. A paper copy may be purchased [prepayment required] from the National Technical Information Service, Springfield, Virginia 22161. The report is also available on microfiche at no charge. To obtain a microfiche copy, Circle 28 on the TSP Request Card.*
MFS-25444

Solar Heater/Cooler for Mass Market

Project aims for an affordable, easy-to-install system.

A 106-page report describes a project to design, build, and test a family of solar-heating/cooling systems for a mass market. Four basic systems were developed:

- Heating and Domestic Hot Water for Single-Family Dwellings;
- Heating and Domestic Hot Water for Commercial Buildings;
- Heating, Cooling, and Domestic Hot Water for Single-Family Dwellings; and
- Heating, Cooling, and Domestic Hot Water for Commercial Buildings.

The systems have been installed, or are planned for installation, in seven buildings scattered around the United States.

To keep manufacturing costs low, the systems use common parts and modular subsystems. To keep installation costs low, they are compatible with many types of heating, ventilating, and air-conditioning (HVAC) equipment and employ prepackaged controls and auxiliary units.

The solar collector for all systems has evacuated glass outer tubes, a metal reflector, and a heat-transfer fluid circulating in selectively-coated metal tubes. The control of fluid flow is based on a time average of insolation, as measured by an integrating sensor in the collector, rather than on instantaneous insolation; this reduces on/off cycling of the pump.

For heating, the fluid transfers its heat to water in a storage tank, which transfers its heat to forced air. For cooling, the stored water delivers its heat to a heat pump, which cools air or water circulating through the building.

The report describes the plan for the project, the systems and their components, the test sites, and performance. The text is complemented by detailed drawings and test data.

This work was done by the Space Division of General Electric Co. for **Marshall Space Flight Center.** *Further information may be found in DOE/NASA CR-161422 [N80-24746/NSP], "Solar Heating and Cooling System Design and Development [Final Report]" [$9]. A paper copy may be purchased [prepayment required] from the National Technical Information Service, Springfield, Virginia 22161. The report is also available on microfiche at no charge. To obtain a microfiche copy, Circle 29 on the TSP Request Card.*
MFS-25452

Data-Acquisition and Control System for Severe Environments

Evaluation test procedures and results

An evaluation test program on a commercial solar data-acquisition and control system is documented in a new report. The program measured the accuracy and performance of the system subcomponents, including the interface wiring unit, power controller, and tape recorder, in a severe environment.

One proposed installation site, at Frenchman's Reef in the Virgin Islands, is an uncontrolled enclosed area near surfaces with higher than ambient temperatures and high relative humidity. Also, the supply voltage in the area varies in magnitude and frequency. Test parameters were established as: temperature 0° to 50° C, relative humidity 0 to 90 percent, supply frequency 54 to 66 cycles/second, voltage 103 to 127 volts, and temporary voltage dropout 10 milliseconds.

The evaluation was conducted in an environmental chamber for controlling humidity and temperature. Initial tests established unit temperature recording accuracy. A custom solar simulator was used to provide a simulated collector system. Two computer programs were written: a program to exercise the discrete digital outputs at 5-minute intervals and a program executed at 30-minute intervals to test thermistor inputs and analog voltage channels. The second program also exercised internal counters, discrete inputs and discrete outputs, and printed the time and system status.

Although the data-acquisition and control system performed as expected at 100° F (38° C) and 87 percent humidity, it failed to operate at 120° F (49° C). In some cases, a failure might result in false triggering of output drivers unless special shutdown precautions are taken.

The report features test program descriptions, sample readouts, and test results. A summary of the custom solar system simulator is included.

This work was done by Wyle Laboratories for **Marshall Space Flight Center.** *Further information may be found in DOE/NASA CR-161449 [N80-25783/NSP], "Test Results on the Frenchman's Reef Solar Data Acquisition and Control System" [$5]. A paper copy may be purchased [prepayment required] from the National Technical Information Service, Springfield, Virginia 22161. The report is also available on microfiche at no charge. To obtain a microfiche copy, Circle 30 on the TSP Request Card.*
MFS-25471

Commercial-Building Solar-Energy System — Stamford, Connecticut

Electrical energy consumption is reduced by half for a 2-1/2-story office building.

An efficient distributed heat-pump system and an electrical boiler backup, together with an almost-completely-empty flat roof that faces nearly due south, made the Executive East office building in Stamford, Connecticut, very attractive for a solar-energy retrofit. Solar energy now replaces more than half the total electrical energy previously used for heating, and it eliminates all the electrical boiler capacity used during peak daytime hours. A 93-page final report on the project includes detailed drawings and photographs, the operation and maintenance manual, the acceptance test plan, and other pertinent information.

The Stamford office building has 25,000 square feet (2,300 square meters) of heated space in 2½ stories. Its aluminum and glass curtain-wall construction is typical of office buildings built prior to the energy crisis. Located next to a major shopping center on a busy highway in Stamford, the building is oriented with its long axis pointing 5° west of south; the roof is flat and almost completely unobstructed. Zoning regulations restrict the construction of any nearby tall buildings that could block the Sunshine to the building.

Nearly 80 water-source heat pumps heat and cool the building. They are connected in series in a hydronic loop, which is always maintained between 75° and 85° F (24° and 29° C). When heating the building, a heat pump extracts heat from the hydronic loop. Prior to installation of the solar system, all the heat needed to maintain the loop temperature was supplied by two 75-kVA electric boilers.

One hundred and thirty-eight liquid flat-plate solar collectors, arranged in six rows, are mounted on the roof of the building. A polished aluminum reflector in front of each row increases the collected energy (by 46 percent during the winter). For protection against overheating or stagnation, the shutters are hinged and can be folded up as a shield for the collectors.

Solar energy is delivered to a 6,000-gallon (23,000-liter) stone-lined storage tank and, from there, to the building heat-pump loop. If the storage-tank temperature drops too low, the building loop can be heated by the electrical hot-water boilers.

This work was done by the Lutz-Sotire Partnership for **Marshall Space Flight Center.** *Further information may be found in DOE/NASA CR-161436 [N80-27800/NSP], "Solar Heating System Installed at Stamford, Connecticut" [$8]. A paper copy may be purchased [prepayment required] from the National Technical Information Service, Springfield, Virginia 22161. The report is also available on microfiche at no charge. To obtain a microfiche copy, Circle 31 on the TSP Request Card.*
MFS-25468

Solar-Heated and Cooled Office Building — Dalton, Georgia

A modern energy-efficient building is heated and cooled by solar energy.

Information on an energy-efficient Georgia office building equipped with solar heating and cooling is contained in a recently released report. Located on a 1.5-acre (6.1 x 10^3-m^2) lot near downtown Dalton, Georgia, the building is a modern two-story structure with 7,000 ft^2 (650 m^2) of office space and workspace. The energy collected in five rows of flat-plate solar collectors supplies a major fraction of the building heating and cooling demand, along with all of its modest domestic hot-water needs. Included in the 132-page final report are detailed drawings and

photographs, manufacturer's literature, performance specifications, acceptance test data (the plan and results), and performance verification statements. The operation and maintenance manual is also included.

The building is constructed with many energy-conserving features. Its western and northwestern first-floor elevations are buried into the sloping contour of the lot, reducing the summertime afternoon Sun load and minimizing the cooling effect of the winter wind. The square shape of the building has minimal exterior wall area, which also reduces the heating and cooling load. The two-story design minimizes the roof area. Window area has also been kept to a minimum and is protected from the Sun by generous roof overhangs. All windows are operable so that natural ventilation is available. The double-glazed insulation is shaded to block direct Sunlight.

Heating for the building is by the direct flow of solar-heated water to an exchange deck in the central air handler. The building is cooled by the flow of chilled water to a separate exchange deck. For cooling, solar-heated water drives a 25-ton (88-kW) absorption chiller. The backup or supplementary supply of heated water to drive the chiller and for building heat is supplied by a conventional oil-fired boiler. A multizone central processor controls the system in each of its heating and cooling modes. Day and night periods of heating and cooling are regulated by a standard automatic timeclock and an overriding thermostat.

This work was done by the North Georgia Area Planning and Development Commission for **Marshall Space Flight Center.** *Further information may be found in DOE/NASA CR-161273 [N80-11555/NSP], "Solar Energy System Installed at the North Georgia APDC Office Building" [$10]. A paper copy may be purchased [prepayment required] from the National Technical Information Service, Springfield, Virginia 22161. The report is also available on microfiche at no charge. To obtain a microfiche copy, Circle 32 on the TSP Request Card.*

MFS-25451

Solar-Heating and Hot-Water System — St. Louis, Missouri

Sunlight supplies about half the heat-energy needs of a small office.

A solar-energy system of more modest size than those of the two preceding articles is described in a new report. The system, installed in a St. Louis office building, supplements the winter heating load for a 900-ft² (84-m²) addition to the building and preheats the service hot water for the entire building. It includes 252 square feet (23.4 square meters) of "mildly-concentrating" commercial solar collectors and a 1,000-gallon (3,785-liter) energy-storage tank. The 67-page report contains a description of the system and its components, drawings and photographs, manufacturer's data, and other related material.

About 50 percent of building hot-water requirements and 45 percent of the space-heating needs of the addition are supplied by Sunlight. To maximize the collection efficiency, the tilt angle of the six solar collectors is variable and is adjusted seasonally. Energy is transferred to the 1,000-gallon storage tank through a tube-in-shell heat exchanger. Incoming city water is preheated in a smaller storage tank equipped with a heat exchanger.

This work was done by William Tao and Associates for **Marshall Space Flight Center.** *Further information may be found in DOE/NASA CR-161420 [N80-24744/NSP], "Solar Heating and Hot Water System Installed at St. Louis, Missouri — Final Report" [$7]. A paper copy may be purchased [prepayment required] from the National Technical Information Service, Springfield, Virginia 22161. The report is also available on microfiche at no charge. To obtain a microfiche copy, Circle 33 on the TSP Request Card.*

MFS-25453

Solar Heating for an Electronics Manufacturing Plant — Blue Earth, Minnesota

Space heating for a 97,000-square-foot plant is supplied partly by solar energy.

The heating system of a large manufacturing plant for tape recorders and other electronics in southern Minnesota has been refitted for solar energy as part of the Solar Heating and Cooling Demonstration Program. Described in detail in a 167-page final report, the system has been delivering space heat since February 1978.

The 97,000-square-foot (9,000-square-meter) building houses assembly areas, administrative offices, and a warehouse. It is constructed of steel, with 6 inches (15.2 cm) of fiberglass insulation between the steel skins. In cold weather, the space-heating load is 9 million to 12 million Btu (9.5×10^9 to 12.6×10^9 J) per day. There is little hot-water demand. Because it uses electric resistance heating, the plant was considered a good choice for adaptation to solar energy.

The 360 flat-plate solar collectors are mounted on a wood-and-concrete support structure adjacent to the building. Arranged in 10 rows of 36 collectors, each 4 by 8 feet (1.2 by 2.4 m), the solar array has a gross area of 11,520 square feet (1,071 square meters). Solar energy is stored as heat in a 20,000-gallon (75,000-l) water tank located inside the building.

The plant is heated by water-to-air heating coils in the nine already-existing air-handling units and three water-to-air heating coils. If the storage-tank temperature is insufficient to meet the heating requirements of a part of the building, the balance of the heat is supplied by electrical resistance heating. The system includes all the necessary control electronics for year-round operation. During the month of December 1978, solar energy supplied about 24.4 percent of the building space-heating load.

This work was done by Telex Communications, Inc., for **Marshall Space Flight Center.** *Further information may be found in DOE/NASA*

CR-161437 [N80-25786/NSP], "Solar Heating System Installed at Telex Communications, Inc., Blue Earth, Minnesota — Final Report" [$12]. A paper copy may be purchased [prepayment required] from the National Technical Information Service, Springfield, Virginia 22161. The report is also available on microfiche at no charge. To obtain a microfiche copy, Circle 34 on the TSP Request Card.
MFS-25469

Costs and Description of a Solar-Energy System — Austin, Texas

Heating and cooling system uses Fresnel-lens concentrating collectors.

The final report on a solar-energy system installed at the site of a Texas corporation includes a detailed breakdown of the costs of the project. Commercial concentrating solar collectors covered by acrylic Fresnel lenses are used in the heating and cooling system. The major system components are 36 concentrating collectors, a 1,500-gallon (5,700-l) thermal storage tank, an absorption cooler, a cooling tower, a heating coil, pumps, a heat exchanger, and backup heating and air-conditioning.

Each concentrating collector has a Fresnel lens [1 by 10 feet (0.3 by 3 meters)] to concentrate Sunlight onto a flattened copper absorber tube that has a black-chrome absorptive coating. A tracking mechanism focuses the Sunlight. Each collector has a pulley attached to a shaft at the lower end. A steel cable looped around the pulleys simultaneously rotates up to 20 collectors. A pair of photovoltaic cells senses the location of the Sun. An unbalanced output from these cells turns on a motor, which rotates the collectors through a gearbox and the cable.

A 3-ton (11 kW) lithium bromide air-conditioner provides space cooling. It requires 55,000 Btu/h ($58{,}000 \times 10^3$ J/h) heat input from solar-heated water to boil the water in the lithium bromide/water solution. The water vapor is passed over the condensing coils in the cooling tower, which extracts heat at the rate of 91,000 Btu/h ($96{,}000 \times 10^3$ J/h), for a net cooling rate of 36,000 Btu/h ($38{,}000 \times 10^3$ J/h).

The performance of this system is monitored by 47 sensors that measure temperature, flow rate, insolation, power, windspeed, and other parameters. Once every 5 minutes, the sensors are sampled, and the data are stored on cassette tape.

Component and installation costs are given for seven subsystems (e.g., collectors, storage tank, and controls). The costs of monitoring sensors, of installation, and of engineering are listed separately. The total of "essential" costs for the system installed in 1977 is $42,082.

This work was done by Radian Corp. for **Marshall Space Flight Center.** *Further information may be found in DOE/NASA CR-161442 [N80-25784/NSP], "Solar Heating and Cooling Demonstration Project at Radian Corporation, Austin, Texas — Final Report" [$6]. A paper copy may be purchased [prepayment required] from the National Technical Information Service, Springfield, Virginia 22161. The report is also available on microfiche at no charge. To obtain a microfiche copy, Circle 35 on the TSP Request Card.*
MFS-25472

Solar Energy in a Historical City — Abbeville, South Carolina

Direct-air solar heating does not alter building appearance.

A solar-heating system installed in the Abbeville, South Carolina, municipal building does not compromise approval of the building design by state and local historical societies. The flat-roofed two-story brick structure, which houses the police and fire departments and the recorder's court, is architecturally compatible with other buildings in this very old and historical city — a factor that was considered very seriously when planning the solar-energy system.

The system that met the architectural standards is a direct-air solar space-heating system with roof-mounted flat-plate collectors and a rock-storage bin. The collectors lie flat against the roof and are not visible from the ground. An air-handling unit coordinates the solar and backup heating systems by monitoring the temperatures of the outside air, the collector, the storage bin, and the building air. From these data, it controls the collection and distribution of solar heat.

"Natural" cooling modes supplement the building air-conditioning. Inside air is circulated through the rock-storage bin, allowing the rocks to absorb some of the heat from the air. When the outside air temperature drops below that of the rocks, the air handler circulates the outside air over the rocks to exhaust the heat to the outside.

Solar preheating of domestic hot water is possible when excess hot air in the collectors would be exhausted to the outside. At these times, water from a storage tank is circulated through a heat exchanger in the exhaust duct. Any additional heat required is supplied by an electric hot-water heater.

The 52-page final report on the system contains performance data, drawings, photographs, and other pertinent information. The installation manual for the air handler is included as an appendix.

This work was done by Gilliland-Bell Associates, Inc., for **Marshall Space Flight Center.** *Further information may be found in DOE/NASA CR-161443 [N80-25788/NSP], "Solar Heating and Hot Water System Installed at Municipal Building Complex, Abbeville, S.C. — Final Report" [$7]. A paper copy may be purchased [prepayment required] from the National Technical Information Service, Springfield, Virginia 22161. The report is also available on microfiche at no charge. To obtain a microfiche copy, Circle 36 on the TSP Request Card.*
MFS-25479

Municipal Recreation Center Is Heated and Cooled by Solar Energy — Dallas, Texas

A major fraction of heating, cooling, and domestic hot-water requirements is supplied by Sun energy.

The final report on the solar-heating and cooling facility at the North Hampton Park Recreation and Health Center, Dallas, Texas, chronicles the demonstration project from its inception in November 1975 through its

completion in July of 1978. Other material in the 115-page document is a summary of the project performance, costs, operating modes, and data-acquisition system. An appendix contains manufacturer's product literature and over 20 pages of engineering drawings.

The North Hampton Park Recreation and Health Center is a single-story structure enclosing a gymnasium, locker area, and health-care clinic. It is surrounded by a recreational area and an athletic field. Total building area is 16,000 square feet (1,486 square meters) of which one-half is the gymnasium, which is conventionally heated and not part of the solar-energy demonstration project.

The solar-energy system is designed to supply 80 percent of the annual space heating, 48 percent of the annual space cooling, and 90 percent of the heat for domestic hot water. It includes a solar-collector loop, hot-water energy storage, a domestic hot-water system, an absorption chiller, and chilled water storage. The collector loop heat-transfer medium is an aqueous solution of 35 percent ethylene glycol.

The 238 commercial flat-plate solar collectors are roof-mounted in 29 arrays. A heat exchanger transfers the collected energy to a 6,000-gallon (22,000-liter) storage tank insulated with 4 inches (10 cm) of urethane.

Space cooling is partly supplied by using solar energy to operate a commercial absorption chiller. The chilled water is stored in a 2,000-gallon (7,600-liter) tank. The balance of space cooling is supplied by two vapor compression units.

Domestic supply water is preheated by heat exchangers on the hot side of the absorption-chiller condenser loop and the hot-water storage-tank loop. A conventional natural-gas heater supplies any additional energy needed for domestic hot water.

This work was done by Travis-Braun and Associates, Inc., for **Marshall Space Flight Center.** *Further information may be found in DOE/NASA CR-161444 [N80-26766/NSP], "Solar Energy Facility at North Hampton Recreation Center, Dallas, Texas — Final Report" [$10]. A paper copy may be purchased [prepayment required] from the National Technical Information Service, Springfield, Virginia 22161. The report is also available on microfiche at no charge. To obtain a microfiche copy, Circle 37 on the TSP Request Card.*
MFS-25478

Solar Energy Meets 50 Percent of Motel Hot-Water Needs — Key West, Florida

When occupancy is less than 50 percent, no auxiliary energy is needed.

A final report describes a solar domestic-water preheat system installed in a 148-room motel in Key West, Florida. The solar equipment meets 50 percent of the domestic hot-water needs when the motel is 100 percent occupied; equivalently, it supplies 100 percent of the hot water when occupancy is 50 percent. Prior to the installation of the solar-energy demonstration project, domestic hot water was heated by an oil-fired boiler feeding a 500-gallon (1,900-liter) storage tank.

The energy demand estimate for the motel is 6.81×10^8 Btu/year (7.18×10^{11} J/year) of which 3.19×10^8 Btu/year (3.36×10^{11} J/year) are to be supplied by solar energy. The system consists of 1,400 square feet (130 square meters) of flat-plate liquid solar collectors, storage tanks, a pump, a controller, and other hardware. Cold water in copper tubing is circulated through the collectors, and the heated water is stored. At times when no hot water is being used, the stored water is continuously passed through the collectors. When hot water is needed, it is either transferred directly to the boiler storage tank or through the boiler to the tank, depending on the water temperature.

This work was done by Quality Inn of Key West for **Marshall Space Flight Center.** *Further information may be found in DOE/NASA CR-161434 [N80-23774/NSP], "Solar Hot Water System Installed at Quality Inn, Key West, Florida — Final Report" [$5]. A paper copy may be purchased [prepayment required] from the National Technical Information Service, Springfield, Virginia 22161. The report is also available on microfiche at no charge. To obtain a microfiche copy, Circle 38 on the TSP Request Card.*
MFS-25454

Solar-Heated Office Complex — Greenwood, South Carolina

System meets 85 percent of heat requirements.

A Greenwood, South Carolina, office complex, completed in 1975, is 85-percent heated by solar energy. The system uses roof-mounted recirculating-water solar panels and underground hot-water energy storage. Aluminum-film reflectors increase the total solar flux captured by the panels. A thorough documentation of the project is contained in a recently-released final report.

Solar energy captured as heat and stored in the underground water tank is transferred to the building air at a coil located in the hot-air duct. A heat pump downstream of the coil and an electric resistance heater in the duct add additional heat when needed. Service water is heated by a single-wall, tube-bundle heat exchanger immersed in the storage tank. Its heat is augmented by an electric water heater.

Domestic city water mixed with a corrosion inhibitor is the heat-transfer fluid in the collector loop. The water is prevented from freezing by automatic drain-down instrumentation.

The solar-heated area of the office complex is 4,284 square feet (398 square meters). A total of 954 square feet (89 square meters) of collector area supplies 85 percent of the heating requirements of this area.

This work was done by W. E. Gilbert & Associates, Inc., for **Marshall Space Flight Center.** *Further information may be found in DOE/NASA CR-161435 [N80-23776/NSP], "Solar Heating System Installed At Blakedale Professional Center, Greenwood, S.C. — Final Report" [$6]. A paper copy may be purchased [prepayment required] from the National Technical Information Service, Springfield, Virginia 22161. The report is also available on microfiche at no charge. To obtain a microfiche copy, Circle 39 on the TSP Request Card.*
MFS-25458

Residential System Tested in an Office — Huntsville, Alabama

A system does not meet its design specifications if it is not matched with its application.

The difficulties in trying to adapt a residential solar-energy system to a commercial building are underscored by the results at one operational test site. Installed in a Huntsville office building, the system designed for a single-family residence supplied considerably less of the annual heat load than expected, although actual hardware problems were minimal. An 85-page report on the project discusses these observations and contains an abundance of design, performance, and test information.

There are two key differences between the office and residential applications. First, the space-heating demand at the office was more than the design value because the thermostat was not held at 70° F (21° C), as specified for the residence. Often the temperature was maintained at 76° F (24° C) during work hours. Second, the hot-water demands of an office are considerably less than those of a residence. Thus, much of the energy collected and stored during the summer went unused because relatively-little hot water was used. In fact, it is estimated that if the solar equipment had been shut off during the late spring, summer, and early fall, energy savings would have increased by 21 percent for the year.

The system, which uses air solar collectors, is designed to supply 50 to 60 percent of the space-heating requirements of a single-family dwelling with 2,200 ft^2 (200 m^2) of floorspace. The hardware is described in more detail in "Prototype Solar-Heating System" (MFS-23916) on page 201 of *NASA Tech Briefs*, Vol. 3, No. 2.

This work was done by the Federal Systems Division of IBM Corp. for **Marshall Space Flight Center.** *Further information may be found in DOE/NASA CR-161464 [N80-25790/NSP], "Solar Energy System Performance Evaluation — Seasonal Report for IBM System 1A, Huntsville, Alabama" [$8]. A paper copy may be purchased [prepayment required] from the National Technical Information Service, Springfield, Virginia 22161. The report is also available on microfiche at no charge. To obtain a microfiche copy, Circle 40 on the TSP Request Card.*
MFS-25481

Solar-Heated Two-Level Residence — Akron, Ohio

Operational tests over a 1-year period

A report available on request describes a 1-year evaluation of a solar-heating and hot-water system for a two-level single-family residence in Akron, Ohio. The system uses flat-plate solar collectors with air as the heat transport medium. A rock-storage bin stores the collected energy. Backup heat is supplied by an air-to-liquid heat pump. [For more details about this system, see "Solar-Heating and Cooling System Design Package" (MFS-25393) on page 38 of *NASA Tech Briefs*, Vol. 5, No. 1.]

Solar energy satisfied 24 percent of the hot-water and space-heating load during the 1-year test. Gross electrical-energy savings were 9.03×10^6 Btu (9.52×10^9 J). Net savings, after 2.15×10^6 Btu (2.27×10^9 J) needed to operate the system are subtracted, were 6.88×10^6 Btu (7.26×10^9 J). If a 30-percent efficiency is assumed for power generation and distribution, then 22.92×10^6 Btu (24.18×10^9 J) of fuel were saved at the power-generating station.

This work was done by the Federal Systems Division of IBM Corp. for **Marshall Space Flight Center.** *Further information may be found in DOE/NASA CR-161465 [N80-25791/NSP], "Solar Energy System Performance Evaluation — Seasonal Report for Solaron-Akron, Akron, Ohio" [$8]. A paper copy may be purchased [prepayment required] from the National Technical Information Service, Springfield, Virginia 22161. The report is also available on microfiche at no charge. To obtain a microfiche copy, Circle 41 on the TSP Request Card.*
MFS-25480

Solar-Energy Workshop — Tucson, Arizona

A showplace for solar-energy utilization includes a complex solar-heating and cooling system.

A complex solar-heating and cooling system, tested onsite at the "Decade 80" house, Tucson, Arizona, supplied 93 percent of the building space-heat requirements between November 1978 and October 1979. As stated in a seasonal report on the project, solar energy saved 202 million Btu (213×10^9 J) of conventional energy sources during that period.

The Decade 80 house, a one-story single-family dwelling, is a showplace and workshop for solar-energy utilization. Superior construction techniques and quality materials were utilized, and a full-time maintenance staff was assigned to keep all systems operating.

An aqueous solution of propylene glycol is the heat-transfer medium in the flat-plate collector loop. The collected energy is transferred to an underground water-storage tank. The collector-to-storage loop also has a heat exchanger that diverts some heat to a swimming pool.

Two absorption-cycle water chillers operating in parallel supply space cooling. Heat from the storage tank is circulated through the generators of the chillers to activate the absorption cycle. The chilled water is pumped to heat exchangers in the building air-distribution system. When the available solar energy is not sufficient, a gas-fired boiler supplies the balance of the energy requirements.

Domestic hot water is circulated through a heat exchanger in the energy storage tank. Additional energy is supplied by electrical heating elements. The domestic water is continuously circulated between a small storage tank and the building plumbing, so that hot water is always available on demand.

This work was done by the Federal Systems Division of IBM Corp. for **Marshall Space Flight Center.** *Further information may be found in DOE/NASA CR-161450 [N80-25787/NSP], "Solar Energy System Performance Evaluation — Seasonal Report for Decade 80 House, Tucson,*

Arizona" [$9]. A paper copy may be purchased [prepayment required] from the National Technical Information Service, Springfield, Virginia 22161. The report is also available on microfiche at no charge. To obtain a microfiche copy, Circle 42 on the TSP Request Card.
MFS-25473

Residential Solar Hot-Water System — Tempe, Arizona

Domestic hot water for a single-story residence is heated by two 4- by 8-foot solar collectors.

A solar hot-water supply saved 5.54 million Btu (5.84 billion Joules) from June 1979 through January 1980 at the Agricultural Department residence at Arizona State University. Since hot-water consumption at the site was low, and consequently much of the solar energy went to make up standby losses, savings with increased usage would be significantly higher. The system is described along with test results in a report that is now available.

The commercial domestic hot-water system uses two 4- by 8-foot (1.2- by 2.4-meter) flat-plate collectors to heat water in either a preheat tank or a domestic hot-water tank, each with a capacity of 52 gallons (196 liters). Additional heat is supplied, if required, by an auxiliary electrical heating element in the domestic hot-water tank.

Energy from the solar collectors is supplied to the domestic hot-water tank whenever the tank temperature is less than 140° F (60° C) and more than 20° F (11° C) below the solar-collector outlet temperature. Should the tank temperature exceed 140° F, excess solar energy is routed to the preheat tank. The system protects against freezing by automatically circulating hot water through the collectors when the collector temperatures approach freezing. Total incident solar energy while the collector was operating during the 6-month period was 15.78 million Btu (16.64 billion Joules). Collected solar energy totaled 8.16 million Btu (8.61 Joules), for a collector efficiency of 52 percent.

This work was done by the Federal Systems Division of IBM Corp. for **Marshall Space Flight Center.** *Further information may be found in DOE/NASA CR-161466 [N80-26778/NSP], "Solar Energy System Performance Evaluation — Seasonal Report for Elcam Tempe, Arizona State University, Tempe, Arizona" [$7]. A paper copy may be purchased [prepayment required] from the National Technical Information Service, Springfield, Virginia 22161. The report is also available on microfiche at no charge. To obtain a microfiche copy, Circle 43 on the TSP Request Card.*
MFS-25490

Residential Solar-Heating Installation — Stillwater, Minnesota

Installer guidelines for each subsystem, including filling and testing

The 179-page "installation guidelines" for the single-family residential heating system at William O'Brien State Park in Stillwater, Minnesota, are now available. The design package for the system is described in "A Solar-Energy System in Minnesota" (MFS-25428) on page 175 of *NASA Tech Briefs*, Vol. 5, No. 2. Information on the operating procedures, controls, caution requirements, and routine and scheduled maintenance is included as written procedures, schematics, detailed drawings, and manufacturer's component data.

The system has 33 liquid flat-plate collectors, a 1,000-gallon (3,790-liter) steel water-storage tank, an auxiliary gas-fired furnace, a domestic hot-water preheater, and accessory pumps, piping, and control equipment. The glycol/water collector loop interfaces with a water-storage loop through a tube-and-shell heat exchanger. A domestic hot-water preheat coil transfers collected energy to the storage tank. A heat exchanger transfers solar-collector heat to the hot-water coil in the return air duct to supply building heat.

Solar-heated water is diverted to charge storage when the building heat demand is met. When available solar energy is inadequate, storage is tapped, or the auxiliary furnace is activated. The domestic hot water is continuously preheated and purged of excess energy.

This work was done by the Energy Resources Center of Honeywell, Inc., for **Marshall Space Flight Center.** *Further information may be found in DOE/NASA CR-161480 [N80-28861/NSP], "Installation Guidelines for Solar Heating System Single-Family Residence at William O'Brien State Park, Stillwater, Minnesota" [$12]. A paper copy may be purchased [prepayment required] from the National Technical Information Service, Springfield, Virginia 22161. The report is also available on microfiche at no charge. To obtain a microfiche copy, Circle 44 on the TSP Request Card.*
MFS-25504

Three-Story Residence With Solar Heat — Manchester, New Hampshire

Heat lost through ducts should be included for an accurate performance assessment.

The performance of a solar-energy system that heats the interior and the domestic hot water of a three-story dwelling on the New Hampshire Vocational Technical College campus is documented in a recently-released 78-page report. The system was evaluated from March 1979 to February 1980. During this period, the measured average outdoor ambient temperature was 53° F (12° C). When the net energy savings are adjusted for heat lost through ducts, but absorbed within the building, solar energy supplied 56 percent of the total measured load for space heating. Average building temperature was maintained at 69° F (21° C).

Compared to an oil-fired furnace efficiency of 60 percent, measurements based on the energy delivered to the space-heating subsystem show a net energy savings of only 14.52 million Btu (15.32 billion Joules). However, solar heat that is lost in delivery to the space-heating subsystem (e.g., through ducts) also contributes to building heat. Including this "unmeasured" contribution, the net savings total 50.48 Btu (53.25 billion Joules).

(continued on next page)

Solar energy is collected by 20 double-glazed flat-plate collectors, connected in parallel, with a total area of 805 square feet (75 square meters). Air is the heat-transfer medium. Thermal energy is stored by a rock bin holding approximately 720 cubic feet (20.4 cubic meters). Six operational modes include heating from the solar collectors, storing heat, heating from storage, auxiliary heating with an oil-fired furnace, summer venting, and hot-water preheating.

This work was done by the Federal Systems Division of IBM Corp. for **Marshall Space Flight Center.** *Further information may be found in DOE/NASA CR-161471 [N80-27802/NSP], "Solar Energy System Performance Evaluation — Seasonal Report for Contemporary-Manchester, Manchester, New Hampshire" [$8]. A paper copy may be purchased [prepayment required] from the National Technical Information Service, Springfield, Virginia 22161. The report is also available on microfiche at no charge. To obtain a microfiche copy, Circle 45 on the TSP Request Card.*
MFS-25499

A High School Is Supplied With Solar Energy — Dallas, Texas

All the domestic hot water and almost half of the annual building heating requirements are supplied.

An 85-page final technical report includes the details of installation, operation and maintenance, contract negotiation, and the acceptance test plan for a retrofit solar-energy system in a Dallas high school building. The system preheats 100 percent of the domestic hot water and supplies 47.5 percent of annual heating requirements for the three-story, concrete-frame, brick-masonry building with basement.

The building, 56 years old and in excellent structural condition, was recently air-conditioned with a 300-ton (1,100-kilowatt) chilled-water system. The new solar system is interconnected with the cooling system to convert it to a two-pipe heating and cooling system.

The flat-plate collectors are roof-mounted utilizing standard steel supports resting in pitch pans on the flat roof deck. The steam-radiation heating system for the building was abandoned, but the boilers supply steam as a backup heat source.

With the summer/winter switch indexed to "winter," three-way valves isolate the chiller from the heating loop. Water from the storage tanks either preheats the hot-water supply or is mixed with cooler water to supply water at 95° F (35° C) to the primary building heating-system pump. In the "summer" mode, the system operates in its normal cooling mode, and the solar storage supplies domestic hot water.

This work was done by the Dallas Independent School District for **Marshall Space Flight Center.** *Further information may be found in DOE/NASA CR-161482 [N80-29847/NSP], "Solar Heating and Domestic Hot Water System Installed at North Dallas High School" [$9]. A paper copy may be purchased [prepayment required] from the National Technical Information Service, Springfield, Virginia 22161. The report is also available on microfiche at no charge. To obtain a microfiche copy, Circle 46 on the TSP Request Card.*
MFS-25514

Materials

Hardware, Techniques, and Processes

Heat-Resistant Polyphosphazene Polymers

Polymers of carboranyl-substituted polyphosphazene are stable at high temperatures and produce an insulating char upon pyrolysis.

Ames Research Center, Moffett Field, California

A new process synthesizes carboranyl-substituted polyphosphazenes and their thermal polymerization to heat-resistant polymers. The incorporation of carboranyl groups in the molecules of conventional polyphosphazenes greatly increases their thermal stability. Upon decomposition at extreme temperatures (about 1,000° C), the new polymers produce a high char yield that insulates other less-resistant materials from heat and flame. In contrast, unsubstituted polyphosphazene totally evaporates at about 400° C.

Carboranyl-substituted polyphosphazenes are prepared by heat-polymerizing a carboranyl halocyclophosphazene at 250° C for about 120 hours in the absence of oxygen and moisture. The cyclophosphazene is obtained by reacting a lithium carborane with, for example, hexachlorocyclotriphosphazene at ambient temperature, under anhydrous conditions. For greater stability in the presence of moisture, the chlorine of the polymer is replaced by aryloxy and alkoxy groups, such as CF_3CH_2O-.

The generalized chemical reactions and the compounds involved are illustrated in the figure. In the formula, R is either a hydrogen atom, a lower alkyl radical having up to six carbon atoms, or an aryl radical of up to nine carbon atoms; R^1 is an alkyl group, an aryl group, a halogenated homolog of these groups, or a mixture of any of these groups.

The following example illustrates the process. A solution of hexachlorocyclotriphosphazene (I) was added to phenyl-*o*-carborane and *n*-butyllithium dissolved in diethyl ether at 25° C. The reaction proceeded for 12 hours at 25° C in an anhydrous environment. The solvent was removed under reduced pressure, and the residue was heated at 80° C and 0.05 mm Hg to remove unreacted starting material. A subsequent increase in temperature to 120° C brought about the volatilization and condensation of phenylcarboranylpentachlorocyclotriphosphazene (II).

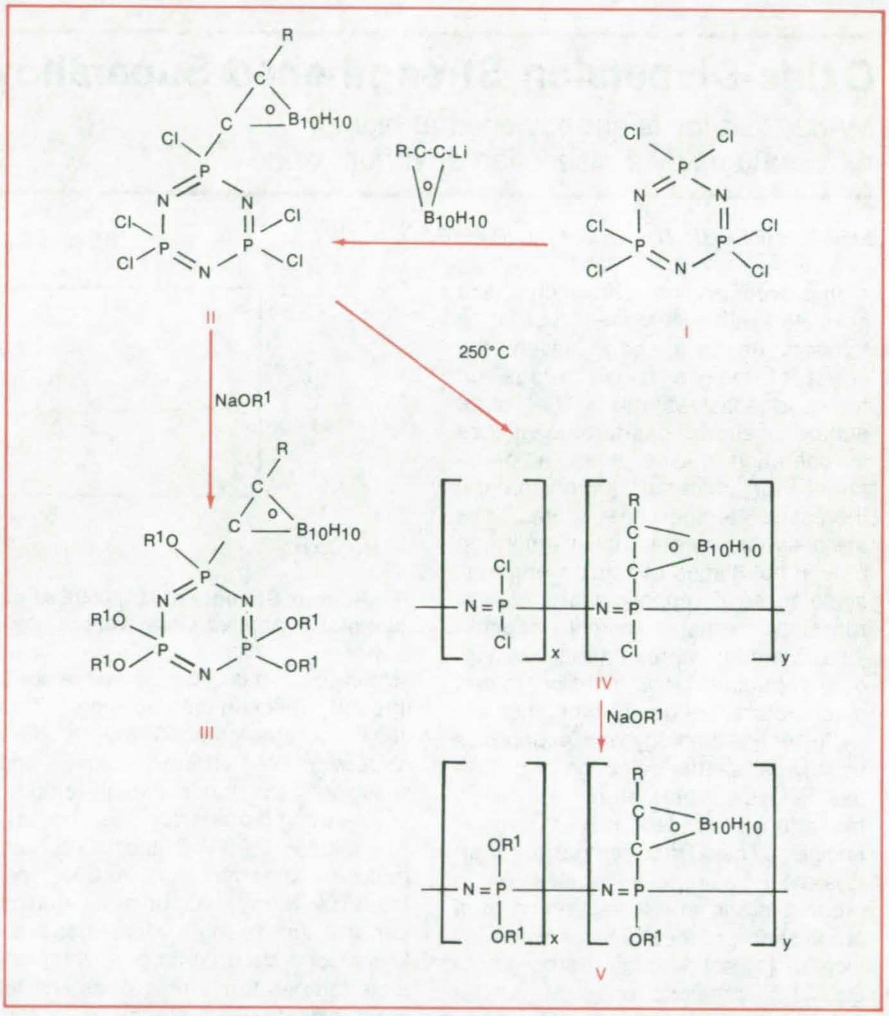

Carboranyl-Substituted Phosphazenes are prepared by heat-polymerizing a carboranyl halophosphazene. R and R^1 in the formulas are members of a number of different groups. In the polymeric formulas IV and V, the ratio of x to y is 2 to 1, the number and type of polymeric units being determined by the structure of II.

Phenylcarboranylpentachlorocyclotriphosphazene was subsequently dissolved in dry THF (tetrahydrofuran) and treated with a solution of sodium trifluoroethoxide in THF for 28 hours at 66° C. After the treatment, the solution was neutralized with concentrated hydrochloric acid and the product isolated by extraction with benzene and dried over magnesium sulfate. Upon filtration and removal of the solvent, phenylcarboranylpentatrifluoroethoxycyclotriphosphazene (III), an oily product, was obtained.

The phenylcarboranylcyclopentachlorotriphosphazene monomer (II) was polymerized by heating in an evacuated tube at 250° C for 120 hours. The next step in the process was chlorine replacement. The polymeric product (IV) was reacted with sodium trifluoroethoxide in boiling THF for 120 hours to yield the fluoroethoxy-substituted polymer (V). The product was concentrated and neutralized with hydrochloric acid and the precipitate filtered off, washed with water, and dried. A fractional precipitation of a

(continued on next page)

THF solution of the product into hexane and benzene gave V. A similar preparation process using methyl-o-carborane, in place of phenyl-o-carborane, yielded methylcarboranylcyclopentachlorotriphosphazene.

This work was done by Larry L. Fewell of **Ames Research Center** *and Harry R. Allcock, John P. O'Brien, and Angelo G. Scopelianos of Pennsylvania State University. For further information, Circle 47 on the TSP Request Card.*

This invention is owned by NASA, and a patent application has been filed. Inquiries concerning nonexclusive or exclusive license for its commercial development should be addressed to the Patent Counsel, Ames Research Center [see page A5]. Refer to ARC-11176.

Oxide-Dispersion-Strengthened Superalloy

MA6000E alloy is strengthened at high temperatures by a dispersion of yttrium oxide.

Lewis Research Center, Cleveland, Ohio

Improved engine efficiencies are possible with increased operating temperatures and can lessen the effect of today's fuel shortage on transportation systems. The large number of aircraft gas-turbine engines in operation makes them a prime target for material improvements. Increased temperature capabilities are desirable for materials used in the critical hot stages of turbine engines, since these components are usually run close to their maximum capabilities. Material improvements are vigorously pursued by both designers and manufacturers of gas-turbine engines.

Current technology and economics usually dictate the selection of nickel-base alloys as the material for use in the critical hot sections of turbojet engines. These high-temperature alloys, as a class, have unique strength properties and are strengthened by a combination of mechanisms that may include (1) solid solution strengthening, (2) precipitation, (3) stable particle dispersion, and (4) grain structure control.

Until the recent development of mechanical alloying, it has not been possible to combine all of these mechanisms successfully together with oxide dispersion strengthening in one alloy system. A new alloy, MA6000E, has been developed through mechanical alloying. This alloy is strengthened by a fine dispersion of yttrium oxide, and possesses outstanding high-temperature-strength properties (see figure). At 2,000° F (1,090° C) the 1,000-hour rupture strength is 20,000 psi (138×10^6 N/m^2), about twice that of current high-strength nickel-base alloys. Good thermal-fatigue, intermediate-temperature strength, as well as good oxidation resistance give this alloy a unique combination of properties not available in any other material.

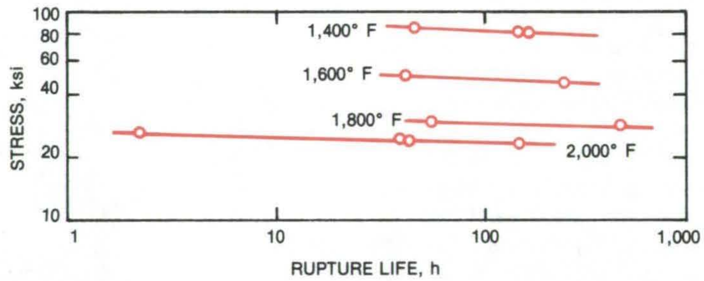

The **Rupture Strength of MA6000E Alloy** is shown for several operating temperatures as a plot of applied stress versus time to rupture.

This work was done by Thomas K. Glasgow of **Lewis Research Center** *and Y. G. Kim, L. R. Curwick, and H. F. Merrick of Inco Research and Development Center. Further information may be found in:*

NASA CR-135150 [N77-22213/NSP], "Development of an Oxide Dispersion Strengthened Turbine Blade Alloy by Mechanical Alloying" [$7],

NASA CR-159493 [N80-13218/NSP], "Characterization of an Oxide Dispersion Strengthened Superalloy" [$6], and

NASA TM-79088 [N79-20180/NSP], "An Oxide Dispersion Strengthened Alloy for Gas Turbine Blades" [$5].

Copies of these reports may be obtained from the National Technical Information Service, Springfield, Virginia 22161.

LEW-13589

Low-Cost, High-Temperature, Duplex Coating for Superalloys

The high-temperature resistance to oxidation and corrosion of nickel-base alloys is substantially improved by a duplex silicon-slurry / aluminide coating.

Lewis Research Center, Cleveland, Ohio

Energy shortages and fuel substitutes place an increasing demand on power systems and their component materials. Efficient use of such systems can usually be improved by increased operating temperatures. These increased temperatures, however, cause accelerated material degradation in the form of oxidation, hot corrosion, and thermal fatigue. Nickel-base alloys that are widely used in critical sections of some power systems (i.e., turbojet engines) require protective coatings to extend their operating capabilities.

A new low-cost coating has been developed that exhibits significant protection for superalloys from high-temperature, high-gas-velocity oxidation, hot corrosion, and thermal fatigue. The coating is a duplex silicon-slurry/aluminide material approximately 0.01 inch (0.03 centimeter) thick. It was applied to the surface of two high-strength nickel-base alloys, NASA-TRW VI A and B-1900. Both alloys were tested at 2,000° F (1,090° C) in a cyclic oxidation rig test at mach 1. Hot corrosion tests [1,650° F (900° C), mach 0.3, with 5 ppm sea salt injection] were also run on the cooled B-1900 material.

Test results indicate substantial life improvements with the duplex silicon-slurry/aluminide coating over the base material as well as standard pack-cementation aluminide coatings. The performance of this new coating was somewhat different with each alloy, and it may not be quite as good, in specific applications, as the more-expensive platinum/aluminum or MCrAlY coatings. However, with additional characterization of alloy/coating interaction, suitable alloys should be identified that will give superior performance under severe operating conditions. This system offers the opportunity to reduce coating costs as well as to increase material operating capabilities.

This work was done by Stanley G. Young and Daniel L. Deadmore of **Lewis Research Center**. *Further information may be found in NASA TM-79178 (N79-29292/NSP), "An Experimental, Low-Cost, Silicon Slurry/Aluminum High-Temperature Coating for Superalloys" [$5]. A copy may be purchased [prepayment required] from the National Technical Information Service, Springfield, Virginia 22161.*

Inquiries concerning rights for the commercial use of this invention should be addressed to the Patent Counsel, Lewis Research Center [see page A5]. Refer to LEW-13497.

Improved Metallic and Thermal-Barrier Coatings

Low-thermal-conductivity two-layer ceramic coatings are efficient thermal barriers between cooled metallic components and high-temperature combustion gases.

Lewis Research Center, Cleveland, Ohio

Two-layer ceramic thermal-barrier systems (TBS) have been developed that are significantly improved, simple, and highly adherent. These TBS consist of an alloy bond coating and a thermal-barrier coating (TBC). In these systems, bond coatings are either M-Cr-Al-Yb (M ≡ Ni, Co, or Fe), Ni-Al-Y, or improved M-Cr-Al-Y (M ≡ Ni, Co, or Fe) compositions. The TBC is an improved $6Y_2O_3$ or $8Y_2O_3$ stabilized zirconia (composition in weight percent). These TBC's have very low thermal conductivity and therefore impart an efficient thermal barrier between cooled metalic components and high-temperature combustion gases. More importantly, they have significantly longer life than those reported earlier.

Metallic components could typically be combustors, blades, and vanes in aircraft engines or power-generating turbines, or any other cooled heat-engine component. The presence of the improved and more efficient two-layer coatings on cooled components can greatly reduce the metal substrate temperature or minimize coolant requirements.

Experimental evidence indicates that improvements in durability result chiefly from the optimization of the reactive metal (yttrium or ytterbium) content of the bond coating, replacement of yttrium by ytterbium, and optimization of the Y_2O_3 content of the zirconia. Optimization studies to date have also indicated that coating durability is sensitive to the concentrations of Cr and Al in the bond coating.

Moreover, experimental results indicate that the compositions of the bond coat and TBC are more critical in limiting coating adherence and life than the thermal expansion coefficient of the substrate material. In rigorous systematic cyclic furnace tests between 1,095° and 280° C, Ni-17.5Cr-6.6Al-0.14Yb coupled with ZrO_2-$6.1Y_2O_3$ or ZrO_2-$7.8Y_2O_3$ withstood 280 and 206 1-hour cycles, respectively; Ni-19.3Al-0.5Y/ZrO_2-$7.8Y_2O_3$ withstood 198 1-hour cycles; and Ni-25.7Cr-6.6Al-0.3Y/ZrO_2-$7.8Y_2O_3$ withstood 246 1-hour cycles. These results indicate that the improved ceramic thermal-barrier coatings are approximately four times superior to the previously reported Ni-16Cr-6Al-0.6Y/ZrO_2-$12Y_2O_3$ thermal-barrier system. In these studies ytterbium-containing bond coatings were found to be more oxidation resistant than

(continued on next page)

similar yttrium-containing bond coatings.

This work was done by Stephan Stecura of **Lewis Research Center**. *Further information may be found in:*

NASA TM-79206 [N79-29293/NSP], "Effects of Yttrium, Aluminum, and Chromium Concentrations in Bond Coatings on the Performance of Zirconia-Yttria Thermal Barriers" [$6]; and

NASA TM-78976 [N78-31212/NSP], "Effects of Compositional Changes on the Performance of a Thermal Barrier Coating System" [$6].

Copies of these reports may be purchased [prepayment required] from the National Technical Information Service, Springfield, Virginia 22161.

Inquiries concerning rights for the commercial use of this invention should be addressed to the Patent Counsel, Lewis Research Center [see page A5]. Refer to LEW-13324.

Resin-Char Oxidation Retardant for Composites

Boron powder stabilizes the char, so that graphite fibers are retained.

Lewis Research Center, Cleveland, Ohio

An effective and simple method has been developed for retarding the oxidation of resin char formed in the burning of resin matrix/graphite fiber composites. The method consists of adding boron to the resin matrix by dispersion in the impregnation mixture applied to the graphite fiber. Addition of as little as 3 percent boron powder by weight effectively maintains the structural integrity of the composite and prevents release of the graphite fibers.

Char formed during the burning of resin matrix composites is a carbonaceous material that oxidizes rapidly in air at temperatures above 1,200° F (650° C). Elemental boron powder added to the composite as a filler material stabilizes the char as it is formed and protects it from oxidation. Resin matrix/graphite fiber composites modified by the addition of boron powder can be exposed to high thermal heat fluxes in air for prolonged periods of time and maintain their structural integrity. The char formed by the thermally decomposed resin is protected from oxidation in air and remains as a functional matrix material that cements the fibers together.

The effectiveness of boron powder as a char oxidation retardant has been demonstrated for both a typical low char forming resin and a typical high char forming resin. Test panels of a low char forming epoxy/graphite composite (HTS/3501-6), such as used in the aircraft industry today, and a high char forming polyimide/graphite composite (HTS/PMR-15) were made both with and without the boron powder filler. The test panels were burned in air by exposure to a radiative heat source of 5.3 Btu/ft^2-s (6.0×10^4 J/m^2-s) for a period of 35 minutes. Results are shown in Figures 1 and 2.

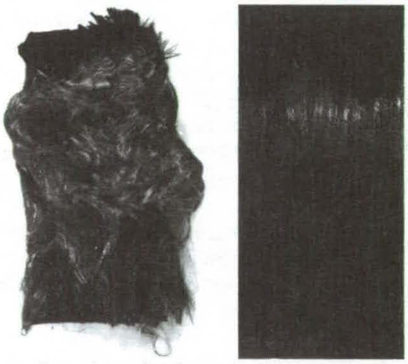

(a) UNFILLED (b) BORON-FILLED

Figure 1. **Graphite /Epoxy Laminates** burned in air by 5.3 Btu/ft^2-s radiation flux are stabilized by boron filler. In (a), the surface of the burned unfilled sample exhibits loose graphite fibers; whereas the surface of the burned boron-filled sample (b) is smooth, shiny, and free of loose graphite fibers.

Figure 1 shows photographs of two panels of the epoxy/graphite composite. The surface of the burned unfilled sample, Figure 1(a), consists of a deep mat of loose graphite fibers. The surface of the burned boron-filled sample, Figure 1(b), is smooth, shiny, and free of loose graphite fibers that are retained within the stabilized char filler material. Panels of the burned polyimide/graphite composite exhibited similar appearances. Both the unfilled epoxy and unfilled polyimide composites were reduced to piles of free graphite fibers after the burning tests were concluded. All boron-filled samples exhibited solid surfaces after burning with no visible free fibers.

Figure 2 shows the comparative resin weight loss for the unfilled and boron-filled (designated /B) epoxy/graphite and polyimide/graphite test panels. (The percent resin weight loss data for the unfilled samples are artificially high because they include a significant amount of fiber weight loss after the first 5 minutes.) Resin weight losses for both the unfilled and boron-filled samples were nearly identical for the first 3 minutes of burning. After 3 minutes, the unfilled samples continued to lose weight while the boron-filled samples stabilized.

Addition of the boron powder filler to resin matrix/graphite fiber composites

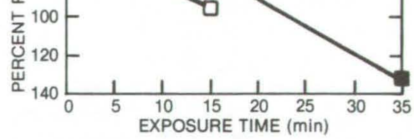

Figure 2. **Resin Weight Loss** of laminates during exposure to 5.3 Btu/ft^2-s thermal radiation in air is nearly identical for the first 3 minutes for both unfilled and boron-filled samples. After 3 minutes, the boron-filled samples (represented by graphs in color) stabilize.

has no significant effect on the mechanical properties of the materials. Density increases by about 1.5 percent. Boron powder addition is easily incorporated into conventional composite processing procedures with minimal modification or interruption.

These resin char oxidation retardant composites can be used in fire-sensitive environments where stringent burnthrough requirements are specified and where structural integrity when exposed to burning is essential.

This work was done by K. J. Bowles and R. E. Gluyas of **Lewis Research Center.** *Further information may be found in:*

NASA TM-79314 [N80-14196/NSP], "Burning Characteristics and Fiber Retention of Graphite/Resin Matrix Composites" [$5], *and*

NASA TM-79288 [N80-13171/NSP], "Improved Fiber Retention by the Use of Fillers in Graphite Fiber/Resin Matrix Composites" [$5].

Copies of these reports may be purchased [prepayment required] from the National Technical Information Service, Springfield, Virginia 22161.

Inquiries concerning rights for the commercial use of this invention should be addressed to the Patent Counsel, Lewis Research Center [see page A5]. Refer to LEW-13275.

Composites With Nearly-Zero Thermal Expansion

Graphite, glass, and resin composite is unusually strong, stiff, and thermally stable.

Lyndon B. Johnson Space Center, Houston, Texas

A new composite has a near-zero coefficient of thermal expansion and a high modulus of elasticity. The material thus combines exceptional dimensional stability over a wide temperature range with unusually high strength and stiffness.

The composite consists of graphite fibers and glass fibers in a plastic resin matrix. The constituents are inexpensive and lightweight, and the composite material is produced by an economical process — "pultrusion" (see figure).

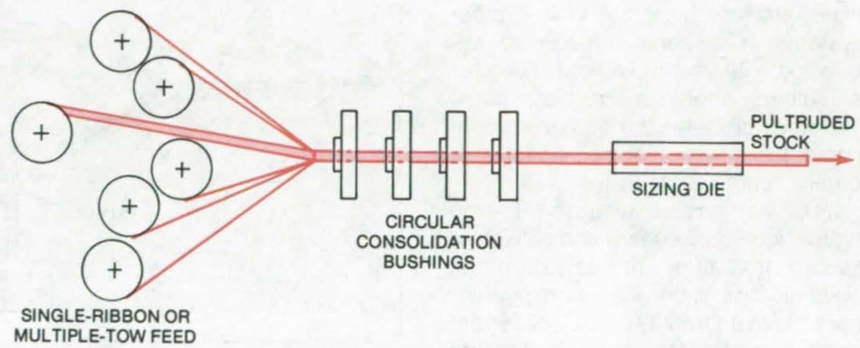

Glass/Graphite Fibers in a Resin Matrix Are Pulled through a sizing die, forming structural rods or bars. The process, which is economical and continuous, may be fed by a single ribbon of resin-impregnated fibers or by multiple reels that pass through a resin bath (not shown). The sizing die has a rectangular cross section or a circular cross section.

Developed for large truss structures in space, the composite is also suited to applications in optics and communications. In the truss structures, the composite is used as narrow rods that overlap in an open lattice; where the rods overlap, they are joined by an encapsulant. As a mounting material for antennas, mirrors, and lenses, the glass/graphite composite can eliminate serious structural distortion.

The graphite fibers have a negative coefficient of thermal expansion, and the glass fibers and resin matrix have a positive coefficient; that is, the graphite contracts and the glass and resin expand as the temperature increases. When the materials are combined in the proper proportion, they produce a nearly thermally-inert composite material.

The matrix for the fiber may be a polysulfone, an epoxy, a polyimide, or other resin. The proportion of the constituents for a nearly thermally inert composite was found to be 14.2 percent glass fiber, 38.5 percent graphite fiber, and 47.3 percent resin (percentages by volume).

For maximum elastic modulus and zero thermal-expansion coefficient, it is important that the fibers be oriented in the same direction and that the glass fibers be uniformly distributed among the graphite fibers. To ensure these conditions, rods of the composite are made by pulling a preimpregnated ribbon of glass and graphite fiber through a die. The ribbon is just wide enough to fill an 0.08- by 0.08-inch (2- by 2-mm) sizing die. Four bushings precede the sizing die and consolidate the ribbon in steps. The bushings are heated to 750° F (399° C) and the sizing die is heated to 500° F (260° C). The pull rate varies from 6 to 20 inches/min (15 to 51 cm/min). As an alternative to preimpregnation, the fibers can be pulled through a resin bath as part of the pultrusion process.

The final product is only three-fifths as dense as aluminum, yet has an elastic modulus of 18 to 24 million psi (1.2 to 1.7×10^{11} N/m^2). The thermal-expansion coefficient can be adjusted negatively or positively by altering the proportions of glass and graphite and

(continued on next page)

by adding fibers at an angle to the main axis of the bars.

This work was done by Thomas J. Dunn of **Johnson Space Center** *and Anthony J. Cwiertny, Jr., Vernon L. Freeman, and Read Johnson, Jr., of McDonnell Douglas Corp. Further information may be found in NASA CR-160558 [N80-19144/NSP], "Development of a Composite Geodetic Structure for Space Construction"* [**$7**]. *A copy may be purchased [prepayment required] from the National Technical Information Service, Springfield, Virginia 22161.*
MSC-18724

Carbon Scrubber

Automated membrane separation is used to remove inorganic carbon from samples to be analyzed for "total organic carbon."

Lyndon B. Johnson Space Center, Houston, Texas

An online flow system utilizes a pH-dependent equilibrium reaction and a semipermeable membrane to remove inorganic carbon from samples to be analyzed for total organic carbon. It was developed for use with automated water-analysis systems. Unlike other systems for inorganic carbon removal, it works passively, without complex machinery, methods, or techniques, and does not alter the composition or content of any nonionized species of organic compounds in the system.

The method is illustrated in the figure. A sample stream is divided into two equal streams. In one stream the aqueous solution is continuously mixed with a strongly acidic reagent to convert carbonate and bicarbonate ions to dissolved carbon dioxide gas. In the second stream the aqueous solution is continuously mixed with an alkaline reagent. The alkaline reagent converts carbon dioxide to carbonate and bicarbonate ions.

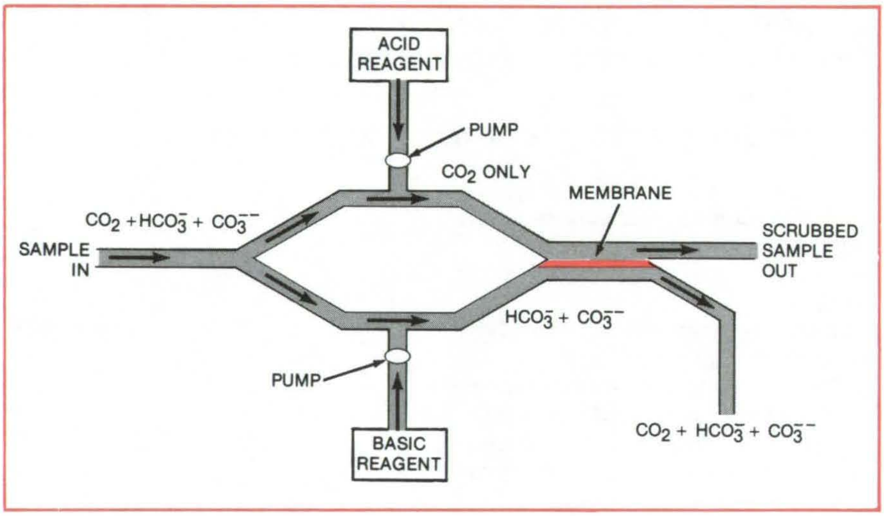

A **Semipermeable Membrane** separates two sample streams, one of which is treated with an acid reagent and the other with a base. Carbonate and bicarbonate ions are converted to dissolved CO_2 by the acid; the reverse process occurs in the basic stream. Only CO_2 is passed by the membrane, from the acid-treated stream to the base-treated stream. Thus, the acidic stream emerges free of all species of inorganic carbon.

The acidic and basic solutions then flow past opposite sides of a membrane permeable to dissolved carbon dioxide gas and impermeable to carbonate and bicarbonate ions. Since there is no carbon dioxide in the basic solution, the dissolved carbon dioxide in the acidic solution tends to flow across the membrane. After crossing the membrane, the carbon dioxide is converted to carbonate and bicarbonate ions and cannot recross. The process continues removing carbon dioxide from the acidic solution. The length of the membrane and the flow rate of each mixed stream determine the degree to which inorganic carbon is removed from the acidic solution. A sample stream containing 1,000 ppm of inorganic carbon prior to stripping was found to contain 1 ppm after 30 seconds of residence in the stripper.

The constant flows of alkaline and acid reagents are maintained by a pump. The use of a single pump, adding equal volumes of reagent to sample streams, results in equal dilution of the sample streams.

The semipermeable membrane used in the method is made from such material as silicone rubber, porous polypropylene, or porous tetrafluoroethylene. A typical acid reagent used in the scrubber is $H_2SO_4(NH_4)_2S_2O_8$, and a typical alkaline reagent used is NaOH.

When the inorganic carbon removal is complete, the alkaline stream contains all the inorganic carbon; and the acidic stream, free of inorganic carbon, can be measured for total organic carbon. The total organic carbon is oxidized in the acidic solution to form carbon dioxide, the concentration of which is monitored with a potentiometric electrode.

This work was done by Martin S. Frant of Orion Research Inc. for **Johnson Space Center.** *For further information, Circle 48 on the TSP Request Card.*
MSC-16531

Electrically-Conductive Palladium-Containing Polyimide Films

Addition of palladium reduces electrical resistivity.

Langley Research Center, Hampton, Virginia

A palladium complex has been added to a polyimide film to make it more conductive. Because polyimide films can be lightweight, thermally stable, and flexible, they are currently being considered as materials for large space structures. To dissipate electric charge in this application, the films should possess antistatic properties with an electrical resistivity of 10^8 to 10^{10} ohm-cm.

Linear condensation polyimides, however, are not conductive by nature, having electrical resistivities of the order of 10^{17} ohm-cm. Attempts to lower the resistivity have been made by doping the polymers with such metals as aluminum or with carbon microspheres. These approaches led to an unwanted increase in weight of the material, a much embrittled film, uneven dispersion of the additive throughout the film, and a degradation in thermal and mechanical properties.

The palladium polyimide film is prepared in four general steps: (1) the preparation of a polyamic acid in a polar solvent, (2) the addition of a soluble palladium complex salt, (3) fabrication of a thin film of the "palladium-polyamic acid" solution, and (4) thermal imidization of the film to the palladium-containing polyimide by heating at 300° C.

The polyamic acid solution is prepared by adding an equivalent amount of 3,3',4,4'-benzophenone tetracarboxylic acid dianhydride (BTDA) to a stirred solution of 4,4'-oxydianiline (ODA) in an amide solvent. The palladium-containing complex is then added using a 1:4 mole ratio of the metal species to the polymer. After several hours stirring, a viscous polymer is formed with the structure shown in the figure.

The electrical conductivity of the polymer is entirely dependent upon the presence of palladium. The best results were obtained using Li_2PdCl_4 or $Pd[S(CH_3)_2]_2Cl_2$ as a source of the metal. As shown in the table, volume and surface resistivities of films containing these two complexes were dramatically lowered when compared to the polymer alone. A lesser decrease in electrical resistivity was achieved with other palladium salts. Good solubility of the palladium salt in the polyamic acid is necessary for achieving conductivity.

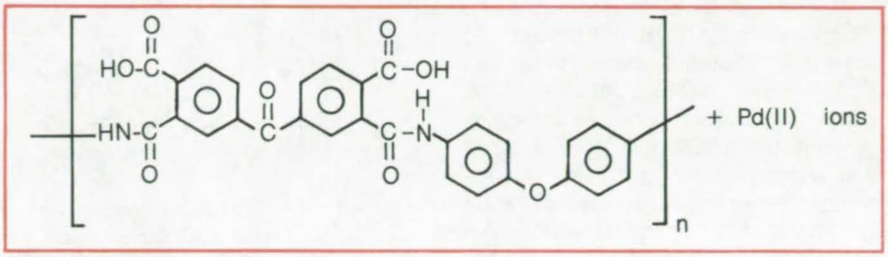

Palladium Polyimide Complex can be used to make a light, flexible film with sufficiently low resistivity to relieve space charging.

Film	Volume Resistivity[a] (ohm-cm)	Surface Resistivity (ohm)	Metal Content	T_g[b] (°C)
Polymer alone	1.0×10^{17}	1.0×10^{17}	0	282
Polymer + Li_2PdCl_4	2.0×10^6	9.5×10^5	0.17% Li 5.33% Pd	338
Polymer + $Pd[S(CH_3)_2]_2Cl_2$	very low[c] $<10^5$	very low[c] $<10^5$	0.23% S 7.02% Pd	343
Polymer + Na_2PdCl_4	2.3×10^{15}	———	1.36% Na 4.69% Pd	372
Polymer + $PdCl_2$	2.3×10^{11}	———	2.97% Pd	281

[a]Electrical resistivities were measured according to ASTM method of test D257-66.
[b]Glass transition temperatures determined by thermomechanical analysis at 5° C/min in static air
[c]Unmeasurable due to overloading at 10 volts

Test Data on Palladium-Containing Polyimide Films

The lowered electrical resistivities of these palladium polyimide films were achieved without a loss in film flexibility and with a minimal increase in the weight of the film. Resistivities obtained (10^6 or lower) by the addition of Li_2PdCl_4 and $Pd[S(CH_3)_2]_2Cl_2$ should be low enough to relieve space-charging effects.

This work was done by Anne K. St. Clair of **Langley Research Center** *and T. A. Furtsch, and L. T. Taylor of Virginia Polytechnic Institute and State University. For further information, Circle 49 on the TSP Request Card. LAR-12629*

Aluminum Ions Enhance Polyimide Adhesive

Adding complexed aluminum ions raises the useful temperature of polyimide adhesive without embrittling it or reducing long-term stability.

Langley Research Center, Hampton, Virginia

Polyimides have been considered as adhesives for bonding titanium and thermally resistant composites and films for aerospace applications. The room-temperature adhesive strengths of linear polyimides are high, but they are thermoplastic and fail in the temperature range from 250° to 300° C. Attempts to improve the adhesive properties have generally reduced the long-term thermal stability of these resins.

Previous modifications that have improved the adhesive properties of linear polyimides include polymer preparation from isomeric meta-oriented aromatic diamines, polymer preparation in certain water- or alcohol-miscible ether solvents, and the addition of large amounts of aluminum powder to the resins prior to bonding. The addition of metal fillers, however, causes a drastic increase in weight and a less-flexible adhesive joint.

It has been discovered that the high-temperature strength of a polyimide adhesive can be improved (see table) by adding complexed aluminum ions without introducing excessive weight or embrittling the adhesive. In the process:

1. A polyamic acid solution is prepared in a solvent or mixture of solvents, one of which is a water- or alcohol-miscible ether.
2. Aluminum ions are added to the solution as tri(acetylacetonato)aluminum, $Al(acac)_3$.
3. The aluminum and polyamic acid solution is applied to a substrate prepared for bonding.

The aluminum-ion-containing adhesives can be applied to a suitably-prepared substrate surface as the neat resin with or without supports such as glass fabric. The substrates can be metal (titanium, steel, aluminum), composite (graphite/polyimide, graphite/epoxy, glass/polyimide, glass/epoxy), or polymeric film (either metalized or unmetalized). The coated substrates are allowed to stand for solvent evaporation or are prestaged to a certain temperature for solvent removal. They are then bonded together using heat (250° to 300° C) and, if necessary, pressure [50 to 200 psi (3.4×10^5 to 1.4×10^6 N/m^2)]. The heat evaporates any remaining solvent and converts the solution to a thermally-resistant cyclic polyimide containing aluminum ions. During this process, an excellent adhesive bond is formed.

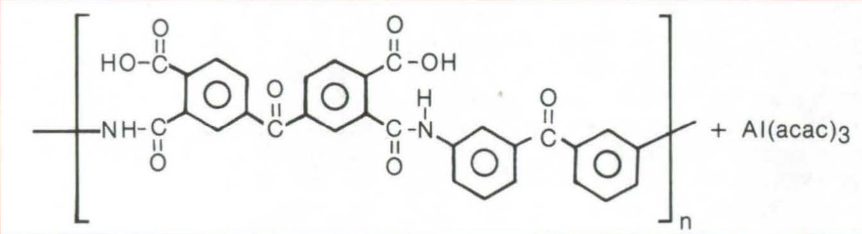

Structural Unit of Aluminum-Ion-Containing Polyimide

Polymer	T_g(°C)[a]	PDT(°C)[b]	Lap Shear Strength (psi)[c] RT	250° C	275° C	300° C
With $Al(acac)_3$	271	555	2,380	1,890	1,640	700
Polymer alone	251	570	2,970	1,570	0	0

[a]Glass transition temperature determined by thermomechanical analysis at 5° C/min in static air

[b]Polymer decomposition temperature determined by thermogravimetric analysis at 2° C/min in air

[c]Lap shear tensile strength on titanium alloy determined according to ASTM D-1002 (CTM No. 26)

Test Data on a polymer formulated from BTDA and 3,3′-DABP with $Al(acac)_3$ are compared to those for the polymer without aluminum ions.

The aluminum-ion-containing polyamic acid is prepared by adding an equimolar quantity of 3,3′,4,4′-benzophenone tetracarboxylic acid dianhydride (BTDA) to a stirred solution of 3,3′-diaminobenzophenone (3,3′-DABP) in a water- or alcohol-miscible ether solvent or mixture of solvents, one being an ether. The $Al(acac)_3$ complex is then added to the solution at a concentration of 2 to 3 percent by weight. The reaction is carried out at room temperature, and the result is a viscous, homogeneous polymeric solution. The polyamic acid is characterized by a recurring unit with the structural formula illustrated.

Ultimate success of the adhesive at high temperature depends upon the presence of the $Al(acac)_3$ complex. The solvents useful for this process are of the aliphatic acyclic and cyclic ether types. Such solvents have a high affinity for the polar chemical groups of the aromatic polyamic acid intermediates, in contrast to aromatic water-immiscible solvents.

During the cure, the $Al(acac)_3$ maintains integrity as a metal complex rather than converting to a free metal. (This behavior has been confirmed by X-ray photoelectron spectroscopy.) This is believed to be the reason that the adhesive is able to maintain excellent strengths at high temperature. Other polyamic acid systems containing metal acetylacetonates are converted upon curing to the polyimide plus free metal and are essentially useless as high-temperature adhesives.

As opposed to a metal-powder-filled polymer, the polymer containing aluminum ions maintains the flexibility of a linear system without embrittlement caused by a free metal filler. This makes the adhesive an excellent candidate where flexibility of the bond line is required. In addition, at a metal-to-polymer weight loading of 2.5 percent, a considerable weight savings is realized compared to a polymer loaded with 80 percent aluminum powder.

This work was done by Anne K. St. Clair and Terry L. St. Clair of **Langley Research Center** *and Larry T. Taylor of Virginia Polytechnic Institute and State University. For further information, Circle 50 on the TSP Request Card.*

This invention is owned by NASA, and a patent application has been filed. Inquiries concerning nonexclusive or exclusive license for its commercial development should be addressed to the Patent Counsel, Langley Research Center [see page A5]. Refer to LAR-12640.

Simultaneous Measurement of Three Atmospheric Pollutants

Proposed method would enable simultaneous concentration monitoring of atmospheric SO_2, NO, and NO_2.

NASA's Jet Propulsion Laboratory, Pasadena, California

Although fluorescence is often used in separate measurements of atmospheric sulfur dioxide (SO_2), nitric oxide (NO), and nitrogen dioxide (NO_2), a sensitive and simultaneous measurement of these three pollutants is needed. Lasers have been used to detect NO_2, which has an absorption band in the visible part of the spectrum; but for SO_2 and NO, fluorescence is usually induced by discharge lamps, because of the lack of a suitable ultraviolet laser.

The three pollutants would be measured simultaneously by a proposed method that utilizes a dye laser with a fundamental output frequency in the visible spectral region and a second harmonic in the ultraviolet. Dye lasers with output wavelengths in the visible region and at 217 nm in the ultraviolet region are already in existence.

The method is illustrated in the figure. When both visible and ultraviolet frequencies from the dye laser are passed through the gas sample, the visible frequencies are absorbed by the NO_2 molecules while the ultraviolet frequencies are absorbed by SO_2 and NO. The subsequent fluorescence of these gases is detected by separate photomultipliers, each with optical filters to select the characteristic emissions of one of the three gases. The photomultiplier outputs are then fed to a signal processor unit for storage and subsequent analysis.

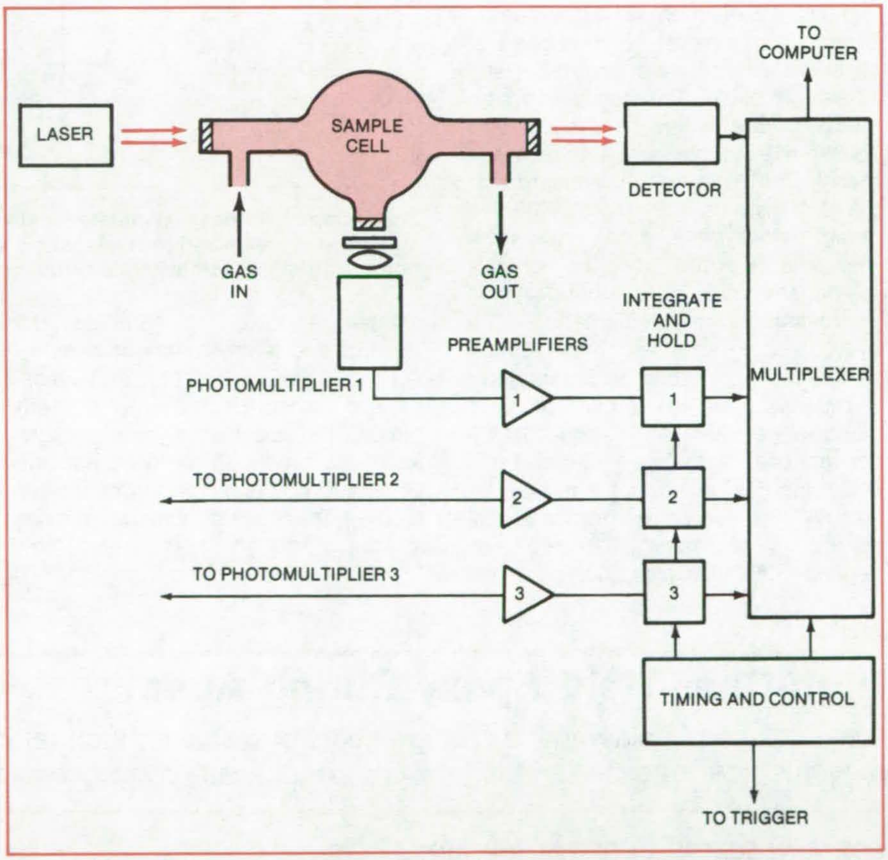

Fluorescing Pollutant Gases in the sample cell are excited by the visible output of a dye laser together with its second-harmonic ultraviolet frequencies. The fluorescence is viewed by three photomultipliers, each with suitable optical filters. For added sensitivity, the sample cell may be placed in a multipass cavity.

This method would eliminate the errors in sequential analysis that occur when the gas concentrations or flow characteristics are rapidly changing. It could be applied to the probe of ambient air, stack emissions, and highway automotive exhausts and may help to provide an understanding of the transport and dispersion properties of these gases.

This work was done by Mahadeva P. Sinha of Caltech for **NASA's Jet Propulsion Laboratory.** *For further information, Circle 51 on the TSP Request Card.*
NPO-14828

Aerosol Lasts up to Six Minutes

Catalytic generator ejects a high-visible lasting mist.

NASA's Jet Propulsion Laboratory, Pasadena, California

A simple, nonpolluting method for generating a highly visible aerosol aids in studying the wakes of aircraft and similar turbulent aerodynamic effects. The aerosol, a mist of dye and water vapor, lasts for as long as 6 minutes at ground level.

An aerosol is generated by the apparatus shown in the figure. Compressed hydrogen peroxide flowing over a catalyst bed is converted, in an exothermic reaction, to superheated steam. The catalyst is composed of silver-plated screens coated with potassium oxide. The steam enters an ejection tube where it vaporizes a liquid dye such as tetraethylene glycol. Baffles in the tube ensure that the dye is completely mixed with the steam before it is ejected. Tests show that the ejected mixture quickly condenses into a fog of particles approximately 1 μm in diameter — the most visible size — that remain suspended for as long as 6 minutes.

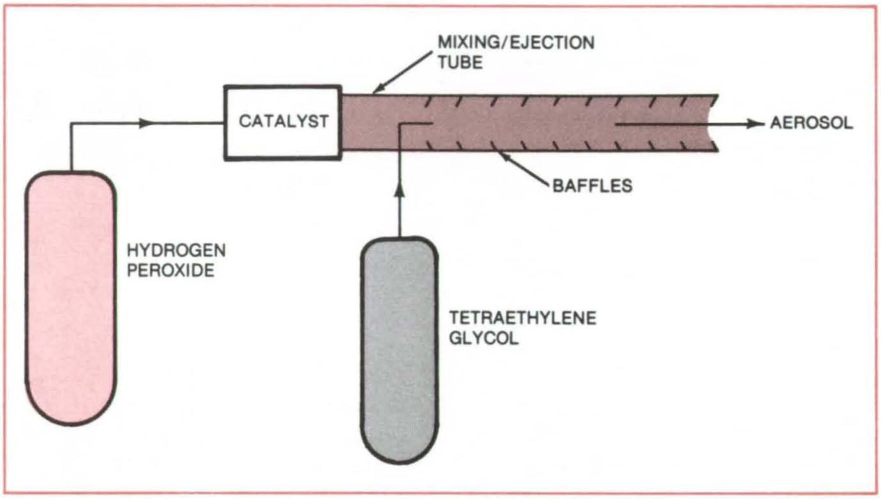

This **Simple Aerosol Generator** catalytically converts hydrogen peroxide to superheated steam and then mixes this steam with a dye. The highly visible mist can be used to study aerodynamic turbulence.

The superheated aerosol persists much longer than those produced by conventional aerosol generators, which last for only about a minute or less. Unlike aerosols produced by skywriting airplanes, it does not depend on the formation of ice crystals at cold high altitudes for visibility and is environmentally safe.

Because of its duration and visibility, the aerosol can be used to study turbulent aerodynamic effects, such as wakes produced by flying aircraft. One important application would be to study vortexes left behind moving aircraft. Though these last only several minutes, they are considered dangerous to following aircraft, particularly near ground level.

This work was done by Marshall A. Appel of Caltech for **NASA's Jet Propulsion Laboratory.** *For further information, Circle 52 on the TSP Request Card.*
NPO-14947

High-Char-Yield Epoxy Curing Agents

A new class of imide-amine curing agents preserves structural integrity, prevents fiber release, and is fully compatible with conventional epoxy resins.

Lewis Research Center, Cleveland, Ohio

Epoxy resins are the most widely used matrix resins in graphite-fiber-reinforced resin matrix composite materials because they are easy to process and because fiber-reinforced epoxies have excellent mechanical properties. However, the char yield of conventional epoxy resins is quite low, usually less than 25 percent. When exposed to a high heat flux such as produced by a fire, these composites lose their structural integrity, and free graphite fibers are released. A novel class of imide-amine curing agents has been synthesized, which more than double the char yield of cured epoxy resins, preserving structural integrity and preventing fiber release.

The imide-amine curing agents are fully compatible with conventional epoxy resins and do not detract from composite properties while greatly increasing char yield.

Conventional graphite-fiber/epoxy-resin composite specimens and neat (unreinforced) epoxy-resin specimens, both with and without the imide-amine curing agents, were fabricated

and tested for mechanical properties, thermo-oxidative stability, and char yield. Processing characteristics with and without the imide-amine curing agents are similar. Mechanical properties are equivalent. All specimens exhibited essentially the same level of thermo-oxidative stability. In char yield tests, the epoxy resins with the imide-amine hardeners exhibited a 200- to 300-percent increase in aerobic char yield and as much as a 100-percent increase in anaerobic char yield.

The development of these imide-amine curing agents is a major breakthrough in achieving high-char-yield epoxy resins. Composite materials utilizing these curing agents can be used in aerospace, automotive, and other structural components where structural deterioration must be minimized and fiber release must be avoided in the event of fire.

This work was done by Peter Delvigs, Tito T. Serafini, and Raymond D. Vanucci of **Lewis Research Center.** *Further information may be found in NASA TM-79226 [N79-29240/NSP], "High Char Imide-Modified Epoxy Resins"* [**$**5]. *A copy may be purchased [prepayment required] from the National Technical Information Service, Springfield, Virginia 22161.*

This invention is owned by NASA, and a patent application has been filed. Inquiries concerning nonexclusive or exclusive license for its commercial development should be addressed to the Patent Counsel, Lewis Research Center [see page A5]. Refer to LEW-13226.

Cap Protects Aircraft Nose Cone

A polycarbonate cap protects aircraft nose cone from erosion.

Langley Research Center, Hampton, Virginia

An inexpensive, easily fabricated cap significantly reduces the costs of repairing nose-cone erosion on aircraft. Made of molded polycarbonate, the cap has been flight-tested and is in use on NASA T-38 aircraft (see figure).

Nose cones and other sections that house radar, radio, or other avionics equipment on some aircraft are usually made of fiberglass to allow transmission or reception of an electromagnetic signal. The fiberglass nose cones, which are especially vulnerable to rain, hail, or dust, eventually erode and must be replaced. For example, on the T-38 aircraft, the unprotected fiberglass nose cones had to undergo inspection twice a year. Roughly 50 percent of the cones had to be replaced annually, at a cost of material and labor for removal, inspection, and repair.

The polycarbonate caps are easily fabricated from commercially available 0.16-cm (1/16-in.) polycarbonate sheets by vacuum forming over a mold. Molding temperatures of only 464 K (375° F) are used. After molding, the interior concave surface of the cap is roughened to enhance adhesion, and the cap is applied to the nose cone with a polyester adhesive. Any required coloring is added to the adhesive resin.

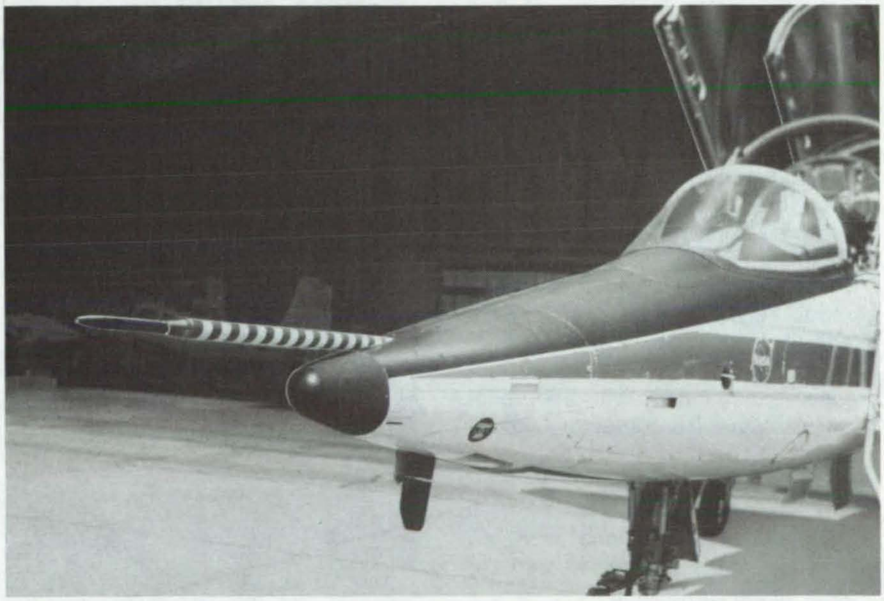

A **Polycarbonate Cap** on the T-38 nose cone protects the fiberglass cone from erosion.

The polycarbonate caps have been under development for several years. Their strength and erosion characteristics are superior to those of the fiberglass cones that the caps protect. Some caps have been tested in-place on T-38 aircraft for over 5 years. Thus far, not a single polycarbonate cap has required replacement. Polycarbonate caps have been tested at both subsonic and supersonic speeds, and a polycarbonate cap on the foresection of the T-38 luggage pod has also been tested. More extensive flight-testing of polycarbonate caps is planned.

This work was done by Charles F. Bryan, Jr., and Donald C. Bryan of **Langley Research Center.** *For further information, Circle 53 on the TSP Request Card.*
LAR-12367

Laser-Beam Methane Detector

Laser instrument determines methane concentration in liquid-natural-gas vapor.

NASA's Jet Propulsion Laboratory, Pasadena, California

A 3.39-μm wavelength helium/neon laser instrument determines the amount of methane in liquid-natural-gas (LNG) vapor. Methane concentration is measured by two InAs infrared detectors that monitor the intensity of the beam passing through the gas. The amount of radiation absorbed by methane at 3.39 μm is proportional to methane concentration. The instrument can be used in modeling the spread of LNG clouds, an important subject in studying the hazards of LNG spills in populated areas, and as a leak detector on LNG carriers and installations.

The laser and its power supply are contained in an enclosure (see photo). The detectors (designated as sensors 1 and 2) are mounted in a column alined with the laser beam. Sensor 1 is located at a height of 2.5 m; and sensor 2, at 1.5 m. A third detector at the column base monitors the laser output, to ensure that the measurements are not affected by power variations.

Gas enters adjustable airgaps adjacent to each sensor. The beam intensity remaining after passage through the absorbing medium decreases exponentially with absorbent concentration. The detector signals are amplified and displayed on a strip-chart recorder. Methane concentration is easily determined from the sensor outputs as long as a few calibration points are known and the system response is linear.

During the initial tests, the detectors remained within their linear-response range up to 6-mV output. The system was tested using a 1-cm-long calibration cell, with methane concentrations from 0 to 100 percent. Linearity and agreement between the two sensor channels were confirmed.

Though not essential to the detection of methane, several thermistors are mounted near the sensors and in the box near the laser and other electronic components to record the operating temperature. (This would be needed to monitor the system in a hot desert environment.) Provision is also made for air-conditioning to maintain stable temperature in hot environments. The unit includes wheels for mobility and can be operated vertically (as shown) or horizontally. A dynamic range of 10^6 is available, assuming operation at 6 mV, with an ultimate detector noise limit of 6 nV.

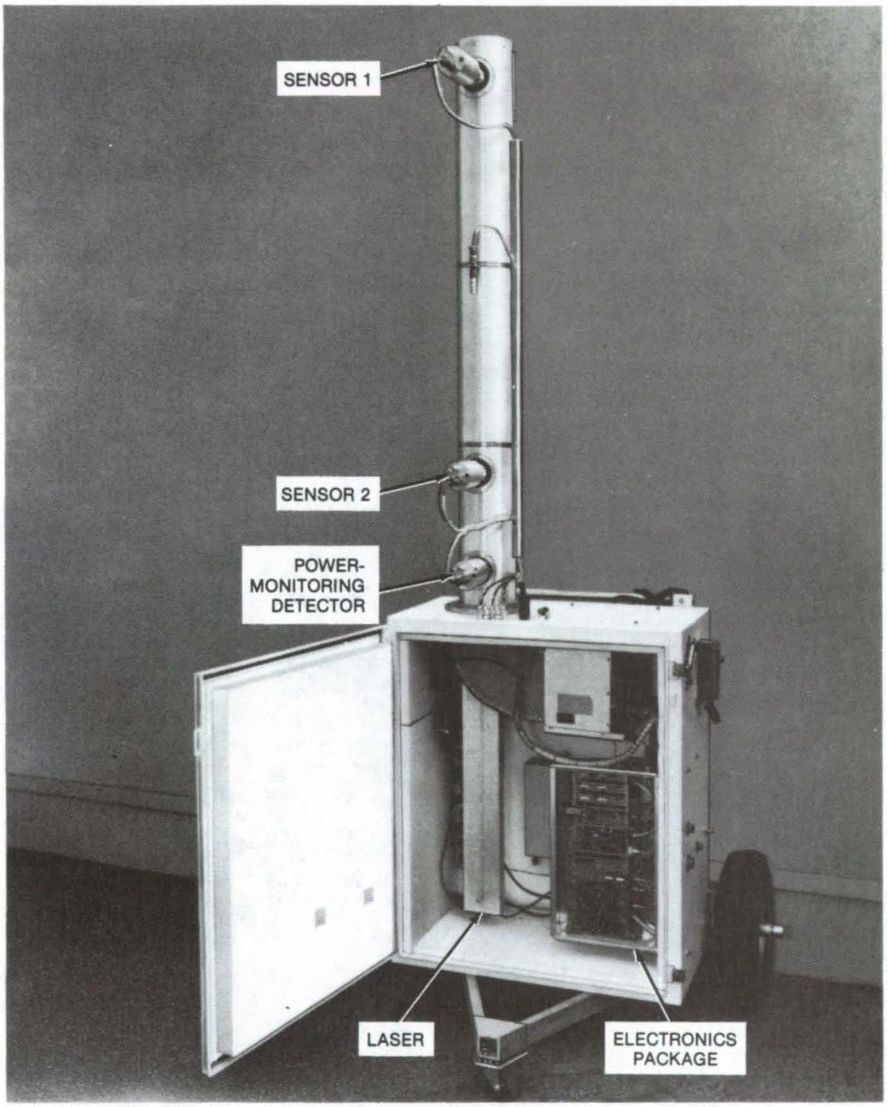

This **Laser System Measures Methane Concentration** by infrared absorption. Two sensors measure the intensity of the 3.39-μm laser beam after it passes through the gas; the absorption is proportional to the concentration of methane.

This work was done by Everett D. Hinkley, Jr., of Caltech for **NASA's Jet Propulsion Laboratory.** *For further information, Circle 54 on the TSP Request Card.*
NPO-14929

Reduced Hydrogen Permeability at High Temperatures

CO and CO_2 reduce hydrogen loss through iron-, nickel-, and cobalt-based alloy tubes.

Lewis Research Center, Cleveland, Ohio

Hydrogen gas is being used as a working fluid in a prototype automotive Stirling engine. Advantages may be achieved over the standard internal-combustion engine in terms of efficiency, fuel consumption, and emissions. The Stirling engine, which is being considered for automotive applications, uses hydrogen gas at high temperatures and high pressures in a closed system. At high temperatures, loss of hydrogen from permeability through the metal containers becomes a serious problem.

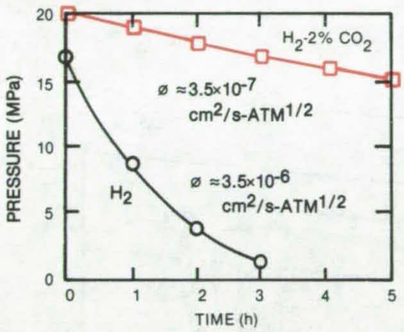

Hydrogen Pressure Loss at high temperatures in Incoloy-800H alloy tubes is up to an order of magnitude smaller when the hydrogen is doped with 2 percent carbon dioxide.

A method has been devised to reduce hydrogen permeability through iron-base, nickel-base, and cobalt-base alloys at high temperature. This method is based on the known concept that an oxide film on a metal surface reduces hydrogen permeability through the metal. The innovation is too add CO or CO_2 to the hydrogen in order to form oxide films continuously during operation. As a result, hydrogen containment at high temperatures is improved.

Tests were run with high-pressure containment tubes at temperatures of 1,400° F (760° C). The iron-, nickel-, and/or cobalt-base alloy tubes were filled with hydrogen gas that had been doped with 0.2 to 5 volume percent of CO or CO_2 gas. Hydrogen permeability rates were reduced by up to an order of magnitude. The necessary factors in reduced permeabilities in addition to an oxygen source such as CO or CO_2 in the hydrogen appear to be the presence of chromium and such other strong oxide formers as aluminum, columbium, or lanthanum in the alloys. The figure shows the reduction in hydrogen permeability, as indicated by loss in pressure, for Incoloy-800H alloy tubes using 2-percent-CO_2-doped hydrogen as compared to undoped H_2.

This research may act as a guide for the development of specific alloys to be used in conjunction with high-pressure, high-temperature hydrogen gas. This should in turn improve the prospects for increased utilization of the Stirling-engine system.

This work was done by J. R. Stephens, W. D. Klopp, and J. A. Misencik of **Lewis Research Center**. *No further documentation is available. LEW-13485*

Chlorinolysis Reclaims Rubber of Waste Tires

A new process reclaims rubber and reduces sulfur content.

NASA's Jet Propulsion Laboratory, Pasadena, California

Disposing of or reclaiming the almost 100 million rubber tires scrapped annually in the United States presents many problems. Traditionally, the reclaim process consists of heating ground-up rubber tires in swelling agents after the cord and metal have been removed. Rubber reclaimed in this manner has poor hysteresis and abrasion resistance, making it unsuitable for premium radial tires.

A new process reclaims waste rubber by using chlorine gas to oxidize the sulfur bonds in preference to other bonds. At the same time, the chlorine gas adds chlorine atoms to the double bonds of the rubber molecules; this reduces depolymerization by preventing oxidation of the carbon/carbon bonds. The chlorinated rubber is less susceptible to swelling by oils and may be used as a paint ingredient. Rubber hydrochloride, a similar product, is an established packing film.

In a typical treatment, 50 grams of acetone-washed ground scrap rubber containing about 5 percent calcium carbonate are slurried with 400 grams of trichloroethane and 10 grams of water. The slurry is heated to boiling and chlorine gas is bubbled through at 0.18 liter/minute for from 1 to 4 hours. The liquid is then filtered through a Buchner funnel and washed with water to remove sulfates. The chlorinated product is washed with acetone to determine if other new compounds are

(continued on next page)

produced. The product is then vacuum-dried to remove all solvent.

Elemental analysis of the carbon, hydrogen, sulfur, and chlorine in rubber treated this way shows a large reduction in sulfur content and a sharp increase in the chlorine content. This process takes place without much depolymerization, though extensive chlorine addition at the rubber-polymer double bonds occurs. There is no measurable substitution of hydrogen atoms by chlorine atoms.

This work was done by Eugene R. du Fresne, Jan Harper Tervet, and Glen G. Hull of Caltech for **NASA's Jet Propulsion Laboratory.** *For further information, Circle 55 on the TSP Request Card.*

Inquiries concerning rights for the commercial use of this invention should be addressed to the Patent Counsel, NASA Resident Office-JPL [see page A5]. Refer to NPO-14935.

Reduced Gravity Favors Columnar Crystal Growth

In zero-gravity, alined columnar microstructures form at the expense of equiaxed growth.

Marshall Space Flight Center, Alabama

Alined columnar crystalline microstructures are preferred in castings for which the directional dependence of physical properties is beneficial (such as in turbine blades). However, many complex alloys preferentially form axial rather than columnar microstructures.

Recent experiments aboard sounding rockets indicate that in low gravity, it should be possible to produce completely columnar microstructures with no equiaxed crystal growth. Small samples of NH_4Cl-H_2O were tested as model systems. Experiments were performed during a 250-second free-fall period, when gravitational acceleration was less than 10^{-4} g.

The heart of the apparatus used in the experiment is a solidification chamber (see figure). A semicylindrical copper chill block has been brazed to a stainless-steel top plate. The plastic (Plexiglas or equivalent) front and rear faces are sealed with O-rings. A copper web transmits heat to and from the cell. The particular cell geometry was chosen to extract heat radially, to simulate weld bead solidification, and to allow a camera to observe the experiment.

At 1 g, depending on the amount of superheating and on the orientation of the chill block in the gravitational field, the columnar zone accounted for 25 to 100 percent of the structure. Equiaxed-grain multiplication occurred by showering and by convection-induced dendrites on remelting. These dendrites act as nuclei for the formation of equiaxed grains.

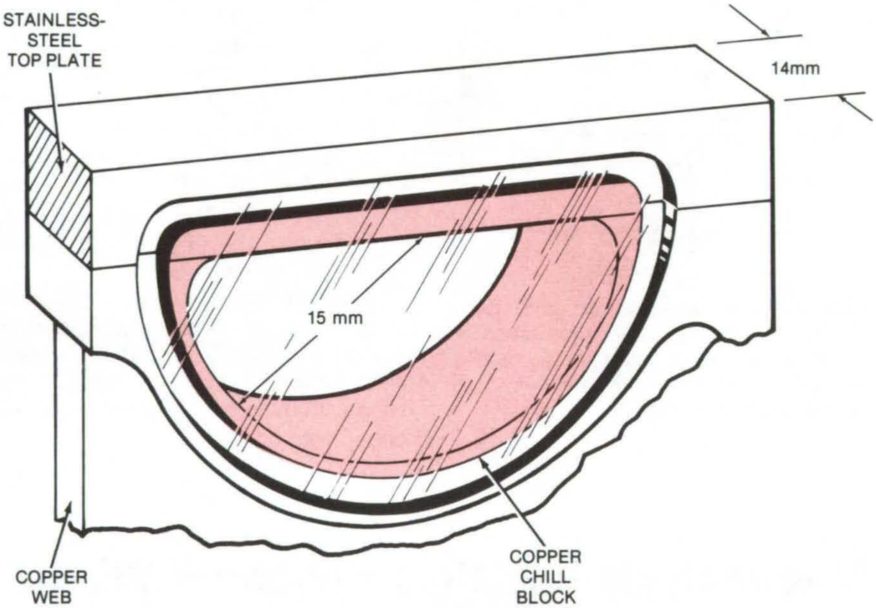

A **Solidification Chamber,** used to grow columnar structures preferentially, consists of a semicylindrical copper chill block brazed to a stainless-steel top plate. In experiments aboard sounding rockets, four chambers were symmetrically arranged about, and attached to, a copper web.

At low gravity, however, completely columnar structures were obtained; all equiaxed-grain multiplication mechanisms were suppressed. Reduced gravity apparently modified the thermal conditions and caused the liquid to cool more slowly. This resulted in steeper temperature gradients in the liquid ahead of the solidification interface. This interface is believed to be a determining factor in the columnar-to-equiaxed transition. The growth rate of the solid was not affected. Although in two cases a spring-loaded expansion piston jammed, causing "big-bang" nucleation and distributing nuclei throughout the liquid, an equiaxed zone did not form. Apparently, low gravity eliminates the columnar-to-equiaxed transition in this system; verification of the results with other metals and alloys is needed.

This work was done by Theodoulos Z. Kattamis and John M. Papazian of Grumman Aerospace Corp. for **Marshall Space Flight Center.** *For further information, Circle 56 on the TSP Request Card.*

MFS-25205

Life Sciences

Hardware, Techniques, and Processes

Books and Reports

Flow Sensor for Biomedical Fluids

Electronic sensor would accurately measure and control flow of plasma, whole blood, or drugs in solution.

Lyndon B. Johnson Space Center, Houston, Texas

A flow-rate sensor shows promise as an instrument for measuring the rate of injection of intravenous biomedical fluids. Originally developed for a water-quality measurement system [see "Meter for Very Slow Flows" (MSC-18112) on page 275 of *NASA Tech Briefs*, Vol. 3, No. 2], the sensor would noninvasively determine the amount of whole blood, plasma, or drug solutions administered to a patient. In combination with a valve or pump, the sensor would control the flow as well as measure it.

The complete apparatus (see figure) consists of intravenous delivery equipment with two metal segments in the delivery tubing, a thermal-flow sensor, control electronics, and a proportioning valve or peristaltic pump. The sensor uses thermistors to measure the temperature of the flowing biomedical fluid at two points in the delivery tube. Before the fluid passes the downstream thermistor, a small resistor heats the fluid just enough to keep the temperature sensed by the downstream thermistor at a predetermined level above that sensed by the upstream thermistor. The electric power consumed by the resistor to maintain the temperature difference is a measure of the flow rate.

The thermistors and resistor embedded in epoxy or other insulating material would contact curved metal plates in a groove on a plastic housing. The insulation insures that the heat from the resistor goes predominantly into the fluid. The fluid delivery tube would be placed in the groove so that its two metal segments, which could be stainless steel or a good thermal conductor such as copper or silver, contact the two metal plates in the housing. The resistor and thermistors thus have a low-thermal-resistance path to the fluid.

Electronic circuits measure the temperature difference between the thermistors, regulate power to the resistor, and calculate and indicate the flow rate. The circuitry also would generate a signal for the flow-control pump or valve.

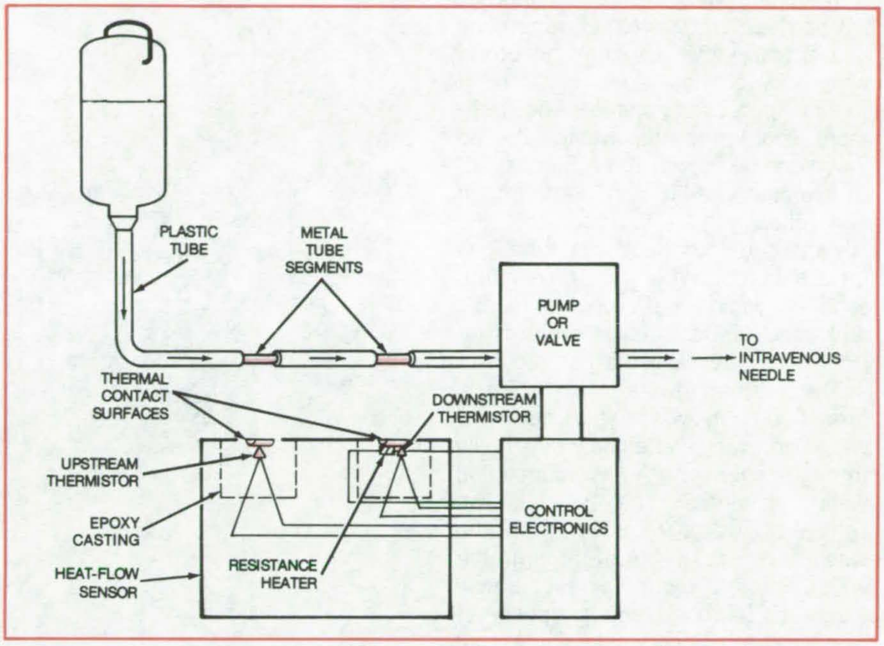

Upstream and Downstream Thermistors have a constant temperature difference maintained between them by a resistance heater. The electric power consumed by the heater in maintaining the constant temperature difference is a measure of the flow rate. This measure is used to control accurately the flow rate through the pump or valve.

The usual way to supply biomedical fluids is from a bottle, elevated to provide a gravity pressure head to force the fluid through a plastic tube and a hypodermic into the patient's body. A small pinch valve is used to control the fluid flow manually, the flow being estimated by counting the frequency of the drops of fluid at the mouth of the glass bottle. The error with this flow estimation method is ±15 percent.

With the new sensor, the fluid flow would be set and maintained at a precise rate. Since infusion-pump rates typically vary from 0.04 cc/hour to 4.00 cc/hour, the new sensor would have to function in this range. The pump would be controlled continuously to compensate for changes in upstream pressure as the bottle empties. Since the sensor responds to a temperature difference, rather than absolute temperature, it would not be very sensitive to the temperature at which the fluid is supplied — an important advantage since biomedical fluids are sometimes used directly as they come from the refrigerator. The sensor would also detect when air replaces liquid in the tube and could stop the pump to prevent air from being injected into the patient's veins when the bottle is empty.

Since the sensor would not directly contact the fluid, it would not have to be sterilized. It is compatible with disposable bottles, tubes, and the hypodermic needles widely used in hospitals. The only modification necessary is in the tube, which must contain two small metal inserts, spaced to fit in the curved thermistor plates.

This work was done by H. Eugene Winkler of **Johnson Space Center.** *For further information, Circle 57 on the TSP Request Card.*

Inquiries concerning rights for the commercial use of this invention should be addressed to the Patent Counsel, Johnson Space Center [see page A5]. Refer to MSC-18761.

Treating Domestic Wastewater With Water Hyacinths

Greenhouse system purifies water, extracts fertilizers, and generates fuel.

Marshall Space Flight Center, Alabama

Waste and wastewater from individual homes can be treated separately and effectively by a system based on water hyacinths, according to a recently proposed concept. The treatment would purify the wastewater so that it can be reused and would extract usable plant nutrients, rich in nitrogen and phosphorus. In addition, the system could produce methane gas for use as fuel. When fully developed, such a system may supplant septic tanks and central sewage systems for rural and undeveloped areas.

The treatment system consists of a greenhouse in which the domestic waste and wastewater flow by gravity through spiral channels containing water hyacinths (see figure). The soluble waste is removed from the wastewater as it flows through the water hyacinth roots where chemical elements (nitrogen and phosphorus) are removed. Solid waste settles out of the wastewater and decomposes in an anaerobic digestion tank, producing enough methane to heat the greenhouse during the winter months. After the solid waste is removed, the purified water is disinfected with ozone, ultraviolet light, or chlorine and recycled to the house.

The waste and wastewater are pumped to the top channel in the greenhouse, and a check valve in the main sewage line prevents backflow. Reflectors are positioned in the greenhouse to light the hyacinths in the bottom channels.

The number of square feet (meters) of plants needed varies according to their growth rate. Under controlled conditions, the water hyacinths grow rapidly, increasing their weight by 5 to 11 percent every day.

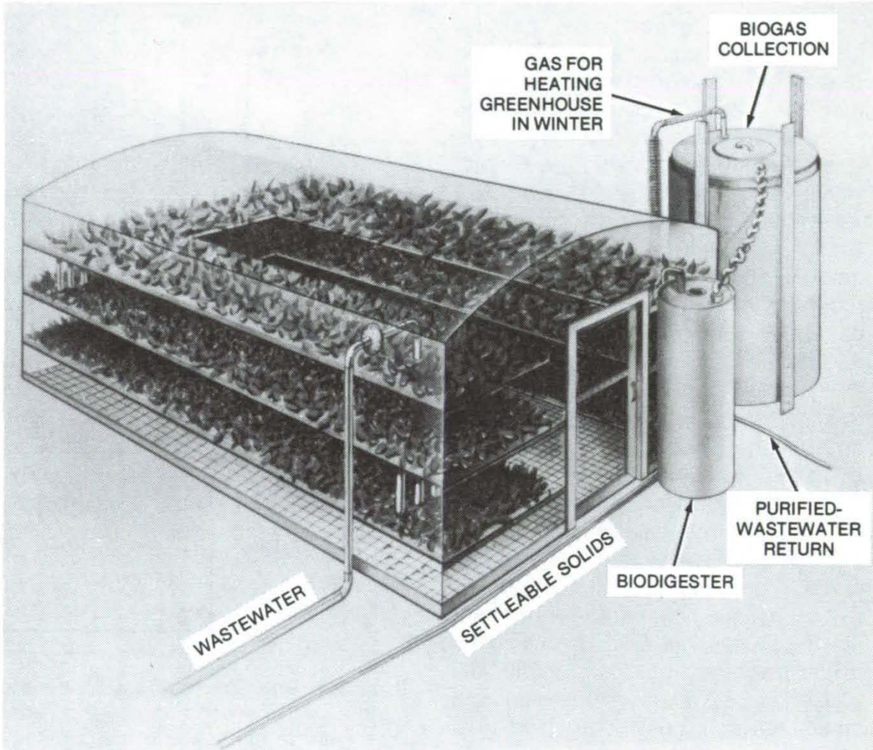

This **Waste-Recycling System** uses water hyacinths to purify wastewater and generate methane gas as a byproduct. A system with 200 ft^2 (18.6 m^2) of water hyacinths would treat the wastewater of a family of four (1,500 liters/day) and would generate 600 to 850 ft^3 (17 to 24 m^3) of biogas.

The flow channels in the greenhouse should furnish 50 square feet (4.65 square meters) of plant surface area for every person or for 100 gallons (378 liters) of wastewater. The channel flow depth should be adjustable from 4 to 12 inches (10 to 31 centimeters) so that the retention time can be varied according to the water quality desired. Once the balance of nutrient loading to plant biomass produced is established, excess water-hyacinth growth can be harvested monthly and converted by anaerobic digestion to additional methane or by composting to organic fertilizer and soil conditioner.

This work was done by Rebecca C. McDonald and B. C. Wolverton of the National Space Technology Laboratory for **Marshall Space Flight Center.** *For further information, Circle 58 on the TSP Request Card.*
MFS-23964

Compliant Transducer Measures Artery Profile

Springy fingers give a continuous recording of artery diameter.

NASA's Jet Propulsion Laboratory, Pasadena, California

A new instrument accurately measures the inside contours of arteries without using X-rays or dyes. Consisting of compliant fingers with attached semiconductor sensors, the instrument is drawn through the artery to allow the fingers to follow the internal contours. Levels of stenosis and plaque can be quantified, along with the artery profile, from a continuous output on a pen recorder.

Two, three, or more compliant fingers may be used, each attached to a base and each with its own semiconductor pickup (see figure). Lead wires transmit electrical signals from the pickups to external processing equipment. The signals are converted to diameter data and displayed as a function of position along the artery.

The contour transducer is emplaced in a catheter, which is inserted in the artery by conventional methods. The catheter is then separated from the transducer, and both are pulled along the artery. As the transducer travels, its fingers press lightly against the artery wall and move in and out to reflect its contours. Because the fingers are thin, they do not interfere appreciably with blood flow.

Tests have shown that the finger pressure is so small that there is no visible enlargement of the artery as the transducer moves along. Reproducibility tests, in which recordings were made by repeatedly drawing the transducer along the same section of an artery, have shown that successive strip-chart traces match each other to a high degree.

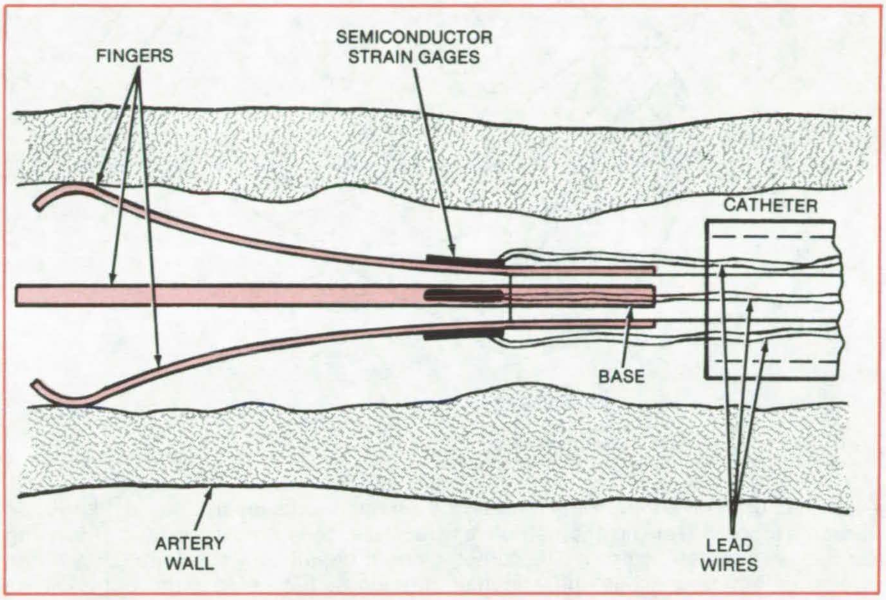

Artery Contour Transducer Has Fingers that move to conform to the walls. Semiconductor pickups convert the finger movements to proportional electrical signals. A catheter is used to place the instrument in an artery.

This work was done by Cyril Feldstein and Virgil H. Culler of Caltech and Donald W. Crawford and James R. Spears of the University of Southern California for **NASA's Jet Propulsion Laboratory.** *For further information, Circle 59 on the TSP Request Card.*
NPO-14899

Improved Ureteral Stone Fragmentation Catheter

An improved catheter would include a fiber-optic viewer, a more reliable ultrasonic probe, and a better contact sensor.

NASA's Jet Propulsion Laboratory, Pasadena, California

Ureteral stones affect about 60,000 Americans every year. Many cases are treated nonsurgically by removing the stones with a Dornier stone basket or, more recently, by using ultrasonic catheters. Catheters using ultrasonically-driven wire probes have already been used with success; however, some improvements are needed.

One of the problems is in guiding the catheters with the assistance of X-rays or fluoroscopes. X-rays and fluoroscopes expose the patient to unnecessary radiation and are not very accurate in verifying when the probe is in contact with the stone. Another problem is the durability of the apparatus. The ultrasonic driver-to-probe coupling can overheat and break.

One suggested improvement is to use fiber-optic viewers to observe the stone directly at distances ranging between 0.5 and 1.0 cm. Two fiber bundles are needed (see figure): one to illuminate the path and the other for viewing.

(continued on next page)

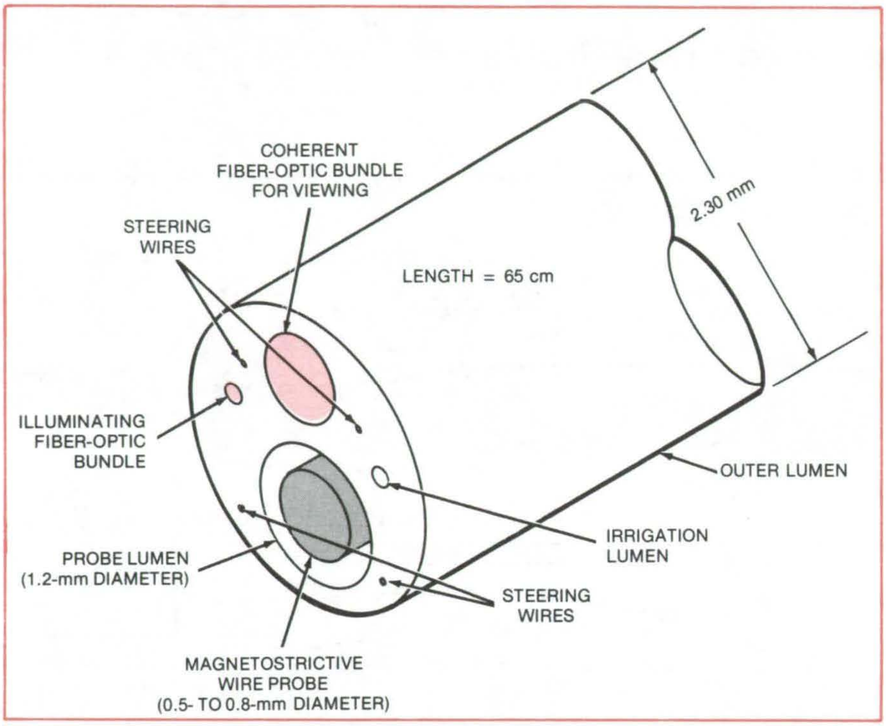

Proposed Ureteral Stone Fragmentation Catheter would incorporate a fiber-optic viewer, a more-reliable magnetostrictive wire probe, and improved means of sensing contact with ureteral calculi. The catheter would be guided by four steering wires, and irrigation fluid would be supplied through a lumen to remove the stone fragments.

Another improvement is to energize the magnetostrictive probe along most of its length. This will help to distribute the stress and prevent probe breakage. To produce 25-μm axial sinusoidal displacements, the probe would be made from magnetostrictive material and wound with a coil that generates a magnetic-field intensity of 200-ampere turns/in.

Finally, contact with stones can be determined by sensing the change in mechanical impedance. This impedance can be sensed photoelectrically or electrically. In the first, an optical sensor comprised of light source, lens, and phototransistor can sense the mechanical displacement and produce a signal to increase the level of the ultrasound when the probe contacts the stone. The displacement could also be sensed electromechanically. In the second, the influence of the mechanical impedance upon the electrical impedance of the driving coils would be sensed.

All of these improvements can probably be incorporated into a 65-cm-long by 2.30-mm-diameter catheter. The catheter would be steered by four wires and equipped with an irrigation lumen. The lumen would supply fluids to remove the stone fragments.

This work was done by Paul M. Gammell of Caltech for **NASA's Jet Propulsion Laboratory.** *For further information, Circle 60 on the TSP Request Card.*
NPO-14745

Miniaturized Physiological-Data Telemetry System

Low-power portable unit has 13 data channels and two-way voice communication.

Lyndon B. Johnson Space Center, Houston, Texas

A portable digital physiological-data telemetry system uses less power, is more compact, and provides better data integrity than two previous systems designed to similar specifications. A block diagram of the portable unit (to be worn by the subject) and the base unit is shown in the figure.

The portable unit transmits 13 data channels to the base unit of which 6 are analog channels (350-Hz-bandwidth each) and 7 are dc data channels (30-Hz-bandwidth each). Three of the analog channels transmit electrocardiogram (ECG) signals (insulated electrodes can be used).

After signal conditioning, the analog data signals are converted to digital form and transmitted serially, using Manchester biphase-coded pulse code modulation (PCM). A modified phase-locked loop decodes the data. The loop has a narrow lock-in range and remains in operation even if the signal from the portable unit is momentarily interrupted.

The telemetry system also has two-way (narrow-band FM) voice communication. Voice transmission from the portable unit interrupts data transmission and is controlled by a voice-operated switch (VOX).

To reduce power drain and to prevent transmission interruption by the subject under crisis, the base unit controls power to most subsystems in the portable unit via a transponder. The base unit also selects the portable-unit operating modes, such as calibrate,

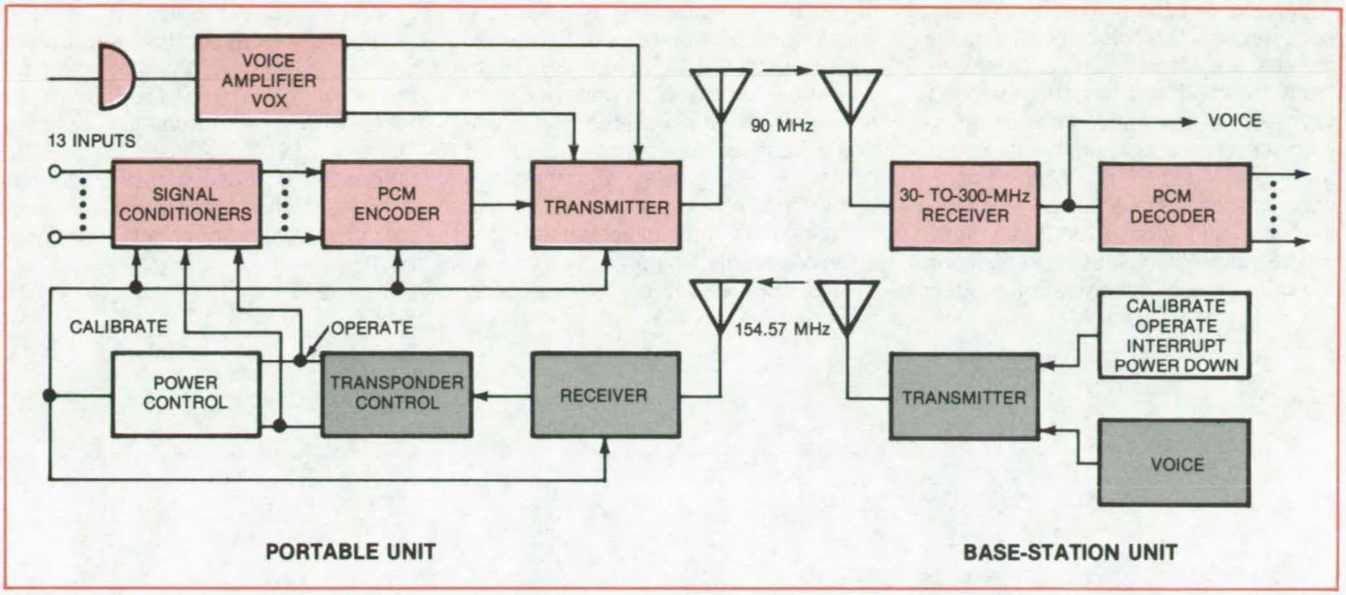

The **Miniaturized Physiological-Data Telemetry System** has a low-power-drain (1/3-watt-maximum) portable unit, worn by the subject, and a base-station unit. The portable-unit transmitter is mounted in the headset. The remaining portable-unit circuitry, measuring 2.5 by 4.5 by 1.25 inches (6.4 by 11.4 by 3.2 cm), is worn in a belt pack.

operate, interrupt (the portable unit receives but does not transmit), or power down (the portable unit samples received signals periodically, until directed to change mode).

All circuits use CMOS flat-pack integrated circuits for minimum power consumption and small size. The RF links in the portable unit operate between 8 and 10 volts and are powered by a standard 9-volt transistor-radio battery. The analog circuits operate at ± 5 and ± 2.5 volts from small nickel/cadmium batteries.

The base station uses a commercially available transmitter and receiver and converts the data received back into analog form. The system operates reliably in all modes at distances of up to 100 ft (30m).

This work was done by William M. Portnoy and Lawrence J. Stotts of Texas Tech University for **Johnson Space Center.** *Further information may be found in CR-160660 [N80-24357/NSP]. "A Miniaturized Digital Telemetry System for Physiological Data Transmission" [$7]. A copy may be purchased [prepayment required] from the National Technical Information Service, Springfield, Virginia 22161.*
MSC-18804

Books and Reports

These reports, studies, and handbooks are available from NASA as Technical Support Packages (TSP's) when a Request Card number is cited; otherwise they are available from the National Technical Information Service.

Manual for Physical Fitness

Personalized programs for becoming and staying fit are included in the *Astronaut Training Manual.*

The 250-page training manual used for preflight conditioning of NASA astronauts will be enjoyable and beneficial reading for anyone interested in physical fitness. Written for an audience with diverse backgrounds and interests, the *Astronaut Training Manual* suggests programs for various levels of fitness, including sample starter programs, safe progression schedules, and stretching exercises. Related information on equipment needs, environmental considerations, and precautions can help readers design safe and effective running programs.

A starter jogging program is recommended for people who can be classified as being in "fair or better" condition according to standards set forth in the manual. Lasting 21 weeks, this program allows beginners to build their cardiorespiratory endurance safely to the point where they can readily jog for 20 minutes continuously, four times a week. Swimming and cycling are among the other exercises for which sample training programs are given.

In addition to endurance training, strength training programs are suggested. The strength programs may be pursued concurrent with the endurance programs and may be performed by lifting free weights, doing isometric exercises, or working out on a mechanical gym. Stretching exercises (which make the body more flexible) are recommended for the morning, during work, before training, after training, during travel, before bed, and for relief of low-back tension. For all programs, performance norms for men and women are included.

The reader is amply furnished with the background needed to design and implement a personalized program. In a discussion of energy sources, fitness

is defined, and the distinction is drawn between anaerobic activities (including golf, baseball, and tennis) and more-effective and efficient endurance-building aerobic activities (including running, cycling, and swimming). Sports are evaluated in terms of their energy consumption, hazard, fitness, development potential, convenience, and fun.

The nature of muscular strength and the principles of schemes for building strength are explained. The relationship between obesity, diet, and exercise is explored, and—in an appendix—busy but weight-conscious fitness trainees are provided with a calories counter for popular fast-food items. (For example, a three-piece crispy fried-chicken dinner furnishes 1,170 calories and can be worked off in a run of roughly 1 hour.)

This work was done by A. Eugene Coleman of the University of Houston at Clear Lake City for **Johnson Space Center**. *Further information may be found in NASA CR-160758 [N80-29024/NSP] "Astronaut Training Manual" [$15]. A copy may be purchased [prepayment required] from the National Technical Information Service, Springfield, Virginia 22161.*

MSC-18915

Mechanics

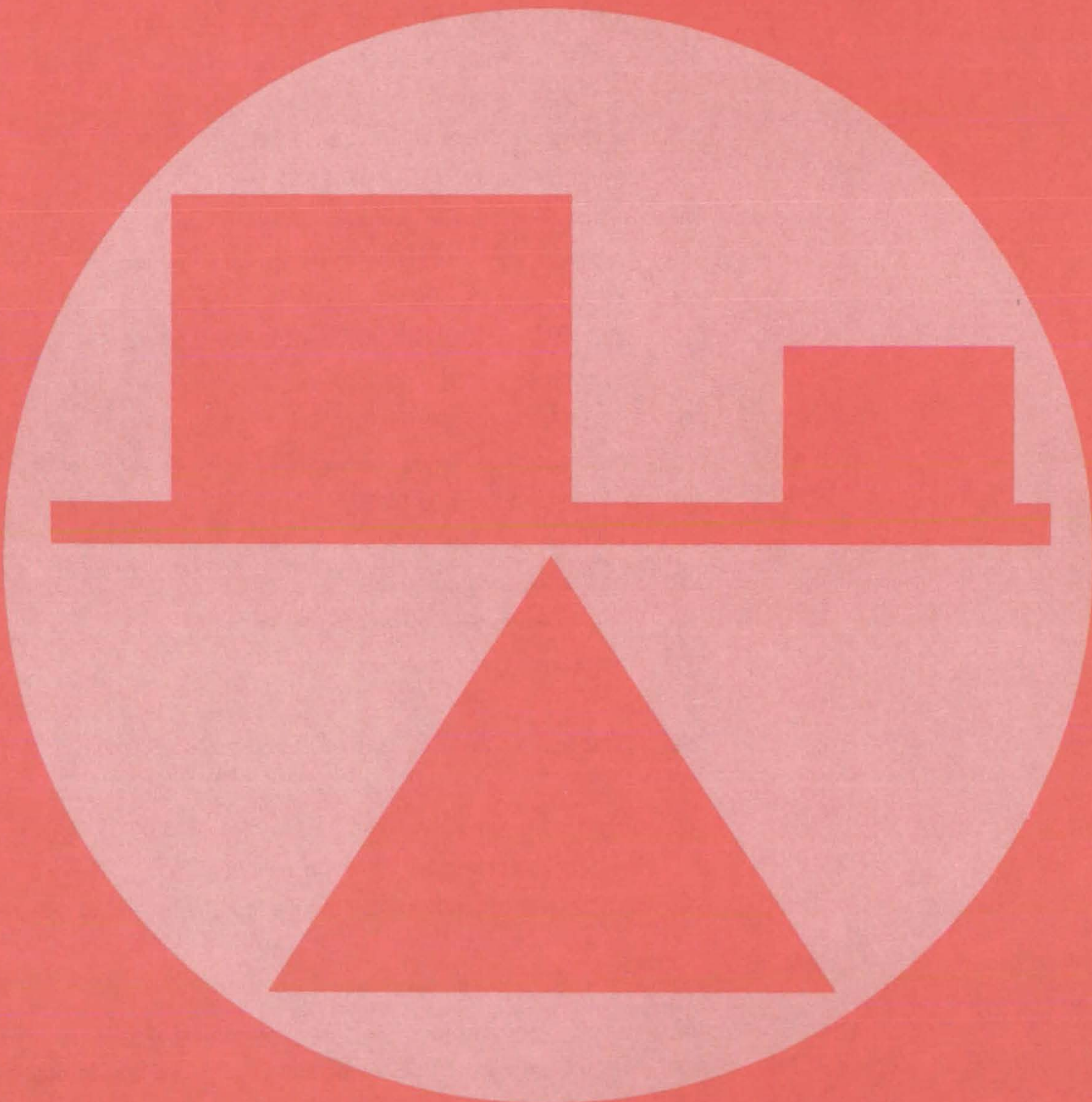

Holes Help Control Temperature

Holes for radiative heat transfer assist in passive thermal control.

Goddard Space Flight Center, Greenbelt, Maryland

Completely-passive temperature control systems — those that use no fans, heaters, or other energy-consuming elements — are often considered for spacecraft because they save weight, cost, energy, and complexity. The same advantages could be realized in some Earthbound systems, particularly those for which convection effects are small.

A recent study of passive thermal control for the Solar Terrestrial Subsatellite (STSS) has found that an array of "see-through" holes substantially improves the performance of the system. The holes in the payload mounting plates allow line-of-sight radiative heat transfer between the hot and cold ends of the spacecraft and between the mounting plates and the ends. Temperature gradients between the plates are thereby reduced, as is the temperature of each plate. The holes and selected exterior paints and finishes keep the payload cool for all orientations and operating modes of the STSS.

Since convective heat transfer is the dominant mode for most terrestrial systems, some forced cooling is usually necessary. However, a passive system can sometimes substitute for some of the active elements; and in evacuated equipment such as flywheel energy-storage devices, a passive system can play a substantial role in controlling the temperature.

For the STSS, a cylindrical enclosure roughly 2 meters in diameter, heat transfer in the vacuum of space is all radiative and conductive. All orientations with respect to the Sun are possible, and the satellite may be spinning at 20 rpm about its axis of symmetry. The scientific payload, which dissipates up to 190 watts, in addition to a "housekeeping" load, is distributed on two interior "isogrid" mounting plates. Originally conceived as a way to save weight and to change modular payloads rapidly, the aluminum isogrid plates are perforated to accept spiderlike payload supports.

(continued on next page)

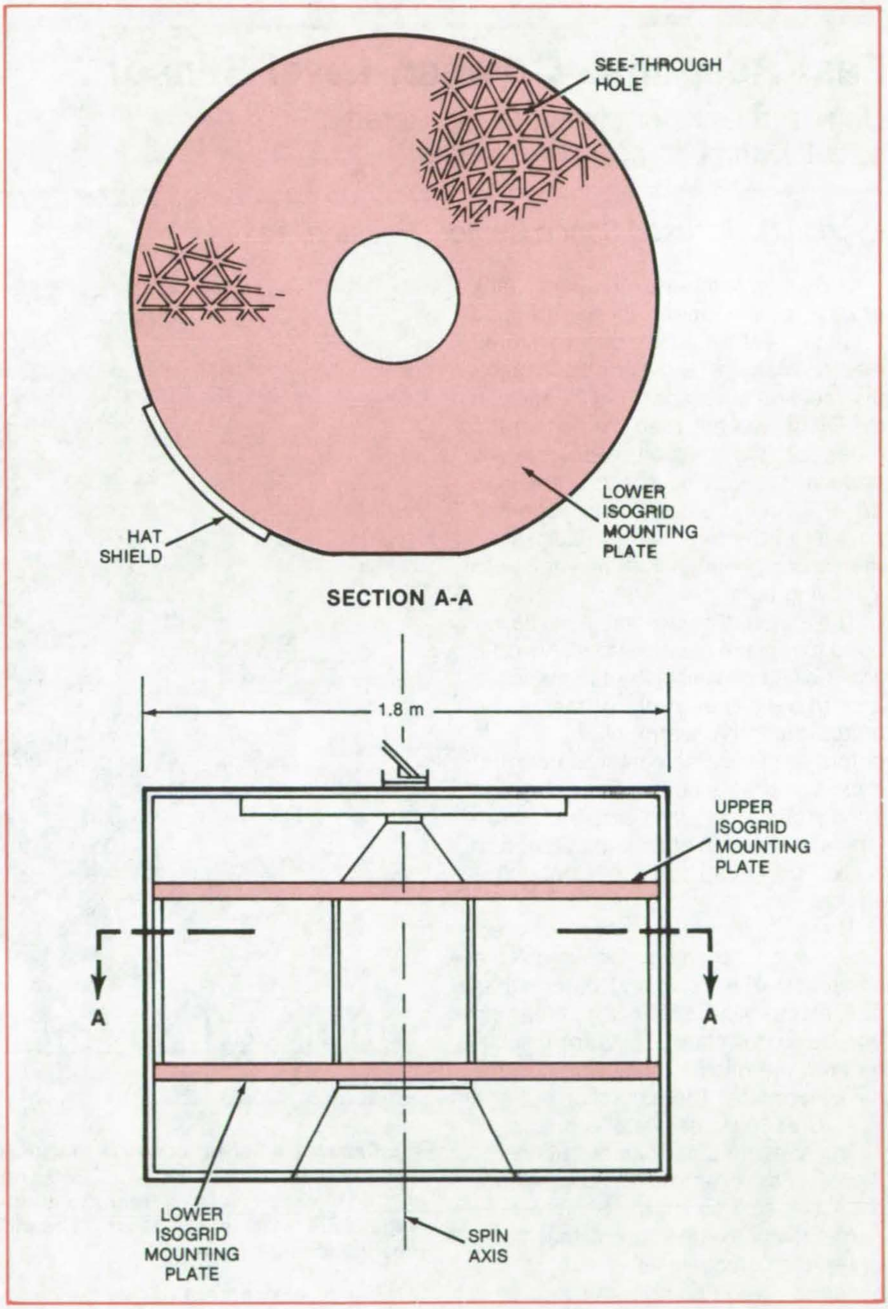

The **Solar Terrestrial Subsatellite** (STSS) is a Space-Shuttle-launched-and-retrieved reusable satellite, operating at an altitude of 250 kilometers. Perforated "isogrid" mounting plates allow rapid interchange of scientific payload modules. A thermal analysis shows that the perforations are essential to effective temperature control.

Analysis of the STSS using a 52-node thermal model shows that the payload temperature can be held between 0° and 30° C for all operating conditions if the scientific instruments do not completely block the holes in the mounting plates. Nominal values for the absorptivity and emissivity of the exterior surfaces were chosen, although these parameters could be adjusted if necessary. Likewise, the total "see-through" area is a parameter that can also be varied. To insure that the radiative paths are not blocked, careful consideration is given to the placement of the payload. In such designs it is advantageous not to be constrained by the shape and size of the enclosure.

This work was done by Chandramohan K. Chhatpar of RCA Corp. for **Goddard Space Flight Center**. *No further documentation is available.*
GSC-12618

Fast-Response Cryogen-Level Sensor

Liquids in tanks or pipes are monitored by a flowthrough capacitive sensor.

Lyndon B. Johnson Space Center, Houston, Texas

The liquid level in a cryogenic tank or pipe, or the amount of gas trapped in pipeline flow, can be monitored electronically by a cylindrical capacitive sensor (see figure). Changes in the liquid level between the concentric tubes of the capacitor change its impedance, varying the current in a drive circuit. Since it is oriented parallel to the direction of liquid flow, the sensor presents little resistance to a moving fluid.

The capacitive sensor was developed to replace a warm-wire sensor in liquid-oxygen vessels. Its response time of 5 ms is an order of magnitude faster than the warm wire, and its output signal is also easier to interpret and is more reliable. By using the conductance of the sensor as an indicator, instead of its capacitance, it could be adapted for conductive liquids.

Three concentric stainless-steel tubes are the main body of the capacitor. The inner and outer tubes are electrically connected, forming one capacitor plate. They are insulated from the middle tube, which forms the other plate. The excitation voltage is a 20-V/6-kHz oscillator signal.

The sensor output can be analog or digital. For example, a comparator may be set so that its threshold corresponds to the current that flows when the cryogen fills half of the capacitor. The comparator can then open a valve if the liquid falls below that level.

For an analog readout, the drive current is monitored by an ammeter. The current gives a reading of liquid level or of the percent of gas bubbles in the liquid. The fast response of the sensor makes possible this quantitative evaluation of gas pockets.

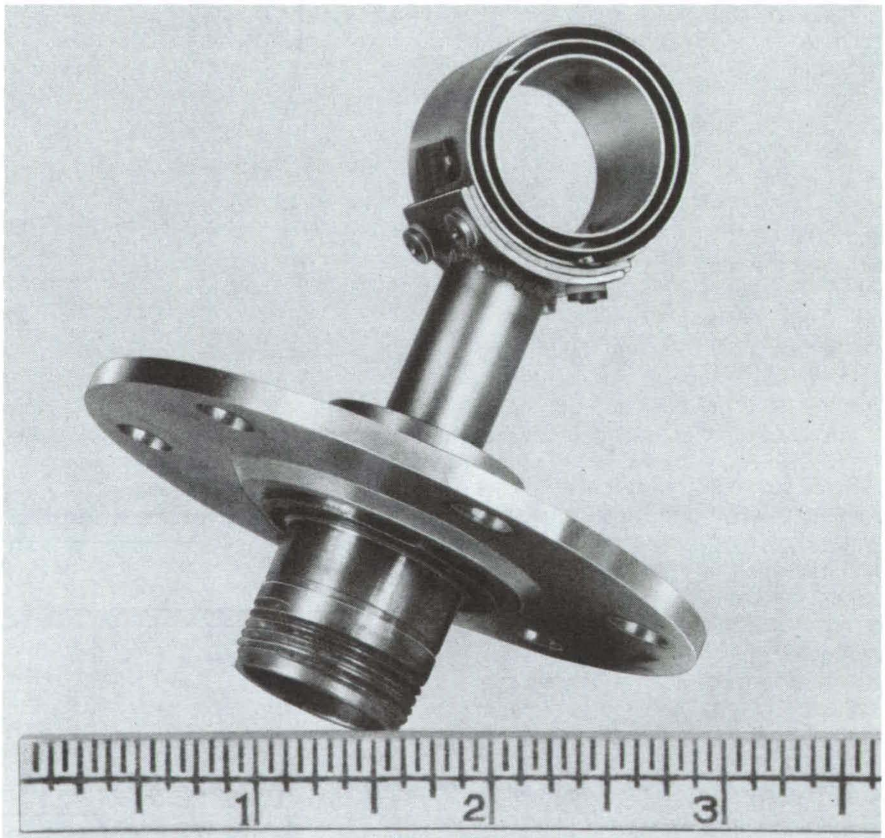

The **Capacitive Sensor** consists of three concentric tubes 0.825 in. (0.210 cm) long; its outer diameter is 1.125 in. (2.859 cm). The inner and outer tubes are connected electrically and insulated from the middle tube by polytetrafluoroethylene spacers. Airgaps are 0.100 in. (0.254 cm). The mounting flange for installing the sensor in a pipeline is also shown.

This work was done by Joel B. FitzPatrick and Lawrence C. Maier of Simmonds Precision Products, Inc., for **Johnson Space Center.** *For further information, including a detailed assembly drawing of the sensor, Circle 61 on the TSP Request Card.*
MSC-18697

Fiber-Optic Level Sensor for Cryogens

Sharp bends in the fiber improve sensitivity with liquids of low refractive index, such as liquid hydrogen.

Lyndon B. Johnson Space Center, Houston, Texas

A new fiber-optic liquid-level sensor is useful in cryogenic environments where liquids of very low index of refraction are encountered. It is a "yes/no" indicator of whether the liquid is in contact with the sensor.

In the new sensor (see figure), sharp bends in the fiber alter the distribution of light among the propagation modes. This amplifies the change in the light output observed when the sensor contacts liquid, without requiring a long fiber that would increase insertion loss. Tests of the sensor in liquid nitrogen show an insertion loss of 20 dB and a change in signal level of 8 dB when the sensor contacts the liquid. A change of 2 dB is expected for liquid hydrogen.

The fiber-optic level sensor uses a bare glass fiber coupled to a light source at one end and to a light detector at the other end. When the fiber contacts a liquid, light propagating in relatively oblique modes passes into the liquid rather than staying in the fiber, because the critical angle for total internal reflection is greater at the liquid interface than it is at the air interface. Thus, light that would remain trapped in the fiber if it were surrounded by air escapes when it is surrounded by liquid. The closer the liquid index of refraction approaches that of the fiber, the more light is lost. Conversely, if the liquid index of refraction is low — as with liquid hydrogen, little light is lost and sensitivity is poor.

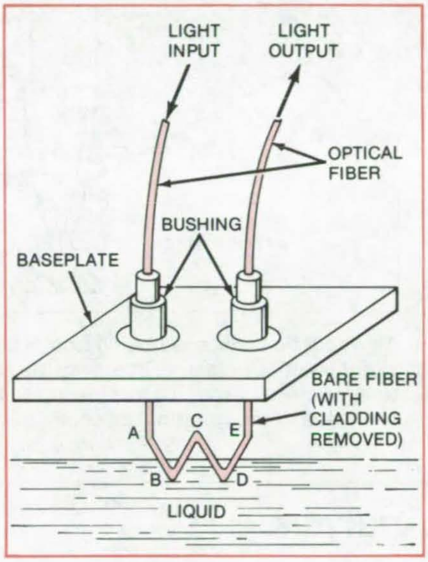

The Improved Fiber-Optic Liquid-Level Sensor has five sharp bends in the glass fiber. Contact with the liquid is sensed at bends B and D. It is driven by an LED that emits 0.2-ms pulses at 50 Hz, which are synchronously detected by a photodiode receiver.

To increase sensitivity, some previous sensors consist of a coil of smooth loops, so that the fiber enters and leaves the liquid several times. However, if the fiber has no sharp bends to generate oblique modes, little additional sensitivity is gained for each added loop, while insertion loss increases. Any mode that does not escape at the first entry into the liquid does not escape at subsequent entries either.

The new sensor uses a glass fiber 0.04 in. (1 mm) in diameter. Special low-loss seals (not shown in figure) are used where the fiber passes through holes in a metal baseplate. The seals have a bushing that assures a very fine band of contact between the epoxy sealant and the fiber.

This work was done by Madan Sharma of TRW, Inc., for **Johnson Space Center.** *For further information, Circle 62 on the TSP Request Card.*

Inquiries concerning rights for the commercial use of this invention should be addressed to the Patent Counsel, Johnson Space Center [see page A5]. Refer to MSC-18674.

Acoustic Lens is Gas-Filled

A fluorocarbon gas contained by a plastic film makes an effective lens for sound waves.

NASA's Jet Propulsion Laboratory, Pasadena, California

A novel acoustic lens is fabricated by clamping together two membranes of thin plastic and filling the enclosed space with a fluorocarbon gas. In tests, the lens substantially improved the accuracy of sound "maps" of turbulent airflow. It could also be used to record sound-intensity patterns in the design of speakers, lecture halls, and auditoriums.

The basic lens configuration is shown in the figure. Two circular membranes of Mylar or equivalent plastic, 0.25 mil (0.06 mm) in thickness, are clamped together around their peripheries. At one point on the circumference, a small tube (not shown) is held by the same clamp and extends into the gastight space. A heavy gas such as Freon (or equivalent) is fed through the tube, stretching the plastic facesheets into the shape of a convex lens.

(continued on next page)

The speed of sound in the gas is considerably less than in air. Thus, the lens refracts and focuses sound waves, in analogy to the focusing of light by a glass lens. (The focal length is adjusted simply by changing the gas pressure, which changes the lens curvature.)

In previous efforts to map the sound from gas flow over an airfoil, a directional microphone was scanned over the flow area. When the new lens was interposed between the flow and the microphone, the sharpness of the sound "image" was improved by a factor of more than 2. The overall gain of the system is also increased because the source energy is focused onto a smaller image area. The inset to the figure is a typical sound map for a sweptwing model tested in a wind tunnel at an airspeed of 28 meters per second. The measurement grid is 1.25 cm between points.

This work was done by James M. Kendall, Jr., of Caltech for **NASA's Jet Propulsion Laboratory.** *For further information, Circle 63 on the TSP Request Card.*
NPO-14757

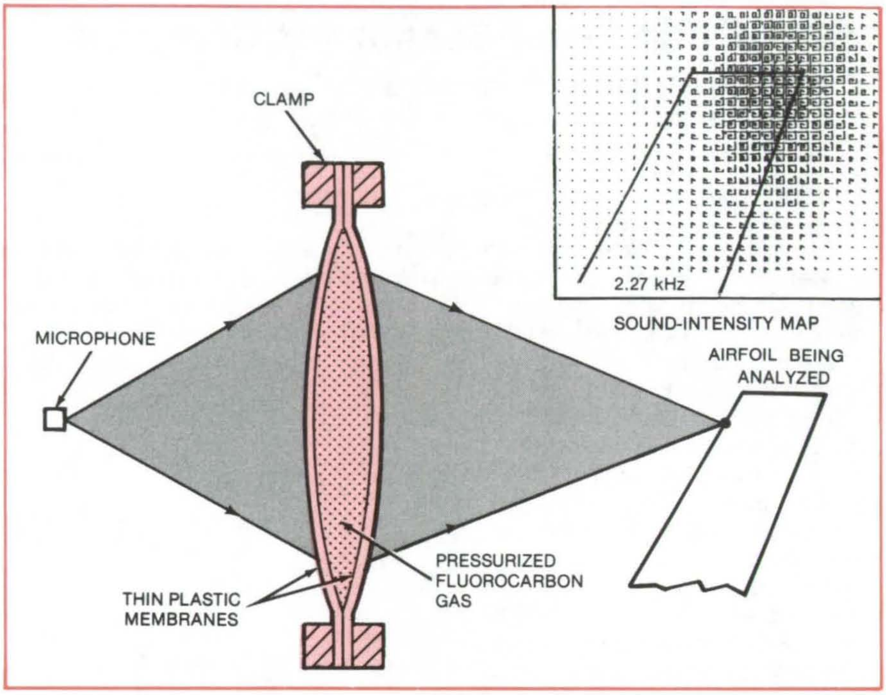

An **Acoustic Lens,** assembled from transparent plastic sheets and filled with Freon at slight positive pressure, improves the accuracy of sound-intensity maps. A typical pattern for airflow around a sweptwing is shown in the inset. It shows a noise source concentrated at the wingtip. The sound frequency is 2.27 kHz.

Ultrasonic Frequency Analysis

Frequency-tracked gated-pulse technique eliminates problems found with current techniques.

Langley Research Center, Hampton, Virginia

An improved technique developed at Langley Research Center for ultrasonic frequency analysis can be used for the evaluation and characterization of materials, fluids, and biological tissue. Normally, short, untuned voltage spikes from a pulser are used to shock-excite a highly-damped piezoelectric transducer. The transducer emits a sharp ultrasonic pulse with a relatively-wide frequency bandwidth, which interrogates the test sample. The signal from the sample is then fed into a spectrum analyzer that displays the magnitude of the Fourier transform of the signal. The spectra, however, are strongly influenced by the shape of the electrical spike used to generate the ultrasonic waveform. Further, the spikes produce unwanted nonlinearities in the emission waveform. This may complicate interpretation of the frequency spectra from the test sample.

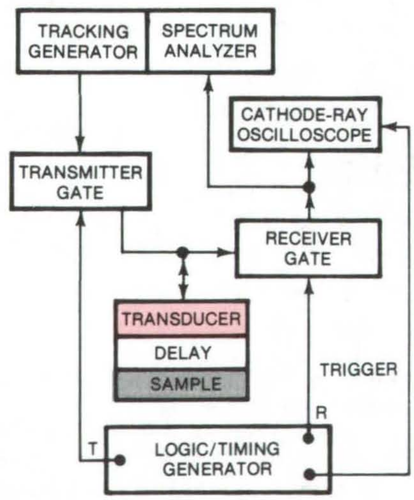

Figure 1. **Frequency Control for an Ultrasonic Analyzer** employs a tracking generator that is slaved to the local oscillator of the spectrum analyzer to produce spectra equivalent to shock-exciting the transducer with a true delta function excitation.

The new method eliminates the problem of the electrical drive-pulse shape by slaving a tracking generator to the local oscillator of the spectrum analyzer, as shown in Figure 1. A logic/timing generator is used to control the pulse transmission and receiving sequence, the pulse width, and the pulse repetition rate. With this arrangement the frequency of the RF input that is pulse-gated to the spectrum analyzer is locked to the frequency in the analyzer at which measurements are being made. Therefore, spectra are produced that are equivalent to shock-exciting the transducer with a true delta function (Figure 2). Since the drive voltages are typically two orders of magnitude lower than those of conventional methods, unwanted nonlinearities in the emission spectra are eliminated. Further, use of the frequency-tracking technique with the

newly-developed phase-insensitive acoustic/electric transducer (AET) permits the AET to extract spectral information; this capability does not exist with the AET using conventional pulse methods.

The practical limitations of the frequency-tracking technique are associated with the frequency limitations of the spectrum analyzer and the electroacoustic bandwidth characteristics of the transducer. For most ultrasonic measurements the spectrum analyzer bandwidths, typically in the tens or hundreds of megahertz, impose little limitation. The development of broadband capacitive transducers should permit maximum exploitation of the frequency-tracking technique for ultrasonic frequency analysis.

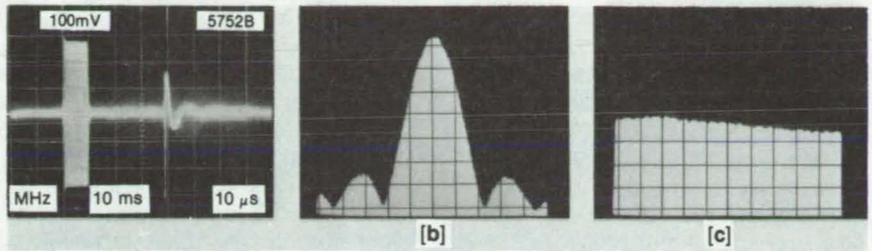

Figure 2. **Ultrasonic Analysis Spectra** are produced by gating an ultrasonic pulse (a) into a spectrum analyzer, using (b) a conventional technique and (c) the frequency-tracking technique.

This work was done by John H. Cantrell, Jr., and Joseph S. Heyman of **Langley Research Center**. *For further information, Circle 64 on the TSP Request Card.*

This invention is owned by NASA, and a patent application has been filed. Inquiries concerning nonexclusive or exclusive license for its commercial development should be addressed to the Patent Counsel, Langley Research Center [see page A5]. Refer to LAR-12697.

Temperature Controller Adapts to Fatigue Tester

Aluminum blocks allow accurate regulation and fast variation over a temperature range of 850° F.

Langley Research Center, Hampton, Virginia

A specimen of material undergoing fatigue tests is maintained at constant temperature or cycled over a wide temperature range by an electronic temperature controller. Cryogenic temperatures near the boiling point of liquid nitrogen and elevated temperatures to 600° F (315° C) are possible with the new unit, which consumes little power and coolant and has low thermal inertia so that rapid temperature changes may be programed.

The temperature controller (see figure) consists of two identical blocks of aluminum placed against the front and back of the test specimen and held together by spring clamps. Thermocouple wires pass through holes in the blocks to monitor the specimen temperature. The temperature signals control either electrical heaters or the valve in a liquid-nitrogen line to small cavities in the blocks.

In the past, relatively-massive commercial systems have been available as either heat sources or cryogenic sources. These, however, are incompatible with fatigue-testing machines designed to test small samples and, because of the large mass, temperature changes occur relatively slowly.

(continued on next page)

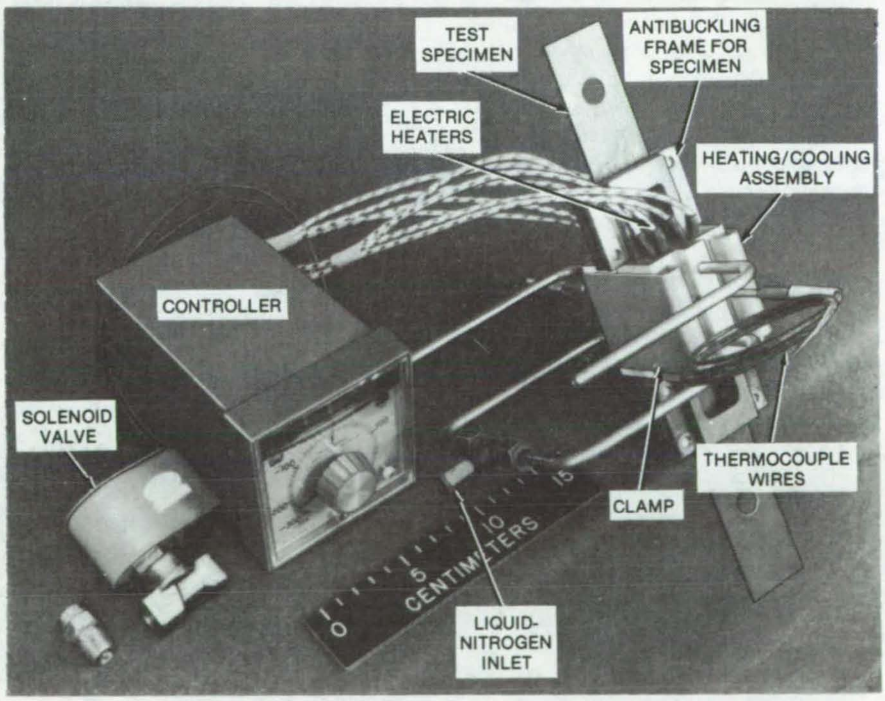

The **Temperature Controller**, designed for compatibility with fatigue-test machines, is shown mounted on a test specimen. Identical blocks of aluminum, held against the front and back of the specimen, each contain electrical heaters, a liquid-nitrogen cavity with input and exhaust tubes, and a thermocouple. The thermocouples are connected to the control unit, which adjusts the specimen temperature during fatigue tests.

The new unit maintains a constant cold temperature on the test specimen by introducing liquid nitrogen from a remote pressurized source through a solenoid valve. The liquid absorbs heat from the surrounding material, including heat from the specimen, and then exhausts the heat to the atmosphere. Liquid nitrogen continues to flow until the thermocouple feedback probe in contact with the specimen senses that the desired temperature has been reached. The solenoid valve controller then closes the solenoid valve. Heat conduction from the surroundings tends to warm the specimen; but the thermocouple probe actuates the solenoid valve controller to allow nitrogen flow, thus maintaining the temperature within a narrow range of the desired temperature.

A similar process maintains a constant elevated temperature on the test specimen. In this case, however, the thermocouple temperature controls electrical power to the heating cartridges. Using a simple timing device the controller was successfully tested over a temperature cycle from 600° F (315° C) to −250° F (−155° C).

This work was done by Leland A. Imig and Mickey R. Gardner of **Langley Research Center.** *For further information, Circle 65 on the TSP Request Card.*

This invention is owned by NASA, and a patent application has been filed. Inquiries concerning nonexclusive or exclusive license for its commercial development should be addressed to the Patent Counsel, Langley Research Center [see page A5]. Refer to LAR-12393.

Environmental Testing Under Load

An inexpensive fixture applies compression loads to specimens exposed to the environment.

Langley Research Center, Hampton, Virginia

Since environmental testing of materials under compressive stress usually requires rather elaborate equipment, engineers and others will be interested in a low-cost, compact test fixture for stressing materials to predetermined compressive stress levels. Intended for compressive loading of structural materials exposed to natural or simulated environments, the fixture can handle relatively large specimens suitable for postexposure analysis of physical, chemical, and mechanical properties.

As shown in the figure, the test specimen is contained in a guide cylinder between two horizontal plates. The plates are held together by two bolts. An adjustable loading bolt through the top plate transmits the load through a piston in the guide cylinder.

The specimen is held in place by adjustable retainers — one pair on the load piston and the other on the bottom plate. The ends of the guide cylinder fit snugly in recesses in the top and bottom plates to ensure axial alinement of the load and the specimen. Two cutouts in the guide cylinder fully expose the specimen to the environment.

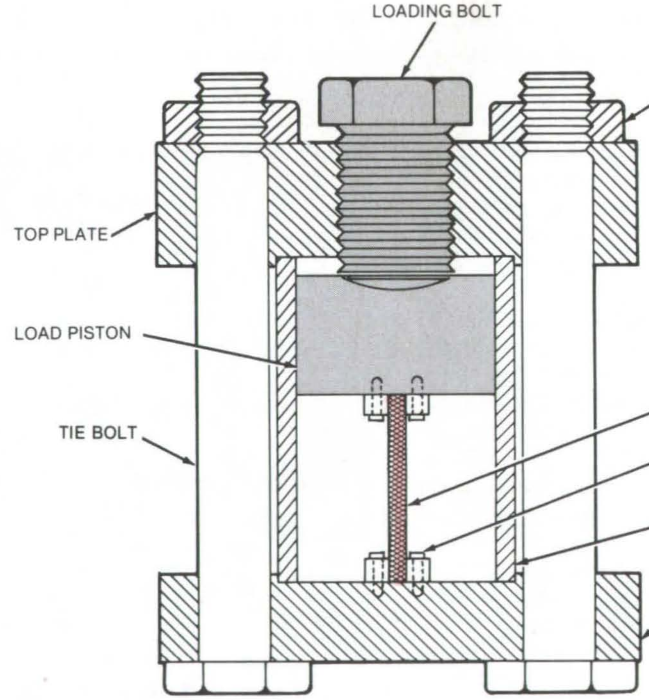

Piston Applies a Load to a specimen, as cutouts (not shown) in the cylinder expose the test sample to the environment. Specimens up to 1 in. (2.5 cm) in width and 1-1/2 in. in length are accommodated. The applied load can be set within ±10 percent of a selected value.

The adjustable loading bolt in the top plate allows the load to be varied; however, since rotation of the bolt could apply a torque to the specimen, the load is not increased simply by advancing the bolt. Instead, the tie-bolt nuts are loosened, the loading bolt is turned to the desired load setting, and a load-test machine applies a purely axial load. When the bolts are retightened, the desired load is locked in the specimen.

Calibration curves are taken to determine the appropriate position of the loading bolt. The curves are developed for a given material and specimen configuration with the aid of a strain-gaged specimen, the axial-load test machine, and a load/strain recorder. The strain and load on the specimen are correlated with the angular position of an index on the loading bolt, as indicated by an angular scale scribed on the top plate.

This work was done by Ronald K. Clark and W. Barry Lisagor of **Langley Research Center.** *For further information, Circle 66 on the TSP Request Card.*

Inquiries concerning rights for the commercial use of this invention should be addressed to the Patent Counsel, Langley Research Center [see page A5]. Refer to LAR-12602.

Testing Panels in Tension and Flexure

A simple jig adapts a tensile-test machine for the simultaneous application of tension and flexure.

Marshall Space Flight Center, Alabama

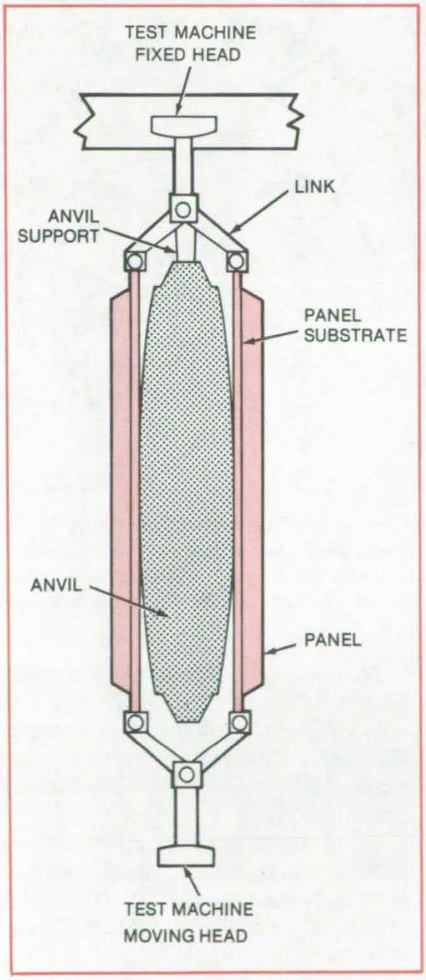

An **Anvil Applies Flexure** while linkages apply tension to panels under test. Loading of the test jig is along a single axis.

Multilayered panels are rapidly tested in both tension and flexure by a novel jig, shown in the figure. The panels are subjected to virtually any combination of tensile and flexural loads simultaneously, for evaluating the panel composition, processing, and design.

The jig is attached to a conventional tensile-test machine. An environmental test chamber can be added so that panel properties can be measured at extreme temperatures.

The tensile-test machine applies a load along a single vertical axis. In the jig, linkages support two panels on opposite sides of a curved anvil. As the panels are loaded by the tensile-test machine, they bend to follow the anvil contours. The bending creates the flexural component of stress.

Anvils having various curvatures — even sharp edges — are used. Smoothly curved anvils of radii from 100 to 500 inches (2.5 to 12.7 m) have been fabricated, as have anvils with more than one radius of curvature.

This work was done by Gustave K. Jung of Martin Marietta Corp. for **Marshall Space Flight Center**. *For further information, Circle 67 on the TSP Request Card.*
MFS-25421

Tracking Falling Objects

Objects in free fall are viewed at constant magnification by an optical carriage on a vertical track and a fixed telescope attached to a camera. A small motor supplies the power needed to overcome the drag on the carriage. The system has been used to study the formation of glass coatings on nuclear-fuel pellets.
(See page 306.)

Photometer Used for Response Time Measurement

In tests of servocontrol systems, a photometer has been used to measure system response time. When the photometer is sighted on a line on the system display screen, it senses output movement on the screen shortly after an operator activates a hand-controlled input. The response time is measured on an X/T recorder.
(See page 293.)

A Construction Technique for Wind-Tunnel Models

Integrally machined orifices and channels offer advantages over traditional miniaturized plumbing.

Langley Research Center, Hampton, Virginia

Miniature wind-tunnel models must satisfy stringent physical requirements, including high strength, good surface finish, and corrosion resistance. Some of the most troublesome problems result from the internal steel tubes that lead to small, pressure-sensing, surface orifices. These tubes may plug or leak, and the cavities they require weaken the model. Since the plumbing cannot be installed until late in the machining process, considerable fabrication time is wasted if defects arise at that point.

These problems are overcome by machining the pressure channels as an integral part of the model. As illustrated in Figure 1 for a sample airfoil built at Langley Research Center, the model with plumbing is assembled from two flat stainless-steel plates, which are joined face to face. The pattern of pressure channels is scribed, machined, or photoetched into the flat surface, and the pressure-sensing orifices are drilled before joining the two halves. The portion of the plates along the central cross section—where the orifice network pierces the airfoil surface—is premachined to minimize the orifice drilling depth.

The mating surfaces of the plates are flashed with a very thin (8×10^{-4}-cm) coat of copper. After they are diffusion-brazed together, the plumbing is checked for plugs or leaks. At that point the block is machined to its final contour. Figure 2 shows the airfoil, with the top surface complete. The tubing shown is brazed in place when the blocks are joined.

In addition to solving construction problems for wind-tunnel models, this technique should be useful in fuel injection, transpiration cooling, and similar applications involving small elements of fluid flow. Since the technique has been developed for 17-4 PH alloy stainless steel, it can be used for corrosive or high-temperature environments.

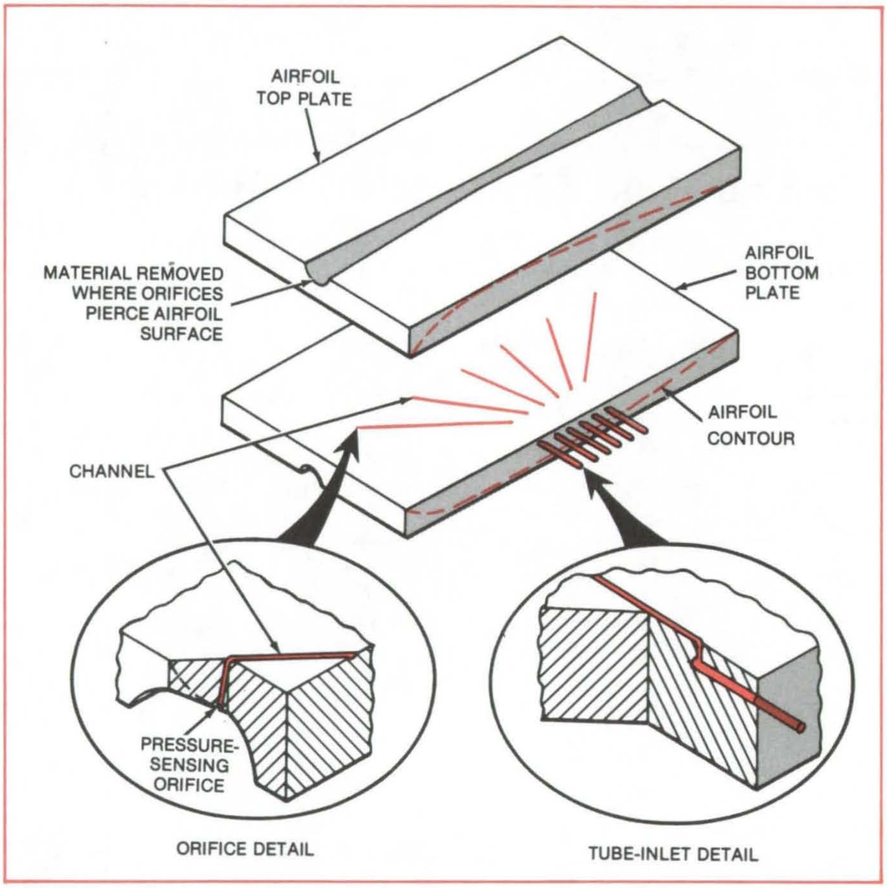

Figure 1. An **Airfoil Model Is Constructed** from two flat plates. The large channel in the top of the upper plate and the channel in the bottom of the lower plate are premachined to remove material along the line where pressure-sensing orifices will pierce the airfoil surface. The small interior channels leading from the orifices to the six tubes are drilled, scribed, or photoetched.

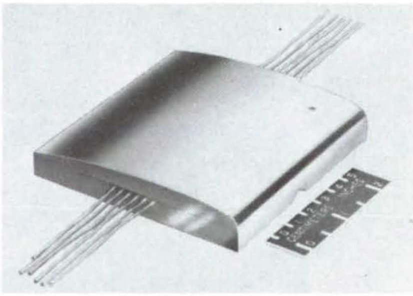

Figure 2. The **Airfoil Has Been Machined to Contour** along one surface in this view, after the plates have been brazed together. The tiny pressure-sensing orifices are too small to be visible in this photograph.

This work was done by Pierce L. Lawing, Paul G. Sandefur, Jr., and William H. Wood of **Langley Research Center.** *For further information, Circle 68 on the TSP Request Card.*

Inquiries concerning rights for the commercial use of this invention should be addressed to the Patent Counsel, Langley Research Center [see page A5]. Refer to LAR-12710

Measuring the Thermal Conductivity of Insulation

Two symmetrical heat sources help determine the thermal transmission properties of an insulating material.

NASA's Jet Propulsion Laboratory, Pasadena, California

The thermal transmission properties of many insulators can be measured with an apparatus that uses two symmetrical heat sources to match temperatures. The heat sources for the apparatus, which has accurately measured the thermal insulation properties of rocket insulation, are saturated steam (though other vapor heat sources can be used) and a wire heater.

To test the thermal transmission of an insulating material (see figure), it is packed in two identical copper tubes. A series of thermocouples measures the temperature along the exterior surface of each tube. The thermal transmission (in W/m °C) of the insulator is determined from a knowledge of the physical dimensions of the test material, the stable and uniform temperature differential across it, and the stable rate of heat flow through it.

In one tube, the constant saturation temperature of steam is maintained at the inner surface of the material. The steam flows from a generator through a copper tube within the test apparatus and is vented to the atmosphere. When the thermocouple readings are constant, a known uniform and stable temperature differential exists radially across the material (different temperatures along the tube could indicate inhomogeneous packing and end losses).

To measure the total power input from the steam and the rate of heat flow, the second tube is used. A heater wire passes through its center and through the insulating material contained within it. The rate of energy input (in watts) to the heater is determined by a voltmeter and ammeter shunt. When the temperature of the steam-heated tube is stabilized, the power output of the wire heater is adjusted until the two sets of thermocouples on the tubes indicate the same temperature. The thermal conductivity of the insulating material can then be determined.

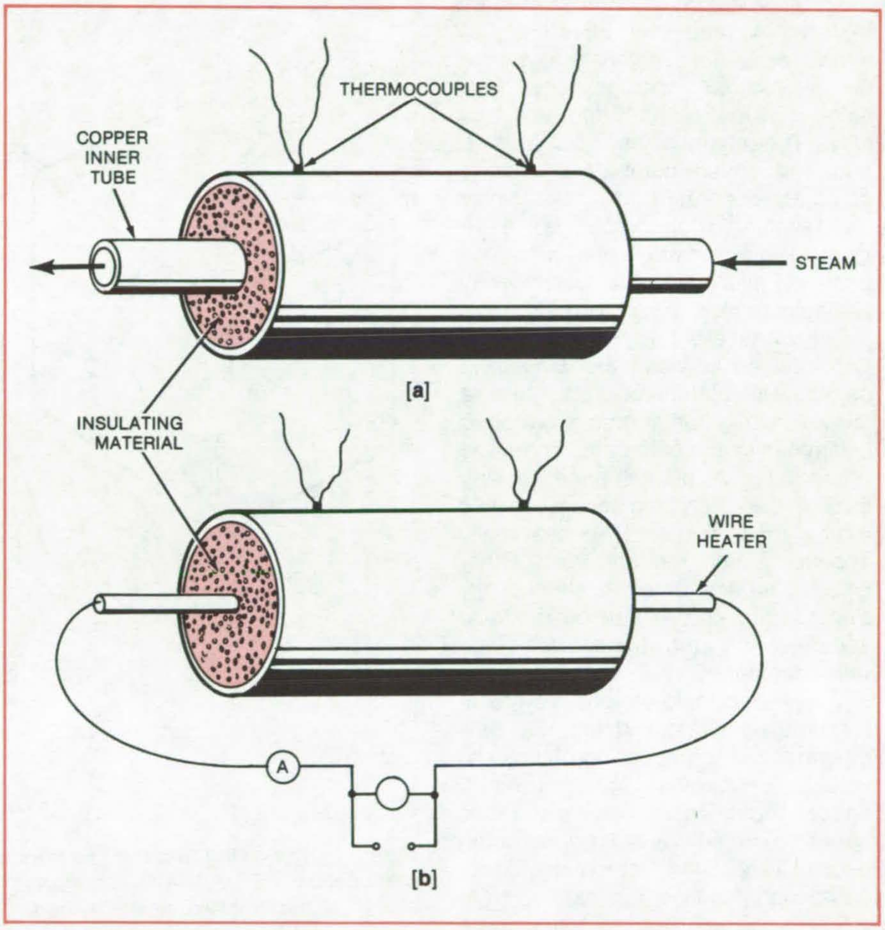

An **Insulating Material** is packed in two copper tubes to measure its thermal transmission properties. In one of the tubes (a), steam is the heat source; in the other tube (b), a wire heats the insulating material. When the thermocouples on the two tubes read the same stable temperature, the thermal transmission of the insulating material can be determined.

This work was done by Christine A. Wilkins, Robert Ash, and Warren L. Dowler of Caltech for **NASA's Jet Propulsion Laboratory**. *For further information, Circle 69 on the TSP Request Card.*
NPO-14871

Rain, Fog, and Clouds for Aircraft Simulators

Moisture chamber realistically reproduces airborne mists for pilot training.

Ames Research Center, Moffett Field, California

An environmental chamber creates realistic fog and rain effects in an aircraft simulator. The chamber reproduces clouds, homogeneous fog, patches of fog, rain and fog, and rain only. The chamber is used with a real-time digital computer, a color computer-generated image display that simulates airport lights, or a color-television camera that produces a moving display of an airport runway as depicted on a model terrain board.

The transparent fog/rain chamber is positioned between the windshield of the simulator cockpit and a television monitor screen showing a collimated image of the airport runway (Figure 1). A pilot trainee looking through the windshield sees a realistic view of the airport as it would actually appear through fog and rain. Other types of optical beam-splitter/mirror systems now in use can be made to accommodate the transparent fog/rain chamber.

Unlike electronic or optical systems for simulating rain and fog, the new chamber can reproduce fog halos like those seen around lights at night, optical attenuation and distortions caused by raindrops splattering on an aircraft windshield from many directions, and "veiling luminance" (the effect by which fog appears more dense when it is viewed in Sunlight, by backscattering as seen by the pilot due to the aircraft landing lights, or from nearby lightning discharges). Windshield wipers in the chamber add to the authenticity of its effects.

Aerosol generators in the chamber are controlled by the computer to produce water droplets in a variety of sizes — from 5 to 20 microns for fog and from 20 to 50 microns for clouds. The mist can be cleared out of the chamber almost instantly, or its density can be increased or decreased abruptly to represent the conditions of a specified runway visual range (RVR) from zero visibility to 30 miles (48.3 km), or that when an aircraft suddenly emerges from fog or clouds or enters a denser or lighter fog bank. The computer low-visibility algorithm synchronizes the control laws of the chamber to generate the desired RVR condition with the simulated movement of the aircraft as the pilot operates the aircraft controls.

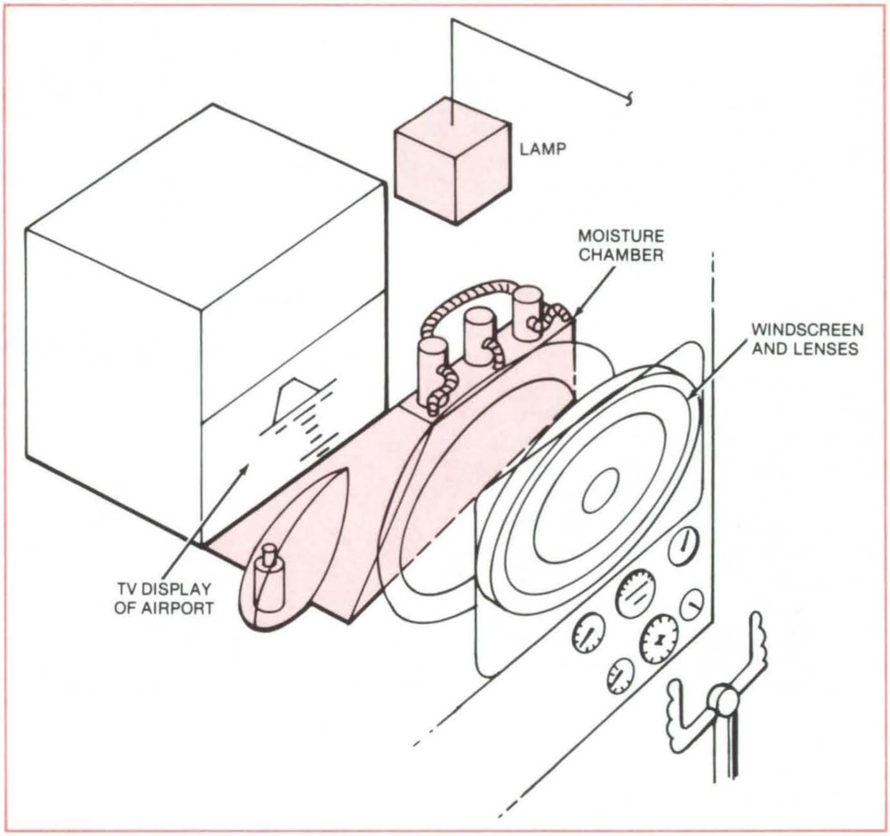

Figure 1. By viewing through **The Windscreen and the Mist Chamber,** a pilot trainee can observe a TV display of an airport. Similar TV screens and mist chambers are placed at the other windows of the cockpit simulator.

Mist is fed into the chamber (Figure 2a) by two primary aerosol units at its sides and auxiliary aerosol generators at its top. To change the density of the mist for a specified RVR condition, two perforated tubes at the bottom inject computer-controlled bursts of high-pressure air to mix with the mist, which is exhausted out the top of the chamber. Rain is simulated by a combination of water and air ejected through orifices in horizontal and vertical tubes and by air alone ejected through a horizontal tube (Figure 2b). Jets from the air tube break up the horizontal and vertical streams of waterdrops into fine droplets.

A xenon lamp (or a fluorescent lamp with a Sunlight-like spectrum) illuminates the chamber from above through its inclined front face. The light from the lamp is visible only when there are water particles in the chamber to scatter it. Thus, the brightness of the haze as observed by the pilot becomes less intense as the simulated aircraft "descends" or as the mist density decreases in the chamber. Finally, when all mist is removed from the chamber, the pilot sees only the runway scene on the TV or computer-generated-image CRT screen. Even though the lamp is still on, its light is not scattered and therefore is not visible to the pilot.

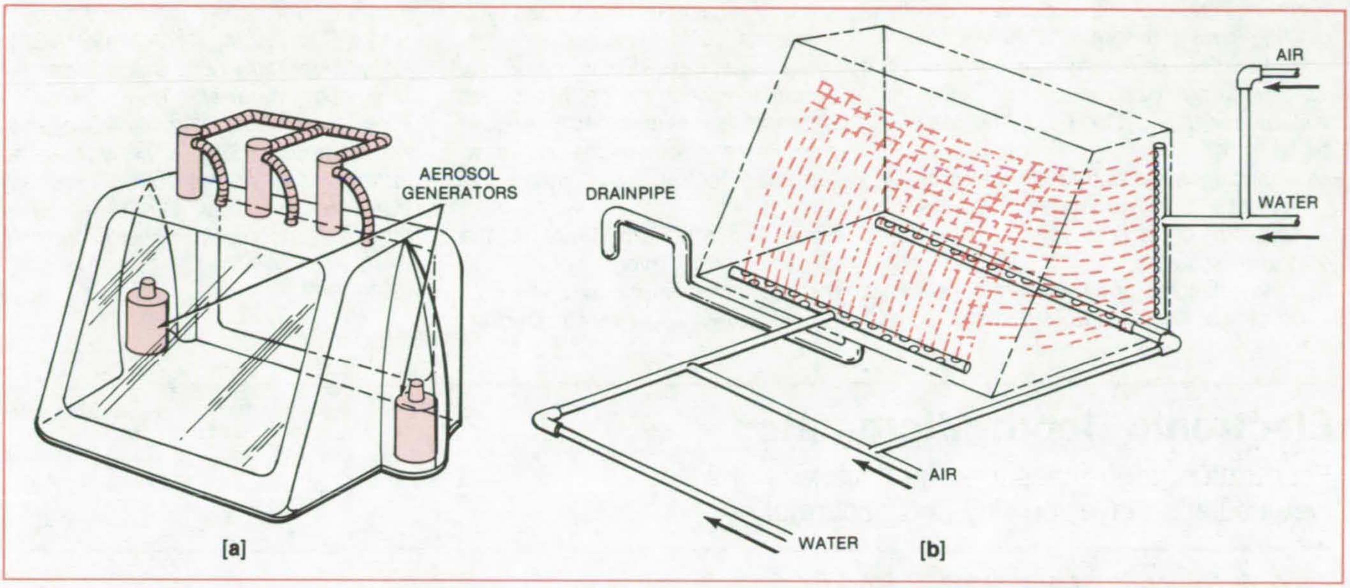

Figure 2. **Under Computer Control,** aerosol generators (a) at the top of the chamber and in side alcoves release mists of predetermined densities. Perforated tubes (b) eject "raindrops" that are broken up into finer drops by jets of high-pressure air from a tube at the bottom of the chamber. The drainpipe prevents water from accumulating.

The lamp can also be controlled by the computer to change brightness to simulate ascent or descent through variable-density clouds. The computer can also flash the lamp intermittently to simulate nearby lightning flashes in a cloud.

For greater realism, the computer controls the brightness of the TV or computer-generated image display so that ground objects are brightest when close to the pilot and gradually fade as they approach the horizon.

This work was done by Wendell D. Chase of **Ames Research Center.** *For further information, Circle 70 on the TSP Request Card.*

This invention is owned by NASA, and a patent application has been filed. Inquiries concerning nonexclusive or exclusive license for its commercial development should be addressed to the Patent Counsel, Ames Research Center [see page A5]. Refer to ARC-11158.

Improved Magnetic Material Analyzer

Core losses at frequencies up to 10 kHz or greater are measured instantaneously.

Lewis Research Center, Cleveland, Ohio

A flux-controlled magnetic-core-loss tester has been developed that produces high-frequency core-loss data (within 2 percent) for any desired waveform excitation and allows the magnetic characteristics of a material to be measured under symmetrical and asymmetrical excitation conditions. It allows the direct control of an additional loss variable, $d\varphi/dt$, rather than just the driving frequency as is the case for all previous sinusoidal core-loss measurements.

Existing core-loss test equipment can measure only sinusoidal low-frequency ($<$400-Hz) core-loss characteristics with respect to frequency and flux density. This new core-loss tester will directly measure core-loss characteristics at high frequency ($>$10 kHz), at saturation, for any type of voltage waveform, instantaneously.

The flux-controlled magnetic-core-loss tester is composed of a drive subsystem, an excitation subsystem, and an instrumentation subsystem. The excitation subsystem consists of a high-power wideband operational amplifier that allows the option of selecting either voltage, current, or the integral of voltage (magnetic flux) as the feedback parameter. This allows a high-frequency voltage source, current source, or flux control configuration to be simulated. Using the flux feedback option, true sinusoidal, square-wave, or impulse voltage excitation conditions may be easily generated. The instrumentation subsystem allows instantaneous core-loss measurements and analyses to be made.

The instrument allows the two core-loss variables, time rate of change of flux ($d\varphi/dt$) and the maximum flux density (B_m), to be directly measured. It also provides the data necessary to calculate Steinmetz coefficients exactly, experimentally verify Warburg's law, and allows examination of domain wall theories under constant and controlled $d\varphi/dt$ conditions.

The magnetic characteristics obtained from this new test unit are extremely useful to the power electronics designer in that they show the

(continued on next page)

functional relationships between induction level and core loss as a function of two key dc/dc, dc/ac converter operating parameters of input voltage and duty cycle. The tester may be used to:

1. analyze magnetic material characteristics and generate core-loss data for any type of voltage waveform excitation;
2. determine the optimum lamination thickness for tape-wound cores;
3. analyze new amorphous magnetic materials;
4. make exact core-loss comparisons among magnetic material core-loss characteristics to determine optimum magnetic designs in transformers, motors, and inductors; and
5. examine magnetic materials at the basic research level.

This work was done by James E. Triner of **Lewis Research Center.** *Further information may be found in NASA TM-79234 [N79-31499/NSP], "Analytical Core Loss Calculations for Magnetic Materials Used in High Frequency High Power Converter Applications" [$9]. A copy may be purchased [prepayment required] from the National Technical Information Service, Springfield, Virginia 22161.*
LEW-13493

Electronic Depth Micrometer

Penetration gage measures the thickness of a wet-insulation layer quickly and accurately.

John F. Kennedy Space Center, Florida

A novel device for measuring depth or thickness reads the distance of penetration by a small-diameter probe. The probe is fastened to the sliding contact on a linear 1,000-ohm potentiometer that has a travel of 1.000 inch (2.54 cm). Thus the resistance between the end of the potentiometer and the sliding contact increases by 1 ohm when the probe moves 1 mil (0.025 mm). The resistance is read on a digital ohmmeter. With the meter set on the 1-kilohm scale, direct readings in thousandths of an inch are obtained.

This device was developed specifically to measure the thickness of wet (uncured) insulation applied to Space Shuttle structures; the thin probe penetrates the wet insulation to the substrate, and the reference surface on the gage is then positioned against the outer surface of the insulation to measure its thickness. The gage is easy to use, even by workers wearing gloves or other protective clothing, and allows remote reading and recording of production data.

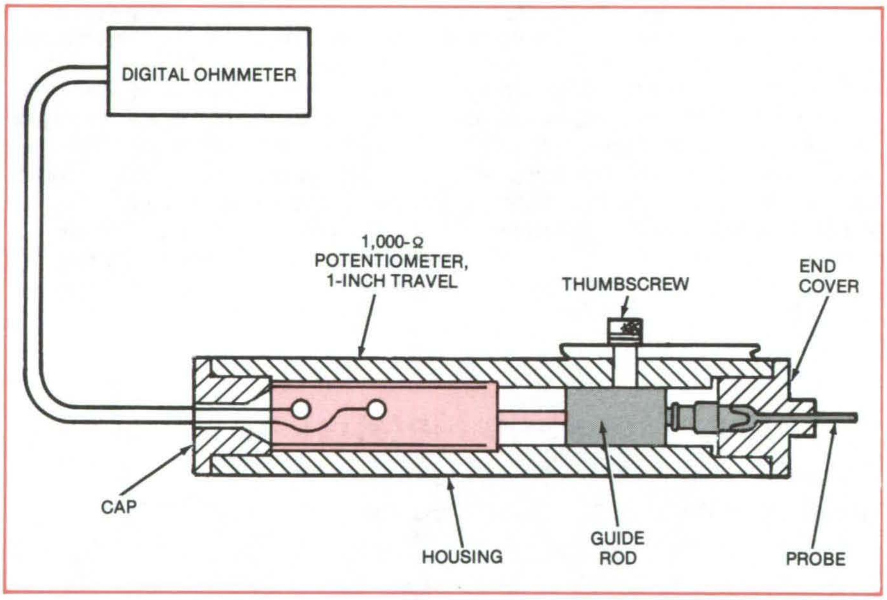

A 1-Kilohm Linear Potentiometer that is 1.000 inch long has a probe fastened to its moving contact. When the probe moves out of its housing, the resistance between the fixed and movable contacts on the potentiometer increases by 1 ohm per mil of probe projection. The digital ohmmeter thus reads probe extension directly when it is on the 1-kilohm scale.

As shown in the figure, the thickness-gage housing has a recess for the linear potentiometer; a cap threaded into the end of the housing has an opening for the potentiometer lead wires. The guide rod attached to the end of the potentiometer shaft is mated to the probe, which is trimmed to length and can project through a hole in the end cover. A thumbscrew applies friction to brake the guide rod so that thickness measurements can be made by placing the probe against the substrate and moving the gage until the end cover just touches the outer surface of the wet film being measured. The thickness measured is the distance from the tip of the probe to the surface of the end cover.

For the insulation thickness measurements, tests showed that a linear 1,000-ohm potentiometer with a tolerance of ± 5 percent gives sufficient accuracy and repeatability. For other applications, a more accurate unit could be used.

This work was done by Richard K. Major of United Space Boosters, Inc., for **Kennedy Space Center.** *No further documentation is available.*

Inquiries concerning rights for the commercial use of this invention should be addressed to the Patent Counsel, Kennedy Space Center [see page A5]. Refer to KSC-11181.

Interchangeable Spring Modules for Inertia Measurements

Spring modules allow rapid adjustment
of the range of an inertia balance.

Langley Research Center, Hampton, Virginia

The operation of an inertia balance is simplified by packaging a set of balance springs in interchangeable modules. This approach has been used with success at Langley Research Center for the balance shown in the figure.

Since models of different weights require crosshair springs with different force constants, the springs must often be removed, replaced, and recalibrated, a procedure that was time consuming and tedious. It was also subject to inaccuracy, since the recalibration step could not always be done reproducibly.

The new spring modules (one of which is shown in the inset to the figure) are prepackaged and precalibrated. They are held in place in the balance pedestal by just two fasteners, making removal and replacement fast and simple. With them, the balance can be readied for a model of different weight in less than 15 minutes, in contrast to more than 2 hours by the previous method.

This work was done by James W. McNamara and John W. Oakley of **Langley Research Center.** *No further documentation is available.*
LAR-12402

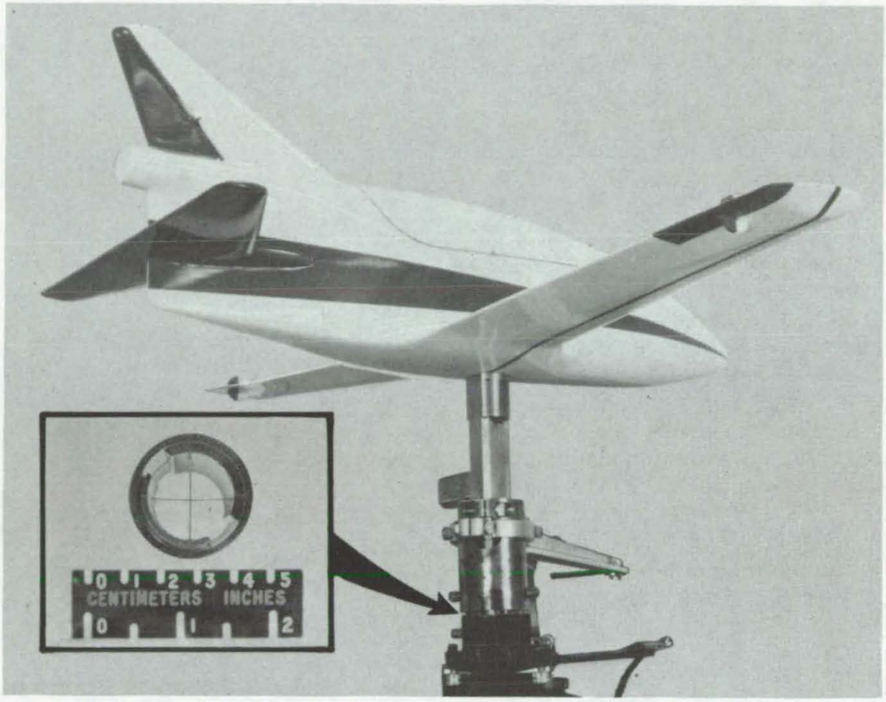

The **Precalibrated Crosshair-Spring Module** shown in the inset is used to determine the moment of inertia of this lightweight model of a low-altitude aircraft. A heavy-duty spring module is rapidly substituted when calibrating heavier models.

Wakeflow Analysis by COST

Turbulent airflow is imaged by computerized
optical-scanning tomography.

NASA's Jet Propulsion Laboratory, Pasadena, California

COST — computerized optical-scanning tomography — is proposed for visualizing the wakeflows of aircraft and wind-tunnel models. Operating very close to real time, COST hardware could be installed at airports to monitor the turbulent flow trailing large aircraft, so that smaller aircraft could be directed to avoid the turbulence. The real-time analysis of jet-engine exhaust plumes, to reduce pollution and optimize performance, is also possible.

COST is similar to CAT (computerized axial tomography), an X-ray imaging technique that is becoming increasingly important as a medical diagnostic. However, COST uses laser radiation rather than X-rays as the probe. By recording the net absorption along different beam paths, the system generates a computer image of a cross section through a sample volume that may be constantly changing. It does so with a laser source (laser 1) and an array of detectors (D_1 through D_n) on opposite sides of the sample volume (see figure, typical for wind tunnels). The laser is pivoted so that the beam path can be changed,

(continued on next page)

falling on each detector in sequence. A second laser and detectors scan the sample at right angles to the first set. All laser sources and detectors are mounted on a mechanism that allows rotation of the beam paths about the sample volume.

The detector outputs, which measure the net absorption along the beam path, are recorded, digitized, and stored in memory. The data are correlated with scan angle to construct an image of the optical density of the sample volume.

By selecting laser emission lines that correspond to absorption frequencies of gases of interest, the system could select only particular gases for analysis. For example a tunable CO_2 laser beam that is selectively absorbed by air pollution gases could be used for imaging the exhaust plume of a jet engine as the fuel/air mixture is adjusted. For wind-tunnel studies, selectively detectable gases could be added to the aircraft-model boundary layer to enhance the COST image.

This work was done by Victor J. Anselmo of Caltech for **NASA's Jet Propulsion Laboratory.** *For further information, Circle 71 on the TSP Request Card.*
NPO-14705

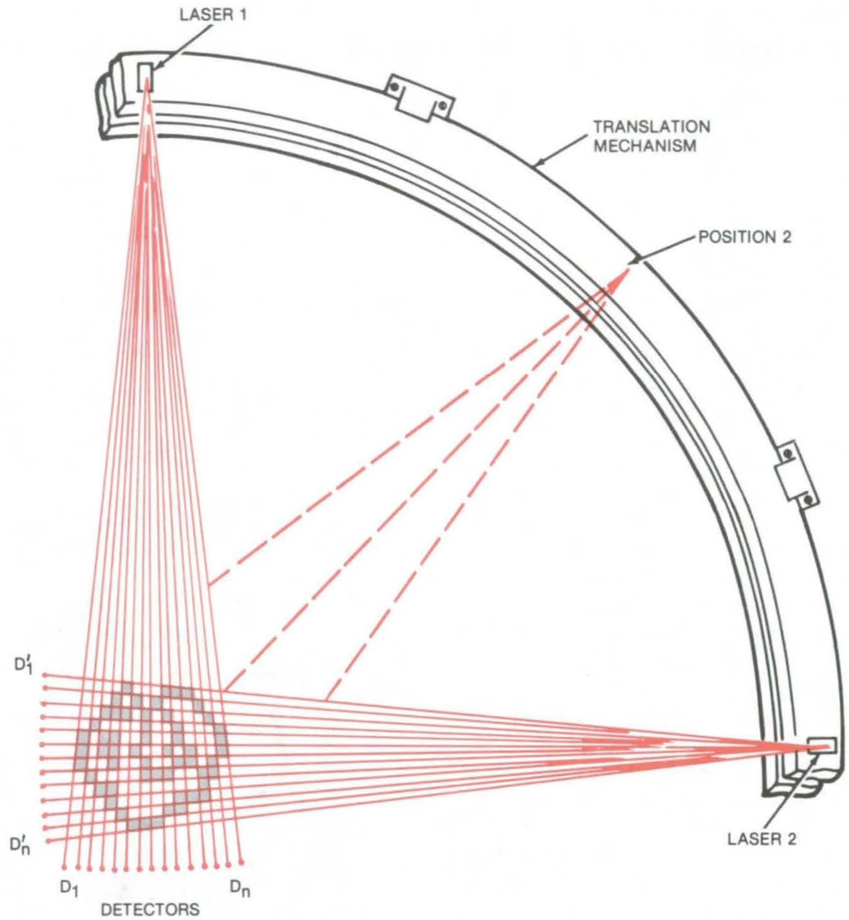

Lasers in the **COST Imaging System** scan a sample volume at right angles. The detectors measure the transmitted light. From these data, an image of the absorption characteristics of the sample is constructed. Scan position 2 would be used to enhance resolution.

Integrated Material-Surface Analyzer

Up to 10 in vacuo surface analyses are performed in one system.

NASA's Jet Propulsion Laboratory, Pasadena, California

Any or all of up to 10 in vacuo surface analyses would be carried out with the proposed module shown in the figure. Such a battery of tests (see table), used to study MOS and other devices, usually requires separate instruments. Combining the tests in one system would speed up testing and would reduce the possibility of sample contamination between tests.

The module concept combines a mass spectrometer, a charged-particle analyzer, and a multiple sample holder. Ultraviolet, X-ray, electron, and ion sources are directed at one sample at a time, as is the analyzer inlet lens. Also included are: a heater/cooler, an electron/ion multiplier, a Faraday cup detector, and digital control circuitry.

The two-section, hemispherical kinetic-energy analyzer is mounted between inlet and exit lenses. From the exit lens, ions ejected from the sample pass symmetrically between four parallel rods in the quadrupole mass spectrometer. When the module is used for one of the ion spectroscopies, an alternating potential superimposed on a steady potential filters out all ions except those of a particular mass. For the electron spectroscopies, the quadrupole mass spectrometer functions as an electron transfer lens between the kinetic-energy analyzer and the electron/ion multiplier.

The different analysis functions are selected by switching to the desired source, applying appropriate potentials to the kinetic-energy and mass analyzers, and controlling the inlet and exit lenses. (A Faraday cup at the spectrometer output is included primarily for calibration.) The potentials are programable and can be set accurately.

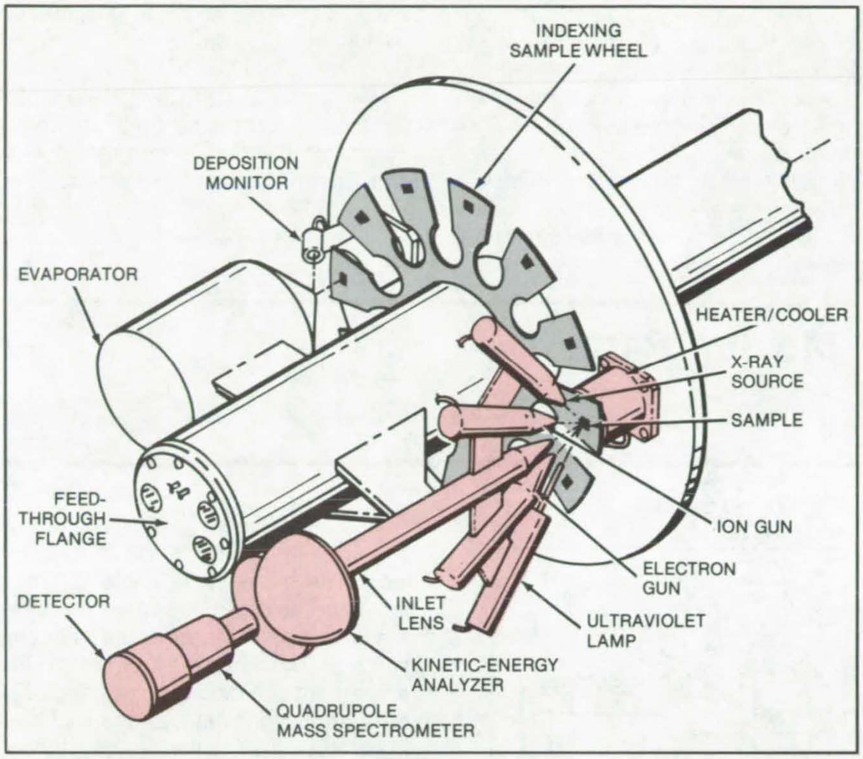

This **Surface-Analysis Module** for installation in a vacuum chamber can run a series of tests without breaking the vacuum between tests. Power for the different tests varies from 100 to 1,500 watts.

- Secondary-ion mass spectroscopy
- Ion-scattering spectroscopy
- Electron-stimulated desorption
- Residual-gas analysis
- Auger electron spectroscopy
- X-ray photoelectron spectroscopy
- Ultraviolet photoelectron spectroscopy
- Characteristic-electron energy-loss spectroscopy
- Scanning electron microscope
- Scanning low-energy electron probe

These **10 Surface-Analysis Tests** can be run without breaking the vacuum. A quadrupole mass spectrometer, used in the first four tests, serves as an electron transfer lens in the last six tests.

An electronics module decodes digital command data and controls the detectors directly or with a prestored sequence from memory. This module also conditions and buffers signals from the detector and from voltage, current, temperature, and position sensors. It also formats the data into a digital stream.

This work was done by Frank J. Grunthaner and Blair F. Lewis of Caltech for **NASA's Jet Propulsion Laboratory.** *For further information, Circle 72 on the TSP Request Card.* *NPO-14702*

Fiber-Optic Accelerometer

Lightweight instrument would convert mechanical motion into digitized optical outputs.

Lewis Research Center, Cleveland, Ohio

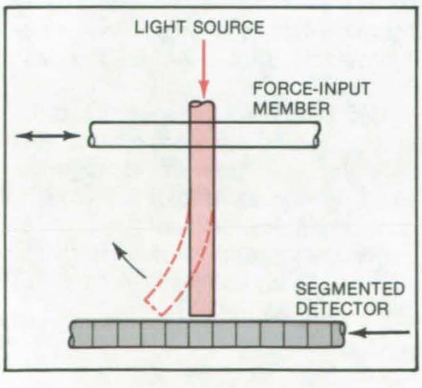

The **Optical Fiber Is Displaced** by the acceleration of the force-input member. The magnitude of the acceleration, which is related to the instantaneous position of the end of the fiber, is indicated as a digital output from the segmented detector.

A low-cost, rugged, lightweight accelerometer has been developed that converts mechanical motion into digitized optical outputs and is immune to electromagnetic and electrostatic interferences. This instrument can be placed in a hostile environment, such as an engine under test, and the output led out through a miscellany of electrical fields, high temperatures, etc., by optic fiber cables to the benign environment of a test panel. There, the digitized optical signals can be converted to electrical signals for use in standard electrical equipment or used directly in optical devices, such as an optical digital computer.

Basically as shown in the figure, a flexible optic fiber is suspended by one end fastened to the instrument case. A light source located at the fixed end introduces light into the suspended fiber. The other end of the fiber is free to move with respect to the case and directs the light onto an array of receptors, fixed with respect to the case. Acceleration applied to the case causes different receptors of the segmented detector to be activated by the light from the end of the oscillating fiber, providing a reading of the instantaneous positions of the fiber. The instantaneous position of the fiber is a direct measure of the acceleration being experienced by the case.

The fiber flexes in a single plane. Three orthogonally mounted instruments can produce three-axis acceleration data, which can, in turn, yield the total acceleration vector.

Variations in the instrument design are possible by controlling length, mass, and optical finish of the oscillating optic fiber, as well as clearance limits and detector design. The light source does not have to be a part of the instrument itself, but can be supplied by an input optic cable. Then the accelerometer itself can be small as well as lightweight. Since optic cables are generally lighter and more flexible than equivalent electric cables, the instrument and associated light cables will have less influence on the structure for which the acceleration is to be measured.

This work was done by R. R. August of Rockwell International Corp. for **Lewis Research Center**. *For further information, Circle 73 on the TSP Request Card.*
LEW-13219

Heat/Pressure Seal for Moving Parts

Articulated graphite segments accommodate dimensional variations.

Lyndon B. Johnson Space Center, Houston, Texas

A prototype seal keeps hot gases from leaking between large, adjacent parts in relative motion. The seal withstands temperatures greater than 1,000° C (1,800° F) and accommodates heat- and pressure-caused distortion of the parts. It is nonabrasive, creates little resistance to the movement of parts, and causes minimal wear and damage to surface coatings.

The seal was developed for the tail of the Space Shuttle orbiter, where it protects rudder/speed-brake components from high temperatures during reentry. It could also find application in manufacturing processes requiring thermal barriers between large moving parts.

The seal (see figure) consists of a housing, for attachment to one of the two adjacent moving parts, and an articulated graphite seal block, located in a channel within the housing. There are two sealing surfaces on the seal block: a rubbing surface that is held against one of the moving parts by helical springs, and a sliding surface that is held against the seal housing by a cantilever spring and a roller. The helical-spring force varies only slightly with deflection so that essentially constant pressure is maintained on the rubbing surface. In addition, the spring force is low enough to minimize rubbing friction and high enough to ensure an adequate seal under atmospheric and aerodynamic pressures.

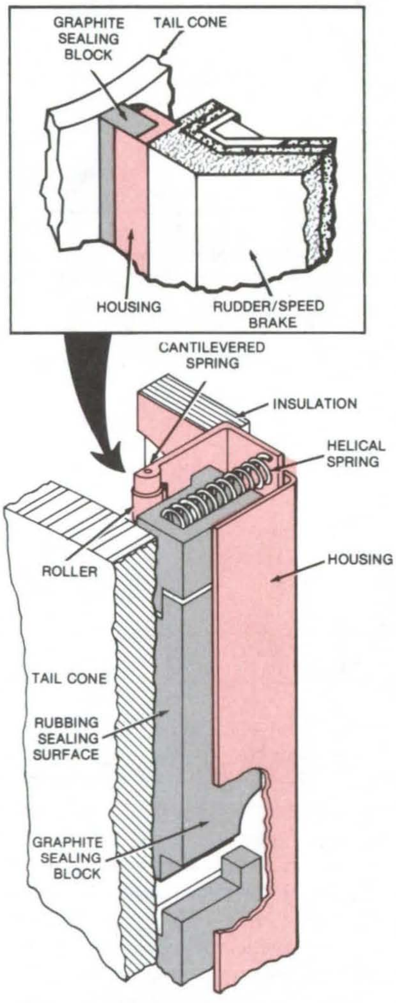

Graphite Sealing-Block Segments move on the Space Shuttle tail cones as the rudder/speed brake moves. Mounted on the rudder/speed brake, the housing contains springs that bias the block segments against the tail cone and housing sealing surface. The block segments accommodate dimensional changes caused by variations in temperature and pressure.

The Shuttle seal is 20 ft (6.1 m) long. The overlapping joints between adjacent seal block segments allow the blocks to conform to the tail cone surface. The opening created by the angle between blocks is so small that only an insignificant amount of gas leaks through. On the Space Shuttle, the seal permits 2-ft (0.61-m) relative rotational motion of the rudder/speed-brake leading edge around the tail cone.

Because of the high-temperature difference between the graphite blocks and the metal housing, each block is positioned by a guide slot and locating pin and is held against the housing by a cantilever spring. The locating pin is attached to the side of the housing, and the guide slot is between projections of the graphite blocks. This allows relative expansion and contraction of the housing without interrupting the seal.

This work was done by Martin L. Stevens of Fairchild Republic Co. for **Johnson Space Center.** *For further information, Circle 74 on the TSP Request Card.*

This invention is owned by NASA, and a patent application has been filed. Inquiries concerning nonexclusive or exclusive license for its commercial development should be addressed to the Patent Counsel, Johnson Space Center [see page A5]. Refer to MSC-18422.

Heat Switch Has No Moving Parts

Thermal link changes from on to off when a getter adsorbs a gaseous heat conductor.

Goddard Space Flight Center, Greenbelt, Maryland

No moving parts would be needed for a proposed new thermally actuated switch. The switch could also operate as a variable thermal conductance, allowing the temperature of the equipment to be regulated with a minimum expenditure of energy.

The switch is a gas-gap type — one in which the presence of a gas in a gap between two plates makes the switch heat-conductive (on) and the absence of gas in the gap makes the switch nonconductive (off). A getter (a gas-adsorbing material) adsorbs the gas to turn the heat switch off and releases the gas to turn the switch on.

The plates, made of a heat-conducting material such as copper or aluminum, are interleaved and are supported by a cylinder of an insulating material, such as fiberglass, nylon, or glass (see figure), which also serves to contain the gas. The gas gap is connected by a capillary tube to a small disk of getter material such as activated charcoal or a member of the zeolite mineral group. An electrical heater is positioned next to the getter. After the gas has been introduced into the switch through a fill tube, the tube is hermetically sealed.

A small current applied to the getter heater turns the heat switch on. The current raises the temperature of the getter enough to expel adsorbed gas into the gap. When the gas pressure in the gap reaches 100 to 200 μm of mercury (0.1 to 0.2 torr), the switch is fully conducting.

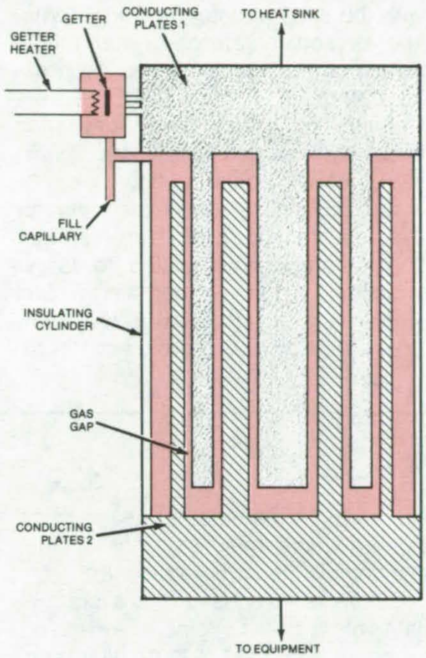

A **Gap Between Interleaved Plates** conducts heat when it is filled with gas and prevents heat transfer when the gas is absent. Controlled by a heater, a getter emits gas into the gap or adsorbs the gas from the gap.

If the heater is turned off and the getter is attached to a sufficiently-cold heat sink, it will adsorb the gas from the gap. When the gap pressure drops to about 10^{-5} torr, the heat switch is in its state of lowest conductance — its off state. In this state, the conductance of the gap is less than that of the insulating cylinder.

The amount of gas that the getter releases into the gap is determined by the magnitude of the heater current. Thus, the current can be regulated to control the amount of gas emitted and hence the conductance of the switch. The heat switch can then be operated as a heat valve with continuously-variable thermal conductance.

The choice of gas and getter depends on the temperature of the heat sink. Helium gas, for example, is the choice for temperatures between 1 and 8 K. The minimum and maximum gas pressures in this temperature range correspond to the required off and on conductances. At higher heat-sink temperatures, krypton (66 to 116 K) or water (233 to 373 K) can be used, for example.

This work was done by Stephen H. Castles of **Goddard Space Flight Center**. *For further information, Circle 75 on the TSP Request Card.*
GSC-12625

Books and Reports

These reports, studies, and handbooks are available from NASA as Technical Support Packages (TSP's) when a Request Card number is cited; otherwise they are available from the National Technical Information Service.

Dynamics of Cavitating Cascades and Inducer Pumps

Annotated bibliography summarizes 19 papers on the dynamics of cavitation.

A report chronicles the advances in understanding and predicting the unsteady dynamic characteristics of cavitating cascades and inducer pumps. It includes a bibliography of 19 papers authored between 1972 and 1980.

Cavitation is a phenomenon in which the fluid pressure of a liquid fluctuates slightly above and below the vapor pressure, causing the alternate formation and collapse of vapor bubbles. This in turn causes localized shock waves that can lead to the pitting of metal surfaces and a marked drop in efficiency. Cavitation phenomena, thus, have very significant

(continued on next page)

implications in liquid-handling and mixing systems.

In early papers simple L,R,C models were used for cavitating pumps, and the types of cavitation occurring in cascades and inducer pumps were identified. Compliance resulting from attached-blade cavities and compliance characteristics of bubbly cavitation were analyzed.

In later papers a more general dynamic-transfer-function concept was developed, and the contributions to the mass flow gain factor due to attached-blade cavities were presented. A test facility was constructed to study the unsteady dynamic response of cavitating inducer pumps. Using water and impellers 3 in. (7.6 cm) in diameter, complete dynamic transfer functions for various mean flow conditions (including cavitation number) were obtained at frequencies up to 42 Hz.

To understand better the dynamics of cavitation, the Bubbly Flow model was developed. It uses a bubbly, two-phase flow representation for the dynamics of cavitation pumps. Its transfer functions are in good qualitative and fair quantitative agreement with the experimental measurements. The essential features of the model are dynamic waves caused by pressure fluctuations and kinetic waves caused by fluctuating cavitation bubble production (near the pump inlet) due to fluctuating flow rate.

Questions about how the data for the test facility with 3-in.-diameter impellers could be scaled to larger impellers led to experiments with impellers 4 in. (10.2 cm) in diameter. These experiments verified that correct scaling behavior had been deduced. Under certain conditions and without external perturbations, flow in the test facility demonstrated large pressure and flow-rate fluctuations. This auto-oscillation instability was also investigated. Studies and theoretical analyses of flow details at or near the inlet to a cavitating impeller showed that the complicated swirling flow at the inlet is an important determinant of both the steady-state performance and the dynamic characteristics of the inducer.

This work was done by C. E. Brennen and A. J. Acosta of the California Institute of Technology for **Marshall Space Flight Center.** *To obtain a copy of the report, "Dynamics of Cavitating Cascades," Circle 76 on the TSP Request Card.*
MFS-25399

Computer Programs

These programs may be obtained at very reasonable cost from COSMIC, a facility sponsored by NASA to make new programs available to the public. For information on program price, size, and availability, circle the reference letter on the COSMIC Request Card in this issue.

Simplified Thermal Analyzer

Program for quick analysis of temperature and power balance is especially easy to use.

The Simplified Shuttle Payload Thermal Analyzer (SSPTA) aids in evaluating the thermal design of instruments to be flown in the Space Shuttle cargo bay. It is a collection of programs that are currently used in the thermal analysis of spacecraft, modified for quick, preliminary analysis of payloads. Although designed primarily to analyze the Shuttle payloads, it can easily be used for thermal analysis in other situations.

SSPTA includes a reduced math model of the Shuttle cargo bay. One of the prime objectives in developing SSPTA was to create an easily used program. With it, the user-required input is simple; and the user is free from many of the concerns normally associated with computer usage, such as disk-space handling, tape usage, and complicated program control.

SSPTA is comprised of a system of data files called "bins," a master program, and a set of thermal subprograms. The bin system is a collection of disk files that contain data required by or computed by the thermal subprograms. SSPTA currently handles 50 bins.

The master program serves primarily as a manager for the bins and their interaction with the thermal subprograms. Inputs to the master program are simple user commands that direct the data manipulation procedures, prepare the data for these procedures, and call the appropriate thermal subprograms. The subprograms of SSPTA are all based on programs that have been used extensively in the analysis of orbiting spacecraft and space hardware.

In subprogram CONSHAD, the user-supplied geometric radiation model computes blackbody view factors, shadow factors, and a description of the surface model. The subprogram WORKSHEET uses the surface-model description, optical-property data, and node-assignment data to prepare input for SCRIPTF, which computes the inverses of the infrared (IR) and ultraviolet (UV) radiation transfer equations. SCRIPTF also computes the radiation coupling between nodes in the thermal model.

Subprogram ORBITAL uses the shadow tables to compute incident flux intensities on each surface in the geometric model. In subprogram ABSORB, these flux intensities are combined with the IR and UV inverses to compute the IR and UV fluxes absorbed by each surface. The radiation couplings from SCRIPTF and the absorbed fluxes from ABSORB are used to compute the temperature and power balance for each node in the thermal model, in subprogram TTA.

Outputs consist of tabulated data from each of the subprograms executed during an analysis. Because SSPTA is modular, analyses may be run in whole or in part, and new subprograms may be added.

SSPTA is written in FORTRAN IV and Assembler for batch execution and has been implemented on an IBM 370-series computer with a central memory requirement of approximately 600K of 8-bit bytes. SSPTA was developed in 1977 and last updated in 1979.

This program was submitted by Michael J. Coyle of **Goddard Space Flight Center.** *For further information, Circle A on the COSMIC Request Card.*
GSC-12638

Resizing Structures for Minimum Weight

Approximation concepts and dual-method algorithms are combined in a new weight-minimization method.

Approximation concepts and dual-method algorithms are combined in a new method of minimum-weight design for structures. The Approximation Concepts Code for Efficient Structural Synthesis (ACCESS3) program is a powerful research tool in which mathematical programing and optimality criteria are coalesced in an efficient structural weight-minimization method.

Approximation concepts convert the general structural synthesis problem into a sequence of explicit problems of separable algebraic form. The dual method exploits this separable form to construct a sequence of explicit dual functions. These dual functions are maximized subject to nonnegativity constraints on the dual variables. This approach is very efficient because the dimensionality of the dual space, where most of the optimization effort is expended, is relatively low for most structural optimization problems of practical interest.

A rather general class of structural optimization problems can be concisely stated as a nonlinear programing (NLP) problem involving the minimization of an objective function subject to a set of inequality constraints. For practical structural design applications, the associated NLP problem is often very complicated due to the large number of design variables, the large set of inequality constraints, and the computational difficulties associated with the constraint functions. The ACCESS3 approach makes such an NLP problem tractable by replacing it with a sequence of relatively small, explicit mathematical programing problems that approximate the original problem while retaining important problem features. This is accomplished through the coordinated use of design variable linking, constraint deletion techniques, and explicit approximations for retained constraints.

Structures with prescribed configurations and given material properties are realized by modifying the dimensions of the finite elements, in particular their cross-sectional areas or thicknesses. Types of finite elements available in ACCESS3 include a truss, an isotropic constant-strain triangular membrane, a constant-strain triangular element with arbitrary orthotropic material properties, an isotropic shear panel, and a thermal shear panel. Thermal load analysis is included for problems involving load vectors that are dependent on design variables.

In addition to the usual Taylor-series expansion with respect to the reciprocals of linked design variables, natural-frequency constraints may be represented as first- or second-order Taylor-series expansions with respect to regular linked variables. Four distinct optimizer algorithm options are available. These are the interior point penalty-function method, the second-order primal-projection method, the second-order Newton-type dual method, and the first-order gradient projection-type dual method.

Input data for ACCESS3 consist of a finite-element model that exhibits the topological form, the geometrical configuration, and the structural materials of the structural system to be optimized, along with a set of structural loads and a selection of program options. Outputs include a description of the resizing of elements required to achieve minimum weight.

The ACCESS3 program is written in FORTRAN IV for batch execution and has been implemented on a CDC CYBER 70-series computer with a central memory requirement of approximately 74K (octal) of 60-bit words. The ACCESS3 program was developed in 1979.

This program was written by C. Fleury and L. A. Schmit of the University of California, Los Angeles, for **Langley Research Center.** *For further information, Circle B on the COSMIC Request Card.*
LAR-12699

NASTRAN Modifications for Recovering Strains and Curvatures

Where required, curvatures and strains can be retrieved in lieu of stresses.

NASTRAN, NASA's general-purpose finite-element structural analysis program, has been modified to allow recovery of surface strains, reference plane strains, and local curvatures at the nodes of the general plane elements. The NASTRAN routines that operate on element stress/strain/temperature relationships and strain/displacement relationships have been modified to incorporate the generation and return of strains and curvatures in lieu of stresses. The strains and curvatures are then transformed to the material axes and interpolated to generate the corresponding strains and curvatures at the nodes of the element. This interpolation is accomplished using a special surface-mapping function.

The recovery of strains and curvatures can be valuable in the performance of certain analyses. These variables are useful in comparing predicted strains with those measured via strain gages. Availability of this information can simplify the use of NASTRAN to solve nonlinear problems. Composite analysts can now couple NASTRAN with composite mechanics via 'pre' and 'post' processors and take advantage of NASTRAN's vast capabilities for designing and analyzing structures.

This program was written by C. C. Chamis of **Lewis Research Center** *and C. H. Hennrich of MacNeal-Schwendler Corp. For further information, Circle C on the COSMIC Request Card.*
LEW-12592

Cost-Minimized Aircraft Trajectories

Climb, cruise, and descent profiles for lowest operating costs

For an aircraft operating over a fixed range, the operating costs are basically a sum of fuel cost and time

cost; but determining a minimum cost trajectory can be complex. A new program optimizes trajectories with respect to a cost function that is based on a weighted sum of fuel cost and time cost. Minimum fuel, minimum time, and various delay trajectories are obtained by specifying particular values for the fuel and time cost factors.

As a research tool, the program could be used to study characteristics of optimum trajectories and to compare them to standard trajectories. It might also be used to generate a model for the development of an airborne trajectory optimization system. The program could be incorporated into an airline flight-planning system, with optimum flight plans determined at takeoff time for the prevailing flight conditions. Trajectory optimization could significantly reduce the cost for a given aircraft mission.

The algorithm incorporated in the program assumes that a trajectory consists of climb, cruise, and descent segments. Each segment is not optimized independently, as in classical procedures, but is optimized to account for interactions between the segments. This is done with optimal control theory.

The climb and descent profiles are generated by integrating a set of kinematic and dynamic equations, where the total energy of the aircraft is the independent variable. At each energy level of the climb and descent profiles, the airspeed and power necessary for an optimal trajectory are determined. The variational Hamiltonian of the problem consists of the rate of change of cost with respect to total energy and a term dependent on the adjoint variable, which is identical to the optimum cruise cost at a specified altitude. This variable uniquely specifies the optimal cruise energy, cruise altitude, cruise mach number, and indirectly, the climb and descent profiles.

If the optimum cruise cost is specified, an optimum trajectory can easily be generated; however, the range obtained for a particular optimum cruise cost is not known a priori. For short-range flights, the program iteratively varies the optimum cruise cost (and therefore the cruise altitude) until the computed range converges to the specified range. For long-range flights, iteration is unnecessary since cruise flight always takes place at the optimum cruise altitude.

The user must supply the program with engine fuel flowrate and thrust data and an aircraft aerodynamic model. The program currently includes data for the Pratt-Whitney JT8D-7 engine and an aerodynamic model representative of the Boeing 727. Inputs to the program consist of the flight range to be covered and the prevailing flight conditions, including pressure, temperature, and wind profiles. Information output by the program includes: optimum cruise tables at selected weights, optimal climb and descent profiles, and a summary of the complete synthesized optimal trajectory.

This program is written in FORTRAN IV for batch execution and has been implemented on a CDC 6000-series computer with a central memory requirement of approximately 100K (octal) of 60-bit words. This aircraft trajectory optimization program was developed in 1979.

This program was written by Homer Lee and Heinz Erzberger of **Ames Research Center.** *For further information, NASA TP-1565, "Computer Algorithm for Fixed Range Optimal Trajectories" [1980], Circle D on the COSMIC Request Card.*
ARC-11282

Aerodynamic Preliminary Analysis

An interactive system for surveying alternative configurations and component geometries.

The computerization of aerodynamic theory has progressed to a state where the analysis of complete aircraft configurations can be performed by a single program. Currently existing programs of this nature abound with subtleties and difficulties attributable to the level of precision of the underlying theory and the sensitivity of the associated numerical solution techniques. In preliminary design stages, it is often desirable to accept some degree of approximation in the interest of faster turnaround, reduced computational costs, the simplification of input, and the stability of results while maintaining generality.

The Aerodynamic Preliminary Analysis System, APAS, is a comprehensive aerodynamic analysis system, based on linearized potential theory. Three-dimensional configurations (with or without jet flaps) having multiple nonplanar surfaces of arbitrary planform and open or closed slender bodies of noncircular contour may be analyzed with the APAS. As a preliminary design aid, APAS allows the designer to survey systematically a large number of alternative configurations and component geometries economically. When combined with realistic assessments of its limitations and estimated viscous characteristics, APAS is a valuable tool for analyzing general aircraft configurations and aerodynamic interactions.

The analysis technique employed by APAS is based on linearized aerodynamic theory. The configuration to be analyzed is simulated by a distribution of source and vortex singularities. Each of the singularities satisfies the linearized small-perturbation-potential equation of motion. The singularity strengths are obtained by satisfying the condition that the flow remains tangent to the local surface.

The bodies, interference shells, and aerodynamic surfaces are each simulated by different types of singularities. First, the strengths of singularities representing the fuselage and nacelles are determined by using a slender body thickness approach to predict the surface and near-field properties. Perturbation velocities induced on the aerodynamic surfaces are evaluated.

Singularity strengths representing aerodynamic surfaces are determined utilizing thin airfoil panel theory, which allows the effects of thickness and lift to be considered independently. A cylindrical, noncircular, interference shell, composed entirely of vortex panels, is used to account for the interference effects of the aerodynamic surfaces on the fuselage and nacelles.

Once all of the singularity strengths are determined, the resulting velocities and pressures throughout the flow are obtained. APAS also performs a drag analysis for determining skin friction, potential form drag, and trim drag.

APAS is a user-oriented interactive system. Once the system is accessed, it is a self-contained interactive environment where the analyst can input vehicle definitions, perform aerodynamic analysis, and display computed results without exiting the system. Geometry and analysis data may be saved for later sessions and are protected from loss due to machine failure. The interactive nature of APAS permits the user to quickly learn how to use the system.

The APAS is written in FORTRAN IV for interactive, or batch, execution and has been implemented on a CDC CYBER 175 computer. The largest program in the system has a central memory requirement of approximately 120K (octal) of 60-bit words. The computer on which APAS is installed must support segmentation and random-access files. The interactive and graphics capabilities of APAS require a Tektronix 4014 graphics terminal, a Tektronix 4096 graphics tablet, and the Tektronix Plot 10 and graphics tablet support software. The APAS was developed in 1978.

This program was written by E. Bonner, W. Clever, P. Divan, K. Dunn, and J. Kojima of Rockwell International Corp. for **Langley Research Center.** *For further information, Circle E on the COSMIC Request Card.*
LAR-12404

Inviscid Transonic Flow Over Axisymmetric Bodies

Outputs include pressure distribution, drag, and flow-field data.

Axisymmetric transonic flow is of interest not only because of its practical application to missile and launch vehicle aerodynamics but also because of its relation, in terms of the area rule, to fully three-dimensional flow. The RAXBOD computer program analyzes steady, inviscid, irrotational, transonic flow over axisymmetric bodies in free air. RAXBOD uses a finite-difference relaxation method to solve numerically the exact formulation of the disturbance velocity potential with exact surface boundary conditions. The nonconservative form of the potential equation is used. Agreement with available experimental results has been good in cases where viscous effects and wind-tunnel wall interference are not important.

The governing second-order partial differential equation describing the flow potential is replaced by a system of finite-difference equations, including Jameson's "rotated" difference scheme at supersonic points. A stretching is applied to both the normal and tangential coordinates, such that the infinite physical space is mapped onto a finite computational space. The boundary condition at infinity can be applied directly, and there is no need for an asymptotic far-field solution.

The system of finite-difference equations is solved by a column relaxation method. In order to obtain both rapid convergence and any desired resolution, the relaxation is performed iteratively on successively refined grids. Inputs to RAXBOD consist of a description of the body geometry, the free-stream conditions, and the desired resolution control parameters. Outputs from RAXBOD include computed geometric parameters in the normal and tangential directions, iteration history information, pressure distribution, drag coefficients, flow-field data in the computational plane, and coordinates of the sonic line.

This program is written in FORTRAN IV for batch execution and has been implemented on a CDC 6600 computer with an overlaid central memory requirement of approximately 40K (octal) of 60-bit words. Optional plotted output can be generated for the CALCOMP plotting system. The RAXBOD program was developed in 1976.

This program was written by Jerry C. South, Jr., and James D. Keller of **Langley Research Center.** *For further information, Circle F on the COSMIC Request Card.*
LAR-12499

Plastic Deformation of Engines and Other Nonlinear Structures

Program analyzes elastic, plastic, and creep deformation for high temperatures and cyclic loads.

The Plastic Analysis Capability for Engines (BOPACE3D) is a nonlinear stress-analysis program based on a very general family of isoparametric finite elements. Although the development of BOPACE3D has been heavily influenced by the requirements for engine analysis (in particular the Space Shuttle main engine), it is a general program applicable to many nonlinear structures.

BOPACE3D analyzes the stresses on structures subjected to very high temperatures, large plastic-creep effects, and geometric nonlinearities, while experiencing cyclic thermal and mechanical loads. It includes several such advanced features as substructuring, an out-of-core Gauss wave-front equation solver, multipoint constraints, combined material and geometric nonlinearities, automatic calculation of inertia effects, follower forces, singular crack-tip elements, and axisymmetric capabilities.

Classical constitutive theory in an elastoviscoplastic program such as BOPACE3D provides the incremental relations between stresses and strains. BOPACE3D uses these relations and the standard finite-element stiffness method to obtain an efficient solution approach for an important class of nonlinear structural-analysis programs.

Elastic, plastic, thermal, and creep deformations and the nonlinear dependence of all deformations on temperatures are accurately accounted for in the BOPACE3D solution. The material theory used includes a combined isotropic/kinematic plastic hardening theory and a generalized approach to cyclic load reversal. A family of isoparametric finite elements is provided for structure modeling. The simplest elements of this family are the two-node rod, the four-node quadrilateral, and the eight-node brick. Various higher

order elements are available with each basic element edge containing up to five arbitrarily spaced nodes.

The ability to space edge nodes arbitrarily and to have different numbers of edge nodes on different edges of the same element provides versatility in representing complex geometries. To relieve the user of much of the effort required in developing a complex finite-element model, the program provides an automated data-generation capability.

The BOPACE3D program is written in FORTRAN IV for batch execution and has been implemented on a UNIVAC 1100-series computer with a segmented central memory requirement of approximately 56K of 36-bit words. Version 6 of the BOPACE3D program was released in 1978.

This program was written by R. G. Vos and J. L. Arnquist of The Boeing Co. for **Marshall Space Flight Center**. *For further information, Circle G on the COSMIC Request Card.*
MFS-23814

Analysis of a Cooled, Turbine Blade or Vane With an Insert

Transient thermal analysis of blades and vanes with a coolant insert

A computer program, TACTI, has been developed to calculate transient and steady-state temperatures, pressures, and flows in a cooled turbine blade or vane with an impingement insert. Coolant-side heat-transfer coefficients are calculated internally in the program, with the user specifying one of three modes of heat transfer at each station: (1) impingement, including the effect of crossflow; (2) forced-convection channel flow; or (3) forced convection over pin fins. A limited capability to handle film cooling is also available in the program. It is assumed that spent impingement air flows in a chordwise direction and is discharged through a split or drilled trailing edge and through film-cooling holes. The program does not allow for radial flow of the spent impingement air. The use of film cooling is restricted by a numerical model requirement for a continuous crossflow.

As turbine-engine core operating conditions became more severe, it was more difficult to effectively cool blades and vanes. Advanced transient thermal calculation techniques were needed to design reliable turbine blades. There was no generally-available computer program that used advanced techniques in combining the required heat-transfer and coolant-flow-distribution calculations. TACTI was developed to perform transient and steady-state heat-transfer and coolant-flow analyses for a cooled blade, given the outside hot-gas boundary conditions, the coolant inlet conditions, the geometry of the blade shell, and the cooling configuration. It can handle a turbine blade or vane that is equipped with a central coolant-plenum insert from which coolant air flows through holes to impinge on the inner surface of the blade shell. The blade is modeled by dividing it by chordwise planes into as many as 15 slices, with each slice having as many as 79 chordwise calculational stations. Temperatures at each station are calculated for four points through the wall and one in the coolant channel. Included in this model is the capability to analyze a blade with a ceramic thermal-barrier coating. The ability of the program to handle film cooling is limited by the numerical modeling of the coolant crossflow.

For inputs to the program, the following basic elements of the geometry are needed for each station: (1) the thicknesses of the wall coating and wall metal and the coolant-channel width, (2) the chordwise distance of each node from the adjacent upstream node, and (3) the radial span for this slice. In addition, depending on the mode of heat transfer specified, the user must supply diameter and spacing for impingement holes or pin fins and data for film-cooling holes. All input values except the radial span are assumed to be the values at the midspan of the slice. Program output includes the temperature at each node, the coolant pressures and flow rates, and the inside heat-transfer coefficients.

The numerical solution for the temperatures throughout the blade involves writing a transient energy equation for each node and forming a set of equations to be solved for the temperature distribution. The nodal energy balances are linearized, one-dimensional, heat-conduction equations at the wall-outer-surface node, at the junction of the cladding and the metal node, and at the wall-inner-surface node. At the midmetal node, a linear, three-dimensional, heat-conduction equation is used.

Similarly, the coolant pressure distribution is determined by writing the transient momentum equation for one-dimensional flow between adjacent fluid nodes and solving the resulting set of equations for static pressures. In the coolant channel, energy and momentum equations for one-dimensional compressible flow including friction and heat transfer are written for the elemental channel length between two coolant nodes.

This program was written in FORTRAN IV for use on an IBM TSS/360-67 computer.

This program was written by R. E. Gaugler of **Lewis Research Center**. *For further information, Circle H on the COSMIC Request Card.*
LEW-13293

Machinery

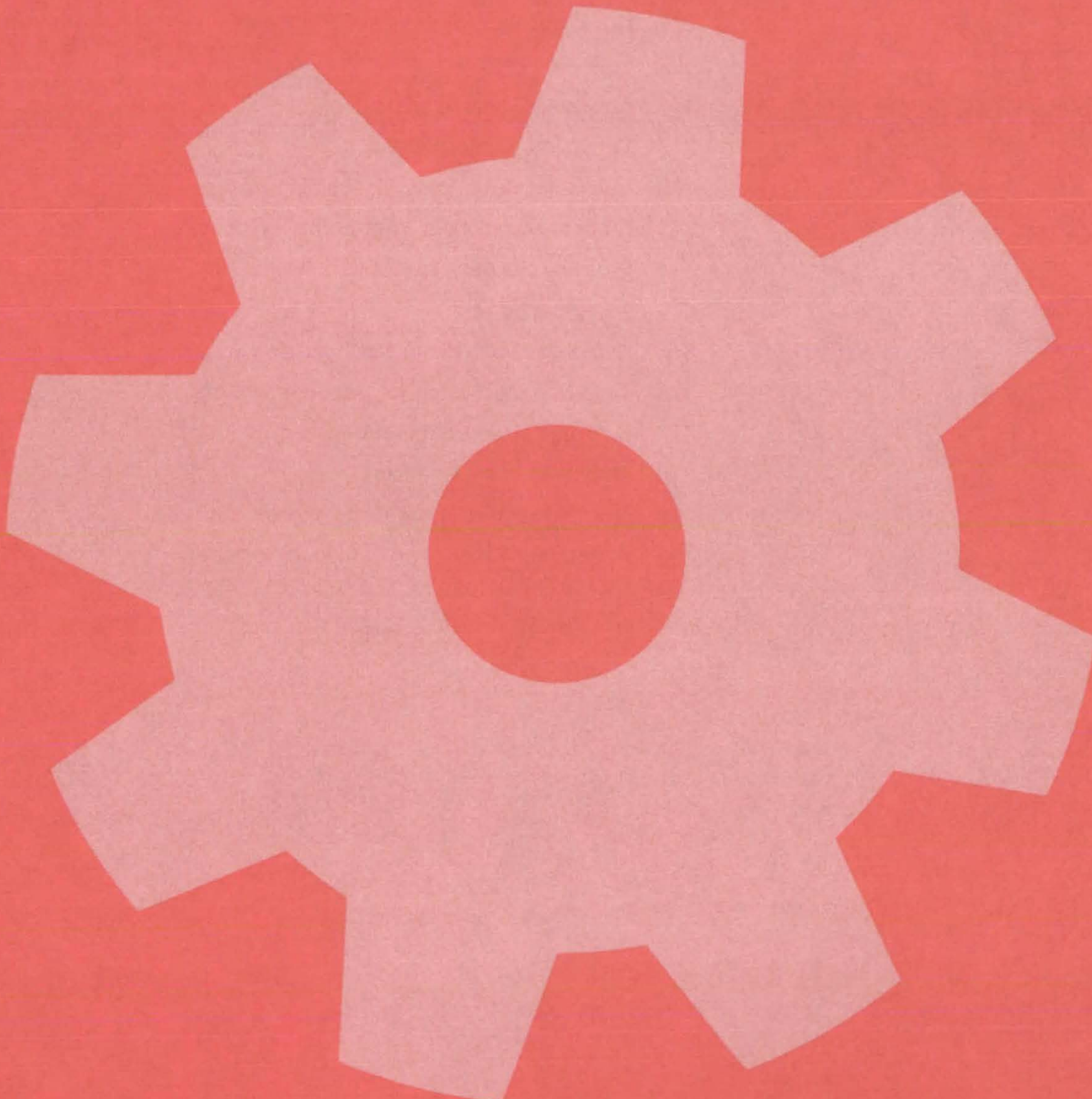

Hardware, Techniques, and Processes

Cleaving Machine for Hard Crystals

Undistorted LiF slices for spectrometers can be prepared quickly and with little waste.

Goddard Space Flight Center, Greenbelt, Maryland

Hard crystalline materials such as lithium fluoride (LiF) can be cleaved in thin sections — precisely and reproducibly — with the aid of a semiautomatic machine. The yield of undistorted LiF crystals is almost 100 percent, even when the cleaved section is only 1/32 inch (0.8 mm) thick. Using the machine, a semiskilled operator can produce uniform crystal slices with greater speed than a skilled hand cleaver.

Previously, lithium fluoride was cleaved by hand with a hammer and knife or razor blade, but learning to cleave by hand was time-consuming and costly in materials. By hand, crystals could not be cleaved reliably to less than 1/16 inch (1.6 mm) thick. Although lithium fluoride crystals measuring 1/32 by 1 by 2 inches (0.8 by 25.4 by 50.8 mm) are required in substantial quantities for such optical devices as crystal spectrometers, it was almost impossible to produce a sufficient number of good-quality slices by hand cleaving.

The new machine contains a spring-activated hammering mechanism that limits the penetration of a blade into the crystal and controls the magnitude of the shock wave that cleaves the crystal. The tension in the spring is adjusted by turning a knob.

A fixture with spring-loaded clamps precisely locates and holds the crystal, restraining it only to the extent that it remains in an ideal position for cleaving until the blade strikes it. The crystal then splays apart as it is cleaved. The holding fixture minimizes damping of the shock wave so that it has full effect in breaking the crystal bonds.

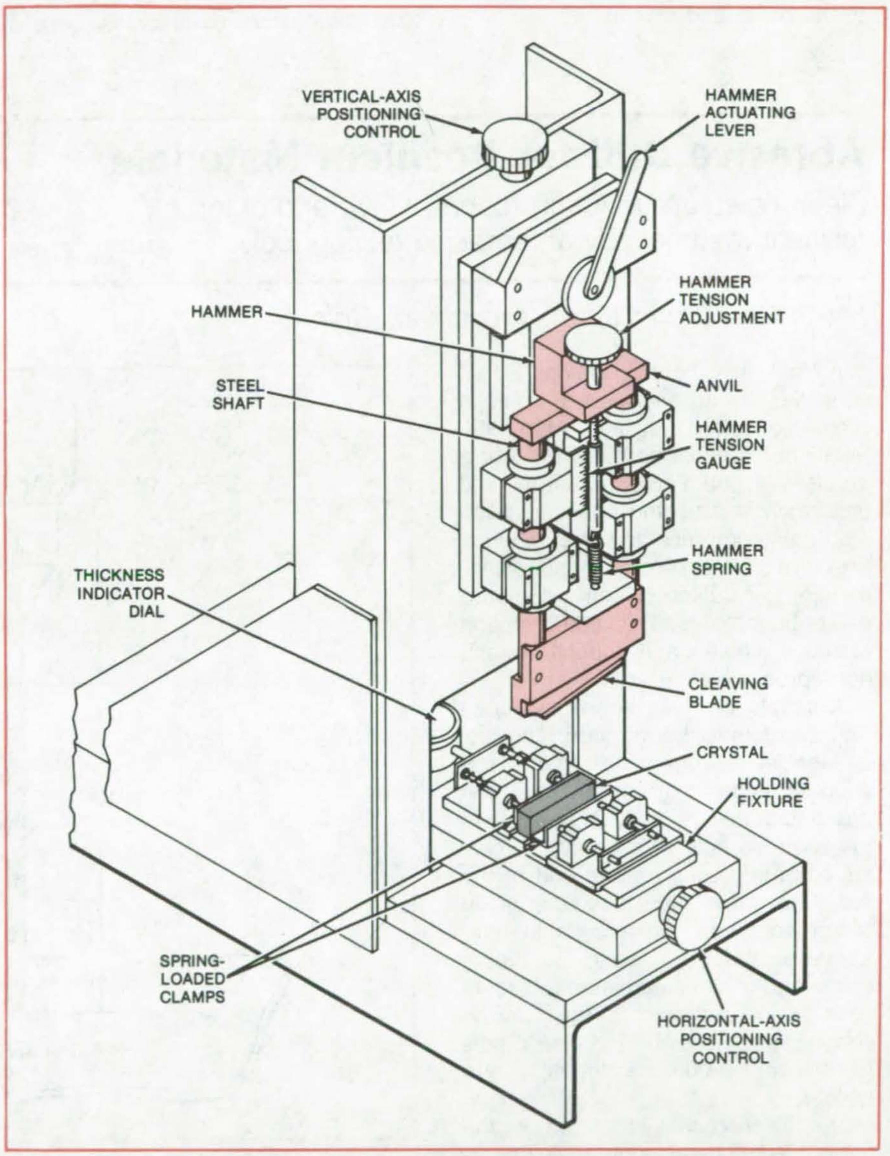

A **Hammer/Anvil/Blade Mechanism** transmits a shock wave that cleaves the crystal. The hard-crystal cleaving machine has controls for adjusting the position of the crystal block and the striking force of the hammer. The machine shown here can accommodate crystals up to 1 by 2 by 1/2 inches (25.4 by 50.8 by 12.7 mm) in size.

To cleave a crystal, an operator:

- Measures the thickness of the crystal block;
- Places the block between the spring-loaded clamps on the holding fixture so that the crystal cleaving plane is alined parallel to the blade;
- Turns the horizontal-axis positioning control until a dial thickness indicator reads one-half the thickness of the crystal block (this step ensures that the blade will contact the block at its midpoint and that shock-wave forces are balanced; otherwise, the crystal may shatter);
- Raises the hammer by pulling the hammer-actuating lever;
- Turns the hammer tension-adjustment knob until the tension gage indicates the proper tension value for the crystal-block thickness (this experimentally determined adjustment ensures that the hammer strikes the blade with sufficient force to completely break the crystal bond along

(continued on next page)

the cleavage plane without shattering the crystal);
- Lowers the blade until it touches the crystal (blade penetration is limited by a fixed stop);
- Trips the hammer-actuating lever, releasing the hammer so that it strikes the anvil, which transfers the shock wave through two steel shafts to the blade and crystal;
- Raises the blade and removes the two crystal slices.

The procedure can be repeated to obtain progressively thinner slices. During a production run, crystals of a given thickness should be cleaved in sequence so that the hammer tension can be kept at a single setting.

This work was done by John S. J. Benedicto and Frederick Hallberg of **Goddard Space Flight Center.** *For further information, Circle 77 on the TSP Request Card.*

This invention is owned by NASA, and a patent application has been filed. Inquiries concerning nonexclusive or exclusive license for its commercial development should be addressed to the Patent Counsel, Goddard Space Flight Center [see page A5]. Refer to GSC-12584.

Abrasive Drill for Resilient Materials

Clean holes are made in rubber, vinyl, and other resilient materials by an abrasive drilling tool.

Lewis Research Center, Cleveland, Ohio

A tool has been developed that simplifies drilling or punching holes in rubber or other resilient materials. Resilient materials normally present a problem in obtaining accurate and uniform hole size and position. Such materials compress and stretch when pressure is applied in punching, piercing, or drilling. When a standard drill or punch is used, this deformation results in a hole that is nonuniform and nonreproducible.

A simple tool has been developed that overcomes the problem. The tool is fabricated from a stiff metal rod such as tungsten or carbon steel that has a diameter slightly smaller than the required hole. A piercing/centering point is ground on one end of the rod. The rod is then plasma-sprayed (flame-sprayed) with a suitable hard abrasive coating. Both aluminum oxide and nickel/aluminum powders have been used as coatings. Spray-coating thicknesses of 1 to 3 mils (0.003 to 0.008 centimeter) are typical.

The finished tool is shown in the figure. High-speed, slow-feed operation of the tool is necessary for accurate holes, and this can be done with a drill press, hand drill, or similar machines. The tool has been used to drill neoprene rubber, vinyl, and polytetrafluoroethylene with maximum deviation of approximately ±0.002 inch (±0.005 centimeter). It is expected that the drill would work well on other resilient materials.

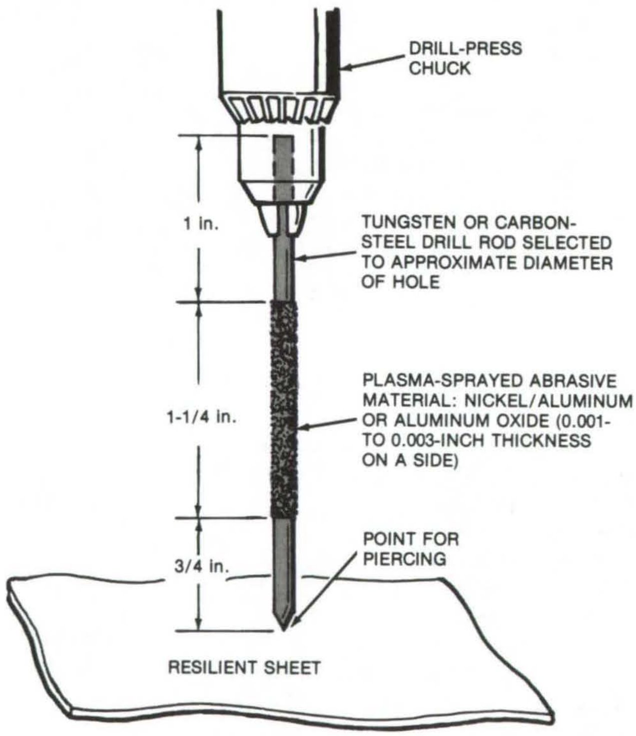

The **Gritty Surface** on the tool turning at high speed reams a smooth hole in rubber, vinyl, and other resilient materials

This work was done by A. J. Koch of **Lewis Research Center.** *No further documentation is available.*
LEW-13411

Drilling at Right Angles in Blind Holes

Flexible shaft in a metal tube guides a carbide cutter through the wall of a blind hole.

Marshall Space Flight Center, Alabama

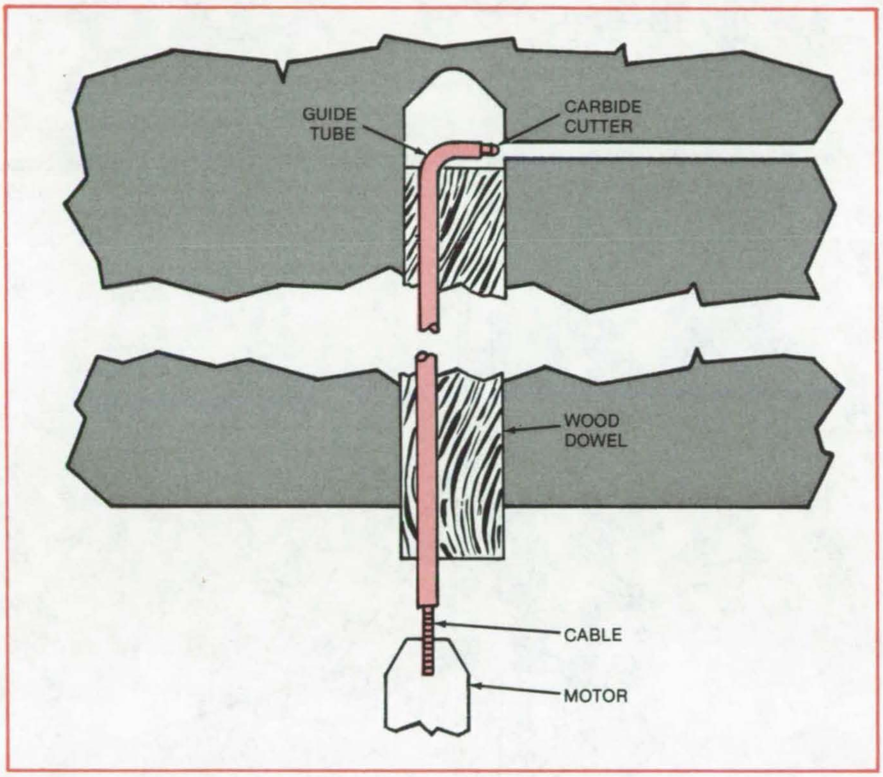

Drill for Hard-To-Reach Areas contains a flexible shaft that transmits torque to a carbide cutter at its tip.

The tool shown in the figure drills a small hole perpendicular to and at the bottom of a blind hole. It consists of a carbide cutter brazed to a flexible shaft, inside a thin metal tube with a 90° bend. A wood dowel holds the tube while a motor turns the shaft and drives the cutter.

The tool was developed for clearing plugged fuel orifices. With it, plugs are cleared on the Space Shuttle main engine without completely disassembling the engine part for offsite electrochemical or electrical-discharge machining. It is used to drill a 3/32-inch (2.4-mm) hole, 3/16 inch (4.8 mm) deep, normal to the wall of a hole 1 inch (2.54 cm) in diameter and 10 inches (25.4 cm) deep. The concept is adaptable to other hard-to-reach drilling situations.

This work was done by Richard Pessin of Rockwell International Corp. for **Marshall Space Flight Center.** *No further documentation is available.* *MFS-19535*

Solar-Powered Aircraft

Cruciform wing allows aircraft to keep solar cells perpendicular to Sun.

Langley Research Center, Hampton, Virginia

A proposed solar-powered aircraft, driven by an electric motor, would have vertical and horizontal wings. This design would allow the aircraft to fly in a straight path while banked, permitting optimal exposure of its wing-mounted solar cells to the Sun. Such an aircraft would fly at an altitude high enough to be above the clouds and to avoid winds with velocities much greater than its own airspeed. Its most likely application would be as a pilotless aircraft to take advantage of its ability to remain aloft for long periods (for very long flights). Excess solar energy could be stored as increased altitude or in batteries or some other energy-storage system. The stored energy would be used to keep the vehicle aloft at night, eliminating fuel as a factor limiting endurance. Because of power limitations, the aircraft would need a very light wing loading.

At least two solar-powered aircraft have been flown successfully; one has an 81-inch (2.1-meter) wingspan, the other a 32-foot (9.8-meter) wingspan. These are conventionally configured with solar cells on top of the wing or fuselage. As a result, the energy available to fly these aircraft is maximum when the Sun is directly overhead, and they can operate only for a few hours near noon in seasons and latitudes in which the Sun is high in the sky.

(continued on next page)

A solar-powered aircraft, to be useful as a monitoring or surveillance platform, should be able to fly indefinitely over any part of Earth and to maintain a station over a desired location. To do this, the plane must be able to recover maximum solar energy throughout the day.

This would be possible, despite the angle of the Sun, if there were solar cells in both the vertical and horizontal planes. For station keeping, the aircraft would have to fly a racetrack pattern, and calculations show that the aircraft would require arrays of solar cells on the upper surface of the wing and an equal number of arrays on each vertical side as shown in Figure 1. However, the weight of the additional solar cells would greatly limit the payload of the aircraft.

One way to eliminate the need for additional cells in the vertical plane would be to bank the aircraft so that the normal to the wing lies along the Sun line, but a conventional aircraft cannot maintain straight flight at a large bank angle. However, by using a vertical wing in addition to the conventional horizontal wing, the aircraft could be flown in a straight line at any bank angle. Thus the solar cells could be kept normal to the Sun line by duplicating the wing rather than by tripling the area of solar cells. A cruciform-winged aircraft (Figure 2) would need solar cells on one wing only. This wing is kept normal to the Sun line.

The racetrack pattern required for station keeping could be flown by banking first in one direction, then in the other, keeping the solar cells normal to the Sun line, and taking full advantage of available solar energy anywhere on Earth throughout the daylight hours. A simplified theoretical analysis shows that as the cruciform aircraft is banked about an axis parallel to the zero lift line, the lift and induced drag remain constant.

In an alternate configuration, the tail and fuselage are eliminated, and the differential thrust of four propellers, one at each wingtip, supplies the pitching and yawing moments required for stability and control. Because of the critical importance of drag and weight in the design of solar-powered aircraft, elimination of the fuselage and tail may be an important factor in meeting the required performance goals.

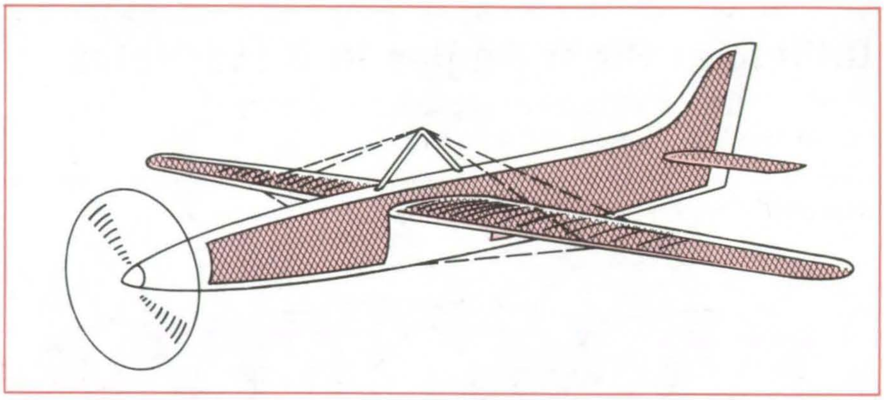

Figure 1. **Conventionally-Configured Solar-Powered Aircraft** would require solar cells (cross-hatched areas) on both vertical sides to provide constant output during daylight hours.

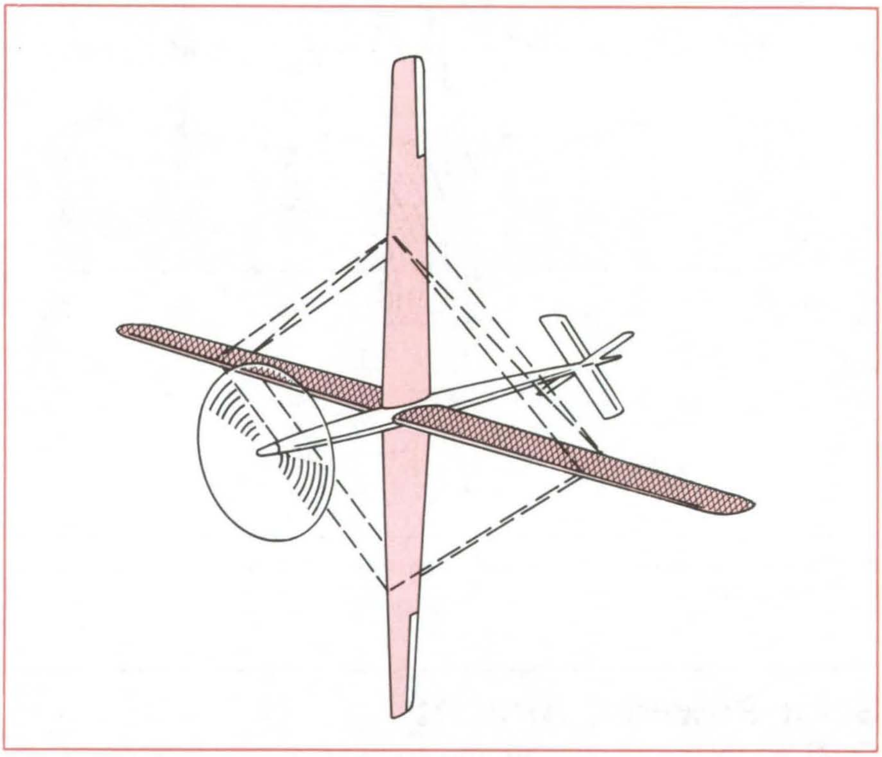

Figure 2. **Cruciform-Wing Solar-Powered Aircraft** could bank steeply to keep its solar cells perpendicular to the Sun line, yet fly a straight course.

Launching and landing for either configuration would be unconventional. The planes could be launched with a motorized dolly or carried aloft on a balloon; they could be recovered by parachute or could return to the motorized dolly.

This work was done by William H. Phillips of **Langley Research Center.** *No further documentation is available.*

This invention is owned by NASA, and a patent application has been filed. Inquiries concerning nonexclusive or exclusive license for its commercial development should be addressed to the Patent Counsel, Langley Research Center [see page A5]. Refer to LAR-12615.

Ball-Joint Grounding Ring

Spring-loaded fingers assure continuous electrical contact across a ball-and-socket joint.

Lyndon B. Johnson Space Center, Houston, Texas

In a ball-and-socket joint where an electrical insulator such as polytetrafluoroethylene is used as a liner to minimize friction, good electrical contact across the joint may be needed for lightning protection or to prevent static-charge buildup. Electrical contact can be maintained by a ring of spring-loaded fingers mounted in the socket (see figure).

This approach is used on the Space Shuttle at the attach points between the orbiter and external tanks. There, the principal hazard is lightning, which could falsely trigger the pyroseparation system. Beryllium copper, an alloy with excellent flexibility and hardness and high conductivity, is used. The ring of springy fingers is attached between the socket wall and its polytetrafluoroethylene liner. They extend over the liner into the socket cavity and bear against the bare-metal portion of the ball.

The full peripheral contact of the grounding ring should be more reliable than a single-path, lanyard connector and less costly than a bellows. It may be useful in industry for cranes, trailers, and other applications requiring a ball-and-socket joint.

This work was done by Peter J. A. Aperlo, Peter A. Buck, and Vincent A. Weldon of Rockwell International Corp. for **Johnson Space Center.** *No further documentation is available. MSC-18824*

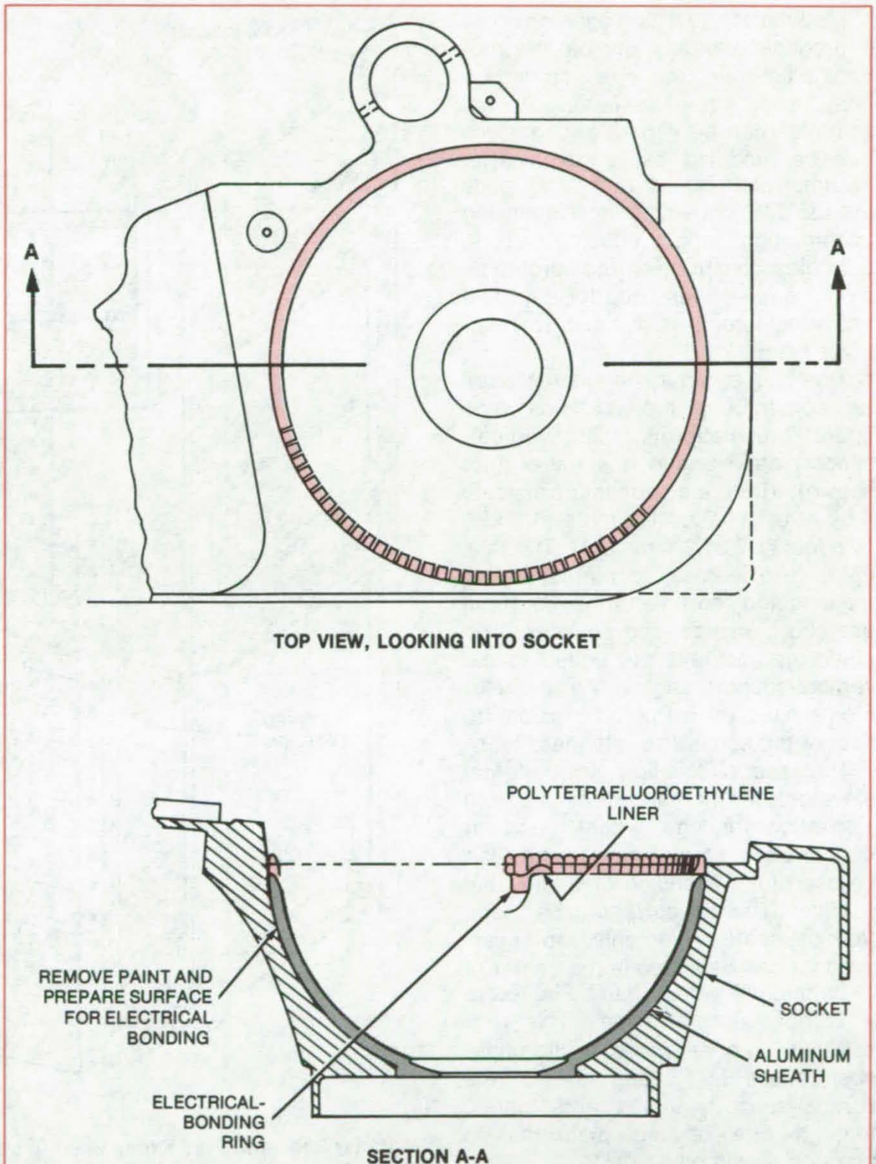

The **Beryllium Copper Electrical-Bonding Ring** (in color) is attached to the metal socket. Part of the polytetrafluoroethylene socket liner overlaps the ring. On the Space Shuttle, 100 equal-sized tabs were used. The ring dimensions are chosen for each application.

Versatile Modular Scaffolds

Movable and fixed modular scaffolds can be tailored to most scaffolding needs.

Goddard Space Flight Center, Greenbelt, Maryland

Modular scaffolds are assembled by interconnecting only four basic structural elements. The size, configuration, and other features of the scaffolds can be varied, and designs can be modified easily, even after assembly. Standard nuts and bolts are used to join elements, simplifying construction and reducing costs. Scaffolds constructed from prototype modules have been used for men and heavy equipment from small to moderate height.

The four structural elements used for constructing the scaffolds (see figure) are platforms, rails, vertical-support angles, and a stiffener (not shown). There are two platform sizes: 4 by 4 feet (1.2 by 1.2 meters) and 4 by 8 feet (1.2 by 2.4 meters). The rails are in two lengths, to correspond to the long and short platforms; each rail has short, vertical end sections. The platforms and rails are bolted to the vertical-support angles. All the elements have the same size holes, to accept the same size, standard bolt.

The scaffolds allow for internal elevators, for men and materials, and also allow for legs, wheels, and air mounts so that the same elements can be used for a standing or a movable scaffold. The elevators can be made from the scaffold elements. Moreover, a ladder can be added in the center of a scaffold platform or can be bolted to a vertical-support angle. The new scaffolds can be made to fit under obstructions by cutting one of the vertical-support angles and cutting through one of the platforms to produce a new platform.

The scaffolds are rigid and can be made any length. They are stable on unlevel ground and can extend to well over 50 feet (15 meters) in height.

This work was done by James Kerley of **Goddard Space Flight Center.** *For further information, Circle 78 on the TSP Request Card.*
GSC-12606

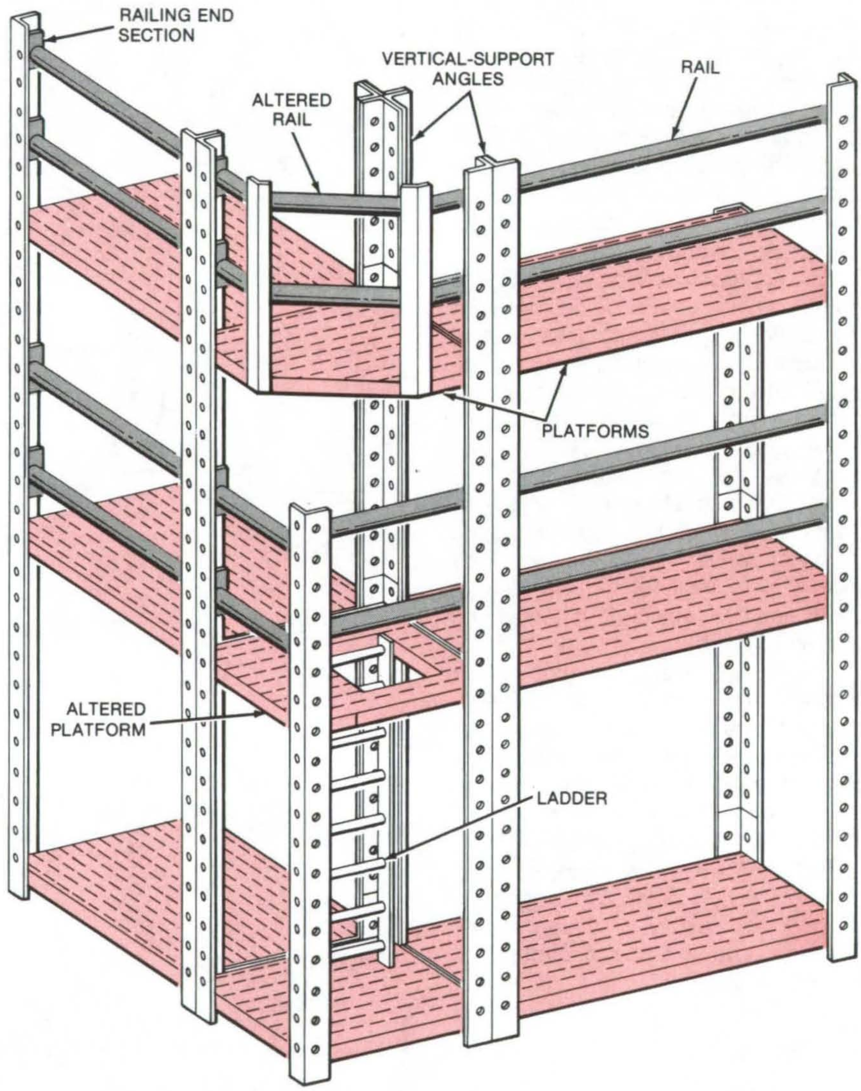

Modular Rails and Platforms, used in constructing scaffolds, come in two different sizes. They are attached with standard nuts and bolts to vertical-support angles. The modules can be altered to accommodate ladders and obstructions and can be used to construct elevators for the scaffolds. They allow easy access to the platforms because no diagonal supports are used.

Reshaping Tube Ends for Welding

A semiautomatic tool rounds deformed tube ends.

Lyndon B. Johnson Space Center, Houston, Texas

A semiautomatic tool rounds tube ends in preparation for welding. It was originally designed for tubes that have been trimmed close to a bend, where deformation is introduced by the bending process. Roundness is restored so that the tube ends can be welded.

The hydraulically operated tool (see figure) can be mounted on a workbench and is small enough to be moved easily from one factory area to another. It consists of two major parts: an "expander" that opens up the out-of-round tube so that a plug can be inserted and a "crimper" that compresses the tube into shape around the plug. Both parts are powered from a single pressurizing line.

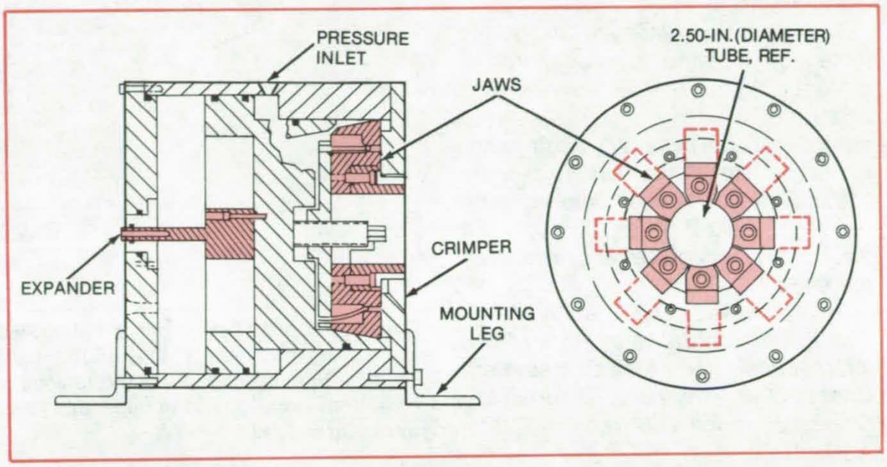

This **Hydraulically Actuated Tool** reshapes out-of-round tube ends in preparation for welding. Six sets of interchangeable jaws handle tube outside diameters from 1/4 to 2-1/2 inches.

An operator first squeezes the out-of-round tube in a vise to restore partially its original shape, then a steel plug is inserted into the tube end. The plug is selected to have the same diameter as the desired inside diameter of the tube. If necessary, the hydraulically actuated expander on the tool is used to enlarge the deformed tube end so that it can accommodate the plug.

Next, the operator inserts the tube end and its plug into the crimping end of the tool. Hydraulic pressure is applied, and the jaws of the crimper swage the tube around the plug so that it assumes the proper shape. Finally, the operator removes the tube from the tool, removes the plug, and places a cap over the tube end to protect it until it is welded. The present design handles a range of tube sizes, from 1/4 to 2-1/2 in. (0.635 to 6.350 cm) outside diameter.

This work was done by William H. Emanuel and Charles A. Headley of McDonnell Douglas Corp. for **Johnson Space Center.** *For further information, including detailed engineering drawings of the tool and its parts, Circle 79 on the TSP Request Card.*
MSC-18462

Remote Manipulator With Force Feedback

Controller gives the user a feel for the force and torque exerted on an object.

Ames Research Center, Moffett Field, California

A controller for a remote manipulator gives a user a "feel" for the forces required to lift, slide, turn, and otherwise handle objects. Because an operator experiences sensations similar to those he would perceive if he handled the objects directly, he needs much less skill and training for this manipulator than for one without force feedback.

The controller was developed to handle hazardous materials, such as radioactive substances, explosives, or corrosive chemicals. Other possible uses include tracking moving objects, vehicle control, and human interaction with computers (for example, via a three-dimensional display of a computer model).

The controller, now in the design stage, allows six degrees of freedom: the translation of an object along x, y, and z axes and the rotation of the object in pitch, roll, and yaw (see figure). It can follow all the angles and positions the hand can assume in a cubic volume about 12 inches (30 centimeters) on a side, while the operator is seated at a table.

A gimbaled handgrip is mounted on a telescopic extension. As the user moves and turns the handgrip, the controller senses its position and orientation with built-in potentiometers and sends appropriate commands to

(continued on next page)

the remote manipulator. At the same time, built-in electric torque motors feed back a force proportional to the force exerted on the object. Cables link the joints to the back-force motors at the end of the telescope joint, through a counterbalanced takeup mechanism. The motors themselves serve as counterweights for balancing the handgrip.

The motors are modular and easily replaced. They furnish a back force of at least 2.2 pounds (9.8 newtons) and a torque of 70 ounce-inches (50 newton-centimeters) on each axis. Friction is low — less than 10 percent of back force or torque. Detailed parts drawings, cabling diagrams, and torque motor specifications have been prepared.

This work was done by John W. Hill and J. Kenneth Salisbury, Jr., of SRI International for **Ames Research Center.** *For further information, Circle 80 on the TSP Request Card.* ARC-11272

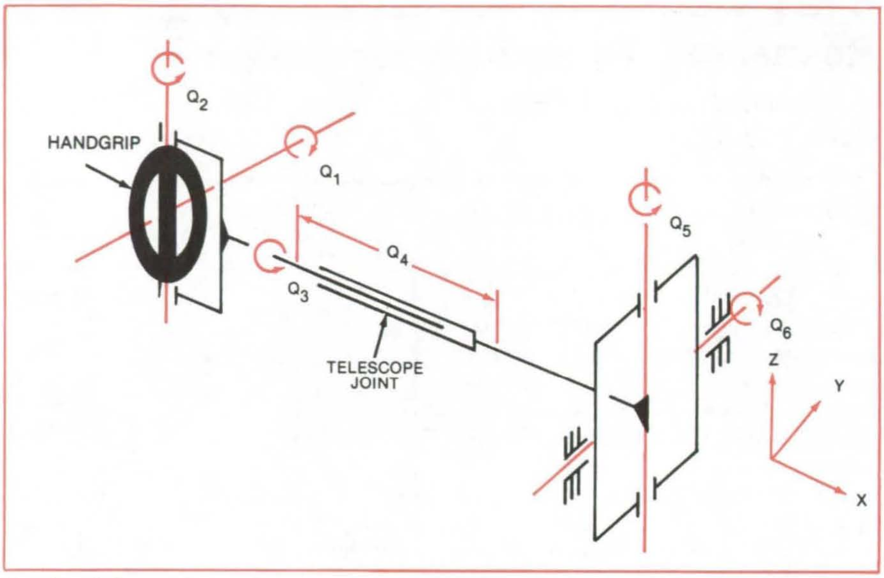

Feedback Controller employs a gimbaled handgrip and a telescope joint. Rotation of the handgrip (axes Q_1, Q_2, and Q_3) produces similar rotation of the manipulated object. Pushing or pulling the telescope joint (axis Q_4) moves the object in the x direction. Rotation of the telescope joint (axes Q_5 and Q_6) moves the object in the y and z directions.

Spraying Suspensions Uniformly

Nozzle contours suppress overspray while preventing suspension components from separating.

Marshall Space Flight Center, Alabama

Coarse, multi-ingredient suspensions can be sprayed on a surface smoothly, uniformly, and without overspray with the aid of a nozzle attachment for a commercial spray gun. The nozzle has been used to apply a protective coating to the aluminum and steel parts of the Space Shuttle rocket boosters, which are recovered from the ocean after they are used. The density of the ingredients in the spray liquid ranges from 0.64 to 1.08 g/cm^3.

In conventional spray nozzles, heavy particles become concentrated on the inside of the jet, and light particles form a fine mist on the outside of the jet. This fine mist drifts onto surface areas on which no spray coating is intended, causing an undesired overspray. As a result, the jet does not deposit a uniform layer on a surface. Removing the overspray can affect material properties, increase labor

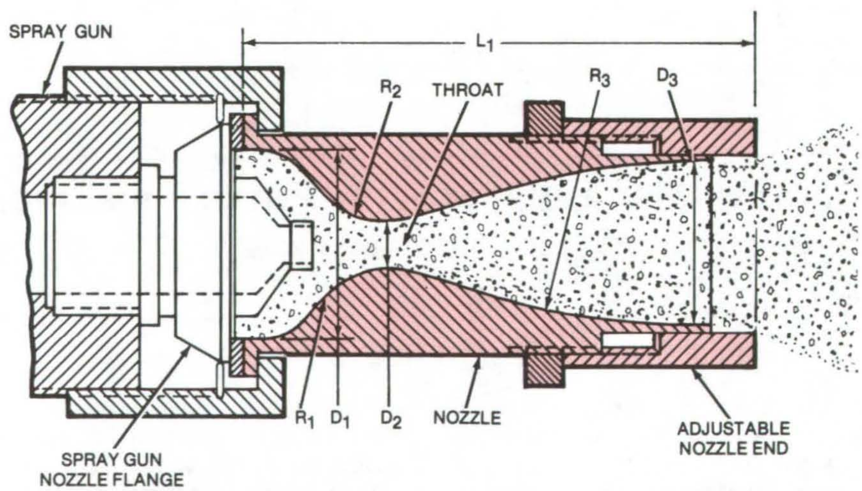

Smooth-Spraying Nozzle is attached to the conventional nozzle of a commercial spray gun. The gently curving contours within the attachment prevent the spray mixture from breaking up into low- and high-density components.

costs, and cause the debonding of subsequently sprayed layers.

The new nozzle attachment (see figure) is contoured internally to suppress overspray and to prevent the spray from segregating. From its conical inlet, the nozzle converges smoothly to a throat section, then diverges in a bell-shaped chamber that allows the suspension to flow uninterruptedly without building up turbulently in the nozzle. The end of the nozzle is adjustable and can be extended or retracted to avoid dripping when the inlet pressure, pump pressure, or density of the mixture changes slightly and to adjust for maximum smoothness on the deposited layer.

The shape and dimensions of the nozzle are critical. A smooth, homogeneous coating with good overspray control can be obtained with the following dimensions:

D_1 = 2.56 cm
D_2 = 0.64 cm
D_3 = 2.18 cm
R_1 = 0.64 cm
R_2 = 1.28 cm
R_3 = 7.95 cm
L_1 = 6.41 cm

A nozzle having a conical divergence chamber also deposits a homogeneous mixture. However, the deposit is not smooth and often requires hand sanding. The bell-shaped nozzle, in contrast, avoids the material waste and labor of finishing the coated surface. Furthermore, it can spray material continuously without stops for removing low-density edge deposits.

This work was done by Willibald P. Prasthofer of **Marshall Space Flight Center**. *For further information, Circle 81 on the TSP Request Card.*

This invention is owned by NASA, and a patent application has been filed. Inquiries concerning nonexclusive or exclusive license for its commercial development should be addressed to the Patent Counsel, Marshall Space Flight Center [see page A5]. Refer to MFS-25139.

Two-Headed Bolt

Machine bolt can be unscrewed from either end.

Marshall Space Flight Center, Alabama

With a head on each of its ends, a new bolt can be disengaged from its blind side. The bolt has a conventional hexagonal head on one end and a smaller hexagonal head on its threaded end (see figure). Since the reduced head is smaller than the bolt diameter, it does not interfere with insertion of the bolt shank in a bolthole. However, it can be turned by a wrench to release the bolt from its blind (threaded) end. The bolt should be tethered on its large-head end so that it does not drop away from the assembly.

The two-headed bolt makes it easier for mechanics to remove a Space Shuttle engine from its engine-handler adapter plate. Formerly, a mechanic had to lean over the edge of the adapter plate to reach the head of a conventional single-headed bolt. Now, the reduced head on the easily accessible side of the plate can be turned to disengage the bolt.

This work was done by G. W. Jeffers of Rockwell International Corp. for **Marshall Space Flight Center.** *No further documentation is available.*
MFS-19619

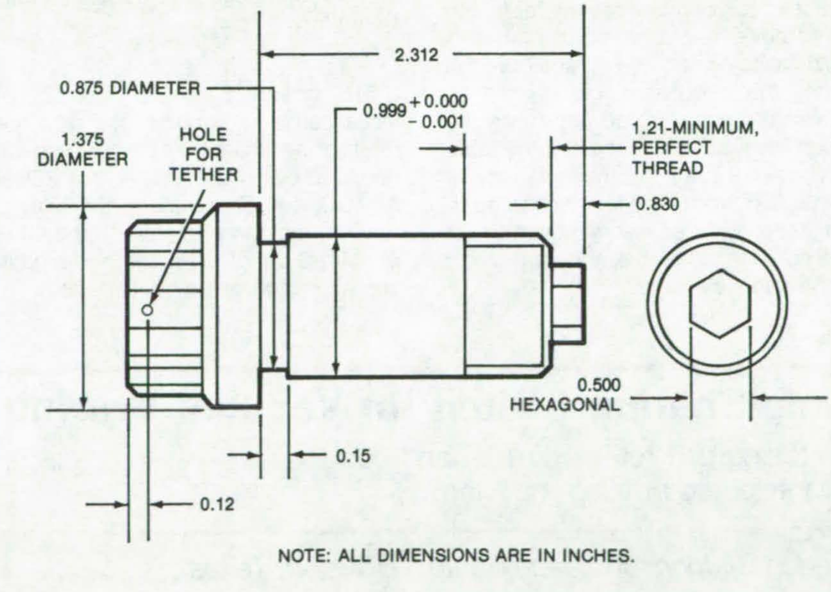

With a Conventional Head at One End and a smaller head at the other, this bolt can be unscrewed from either end. When it is unscrewed by the smaller head, a tether at the conventional head retains the bolt.

Compact Table-Tilting Mechanism

Optical components and other objects are oriented precisely by a simple motorized device.

NASA's Jet Propulsion Laboratory, Pasadena, California

A mechanism proposed for rotating a mirror through a precise angle aboard a spacecraft could have other applications in orienting, positioning, and alining equipment. Offering the advantages of compactness, simplicity, and low backlash, it can manipulate essentially any object that can be attached to a plane tilt table.

As shown in the figure, the device consists of a drive motor, a rotatable disk, a rigid link, and a table. The motor rotates about a vertical axis, and the motion is converted through the disk and rigid link to rotation of the table about a perpendicular axis.

When the motor is activated, the arm attached to the disk moves to the position shown in the illustration at the right of the figure. The bottom edge of the rigid link is carried with the arm. Since the top of the rigid link is attached to the table and the table can only move about a horizontal axis perpendicular to the plane of the paper, the top of the rigid link moves only in the plane of the paper. As the top of the rigid link descends, the table tilts down. Each of the attachment points A, B, and C is a low-friction bearing that allows free rotary movement of one of the joint components with respect to the other.

INPUT/OUTPUT RELATIONSHIP:

$$\mathrm{SIN}\,\frac{\beta}{2} = \frac{1}{2}\,\mathrm{TAN}\,\Theta - \sqrt{\mathrm{TAN}^2\,\Theta - \left(2\,\mathrm{SIN}\,\frac{a}{2}\right)^2}$$

a = INPUT MOTOR ROTATION
β = OUTPUT TABLE ROTATION
Θ = PIVOT-GEOMETRY ANGLE

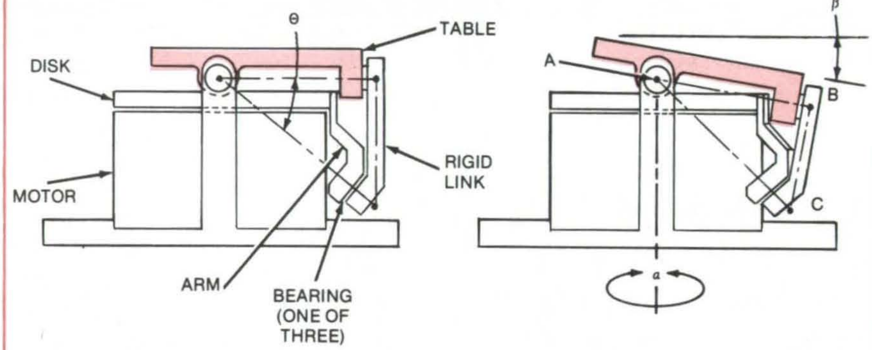

The **Table Is Tilted** from the horizontal plane in the illustration at the left to the orientation in the illustration at the right. The rotation of the motor about a vertical axis through point A is translated into rotation of the table about a horizontal axis through A.

The action of the device can be visualized as a rotation and displacement of an imaginary triangular plane bounded by pivot points A, B, C. Lines AB, BC, and CA lie along the axes of the bearings. In response to the lifting of point C out of the plane of the page, line AB rotates down about point A.

This work was done by Frank R. Mitchell of Frank R. Mitchell and Associates for **NASA's Jet Propulsion Laboratory.** *For further information, Circle 82 on the TSP Request Card.*
NPO-14800

Time-Sharing Switch for Vacuum Brazing

Switching unit routes current and coolant to a selected brazing machine.

Lyndon B. Johnson Space Center, Houston, Texas

A switching unit changes power and cooling-water connections between two vacuum-brazing machines. The switch allows both units to be powered by a single radio-frequency (RF) generator. One of the machines can be used for brazing while the bell jar of the other is being evacuated (a 20-minute process) in preparation for brazing or is being cooled after brazing (a 10-minute process).

The switch, as shown in the figure, eliminates manual interchange of power cables from each brazing machine at the RF generator. The manual interchange operation is not only time-consuming but potentially hazardous as well, since some cooling water is inevitably spilled and can cause arcing around the cable coupling.

The unit is linked to the RF generator by a coaxial cable and to each of the vacuum-brazing machines by two square-cross-section copper conductors. Temperature indicators on the unit allow the operator to monitor pyrometers in the vacuum bell jars. A separate control box controls the RF generator output.

Cooling water flows through the coaxial cable from the RF generator through a tee fitting in the switching unit. From the tee, it passes through a flexible dielectric tube, a check valve,

and one of the square copper tubes to the cooling coil on a bell jar. The water returns to the RF generator through a channel in the return square conductor, an on/off valve in the switching unit, and the coaxial cable.

The brazing-machine operator selects a machine for use by moving the switch handle to the left or right of its center position, thereby engaging the on/off valve so that water flows to the selected bell jar. At the same time, the handle completes the circuit for current from the RF generator to the selected bell jar. The current path is through a copper section on the handle, through the square copper conductors, the bell jar, and a jumper around the on/off water valve to the coaxial cable.

The square conductors offer greater surface area for the transmission of RF current than does the coaxial cable and allow the supply and return lines to be placed closer together so that power losses are minimized. Each tube is covered individually with insulating shrink tubing, and each pair of supply and return copper tubes is held together with another shrink tube.

For safety, an interlock cuts off RF power unless the bell jar is lowered, the switching-unit cover is in place, and the cooling water is flowing.

This work was done by John A. Stein of Rockwell International Corp. for **Johnson Space Center.** *For further information, including detailed engineering drawings, Circle 83 on the TSP Request Card.*
MSC-18600

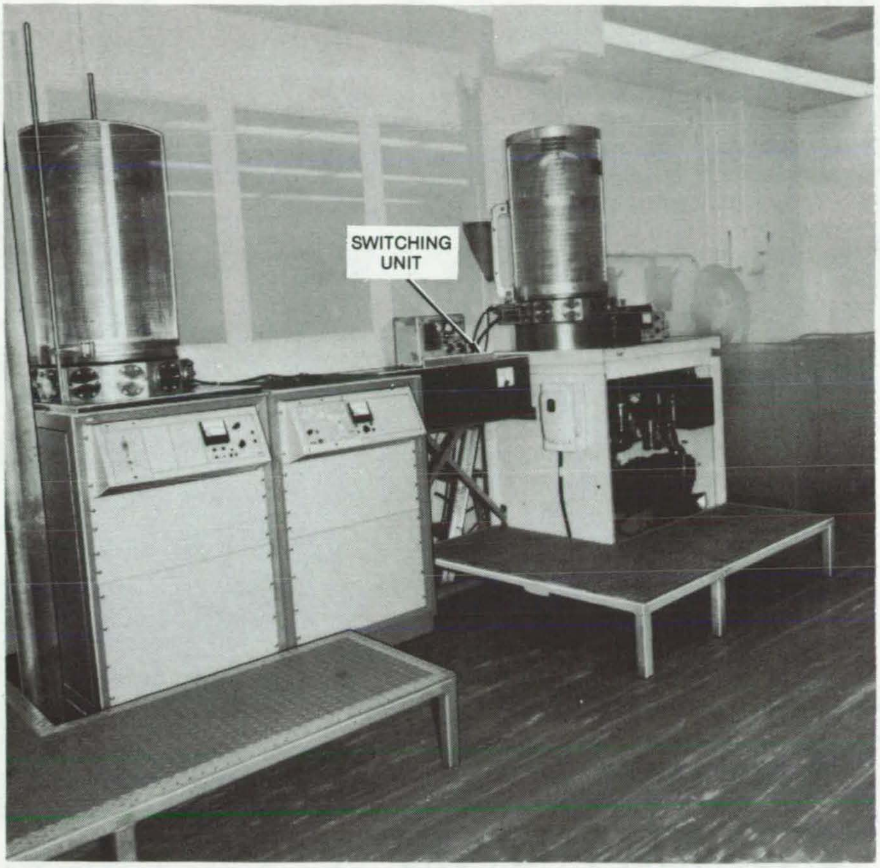

Switching Unit Sends RF Power and cooling water to either vacuum-brazing machine, depending on the position of the switch handle. Meters indicate the temperatures in the bell jars. The control box atop the switching unit controls the remote RF generator.

Limiting Current in Electron-Beam Welders

Mechanically adjustable separation between anode and cathode regulates maximum current.

Marshall Space Flight Center, Alabama

Damage to a workpiece by excessive current in an electron-beam welder is prevented by a mechanism that accurately adjusts the anode-to-cathode spacing. The mechanism is installed on a standard Sciaky (or equivalent) electron-beam gun with only minimal modification. By turning a knurled knob and observing a digital readout of anode/cathode separation, the machine operator adjusts the welder for a safe maximum current before welding begins.

The mechanism consists of an internally-threaded knurled adjustment barrel and an externally-threaded mating anode retainer (see figure). The adjustment barrel is press-fit in an acetyl copolymer roller bearing with nonmagnetic stainless-steel balls. The barrel is free to rotate clockwise or counterclockwise to move the anode retainer, and in turn the anode, toward and away from the cathode.

The electron-beam gun and cathode are rigidly mounted in a vacuum chamber, and the mechanism housing is attached to the lower part of the electron-beam gun. The anode retainer is fitted with either a standard or french anode and a focus coil. When the operator turns the adjustment barrel, the anode

(continued on next page)

and its retainer move up and down relative to the adjustment barrel. The anode motion is sensed by a linear voltage differential transformer and is displayed continuously as the distance between cathode and anode. Because the threads on the adjustment barrel and anode retainer are extra fine [40 threads per inch (16 threads per centimeter) on a 3-inch (7.6-cm) diameter], fine adjustment of the spacing is possible; one complete revolution of the barrel changes the spacing by only 0.025 inch (0.64 mm).

The anode retainer also holds an electron-beam focusing coil and a slipring, which provides an electrical contact for the anode. Tetrafluoroethylene vapor shields prevent gas from entering the vacuum chamber through the threads or bearing.

This work was done by Kirk W. Spiegel of Rockwell International Corp. for **Marshall Space Flight Center.** *No further documentation is available.*
MFS-19503

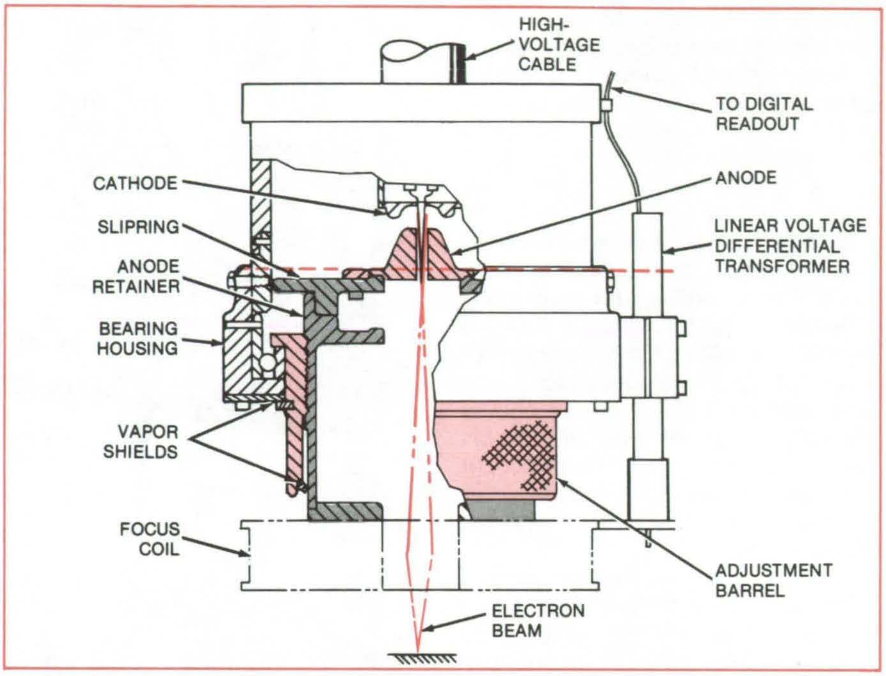

A Knurled Adjustment Barrel is turned to change the separation between anode and cathode and, thereby, alter the maximum electron-beam current. The section above the dashed line in this drawing is a standard electron-beam gun. The section below the dashed line is the new current-limiting mechanism. The shaded portion represents the anode-retainer assembly, which is moved vertically by rotation of the knurled barrel.

Torque-Wrench Extension

Tool made from two bevel gears and an extension shaft reaches difficult locations and allows accurate torque readings.

Lyndon B. Johnson Space Center, Houston, Texas

A novel torque-wrench extension makes it easy to install and remove fasteners that are beyond the reach of typical wrenches or are located in narrow spaces that prevent full travel of the wrench handle. At the same time the new tool allows the applied torque to be read accurately.

The figure shows a tool with an overall length of 28 inches (71 cm), although it could be scaled up or down in size for different applications. The drive system for torques up to 125 inch-pounds (14 N-m) uses two standard 1/4-inch (0.6-cm) drive-socket extensions in an aluminum frame that also holds a pair of 90° bevel gears.

The extensions are connected to one of the bevel gears, which turns the other bevel gear. The gears produce a 1:1 turns ratio through a 90° translation of the axis of rotation. The output bevel gear has a short extension that is used to attach a 1/4-inch drive socket.

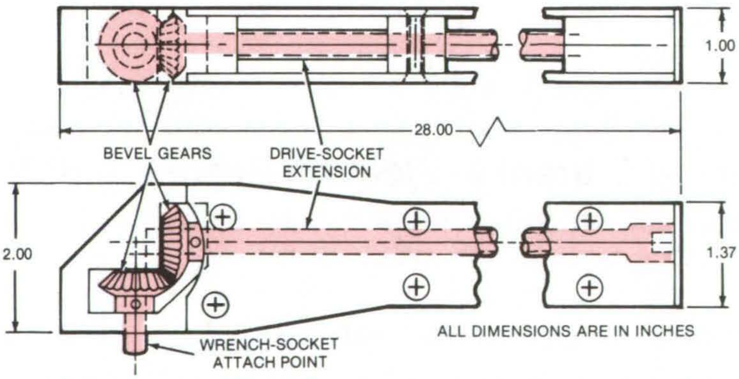

Drive-Socket Extensions and Bevel Gears are housed in the aluminum frame of a torque-wrench extension. The tool facilitates the installation and removal of fasteners that are difficult to reach. A short extension on one of the bevel gears is for the attachment of a wrench socket.

Some commercially available wrench extensions have a flexible shaft that can affect the accuracy of torque readings. The new design with bevel gears has a substantially-greater torque-drive range in addition to giving accurate readings. The torque-wrench extension should be useful in aircraft assembly and automated machine-equipment repair.

This work was done by David H. Peterson of Rockwell International Corp. for **Johnson Space Center.** *No further documentation is available.*
MSC-18769

Quick Mixing of Epoxy Components

In a proposed cartridge, the curing agent would be combined quickly and thoroughly with the base material.

Lyndon B. Johnson Space Center, Houston, Texas

Two materials would be mixed quickly, thoroughly, and in precise proportion by a proposed disposable cartridge. The cartridge would make it possible to mix components of fast-curing epoxy resins, with no mess, just before they are used. Developed to enable astronauts to mix epoxy for repairs in space, the cartridge would also be useful in the home and in industry for such jobs as caulking, sealing, and patching.

The materials (A and B) to be mixed are initially isolated within the cartridge by a cylindrical wall (see figure). The cylinder has vanes at one end and a handle at the opposite end. The vanes have holes through which material A, within the cylinder, can enter material B. To prevent premature mixing, the holes in the vanes are blocked by a gasket; the piston seals the cylinder at the other end.

To mix the materials, the handle on the cylinder is pulled, disengaging the vanes from the gasket. As the cylinder is pulled, material A extrudes through the holes in the vanes and into material B. The cylinder rides on a helically grooved shaft that rotates the vanes so that material A is homogeneously dispersed in material B in a single stroke of the piston. The shaft is rigidly attached to the cartridge by a diaphragm. Mixing would be easier for the user if the materials are formulated so that they are less viscous than usual.

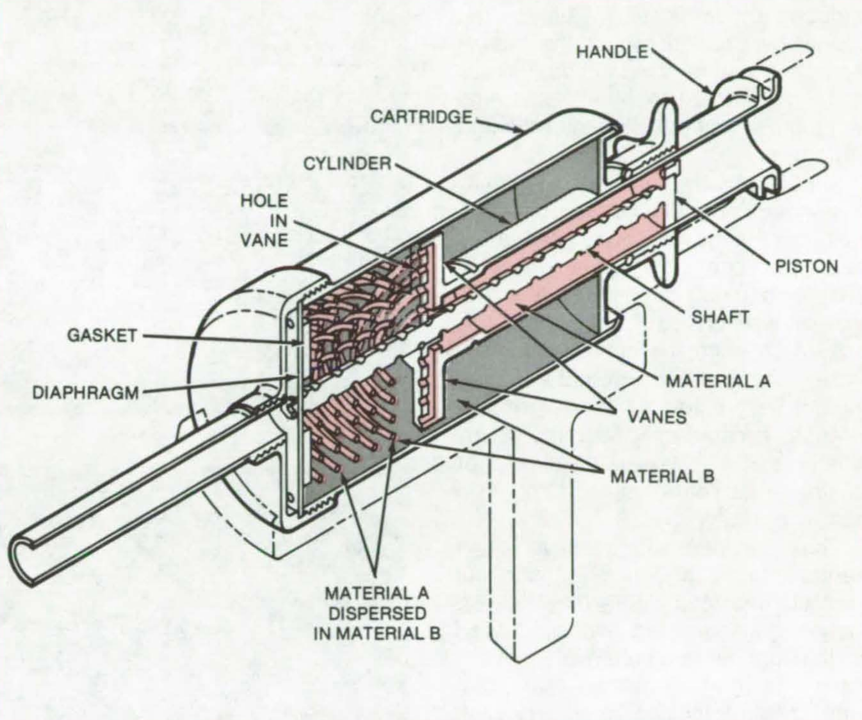

Material A is initially contained within the cylinder. When the handle on the cartridge is pulled back, materials A and B mix. The grooves on the shaft rotate the cylinder as it is pulled back so that the vanes rotate to extrude material A uniformly into material B.

Although mixer capsules have previously been available in which materials A and B are arranged in tandem, separated by a breakable diaphragm, repeated plunging or stirring is needed to ensure a homogeneous mixture. As many as 50 strokes of a plunger may be needed, whereas mixing and stirring would occur in one step with the proposed cartridge.

This work was done by David E. Dunlap, Jr., of McDonnell Douglas Corp. for **Johnson Space Center**. *No further documentation is available.*
MSC-18731

Cutting Holes in Fabric-Faced Panels

A new tool has two carbide inserts that bore clean holes through fibrous material with a knifelike slicing action. The cutting edge of the insert is curved, with a plane inner surface at a 30° angle to the tool axis. A drill press or a hand-held drill can be used to hold the cutting tool.
(See page 391.)

Contour-Measuring Tool for Composite Layups

A simple handtool helps to form contours and complex shapes from laminae of resin-impregnated fabric. The tool, which consists of a yoke having a ballpoint pen and a spindle and gage, is placed so that it straddles a model. As the tool is moved, the pen draws a constant-thickness locus that is used as a template.
(See page 383.)

Compliant Transducer Measures Artery Profile

An instrument consisting of compliant fingers with attached semiconductor pickups measures the inside contours of narrow vessels. The instrument, originally designed to monitor human arteries, is drawn through the vessel to allow the fingers to follow the contours. Lead wires transmit the electrical signals to external processing equipment.
(See page 337.)

Wrench for Smooth or Damaged Fasteners

Serrated tool removes fasteners that cannot be gripped by conventional wrenches.

Lyndon B. Johnson Space Center, Houston, Texas

A special wrench unscrews smooth-surfaced or damaged fasteners that cannot be gripped by a conventional wrench. It can be used in tight spaces and, in contrast to other tools and techniques, will not damage adjacent structures.

The new wrench was originally developed to remove commercial two-part nuts that have a round body and a hexagonal cap. The hexagonal section, needed only during installation so that a wrench can be applied, is broken off once the nut is tightened. Since the smooth round section cannot be gripped by a conventional wrench, it could only be removed by twisting with pliers, chiseling, or drilling — at some risk of damage to nearby parts.

The new wrench consists of a central handle and two independent jaws with serrated teeth (see figure). To use it, the serrated jaws are placed on the fastener to be removed, and the handle is rotated until its teeth grip with a positive locking action. Rotation of the wrench handle safely removes the fastener.

This work was done by Ray Carrillo of Rockwell International Corp. for **Johnson Space Center.** *No further documentation is available.*
MSC-18772

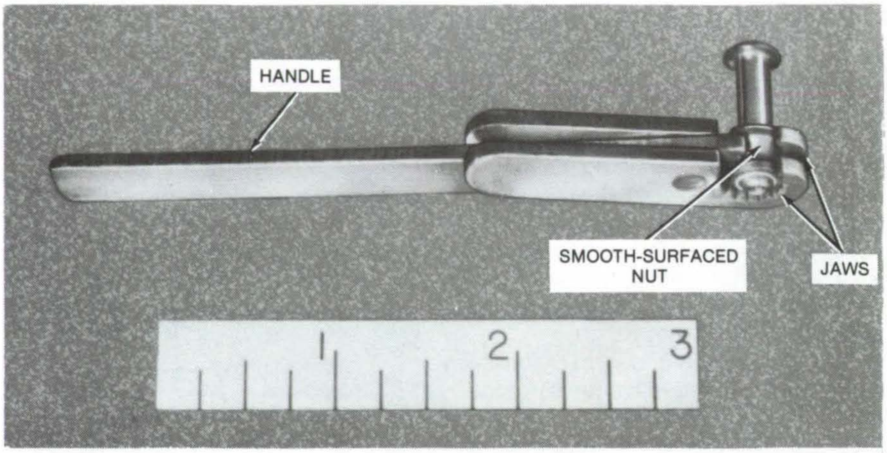

[a]

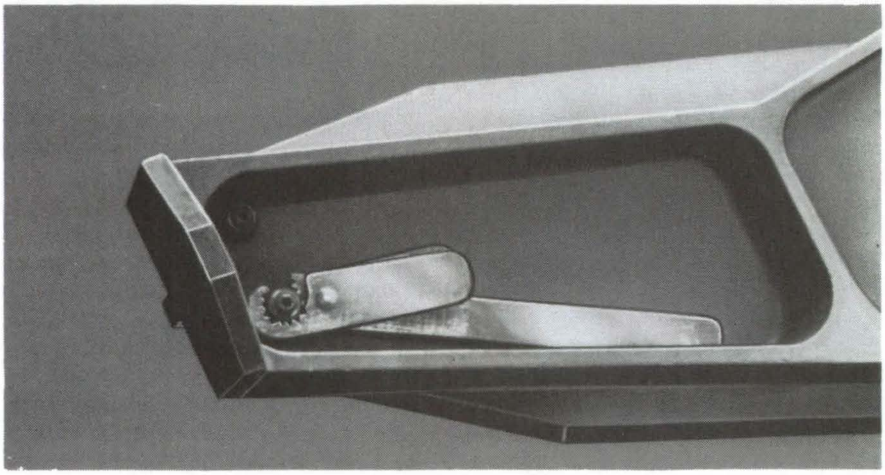

[b]

Three Sets of Teeth on the wrench clamp the smooth cylindrical surface of the nut in (a). The wrench is well suited for use in limited-access areas (b).

Fabrication Technology

Hardware, Techniques, and Processes

Books and Reports

Computer Programs

Contour-Measuring Tool for Composite Layups

Resin-impregnated fabric is marked for cutting with the help of a simple handtool.

Ames Research Center, Moffett Field, California

Contours and complex shapes are formed from laminae of resin-impregnated fabric, with the help of a simple handtool. In the layup technique, sheets of carbon-fiber-reinforced fabric composite are cut into shapes that, when stacked and cured, give the proper contour to the finished part. The new tool, which resembles a micrometer, is used to make paper templates prior to cutting the laminae.

A model of the part (for example, the propeller shown in the figure) is first sprayed with a thin coating of a contact adhesive. A thin sheet of paper is then placed over the model. Care is taken to eliminate bulges and wrinkles.

The contouring tool, which consists of a yoke having a ballpoint pen at one extremity and a spindle and gage at the other, is placed so that it straddles the model. With the gap between writing ball and spindle adjusted so that it is slightly less than the maximum thickness of the model, the tool is moved along a path that keeps the pen and the spindle in contact with the opposite surfaces of the model. The pen thus draws a line on the paper that represents a constant-thickness locus. The paper is peeled away from the model, and a layer of resin-impregnated fabric is cut to conform to the shape of the closed contour line.

Next, the thimble and sleeve on the micrometer gage are rotated to close the gap by an amount that corresponds to the thickness of a single layer in the laminated composite. A new sheet of paper is stuck on the model, and the tool is moved so that it draws a new constant-thickness contour. A ply of fabric is then cut to the new contour. The procedure is repeated until all the plies needed for the composite have been cut.

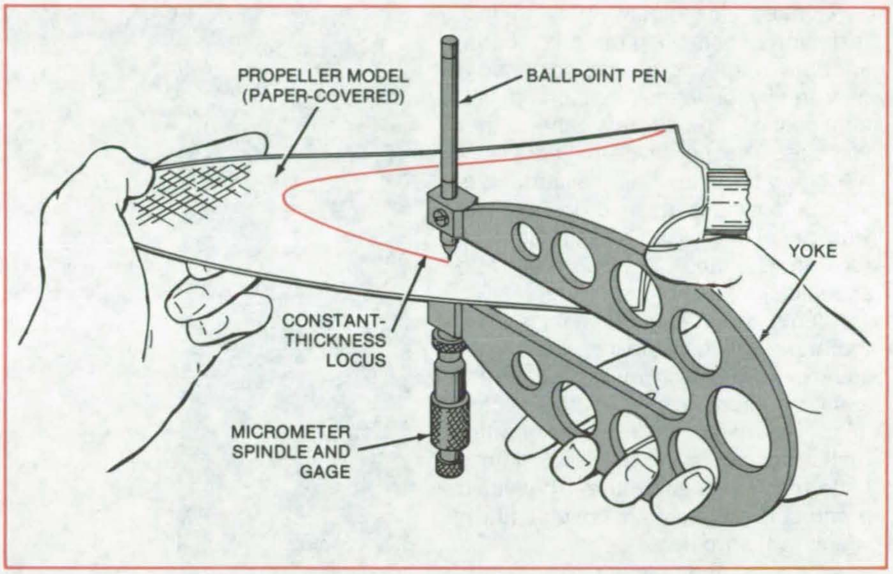

The User Moves the Handtool, scribing a locus of constant thickness on a paper-covered part (here, a propeller). The paper is then used as a template to cut a sheet of resin-impregnated fabric. Several such layers are stacked and cured to form a composite layup with the same shape as the original part.

The plies are assembled in the proper sequence in two half-molds and baked in vacuum bags at 250° F (121° C) for 1 hour. After the two halves have cooled, they are mated and heated so that they coalesce. Finally, the assembly is cured under controlled temperature and pressure in a mold having the exact dimensions required of the final part.

Even though the paper is not flat when a contour is drawn, but is flat when used as a template for a ply, there is enough "give" in the plies during curing to compensate for most distentions during patternmaking. If it is necessary to eliminate distentions completely, a pantograph can be used to transfer a contour from a paper while it is still on the model; or, the contour can be photographed from above and the negative enlarged to the correct scale.

Usually, the fabric will be oriented before each cut so that the fibers of adjacent layers make a 90° angle with each other. This alternating orientation increases strength and fracture resistance and ensures more uniform properties in all directions.

This work was done by Manuel J. Fontes of **Ames Research Center.** *For further information, Circle 84 on the TSP Request Card.*

This invention is owned by NASA, and a patent application has been filed. Inquiries concerning nonexclusive or exclusive license for its commercial development should be addressed to the Patent Counsel, Ames Research Center [see page A5]. Refer to ARC-11246.

A New Family of Fire-Resistant Foams

Polyimide-based foams have potential applications in the interiors of aircraft and other vehicles.

Lyndon B. Johnson Space Center, Houston, Texas

A need for lightweight, flame-resistant, nonsmoking materials in the interiors of spacecraft has spawned a new family of foams that could find applications in aircraft and other vehicles. The polyimide-based foams are being developed as resilient fillers for seat cushions, as rigid, low-density wall panels, as high-strength sheets for floors, and as thermal and acoustical insulation (see figure).

Foams of varying mechanical and thermal properties are prepared from liquid or powder polyimide precursors, some of which are mixed with selected fillers. Heating by microwaves or other method expands the precursor into a uniform cellular structure (the liquid precursor is dried to a powder first), which is then cured.

Aromatic and aliphatic diamines and tetracarboxylic acid dianhydrides are used as starting materials in preparing the precursors; the exact choices depend on the properties desired. For example, foams produced from heterocyclic aromatic/aliphatic diamines at high molecular ratios show good flexibility and compression set and are therefore good candidates for seat-cushion material; foams with various reinforcing fillers, such as carbon or glass, have potential as floor and wall materials; and glass fibers, glass microballoons, and other additives are combined with flexible foam precursors to produce thermal/acoustical insulation.

The many variables that affect foam properties have been examined during an extensive development program, with the objective of optimizing the process. Some significant developments, described in more detail in the articles that follow and in the reports cited at the end of this article, are:

- new terpolyimide precursors for use in seat-cushion foams;
- a continuous spray-drying process for producing large quantities of polyimide powder precursors;
- polyimide powder precursors mixed with conductive fillers are microwave foamed and cured in one step;
- constrained-rise microwave foaming has successfully produced rigid foams;
- the fire resistance of polyimide foams is significantly improved by adding ceramic fibers to the powder precursor; the foams produced from these mixtures are flexible and have good acoustical attenuation; and
- optimum foam compositions have been selected for each final product studied (seat-cushion material, wall material, floor material, thermal/acoustic insulation).

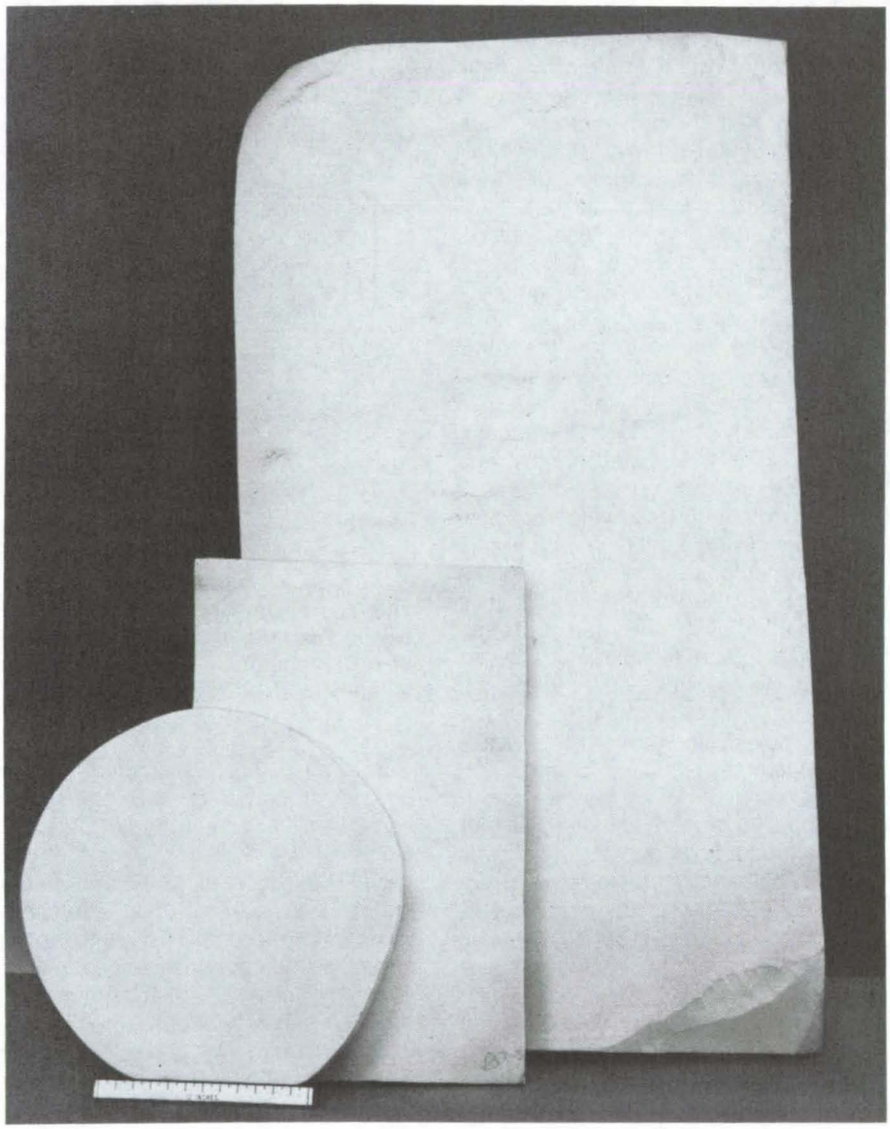

Finished Polyimide Foams such as these are prepared by heating a powder precursor in a 15-kW microwave oven. The large slab measures 160 by 89 by 18 cm. Final curing of the slabs was done in a conventional oven.

Early work on this fire-resistant-foam technology is reported in "Fire-Retardant Foams" (MSC-16222) on page 59 of *NASA Tech Briefs*, Vol. 3, No. 1.

This work was done by John Gagliani of International Harvester Co. for **Johnson Space Center.** *Further information may be found in:*

NASA CR-160576 [N80-22492/NSP], "Development of Fire-Resistant, Low Smoke Generating, Thermally Stable End Items for Commercial Aircraft and Spacecraft Using a Basic Polyimide Resin" [**$***11*]*, and*

NASA CR-151472 [N77-28301/NSP], "Development of Fire-Resistant, Low Smoke Generating Thermally Stable End Items for Aircraft and Spacecraft" [**$***10*].

Copies of these reports may be purchased [prepayment required] from the National Technical Information Service, Springfield, Virginia 22161.

Inquiries concerning rights for the commercial use of this invention should be addressed to the Patent Counsel, Johnson Space Center [see page A5]. Refer to MSC-16921.

Modified Fire-Resistant Foams for Seat Cushions

Aliphatic diamines improve the flexibility and resilience of polyimide foams.

Lyndon B. Johnson Space Center, Houston, Texas

Modified polyimide-polymer resins are the precursors for a new family of resilient fire-resistant foams (see preceding article). The terpolyimide foams containing long-chain aliphatic diamines withstand 50,000 cycles of compression under a 200-pound (890-N) load — an equivalent of 3 years of continuous use as seat-cushion filler.

Although terpolyimide resins usually increase the flexibility of polymers, this is not the case for totally-aromatic terpolyimide systems. When considered as possible seat-cushion material, foams derived from such terpolyimides do not meet minimum specifications for fatigue resistance or elasticity. In fact, the aromatic terpolyimide foams fail after less than 10,000 compression cycles, as do more-conventional copolyimide foams.

When the resin composition is modified by preparing terpolyimides with long-chain aliphatic diamines (see figure), the foam elastic properties improve markedly, although some flame resistance is lost. In trading off between flexibility and flame resistance, it is found that 0.2 mole of aliphatic diamine per mole of tetracid dianhydride give a good combination of properties. Foams produced from these precursors are flexible, do not burn, and meet fatigue requirements for seat-cushion material.

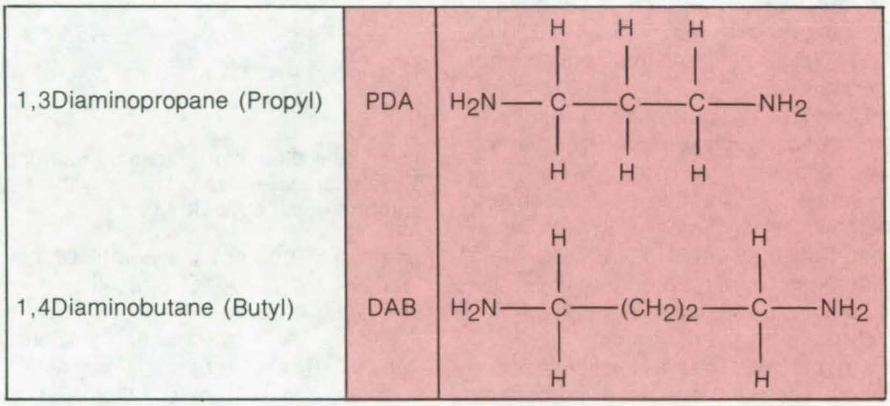

Aliphatic Diamines such as these are combined with aromatic diamines to form terpolyimide precursors for resilient fire-resistant foams. Precursors prepared at an aliphatic diamine ratio of 0.2 showed the best combination of mechanical and thermal properties.

This work was done by John Gagliani, Raymond Lee, Usman A. K. Sorathia, and Anthony L. Wilcoxson of International Harvester Co. for **Johnson Space Center.** *Further information may be found in:*

NASA CR-160576 [N80-22492/NSP], "Development of Fire-Resistant, Low Smoke Generating, Thermally Stable End Items for Commercial Aircraft and Spacecraft Using a Basic Polyimide Resin" [**$***11*]*, and*

NASA CR-151472 [N77-28301/NSP], "Development of Fire-Resistant, Low Smoke Generating, Thermally Stable End Items for Aircraft and Spacecraft" [**$***10*].

Copies of these reports may be purchased [prepayment required] from the National Technical Information Service, Springfield, Virginia 22161.

Inquiries concerning rights for the commercial use of this invention should be addressed to the Patent Counsel, Johnson Space Center [see page A5]. Refer to MSC-18704.

One-Step Microwave Foaming and Curing

Simpler process scales up fire-resistant foam slabs to production sizes.

Lyndon B. Johnson Space Center, Houston, Texas

A process that combines microwave foaming and curing of polyimide precursors in a single step produces fire-resistant foam slabs of much larger volume than has previously been possible (see figure). By adding selected conductive fillers to the powder precursors and by using a high-power microwave oven, foam slabs with dimensions in excess of 61 by 61 by 7.6 cm are made. Typical foaming and curing time is 35 minutes in a microwave oven with an additional 1- to 2-hour postcure in a conventional oven.

Previously, polyimide precursors without conductive fillers were foamed in a microwave oven at 5 kW for 3 to 6 minutes, then transferred to a conventional oven for curing. However, since the fragile uncured foam was often damaged during the transfer, this two-step process was not suitable for full-scale production runs.

In the new process a conductive filler, such as activated carbon or graphite, is mixed with the powder precursor. The filler heats up in the microwave field, transferring more energy to the charge than is possible for the powder precursor alone. The additional energy is directly related to the concentration of the conductive filler and can be controlled to foam and cure the charge in one step. Typical loading of the conductive filler is about 5 percent by weight of the total charge. (Also see the two preceding articles.)

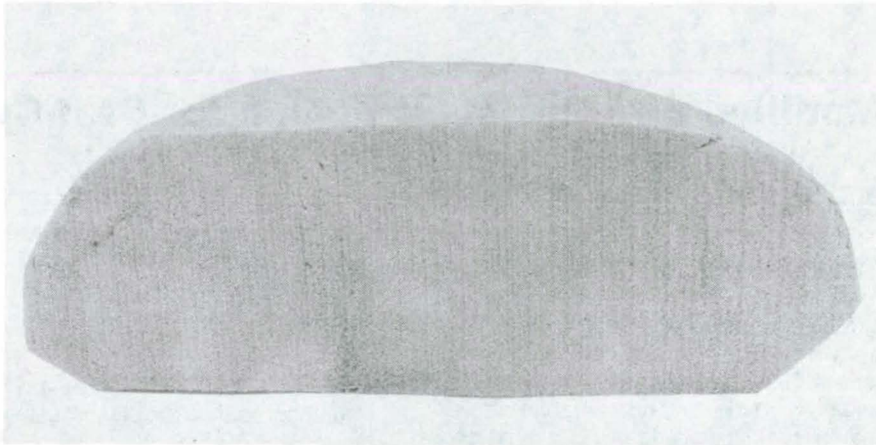

This Foam Slab is produced by foaming and curing 600 g of powder precursor in a 5-kW microwave oven. The polyimide precursor contained 5 percent by weight of graphite conductive filler.

This work was done by John Gagliani, Raymond Lee, Usman A. K. Sorathia, and Anthony L. Wilcoxson of International Harvester Co. for **Johnson Space Center.** *Further information may be found in:*

*NASA CR-160576 [N80-22492/NSP], "Development of Fire-Resistant, Low Smoke Generating, Thermally Stable End Items for Commercial Aircraft and Spacecraft Using a Basic Polyimide Resin" [**$**11], and*

*NASA CR-151472 [N77-28301/NSP], "Development of Fire-Resistant, Low Smoke Generating, Thermally Stable End Items for Aircraft and Spacecraft" [**$**10].*

Copies of these reports may be purchased [prepayment required] from the National Technical Information Service, Springfield, Virginia 22161.

Inquiries concerning rights for the commercial use of this invention should be addressed to the Patent Counsel, Johnson Space Center [see page A5]. Refer to MSC-18707.

Rigid Fire-Resistant Foams for Walls and Floors

Constrained-rise produces stronger foams than does compression.

Lyndon B. Johnson Space Center, Houston, Texas

Previous techniques for fabricating rigid fire-resistant polyimide foams by compressing an already-foamed precursor have been supplanted by a new one-step constrained-rise process. A precursor mixed with reinforcing fillers is placed between rigid substrates that constrain the expansion of the foam as it is heated by microwave energy. The process works for both liquid and powder precursors and can also be adapted to attach woven fiberglass skins at the same time as the precursor is being foamed.

Previously, rigid polyimide foams were produced by compounding fillers and fibers into a liquid or powder polyimide precursor, coating a substrate with the mixture, and drying it in a conventional oven at 120° to 130° F (49° to 71° C) for 6 to 8 hours. The dry

composition would then be heated at 500° to 600° F (260° to 315° C) to foam the polyimide resin. The foam, which has very irregular cellular structure, thickness, and flatness at this stage, is compressed at 500° to 550° F (260° to 290° C) and 5 to 50 psi ($34x10^3$ to $340x10^3$ N/m^2). When tested, such "rigid" foams were found to have poor compressive strength, since the cellular structure collapses in the press.

In the new process (see figure), the polyimide resin is spread on a substrate and dried in a microwave oven at a power of about 1.25 to 2.5 kW. The dried resin is placed between two rigid panels and is foamed at a power of 5 kW. Spacers between the substrates control the panel thickness. By eliminating the compression, this method prevents collapse of the cell structure and produces foams with higher compressive strength. (Also see the three preceding articles.)

This work was done by John Gagliani, Raymond Lee, Usman A. K. Sorathia, and Anthony L. Wilcoxson of International Harvester Co. for **Johnson Space Center.** *Further information may be found in:*

*NASA CR-160576 [N80-22492/NSP], "Development of Fire-Resistant, Low Smoke Generating, Thermally Stable End Items for Commercial Aircraft and Spacecraft Using a Basic Polyimide Resin" [**$11**], and*

*NASA CR-151472 [N77-28301/NSP], "Development of Fire-Resistant, Low Smoke Generating, Thermally Stable End Items for Aircraft and Spacecraft" [**$10**].*

Copies of these reports may be purchased [prepayment required] from the National Technical Information Service, Springfield, Virginia 22161.

Inquiries concerning rights for the commercial use of this invention should be addressed to the Patent Counsel, Johnson Space Center [see page A5]. Refer to MSC-18708.

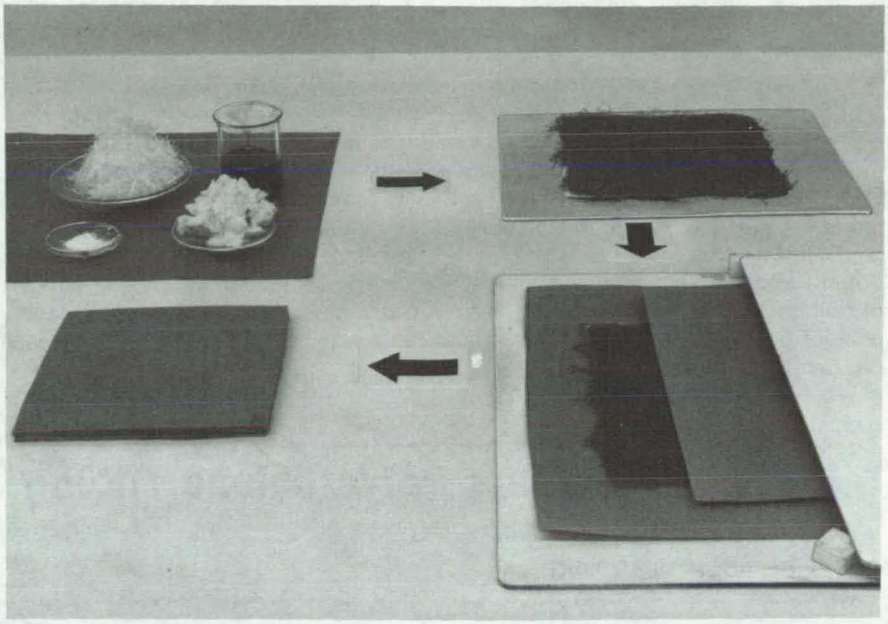

Steps in Fabricating a Rigid Foam Slab from liquid precursor are shown here. The precursor, containing rigidizing fibers and other additives (top left), is dried on a polytetrafluoroethylene-coated glass substrate (top right) and is then heated (by microwave energy) between two rigid sheets (bottom right). The completed slab is seen at the bottom, left.

Hot Forming Graphite/Polyimide Structures

Storable, stabilized preforms simplify fabrication.

Langley Research Center, Hampton, Virginia

Graphite/polyimide structures are generally fabricated by making the shaped structure out of graphite-fiber-reinforced polyimide prepreg. The shaped prepreg is then vacuum-bagged, staged in an oven or autoclave, rebagged, cured, and postcured. Most polyimide resins used for graphite/polyimide prepreg materials are chemically unstable and degrade when stored, which can significantly alter the processability of the material. In addition, the autoclave (or sometimes a captive environment press) can cause problems arising from vacuum bag systems, equipment control limitations, and layup movement.

A hot forming process has been developed in which structural shapes and panels are fabricated directly from stabilized graphite/polyimide preforms. The process can be used with thermosetting polymers that have a high-temperature melt phase just before final cure. This phase allows the fibers to move without destroying the matrix-to-fiber adhesion. It does not require such elaborate equipment as an autoclave or vacuum-augmented heated platen press. A heated platen press and simple matched metal tools are the only processing equipment required to mold the prestaged preforms into fully-cured graphite/polyimide shapes.

(continued on next page)

The first step is to assemble sheets of the prepreg in the desired orientation and thickness. These are staged in an air circulation oven under modest vacuum pressure and appropriate temperature to remove the free solvents and imidization byproducts. The flat preform is then placed in the mold cavity of the preheated tool and heated to the appropriate polymer "melt" temperature; then the tool is closed to shape the preform to the desired contour. The temperature of the tool is next increased to the cure temperature of the polymer and is held there until the structural shape is totally cured.

One of the key advantages of this process is that the prestaged preforms are very stable and do not require refrigerated storage. The flat shape of the preforms simplifies storage, which can be at ambient temperature for an indefinite time. The process lends itself to semiautomated or automated production of prestaged flat panels and has been successfully demonstrated in the manufacture of Celion 6000/PMR-15 and Celion 6000/LaRC-160 graphite/polymide structural sections.

This work was done by Robert M. Baucom of **Langley Research Center** *and Paul W. Kidder of LTV. No further documentation is available.*

Inquiries concerning rights for the commercial use of this invention should be addressed to the Patent Counsel, Langley Research Center *[see page A5]*. *Refer to LAR-12547.*

Method for Shaping Polyethylene Tubing

An insulated copper wire is inserted and bent, then heat is applied.

Lyndon B. Johnson Space Center, Houston, Texas

A new method forms polyethylene plastic tubing into configurations previously only possible with metal tubing. By using polyethylene in place of copper or stainless-steel tubing in low-pressure systems, fabrication costs are significantly reduced. The polyethylene tubing can be used wherever low-pressure tubing is needed in oil operations, aircraft and space applications, powerplants, and testing laboratories.

To shape the tubing, a tetrafluoroethylene-insulated stranded copper wire is inserted into it. When the tubing is bent to the desired shape, heat is applied with a 500° F (260° C) heat gun until the tubing is pliable to the touch. The heat gun is held about 12 inches (30 cm) from the tube. After about 3 minutes of cooling, the wire is removed, and the tubing retains its new shape. For ¼-inch (0.64-cm) tubing, for example, 12-gage stranded wire is used.

A pneumatic power supply using polyethylene tubing formed by this method is shown in the figure. After the tube is shaped, the end is heated and pressed on a 37° cone so that it will fit on a standard B-nut.

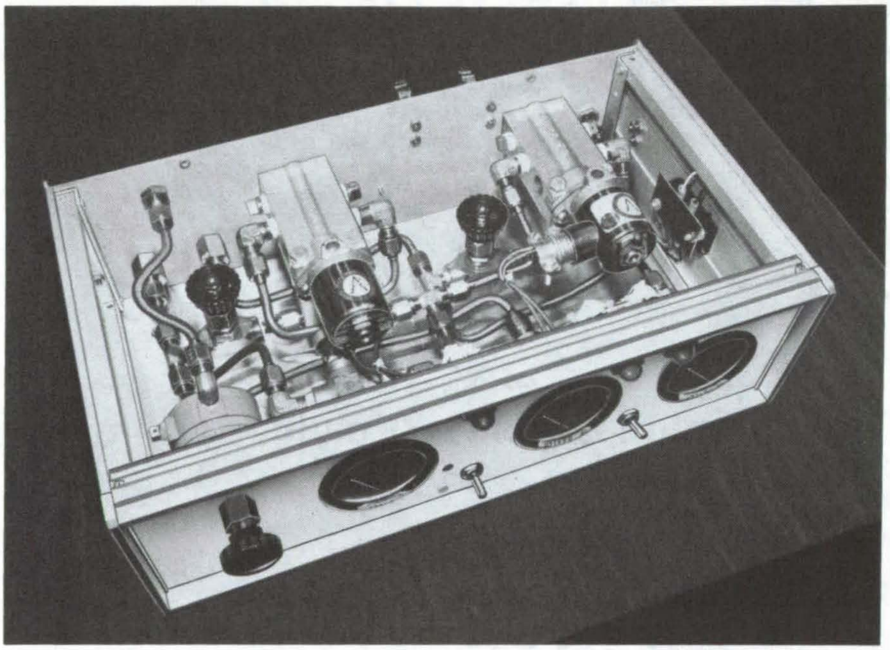

Shaped Polyethylene Tubing is used in this pneumatic power supply to minimize its weight and size. The bends in the tubing were formed by inserting a tetrafluoroethylene-insulated stranded copper wire and then applying heat until the tubing becomes pliable. Upon cooling, the tubing retains its shape.

Previously, polyethylene tubing was conventionally used in simple shapes. Special plastic fittings were needed to provide bends between straight tubing sections. Otherwise, only large-radius bends were allowed, to avoid collapsing the tubing walls.

This work was done by Ralph C. Kramer of Rockwell International Corp. for **Johnson Space Center**. *No further documentation is available.*
MSC-18771

Alining Sleeve for Optical Fibers

Loss at a butt joint of two light-guide sections is only 0.3 dB when the fibers are slipped into a molded resin sleeve.

Lyndon B. Johnson Space Center, Houston, Texas

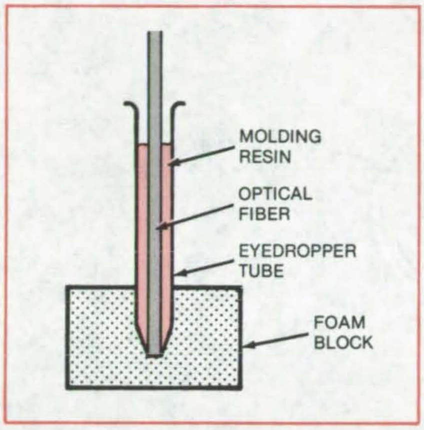

A **Sleeve is Formed** by letting resin set around a length of optical fiber that is used as a mandrel. The mandrel is removed while the resin is still slightly gellike; the sleeve is removed from its glass-eyedropper mold when completely hardened. A typical fiber length, in tests, was 5 inches (13 cm).

A sleeve for alining two optical fibers is made with precisely the correct inside diameter by using a section of the fiber as a mandrel. Because optical fiber is manufactured to very close tolerances, the diameter of the section serving as the mandrel will be the same as the diameters of the two fibers that are mated in a butt joint inside the sleeve. The result, determined by experiments, is a loss of no more than 0.3 dB at the joint.

The sleeve can be made in an eyedropper as shown in the figure. The glass tube of the eyedropper is inserted into a block of polystyrene foam to hold it vertically and to block the small end. A selected resin (a polyester, for example) mixed with its catalyst is poured into the vertical eyedropper, and then a length of the optical fiber (cleaned of its sizing with acetone or other solvent and coated with mold release) is inserted into the resin. After the resin has set to a strong gel (i.e., when it is no longer a liquid), the fiber is removed. Upon completing curing, the resin is removed from the eyedropper cylinder.

The required lengths can be cut from the resin cylinder and shaped and polished if desired. The sleeve may be used for a temporary field splice or even for a permanent joint.

This work was done by Kenneth L. Austin of Lockheed Electronics Co., Inc., for **Johnson Space Center**. *No further documentation is available.*
MSC-18756

Film Coatings for Contoured Surfaces

Spray process leaves thin-film coatings on convoluted surfaces.

Lyndon B. Johnson Space Center, Houston, Texas

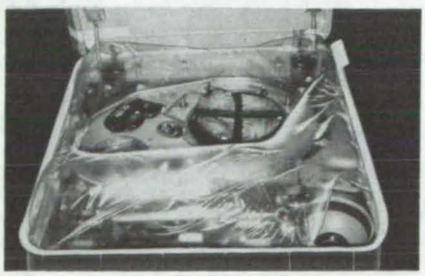

Contoured Fluorocarbon Film of uniform strength and thickness was spray-formed to cover the external tank umbilical cavity on the Space Shuttle.

The thickness of fluorocarbon elastomer films applied to contoured or convoluted shapes by vacuum forming is difficult to control at sharply curved areas. If the film is too thin in these regions, it may fail under applied pressure.

A process for spraying contoured fluorocarbon elastomer films of uniform strength and thickness has been used instead of vacuum forming to fabricate a curtain covering the external tank of the Space Shuttle (see figure). A solution of KEL-F-800 (or equivalent) fluorocarbon elastomer resin, dissolved in a ketone or other suitable solvent, is sprayed over a contoured form or mandrel. Conventional spray equipment may be used, and thicknesses are controlled to 0.003 ± 0.0005 in. (0.008 ± 0.001 mm).

While still on the mold, the film is air-dried by heating at 425° F (218° C) for 30 minutes. Two molds are used, each fabricating half of the curtain. The dried film is then placed on an assembly fixture to trim the periphery.

A rubber bead, installed along the perimeter of the film, is held in place by Kapton (or equivalent) tape. Polytetrafluoroethylene tape holds the two halves of the curtain together.

This work was done by Henry E. Flanery, Roger K. Frost, and Arnold J. Olson of Rockwell International Corp. for **Johnson Space Center**. *No further documentation is available.*
MSC-18784

Kilovolt Vacuum Feedthrough Is Less Noisy

Electrical feedthrough has low capacitance
and low microphonic sensitivity.

NASA's Jet Propulsion Laboratory, Pasadena, California

A new electrical feedthrough connects both low-voltage and high-voltage signals between a cryogenic environment and the "outside world." Developed for a cooled germanium gamma-ray detector, the feedthrough has especially low capacitance and low sensitivity to microphonic noise. Its high-voltage lead is free of corona discharge and electrical breakdown to at least 5 kV.

As shown in the figure, the new feedthrough has two high-thermal-resistance leads, one for high voltage and one for low voltage. Each lead is supported by four insulating disks and an insulating rod (for the low-voltage lead) or an insulating tube (for the high-voltage lead). When the feedthrough is installed, the disks rest in alined holes in the parallel walls of the cooler. They are then epoxied in place to form vacuum-tight seals.

In the low-voltage lead, microphonic sensitivity is reduced by the disks and the insulating rod supporting the thin wire. The rod prevents vibration without seriously increasing the capacitance.

In the high-voltage lead, the conductor is shielded by a guard electrode, which is connected to the same voltage to prevent corona discharge and electrical breakdown. The guard electrode is a thin vapor-deposited coating on the inside surface of the insulating tube. The coating is thin enough to avoid increasing thermal conductance appreciably but thick enough to offer electrical continuity.

The strongest electric field in the vicinity of the high-voltage electrode occurs in the wall of the insulating tube; but even at 5 kV, the field is less than half the breakdown strength of the insulator. As in the low-voltage electrode, the stiff insulating tube and the disks prevent vibration and microphonic noise, and the small inner diameter and thin wall keep the capacitance low.

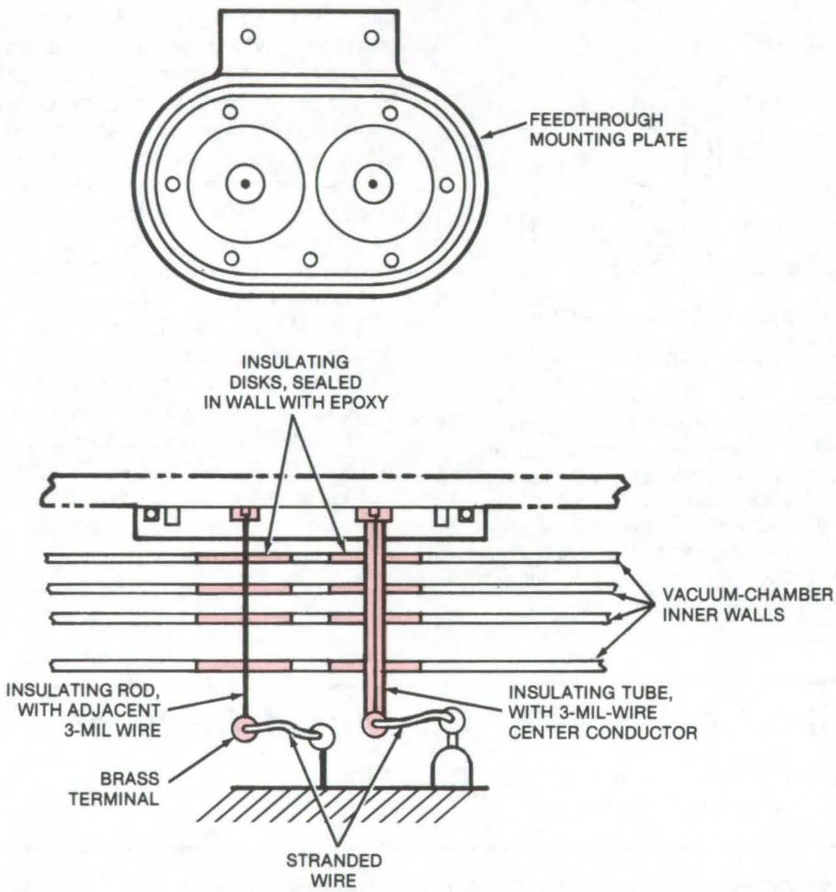

Cryogenic Electrical Feedthrough has two leads. The one on the left is for low-voltage signals; the one at the right is for high voltage (up to 5 kV). Electrical connections are soft-soldered to the terminals at the bottom of the figure. The conductors are 3 mils (7.6 μm) in diameter.

This work was done by Larry D. Howell of IT&T Corp. for **NASA's Jet Propulsion Laboratory**. *For further information, Circle 85 on the TSP Request Card.*
NPO-14802

Cutting Holes in Fabric-Faced Panels

A carbide cutter splices, rather than snags, fibrous material.

Lyndon B. Johnson Space Center, Houston, Texas

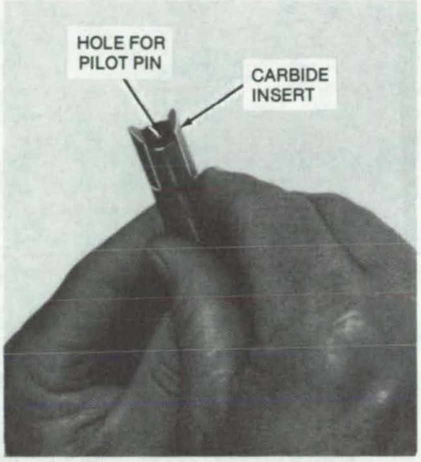

Carbide Inserts on the Cylindrical Tool have curved edges that cut cleanly through fibrous material. The outside diameter of the tool is ground to the required hole diameter. An existing model bores holes 0.561 in. (1.425 cm) in diameter; it is alined with a pilot pin 0.187 in. (4.75 mm) in diameter.

A new tool (see figure) has two carbide inserts that bore through fibrous material with a knifelike slicing action. The tool cuts clean holes in aramid fabric-faced sandwich panels and should be effective for other fabric- or fibrous-faced materials.

Conventional hole cutters have one or more teeth that can snag surface fibers rather than cut them cleanly. In contrast, the carbide inserts in the new boring tool cut like knives, pressing down on the fibers as they slice through them.

The cutting edge of the insert is curved, with a plane inner surface at a 30° angle to the tool axis. To aline the cutter perpendicularly to the work, a pilot pin or guide plate may be used. For a pilot pin, an axial hole is drilled in the body of the cutter.

The cutter can be placed in a drill press or a hand-held drill. To assure a clean hole on both sides of the panel, a backup plate may be required, or the hole can be cut about half way through from each side.

Previously, it took about 1 hour using a grinding jig to bore a clean hole through an aramid sandwich panel used in the Space Shuttle orbiter. It takes about 3 minutes to bore the hole using the new tool in a hand-held drill motor.

This work was done by Scott A. Peterson of Rockwell International Corp. for **Johnson Space Center.** *No further documentation is available.*
MSC-18786

Sealing Micropores in Thin Castings

A surface pretreatment produces hermetically sealed aluminum chassis.

Lyndon B. Johnson Space Center, Houston, Texas

Microscopic pores in thin-walled aluminum castings are sealed by an impregnation pretreatment. The pretreatment was developed for investment castings used in hermetically sealed chassis for electronic circuitry (see figure). Excessively high leakage rates were previously measured in some chassis.

The aluminum chassis are impregnated with a resin that fills the pores in the metal so that it can contain a pressurized gas. With the pretreatment, leakage is reduced below 1×10^{-4} atm-cm^3/s. The principle of the pretreatment is to open the micropores to accept more resin and to control the resin viscosity for maximum penetration.

(continued on next page)

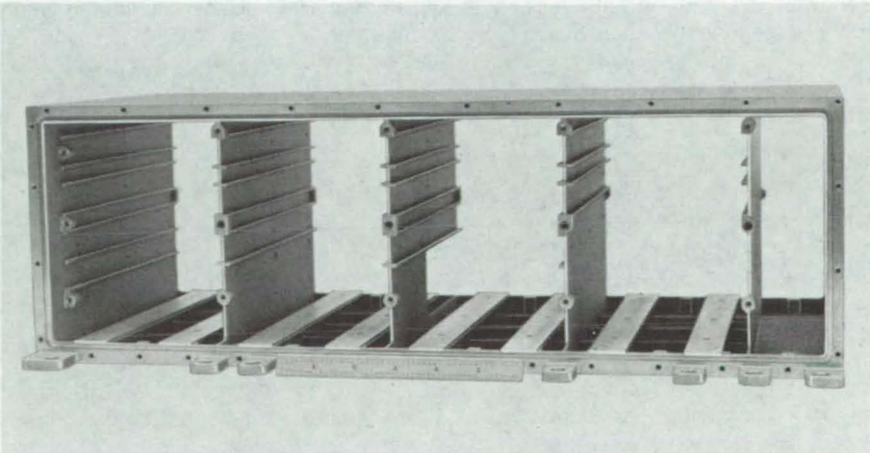

Aluminum Investment Castings like this one hold electronic circuit boards in space vehicles and aircraft. When the openings are sealed with cover plates and electrical connectors, the cast-aluminum chassis is leaktight.

The machined investment casting is first chemically etched in a solution of nitric acid and Actane 70 (or equivalent). With a solution temperature of 20° to 30° C and an immersion time of 3 to 5 minutes, 0.0001 to 0.0006 inch (0.0025 to 0.015 mm) of material are removed from the surfaces of the casting. This amount is small enough to keep the part within dimensional tolerance for most applications, but it is large enough to expose micropores that might have been smeared over by sandblasting and machining.

Next the casting is preheated to 65° C to expand the micropores. The impregnant resin is diluted so that its viscosity measures 15 seconds in a No. 4 Zahn cup. This value of viscosity ensures that the resin permeates deeply into the micropores. The resin impregnated casting is cured at 135° C for 45 minutes.

This work was done by George A. Mersereau, George O. Nitzschke, Hal L. Ochs, and Frank S. Sutch of Honeywell Inc. for **Johnson Space Center.** *For further information, Circle 86 on the TSP Request Card.*
MSC-18623

Lightweight Terminal Board

Sandwich construction reduces cost and weight.

Lyndon B. Johnson Space Center, Houston, Texas

A new sandwich construction for terminal boards reduces fabrication time and produces thinner boards that have better insulation consistency, better appearance, and less weight. The new method also permits closer spacing of the terminal posts.

As the figure shows, the previous fabrication started with a thick (0.12-inch, or 3.0-mm) polyimide board. Slots were end-milled to a controlled depth, holes were drilled, and the terminal posts were inserted. After the "upset" ends of the posts were expanded, the slot was filled with epoxy for insulation.

The new method starts with a thin (0.031-inch, or 0.8-mm) sheet of polyimide and consists of drilling, inserting the terminal posts, upsetting the ends, and then bonding a second sheet to the upset side as a continuous insulation member. The resulting sandwich is lighter and much cheaper to fabricate than the single board.

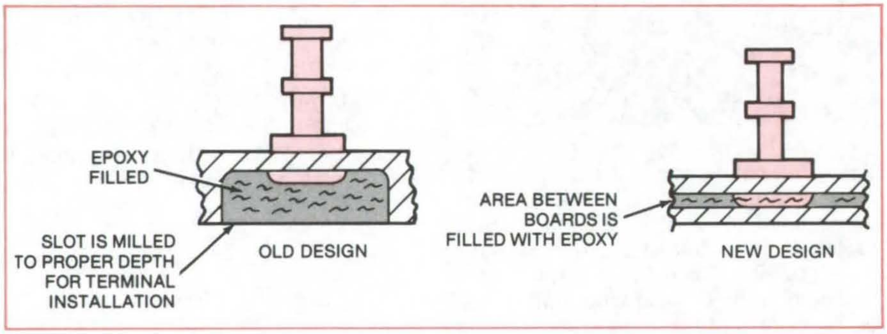

The **Old and New Methods** for making terminal boards are shown here. In the old method (left), slots are end-milled in a thick board; after the posts are mounted, the slot is filled with epoxy. In the new technique (right), the posts are mounted on a thin sheet, and then a second sheet is epoxied to the upset side. The result is a lighter, cheaper product.

Thirty boards made by the new method saved an estimated 8 pounds (4 kg) in the weight of the Space Shuttle orbiter. Further reduction in size and weight is possible, because the elimination of slot milling allows terminal rows to be installed closer together.

This work was done by James D. Drechsler and Harry G. Eaton of Rockwell International Corp. for **Johnson Space Center.** *No further documentation is available.*
MSC-18787

A Construction Technique for Wind-Tunnel Models

High strength, good surface finish, and corrosion resistance are imparted to miniature wind-tunnel models by machining the pressure channels as an integral part of the model. The pattern for pressure channels is scribed, machined, or photoetched before the channels are drilled. The mating surfaces for the channels are flashed and then diffusion-brazed together.
(See page 350.)

Cooling/Grounding Mount for Hybrid Circuits

Extremely-short input and output connections, adequate grounding, and efficient heat removal for hybrid integrated circuits are possible with a new mounting. A rectangular clamp holds the hybrid on a printed-circuit board, in contact with a heat-conductive ground plane. The clamp is attached to the ground plane by bolts.
(See page 274.)

Reshaping Tube Ends for Welding

Tube ends are rounded in preparation for welding by a new semiautomatic tool. Tubes that have been trimmed close to a bend may be deformed by the process. To restore roundness, the out-of-round tube is opened, a plug is inserted, and a crimper compresses the tube into proper shape around the plug.
(See page 373.)

Transistor Package for High-Pressure Applications

With an alumina disk brazed to cap and terminals, a TO63 transistor package can withstand 200 psi.

Lyndon B. Johnson Space Center, Houston, Texas

A TO63 transistor package can operate in hydraulic oil at pressures of 200 psi (1.4×10^6 N/m^2) or greater without leakage failure if it is reinforced by an alumina disk brazed to the cap and terminals. This inexpensive modification has been used successfully on power transistors in hydraulic circulating-pump assemblies for the Space Shuttle orbiter and should be effective in other pressurized environments, such as in oil exploration equipment. The modified package has been proof-tested at 500 psi (3.5×10^6 N/m^2).

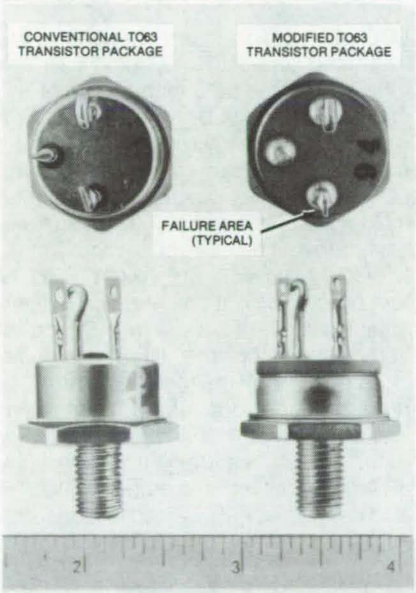

Figure 1. **Modification of a TO63 Transistor Package,** by brazing an alumina disk to the cap and terminals, prevents leaks at the terminals under high pressures.

The TO63 is a stud-mounted transistor package with three terminals emerging through the top cap (see Figure 1). When submerged in oil under high pressure, it was subject to failure at the base of the terminals where they enter the cap.

The alumina disk is added to the cap when the transistor is manufactured. As a preparatory step, molybdenum/manganese alloy is metal-screened (a process similar to silk screening) onto the areas to be brazed (see Figure 2). The disk is then heat-treated by raising its temperature to 1,300° C over 30 to 60 minutes, holding it at that temperature for 15 minutes, and then cooling it back to ambient temperature over another 30- to 60-minute period.

The three terminals are inserted through the holes in the disk and then brazed to the molybdenum/manganese pads. Following this, the disk with terminals is brazed to the transistor cap. For this step, a ring of preformed BT braze alloy that matches the screened area on the disk is used. This brazing operation is done over the same time cycle as in the preparatory step, but the temperature is held at 1,050° C, rather than 1,300° C. The modified cap is then ready for standard transistor assembly.

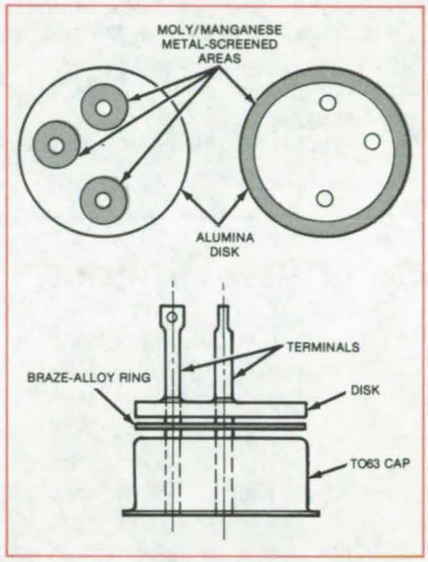

Figure 2. The **Brazing Process** begins (top) when molybdenum/manganese pads are metal-screened around the terminal holes on one side of the alumina disk and around the perimeter of the disk on the reverse side. After a heat treatment, the disk is brazed to the transistor cap, using a preformed braze-alloy ring (bottom).

This work was done by Peter J. Zantos of Rockwell International Corp. for **Johnson Space Center.** *No further documentation is available.*
MSC-18743

Books and Reports

These reports, studies, and handbooks are available from NASA as Technical Support Packages (TSP's) when a Request Card number is cited; otherwise they are available from the National Technical Information Service.

Automatic Chemical Vapor Deposition

Characteristics of the process and equipment are detailed.

A report reviews chemical vapor deposition (CVD) for processing integrated circuits and describes a fully automatic machine for CVD. In chemical vapor deposition, gases react next to the surface of a wafer (silicon, sapphire, or spinel, for example) and form a thin layer of solid material on the wafer. In integrated-circuit manufacturing, CVD is sometimes favored over such other methods as the thermal oxidation of silicon substrates or the deposition of evaporated materials. This is primarily because CVD proceeds at a relatively low temperature, allows a wide choice of film compositions (including graded or abruptly

(continued on next page)

changing compositions), and deposits uniform films of controllable thickness at a fairly high growth rate.

The report surveys CVD techniques for "glassing" chips — that is, for coating integrated-circuit chips with an impermeable protective layer of glass. Glasses composed of silicon dioxide, borosilicates, aluminosilicates, phosphosilicates, and laminates of these materials are considered. Methods of densifying glass films are reviewed, and appropriate substrate materials are surveyed.

The report also deals with CVD for applying insulating, conducting, and semiconducting films — that is, films that form part of the functional structure of an integrated circuit, in contrast to glass films, which are primarily protective.

The automatic CVD machine covered in the report is a continuous system under computer control. It automatically loads 3-inch (7.6-cm) substrates in a "boat," deposits a film on them, and unloads the substrates. Some of the preliminary considerations that go into the design of an automatic CVD machine are described in the report, though details of the system subcomponents are not included. The report gives an overview of hardware, reactants, and temperature ranges used with the CVD machine.

This work was done by Bobby W. Kennedy of **Marshall Space Flight Center**. *To obtain a copy of the report, "Chemical Vapor Deposition for Automatic Processing of Integrated Circuits," Circle 87 on the TSP Request Card.*
MFS-25459

Computer Programs

These programs may be obtained at very reasonable cost from COSMIC, a facility sponsored by NASA to make new programs available to the public. For information on program price, size, and availability, circle the reference letter on the COSMIC Request Card in this issue.

CADAT Logic Simulation Program

Program checks logic functional correctness, accounting for realistic propagation delays.

The CADAT Logic Simulation Program (LOGSIM) checks the functional correctness of an electronic logic circuit by simulating the circuit at the logic gate level. LOGSIM also checks the propagation delay through the logic nets and indicates any timing or "race" problems.

LOGSIM simulates very large logic networks within a modest amount of computer core memory. The program has an internal library of 15 logic elements, to which the user may add new elements by simply defining their operation. In addition, the user can define complex logic functions in terms of read-only memories, each with up to 15 inputs.

LOGSIM is divided into three phases: the preprocessor, the simulator, and the postprocessor. Each phase can run independently or in a stream. The preprocessor validates the input data and sends diagnostic messages whenever necessary. It also generates a connectivity list showing each gate and its loads, to aid the user in determining that the input data describe the circuit intended. The preprocessor also prepares a circuit data file for use by the simulator.

The simulator first establishes the initial levels of each of the logic elements. Next, the user-specified input signals are propagated through the circuit. Specified level changes are entered into an element status table. Each element loaded by the changed signals is then examined to determine if its output is changed. Appropriate logic delay and decay times are added to the current time to find the times at which future events are to be scheduled. When all loads have been examined, the current time is advanced to that of the next scheduled event, and the process is repeated. As the new levels of each scheduled event are entered in the element status table, the event is also recorded on tape for input to the postprocessor.

The postprocessor reads the list of input circuit element names and the initial conditions and prints a list of the output signals. A timing diagram may be printed with the initial condition of each element or a list of all initial conditions. Logic events are read from the simulator data tape, and the status of the user-selected elements is printed for each time within the specified interval at which an event occurs. The postprocessor is controlled by user directives and can generate any number of timing diagrams in any user-specified format during a single run.

For logic circuitry to be simulated on an ideal binary-valued basis, a relationship must be established between the ideal low and high levels and the realistic delayed level transitions. The LOGSIM approach is to establish the switching time as the time when the gate output reaches nine-tenths of the maximum change between levels. The rise and fall delay times are supplied by the user for each circuit element. Thus, LOGSIM simulates such occurrences as logic fall decay of an MOS transmission gate and a logic spike condition.

LOGSIM is written in FORTRAN IV for batch execution and has been implemented on a Xerox Sigma V computer using the CP-5 operating system. Program central memory requirement is dependent on problem size and complexity with a 5,000-logic-gate circuit requiring approximately 50K of 32-bit word memory. LOGSIM was developed in 1972 and last updated in 1976. [See related article, "CADAT Integrated-Circuit Mask Analysis" (MFS-25054), on page 396.]

This program was written by C. L. Mitchell and J. F. Taylor of M&S Computing, Inc., for **Marshall Space Flight Center**. *For further information, Circle J on the COSMIC Request Card.*
MFS-25183

CADAT Test Pattern Generator

Checkout and testing of complex digital circuits are reduced and done in a few days instead of months.

The CADAT test pattern generator (TPG) aids in the checkout, fault detection, and fault isolation of complex digital circuits. The time and the effort of manually generating digital test pat-

terns can be a major limiting factor in effectively utilizing automatic testing. This time and effort are reduced from several months to several days by TPG.

TPG performs the three major tasks associated with test program design. After examining the circuit, it develops a set of stimulus-and-response patterns for checkout, fault detection, and fault isolation. TPG then verifies the diagnostic potential of the patterns, and finally, it creates a data file that can be interfaced with automated circuit-testing equipment.

Input to TPG consists of a nodal description of the digital configuration. A large, expandable digital component library is available for describing the circuit. Once the complete circuit has been introduced, TPG generates a NAND-gate equivalent circuit as the basic model for test pattern generation. The use of NAND equivalents facilitates a realistic failure simulation, which has proved more effective and efficient than individual component simulation. Signal propagation delay is simulated by using a fixed time delay across each NAND. This NAND-gate time accounting has higher resolution than fixed component delay, since nodes are processed simultaneously throughout the circuit. By checking for node-status oscillations, TPG has a high probability of spotting "race" conditions that might otherwise go undetected.

Once TPG has analyzed the model, generated a test pattern, and verified the validity of the pattern, the stimulus data for testing the actual device are prepared. In order actually to test or simulate the device accurately, the TPG-generated stimulus data must be transformed into acceptable inputs for logic test equipment or for a logic simulator. The TPG package includes an interface program (TPGITF) to utilize the TPG stimulus data to generate TOIL test sequences for the MACRO-DATA-200 LSI tester and to generate excitation input for the CADAT system logic-simulator program LOGSIM.

The TPG program is written in FORTRAN IV for batch execution and has been implemented on a Xerox Sigma V computer. The TPG program was originally developed in 1971 and was last updated in 1976.

This program was written by M&S Computing Co., for **Marshall Space Flight Center.** *For further information, Circle K on the COSMIC Request Card.*
MFS-25066

CADAT Field-Effect-Transistor Simulator

A versatile designer tool for analyzing MOS circuits

The CADAT field-effect-transistor simulator (FETSIM) analyzes the dc and transient behavior of metal-oxide-semiconductor (MOS) circuits. Both N-MOS and P-MOS transistor configurations in either bulk or silicon-on-sapphire (SOS) technology and almost any combination of R/C elements are analyzed.

As inputs, FETSIM requires the complete circuit topology and device, process, and control parameters. The user may also specify initial node conditions and the input pulse format. For example, pulse rise time, fall time, width, and time between succeeding pulses are all independently controlled.

FETSIM is based on a sophisticated mathematical model that can accurately handle N-MOS, P-MOS, bulk, and SOS devices. By considering doping of the ionized acceptors (or donors) in the substrate, several second-order physical effects are implicitly accounted for. They include the apparently-decreased carrier mobility resulting from heavy substrate doping and the gating effect associated with stacked devices. Sensitivity to process changes is maintained by requiring such data as threshold voltages and doping levels as inputs. Such intrinsic MOS phenomena as parasitic feedback capacitance and variation of threshold voltage with source potential are handled implicitly.

FETSIM transforms the input data into a set of nodal equations. These ordinary differential equations are numerically integrated. As outputs, FETSIM lists node voltages and all transistor currents as a function of time.

The FETSIM program is written in FORTRAN IV for batch execution and has been implemented on Xerox Sigma V with a central memory requirement of approximately 45K of 32-bit words. The FETSIM program was developed in 1974 and was last updated in 1977.

This program was written by RCA Corp. for **Marshall Space Flight Center.** *For further information, Circle L on the COSMIC Request Card.*
MFS-25067

CADAT Place-and-Routine in Two Dimensions

An interactive program for converting a logic design to final LSI/MOS chip artwork.

The CADAT place-and-route-in-two-dimensions program (PR2D) is a standard-cell automatic-layout program for generating large-scale-integrated/metal-oxide-semiconductor (LSI/MOS) arrays. PR2D translates the logic designer's cell interconnection requirements into a physically-defined MOS chip. Input data consist of program control parameters, logic pattern assignments, and the interconnecting nets. PR2D reads the input data, searches the pin data file for data on each pattern type, generates a placement of the patterns, and interconnects the patterns. As output, it generates the artwork for the layouts.

The program control parameters allow the individual functions of PR2D to be executed in separate steps. This increases the flexibility of the program and can reduce computer run time. By inspecting the output at each step, changes can be made to improve the placement and routing on the final chip design.

PR2D produces a map, or printer plot, that is assembled into the final chip layout. All pertinent data regarding the layout are shown on the map. In addition, a printout of chip statistics is generated for review by the designer. Once the design is finalized, an artwork data file is generated for fabricating the chip mask.

PR2D is written in FORTRAN IV for batch execution and has been implemented on a Xerox Sigma V CP-V computer with 64K of 32-bit memory. The program was developed in 1978.

This program was written by RCA Corp. for **Marshall Space Flight Center.** *For further information, Circle M on the COSMIC Request Card.*
MFS-25058

CADAT Multiport Placement and Routing

Substantial chip area is saved by unique multiport cells.

The CADAT multiport-in-two-dimensions program (MP2D) is a powerful placement and routing aid for processing double-ended cell equivalents of the high-speed silicon-on-sapphire (SOS) standard-cell family. The basic purpose of MP2D is to design high-density large-scale-integrated (LSI) arrays. Using inputs that consist of control parameters, logic pattern assignments, and node connectivity data, MP2D determines a two-dimensional placement of the cells and a two-dimensional routing of interconnections. The outputs include artwork-plotting instructions for generating the final mask. Innovative double-entry and "feedthrough" multiport cells allow MP2D to reduce substantially the chip area and wiring.

Two major innovations in LSI array design make MP2D substantially better than typical single-entry placement and routing programs. One of these innovations enables the program (1) automatically to route interconnections to either the top or bottom of each cell in such a way as to minimize total wire length and interconnection area and (2) to make connections between cells on nonadjacent rows by routing the interconnections directly across or through intermediate cell rows.

The other innovation relates to the unique feature of the circuit cell that permits the input/output connections to be accessed at either the top or the bottom of the cells. This multiport placement and routing can save substantial chip "real estate" because of the reduced requirements for wiring, which previously was the largest user of chip area.

MP2D is written in FORTRAN IV for batch execution, has been implemented on a Xerox Sigma V computer with the CP-V operating system, and has a central memory requirement of approximately 56K of 32-bit words. The program was developed in 1977.

This program was written by RCA Corp. for **Marshall Space Flight Center.** *For further information, Circle N on the COSMIC Request Card.*
MFS-25065

CADAT Integrated-Circuit Mask Analysis

Program verifies artwork, checks logic equations, and evaluates other mask design parameters.

The CADAT System Mask Analysis Program (MAPS2) is an automated software tool for analyzing integrated-circuit mask design. Included in MAPS2 functions are artwork verification, device identification, nodal analysis, capacitance calculation, and logic equation generation.

To simplify the data base, MAPS2 operates on mask data that have been converted from their original forms to orthogonal rectangles with identification numbers. MAPS2 accepts and automatically converts mask data in MAP, PRF, MANN, AIDS, and Banning Cell Library formats. The resultant rectangular mask data file allows MAPS2 to analyze circuit masks quickly and efficiently.

Once the mask data file is created, the user controls the analysis through a versatile command language. The user commands a wide range of processes, including qualitative and quantitative testing of selected mask areas, the modification of masks, the creation of new masks, and the computation and sorting of mask data.

MAPS2 processing is divided into two major processes: rectangular refinement and command execution. In the rectangular refinement processing, user-supplied mask data are converted into the orthogonal rectangle format that approximates the mask to any user-specified accuracy. Once the rectangular mask data have been generated and stored, user-supplied commands are processed one at a time. Data are read from the mask rectangle file, the requested processing is performed, output data files are generated, and any user-requested information is printed.

MAPS2 is written in FORTRAN IV for batch execution and has been implemented on a Xerox Sigma II computer with a central memory requirement of approximately 33K of 16-bit words. MAPS2 was developed in 1976. [See related article, "CADAT Logic Simulation Program" (MFS-25183), on page of this issue.]

This program was written by C. L. Mitchell of M&S Computing, Inc., for **Marshall Space Flight Center**. *For further information, Circle P on the COSMIC Request Card.*
MFS-25054

Mathematics and Information Sciences

Hardware, Techniques, and Processes

An Image-Data-Compression Algorithm

A proposed algorithm simplifies image data processing.

NASA's Jet Propulsion Laboratory, Pasadena, California

A recently-proposed Cluster Compression Algorithm (CCA) preprocesses Landsat image data immediately following the satellite data sensor (receiver). The data are reduced by extracting pertinent image features and compressing this result into a concise format for transmission to a ground station. This results in a narrower transmission bandwidth, increased data-communication efficiency, and reduced computer time in reconstructing and analyzing the image. A similar technique could be applied to other types of recorded data to cut the costs of transmitting, storing, distributing, and interpreting complex information.

Basically, the CCA uses spatially local clustering to extract features from the image data to describe spectral characteristics of the data set. These features form a sequence of scalar numbers that define each picture element in terms of the cluster features. The sequence, called the feature map, is encoded into a compressed format for transmission. The preprocessed data can be decoded via a simple lookup table for image reconstruction or computer analysis.

The CCA can use any of the several clustering techniques all derived from the basic iterative approach known as the Basic Clustering Algorithm (BCA) for automatically grouping the multidimensional data. The BCA involves simple repetitive computations and can be structured in a highly parallel manner for very high data rates.

The BCA assigns each data vector to the closest cluster and generates a predetermined number of features per data set that correspond to a rate-controlled mode for a data compressor. There are many ways to modify the BCA to make it adaptive. For example, clusters might be split, combined, or deleted during the iterative clustering based on intracluster and intercluster distance measures.

The most basic version constitutes the Uncoded CCA. This version applies measurement vectors from every local source to cover the entire image.

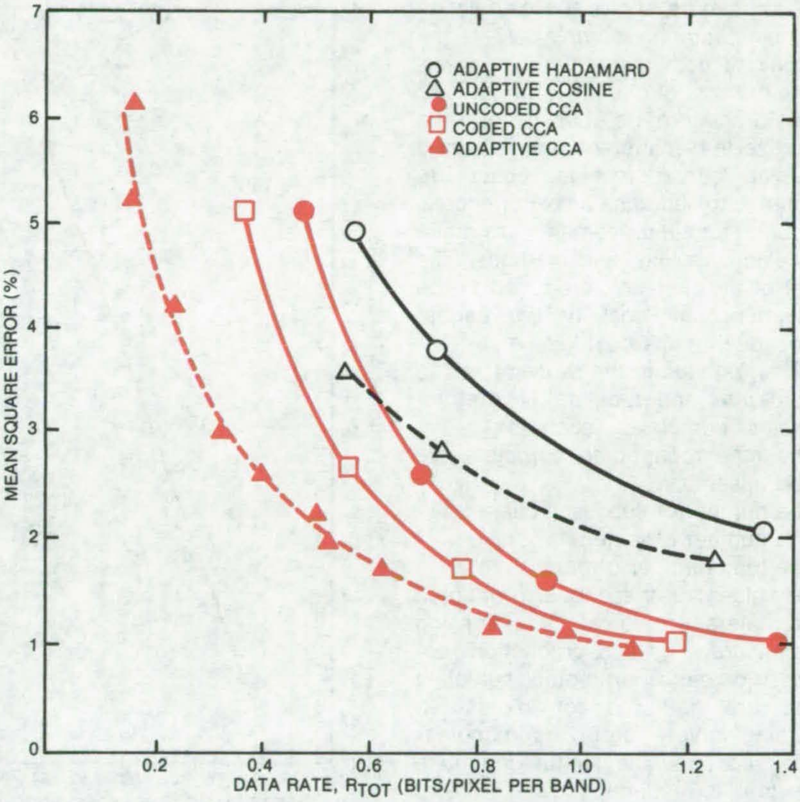

A **Comparison of New CCA Configurations** with adaptive Hadamard and Fourier techniques shows that the former CCA technique has fewer errors as a function of data rate. Algorithm performance was defined in terms of data quality as a function of data rate. The data quality was defined in the most commonly used terms of percent mean-square error (%MSE), classification accuracy, and subjective appearance. The results have shown that in addition to reducing the data volume, the CCA data compression also reduces the number of required classifications.

A more sophisticated version is the Coded CCA. It is based on the fact that in image data there is significant spectral correlation between spatially-close picture elements and correspondingly adjacent elements on the feature map. This correlation lends itself to entropy encoding techniques.

Other versions include the Adaptive CCA and the Cascaded CCA. The Adaptive form is as the Coded CCA except the clustering is adaptive. The clusters may be deleted, split, or combined according to the user supervision thresholds. The Cascaded CCA can modify the local source clustering based on the knowledge of clustering results from surrounding local sources. This characteristic can be used to reduce the spatial and spectral data rates.

The figure shows a comparison of the performances of the new CCA configurations. Performance is measured as the percentage of errors introduced at a given data rate.

This work was done by Edward E. Hilbert and Robert F. Rice of Caltech for **NASA's Jet Propulsion Laboratory.** *For further information, Circle 92 on the TSP Request Card.*
NPO-14496

Determining Manufacturing Cost From Product Complexity

Analytical method exploits the special relationship between complexity and manufacturing improvement trends.

Marshall Space Flight Center, Alabama

A procedure allows the calculation of manufacturing complexity — the totality of cost elements that determine the cost of manufacturing a unit. The procedure is based on the premise that manufacturing follows a learning curve; that is, costs are assumed to decrease as experience is acquired and improvements are made in design, tooling, and methods. The cost of the first unit produced is the maximum unit cost of the series. Subsequent units cost less.

The first step in the procedure is to enumerate and tabulate several indexes of complexity, such as:

- The time required to complete the first assembly,
- The number of subassemblies,
- The number of fasteners, and
- The total number of parts.

The values of these design-oriented parameters are found by examining design drawings and production records. For each parameter, sufficient data are gathered for plotting a learning curve — a curve of manufacturing cost vs. the length of time a design is in production.

Learning curves are plotted on double logarithmic paper for at least six values of each parameter. This step is repeated for each of the subsystems (e.g., electrical, mechanical) in a production unit. For example, if a production unit consists of four subsystems, at least 24 learning curves must be plotted for the number of fasteners and for each of the other design parameters. The slopes of the learning curves for the various parameter values are plotted for each subsystem to give a trend curve (see Figure 1). In general, the slope will increase more or less along a straight line as the parameter value increases.

At that point, a decision is made about the parameters to be included in the calculation. If a parameter appears to be unrepresentative of the overall system, it is omitted from further consideration. Different subassemblies may have different parameters; for example, the set chosen for an electrical assembly may be different from that for a mechanical assembly.

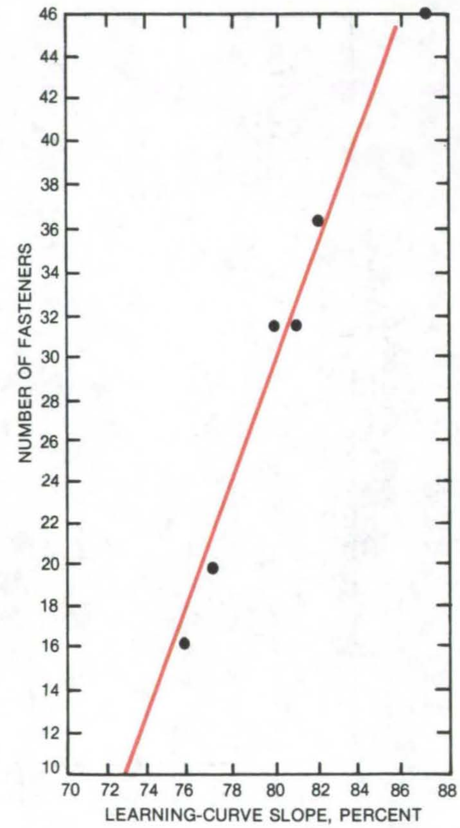

Figure 1. A **Trend Curve** shows how the learning-curve slope varies for different values of a manufacturing parameter (in this case, the number of fasteners).

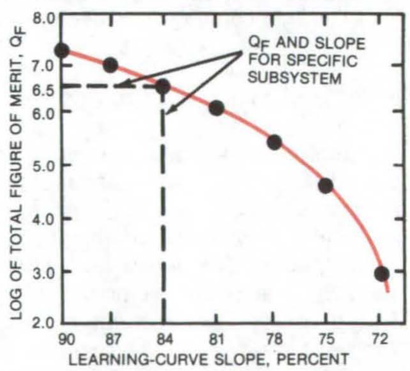

Figure 2. A **Figure-of-Merit Curve** shows how complexity varies with the learning-curve slope of a subsystem.

The next step is to determine a figure of merit representing the complexity of a specific subsystem design. The figure of merit, called Q_F, is found for each of the subsystems in the unit. Q_F is equal to the product of the parameter values at a given value of the learning-curve slope. The logarithm of Q_F is plotted as a function of slope (see Figure 2). This curve applies to a subsystem. The learning-curve slope for a specific subsystem design is found by interpolating from the known Q_F value for the design.

Finally, a composite slope for the complete unit is calculated by a formula that takes into account the slopes of the individual subsystems, the value in dollars of worker hours of each of the subsystems, and the total value of the complete unit. The formula weights the contribution of the individual subsystem slopes according to the value of the subsystem.

With the composite slope, it is possible to compute the cost of the nth unit turned out on the production line. The computation is reduced to finding the ordinate (cost of the nth unit) that corresponds to a particular abscissa (nth unit) on a straight line on double logarithmic paper. Both the slope and intercept (the cost of the first unit produced) are known.

This work was done by Leon M. Delionback of **Marshall Space Flight Center.** *For further information, Circle 88 on the TSP Request Card.*
MFS-25371

SUBJECT INDEX

National Aeronautics and
Space Administration

Washington, D.C.
20546

NASA

New sound-absorbing products, such as the noise-blocking green wall in this light-socket manufacturing facility, are an outgrowth of an early NASA search for better vibration-absorbing encapsulants for spacecraft electronics. Based on a unique liquid plastic compound, the products could reduce noise in a variety of industrial and nonindustrial applications. [*See the bottom of page A1.*]